Gravitational Waves
through the Cosmic Web

Proefschrift

ter verkrijging van
de graad van doctor aan de Universiteit Leiden,
op gezag van rector magnificus prof.dr.ir. H. Bijl,
volgens besluit van het college voor promoties
te verdedigen op dinsdag 4 juli 2023
klokke 13:45 uur

door

Alice Garoffolo

Geboren te Milaan, Italië
in 1993

The cover is generated with DALL-E 2. The inputs are inspired by the paintings of
Jan Toorop and Hieronymus Bosch.

Contents

1

Introduction

Cosmology is a purely observational science: we cannot put the Universe in a laboratory and reproduce its history at our will, tweaking parameters to see how its constituents react. It always has to rely on the detection of a signal, whether it is a photon, or since 2016 [1], a gravitational wave (GW). Basing its hypothesis exclusively on observations, cosmology attempts at providing a single description of the Universe, from its early stages to the present, in terms of only few parameters. In this sense, the first GW direct detection marked a breakthrough for the sciences of the Universe: it opened up a new observational window affected by an entirely different set of systematics compared to electromagnetic signals. The observation of the Cosmic Microwave Background (CMB) by WMAP and Planck [2–4], confirmed that the photons comprising this signal are described by a black-body spectrum with a temperature of 2.73 K, up to one part in 10^5. Since the Universe is expanding, the temperature of photons increases as we go backward in time so that, at the time of the CMB emission, it was about 10^3 K. One can think of extrapolating this increasing behavior to even earlier times, before the moment when nuclei and free electrons combined to form neutral atoms and the photon-baryon fluid was kept in thermal equilibrium by Compton scattering, or even before that, until one reaches the typical energy scale of the Universe at the moment of the formation of the first nuclei: $\sim 10^1 0$ K [5]. So, the ultimate goal of a cosmological model is to build a unique description of the Universe across (at least) roughly 10 orders of magnitude of different energy regimes. This heroic effort has successfully produced the standard cosmological model, ΛCDM: gravity follows the laws of General Relativity, a cosmological constant Λ embodies the *dark energy* driving the recent accelerated expansion of the Universe, and *cold dark matter* (CDM), an unknown form of matter electromagneti-

1

cally neutral, is responsible for structure formation. The last two components make up almost 96% of the current energy budget of the Universe, while the remaining portion is composed of standard model particles, which in cosmology are divided into two categories: radiation and baryons, where in the latter leptons are included as well.

The ΛCDM model's success, lies in its ability to fit a wide range of observational data, not only the CMB, but also type Ia Supernovae (SNe) datas [6, 7], and the mapping of cosmic structures, with the baryon acoustic oscillation (BAO) peak [8]. Yet, ΛCDM still fosters in its dark components large areas of theoretical uncertainties. Enlarging the volume of data, with ongoing and upcoming galaxy and weak-lensing surveys [9–12], will necessarily subject the standard model to a new level of scrutiny. The rise of precision cosmology, has already seen the emergence of tensions between datasets when interpreted within the ΛCDM framework [13, 14], which could signal the first cracks in the model as we achieve a new level of precision in measuring its parameters [15]. Since one of the assumptions of ΛCDM is General Relativity, testing this model also mean testing the theory of gravity on cosmological scales: after passing a battery of tests in the Solar System and on galactic scales, we can investigate gravity at work at low energies.

Thanks to the LIGO-Virgo-Kagra (LVK) [16, 17] collaboration, we can now add GW observations to the pool of different datasets, giving us direct access to the dynamical regime of gravity. The waves observed by these interferometers are produced during the inspiral of a compact object binary. When two black holes or two neutron stars, or a black hole and a neutron star, orbit around each other, they emit gravitational waves. The energy lost through this channel makes the orbit of the binary shrink until the two objects merge into one. In the coming years, the next generation of ground-based interferometers is expected to provide us with a "dark map" of the Universe by observing tens of thousands of GW events [18, 19]. Comparing this map with those compiled by galaxy surveys, will boost our understanding of the electromagnetically neutral species of the Universe. For example, we may be able to determine whether all astrophysical GW sources are located inside galaxies. If so, this would suggest that GWs and galaxies trace the underlying dark matter gravitational potential wells equivalently, so that these two probes can be used jointly, maximizing the scientific return from the two missions. Alternatively, if some astrophysical GW sources are found to be outside of galaxies, it would open up new avenues for scientific inquiry [20]. The observation of exotic compact objects through GWs could have significant implications for cosmology. A particularly intriguing possibility is the existence of *primordial black holes* [21] potentially accounting for part of the Universe's dark matter, which might have formed from the collapse of large, small-scale inflaton perturbations in the early Universe, or through other exotic channels (see [20] and references therein).

The concept that GW observations can enhance our understanding of the early Universe is not new. The detection of *primordial tensor modes*, through a B-mode polarization pattern of the CMB, would have significant implications for our comprehension of the primordial Universe [22–24]. According to the current model, during the pre-standard model era, at least two quantum fields existed in the Universe: the metric and the inflaton, driving a phase of exponentially accelerated expansions. Their fluctuations were first stretched beyond the Hubble horizon, and then slowly re-entered during standard cosmic history setting, for instance, the initial seeds for the development of gravitational potentials, eventually leading to the formation of cosmic structures. Since the inflationary paradigm treats scalar and tensor perturbations on the same footing, primordial gravitational waves are a key prediction of it. These types of GWs are substantially different from astrophysical events seen by LVK. Since their source is a quantum process, they would constitute a *stochastic gravitational wave background* (SGWB), similar in nature to the CMB's photons. From the first GW detection, the literature on SGWB has expanded considerably, as there are a number of mechanisms thought to take place in the early Universe that can produce a diffuse GW signal. The SGWB can also be of astrophysical origin: if the single GW events are not distinguishable one from the other, they are expected to form a background too. Because of the incredible wealth of information, detecting the SGWB is a key science goal for the future GW missions, target of space-based interferometers and pulsar-timing arrays [25–31].

The waveform of a GW and the frequency spectrum of the SGWB depend on the specifics of their sources. Regardless of the generation mechanism, propagation effects can have a significant impact. For instance, a wave traveling through an expanding Universe is damped faster than one traveling through a static one, or objects along the way can cause various distortions. As a result, GWs also convey information about the dynamics of the Universe, including the late-time cosmic expansion, so dark energy, and the cosmic structures tracing the gravitational potential wells of dark matter. Propagation effects introduce an irreducible error, setting an upper limit on the precision with which we can measure the source parameters. However, one can turn this around and look at propagation effects as a rich resource of cosmological information, both at the background and perturbed level.

Photons undergo similar effects during propagation, making it possible to use both probes jointly. Joint observations of GWs and photons are particularly promising for testing proposals for dark energy, where the two messengers behave differently. Such proposals are widespread in the literature and, thanks to the degeneracy breaking between the two sectors, they can be thoroughly investigated in the near future. Despite the similarities, GWs and photons can also exhibit very different behaviors, especially when comparing them at different frequencies. The typical energy of a photon, whether it belongs to the CMB or if it was emitted by an astrophysical event,

is much higher than the energy scale associated to any (known) object it may encounter during propagation. In particular, an obstacle can be a large-scale structure, roughly at the energy scale of 10^{-17} Hz, or a compact object, ranging from supermassive to stellar black holes in the $\sim 10^{-3} - 10^{1}$ Hz band. Even the low-energy CMB photons have frequencies of approximately 160 GHz. This implies that photons are always well described by the *ray-optics* limit. By contrast, there are no limitations for the wavelengths of GWs and, depending on the situation, *wave-optics* effects may arise. The validity of these two regimes, and the kind of description they allow, will be profusely discussed in this Thesis. However, we can already appreciate the fact that GWs not only carry new valuable cosmological information, but also they offer new theoretical challenges.

The main focus of this Thesis is characterizing the propagation effects affecting GWs in the late time Universe, both in the ray-optics limit and in the wave-optics one. We use the former to describe resolved astrophysical GWs, with frequencies higher than the mHz, when these travel through the large-scale structures of the Universe. In this case, we will explore their potentialities in testing particular models for dark energy called *scalar-tensor theories*. Finally, we will give up the high frequency approximation and, in General Relativity, explore the wave-optics effects, paying particular attention to the polarization content of the gravitational waves. The purpose of this Introduction is to provide the reader with all the necessary tools to understand the topics covered in the following Chapters.

1.1. The standard cosmological model

Two very important aspects which any proposed cosmological model has to describe are the expansion of the homogeneous and isotropic Universe and the growth of linear perturbations. In the two sections below, we describe their phenomenology in ΛCDM.

1.1.1. Friedmann equations

Observations suggest that on scales $\gtrsim 100$ Mpc, the *cosmological principle* holds, namely that the properties of the Universe are the same for all observers comoving with the expansion. Observations also suggest that the Universe, on large scales, does not display a preferred direction. These two facts together, fix the metric describing the Universe at these scales to

$$ds^2 = g_{\mu\nu}\,dx^\mu\,dx^\nu = a^2(\tau)\left[-d\tau^2 + \frac{d\chi^2}{(1-\kappa\chi^2)} + \chi^2\left(d\theta^2 + \sin^2\theta\,d\varphi^2\right)\right],\qquad(1.1)$$

also known as the Friedmann-Lemaître-Robertson-Walker (FLRW) metric [32], where τ is the conformal time, $a(\tau)$ is the scale factor, describing how the Universe

expands over time, κ is the intrinsic curvature of the 3D spatial hypersurfaces, and it can take the discrete values $\kappa = 0, +1, -1$, representing *flat*, *positively* or *negatively curved* spatial slices. In the metric above, χ is the *comoving distance*, related to the scale factor as in Eq. (1.8). The FLRW metric (1.1) describes a Universe as *spatially homogeneous* and *isotropic*. The cosmological principle also fixes the form of the possible energy content of the Universe to that of a perfect fluid described by a stress-energy tensor of the form [32]

$$T_{\mu\nu} = \rho\, u_\mu u_\nu + P\Lambda_{\mu\nu}, \tag{1.2}$$

here $\Lambda_{\mu\nu} \equiv g_{\mu\nu} + u_\mu u_\nu$, is the orthogonal projector to the worldlines of the observers whose 4-velocity is u^μ, while ρ is the energy density and P is the isotropic pressure of the fluid element. Then, in the standard cosmological model, the FLRW metric is a solution of Einstein's equations

$$G_{\mu\nu} = 8\pi G \left[T_{\mu\nu} + T^\Lambda_{\mu\nu} \right], \qquad T^\Lambda_{\mu\nu} = -\frac{\Lambda}{8\pi G}\, g_{\mu\nu} \tag{1.3}$$

where $G_{\mu\nu}$ is the Einstein tensor, $T_{\mu\nu}$ is given by Eq. (1.2). In the expressions above, we have introduced Λ, the cosmological constant driving the late time cosmic expansion in the ΛCDM model. To close the system, it is necessary to supplement an equation of state relating pressure and energy density of the perfect fluid, usually in the form $P = w\rho$. In the ΛCDM model, the matter species contributing to the stress-energy tensor are: pressureless non-relativistic matter (CDM and baryons), described by the equation of state $w_m = 0$ and radiation supported by its pressure and characterized by $w_r = 1/3$ [32]. Also, $T^\Lambda_{\mu\nu}$ can be written in a similar fashion of Eq. (1.2), with equation of state $w_\Lambda = -1$ and $\rho_\Lambda = \Lambda/(8\pi G)$. The independent conservation of their stress-energy tensors, gives the continuity equations

$$\Omega'_i + 3\mathcal{H}\,\Omega_i(1 + w_i) = 0, \qquad \text{with} \qquad {}' = \partial_\tau, \tag{1.4}$$

where we defined the time dependent density parameters

$$\Omega_i(\tau) \equiv \frac{\rho_i(\tau)}{\rho_{crit}}, \qquad \rho_{crit} = \frac{3H_0^2}{8\pi G} \tag{1.5}$$

with $i = r, m, \Lambda$. Note that $\Omega^0_\Lambda = [\Lambda/(8\pi G)]/\rho_{crit} = \Lambda/(3H_0^2)$. According to the value of the equation of state parameters, w_i, the continuity equation takes the different solutions

$$\Omega_r(a) = \Omega^0_r/a^4, \qquad \text{and} \qquad \Omega_m(a) = \Omega^0_m/a^3, \qquad \text{and} \qquad \Omega_\Lambda(a) = \Omega^0_\Lambda, \tag{1.6}$$

where Ω^0_i are the values of the density parameters today, i.e. at $a = a_0 = 1$, choosing the spatial curvature to be zero, $\kappa = 0$. The different power laws dictate that the various species "dilute" at different rates, in such a way that we can consider one

χ_M	χ_Λ	χ_*	$\chi_{M\Lambda}$	χ_i
$\left[H_0(\Omega_m^0)^{1/2}\right]^{-1}$	$\left[H_0(\Omega_\Lambda^0)^{1/2}\right]^{-1}$	$\left[H_0(\Omega_m^0)^{1/3}(\Omega_\Lambda^0)^{1/6}\right]^{-1}$	$\chi_* - \chi_\Lambda$	$3\chi_* - \chi_\Lambda$
0.027	0.017	0.023	0.0054	0.052

Table 1.1: List of special comoving distance values entering in Eq. (1.9). The first row contains their definition, while the numerical values are computed considering $H_0 = 67.3$, $\Omega_m^0 = 0.31$ and $\Omega_\Lambda^0 = 0.69$ [4].

element at a time to drive the expansion of the Universe. In order, we will have: radiation first, being the most abundant in the early stages of the Universe, succeeded by a matter dominated phase and finally the cosmological constant in the very recent time. Since we are interested in describing the late time Universe, in our discussion we will always neglect the contribution of radiation to the energy budget. This results in another simplification: we will treat CDM and baryons in the same way.

From Eq. (1.3), one can find Friedmann's equation, relating the scale factor to the energy density of the constituents

$$\mathcal{H}^2 = a^2 H_0^2 \left(\Omega_m + \Omega_\Lambda\right), \tag{1.7}$$

where $\mathcal{H} \equiv a'/a$ is the Hubble parameter in conformal time. We solve analytically Friedmann's equation separately in the *matter* and Λ *dominated* epochs, and match the solutions at the moment of their equivalence, $a_{M\Lambda} = \sqrt[3]{\Omega_m^0/\Omega_\Lambda^0}$. For later convenience, we write the solution in terms of the comoving distance

$$\chi \equiv \tau_0 - \tau = \int_a^1 \frac{d\tilde{a}}{(\tilde{a}\mathcal{H}(\tilde{a}))}, \tag{1.8}$$

where τ_0 is the value of conformal time today, i.e. such that $a(\tau_0) = 1$. From this definition, it is clear that $d\chi = -d\tau$. The scale factor and the comoving distance belong respectively to the range $[0,1]$ and $[0,\chi_i]$, where χ_i is the value of χ corresponding to $a = 0$. Such initial value does not have any particular physical meaning, and it is merely a consequence of having neglected the radiation contribution. We find the solutions

$$a(\chi) = \begin{cases} \dfrac{[\chi - \chi_i]^2}{4\chi_M} & \chi \in [\chi_{M\Lambda}, \chi_i] \\ \dfrac{\chi_\Lambda}{\chi_\Lambda + \chi} & \chi \in [0, \chi_{M\Lambda}] \end{cases}, \qquad \mathcal{H}(\chi) = -\frac{1}{a}\frac{\partial a}{\partial \chi} = \begin{cases} \dfrac{2}{\chi_i - \chi} & \chi \in [\chi_{M\Lambda}, \chi_i] \\ \dfrac{1}{\chi + \chi_\Lambda} & \chi \in [0, \chi_{M\Lambda}] \end{cases} \tag{1.9}$$

where all the quantities defined in the equation above can be found in the Table 1.1. We point out that a solution of Eq. (1.7) interpolating between matter and Λ domination eras exists [33], however it is quite intricate and impractical, therefore in this Thesis we will use the explicit expressions given above when needed.

In the ΛCDM model, dark energy (DE) is modeled with the cosmological constant. To better understand the character of the accelerated expansion it drives, it is best to rewrite the scale factor in terms of cosmic time $dt \equiv a d\tau$. In this case, and neglecting the matter contribution in Eq. (1.7), it is easy to find that

$$\frac{\partial a}{\partial t} = \sqrt{\frac{\Lambda}{3}}\, a\,, \qquad \rightarrow \qquad a(t) = e^{\sqrt{\frac{\Lambda}{3}}\, t}\,. \qquad (1.10)$$

Because of this exponential behavior of the scale factor, the cosmological constant is said to drive the *accelerated expansion* of the Universe in the very recent epoch, a phenomenon detected via the observation of Supernovae type Ia (SNe) which was worth a Nobel Prize [6, 7] .

Another important quantity in background cosmology is the *cosmological redshift*, related to the scale factor as

$$1 + z = \frac{1}{a}\,, \qquad (1.11)$$

determining also the red-shifting of the wavelengths of photons and GWs as they propagate through the expanding Universe.

1.1.2. Cosmological perturbation theory

Departures from the homogeneous and isotropic configuration characterize *large-scale structures* (LSS) of the Universe. On scales between $\sim 100 - 50$ Mpc, these deviations are still small in amplitude, and thus can be treated with linear relativistic perturbation theory.

Prior to the emission of the CMB, photons and electrons were tightly coupled through Compton scattering, forming a unique *photon-baryon fluid*. As a result, ordinary non-relativistic matter was supported by the radiation pressure of photons, preventing it from collapsing under gravitational interaction. In contrast, the electromagnetically neutral and non-relativistic (pressureless) CDM could form clumps, preparing the gravitational potential wells for the baryons to fall into, after the moment of recombination, when the Universe became transparent to photons. This process eventually led to the formation of stars, galaxies, and galaxy clusters inside the wells and filaments of the dark matter distribution. Therefore, it is often said that galaxies *trace* dark matter introducing the concept of *galaxy bias*, as we will see later. In the late-time Universe, relativistic species, such as photons, constitute a subdominant part of the total energy density budget as they dilute faster than the other components (see Eq. (1.6)). Since this is the period we are most interested in, we neglect them when studying LSS and treat baryons and CDM jointly as a non-relativistic pressureless component.

The equations of motion ruling the growth of LSS can be found by linearizing the

1

gravitational field equations around the FLRW background,

$$g_{\mu\nu} = a^2(\tau)\eta_{\mu\nu} + \epsilon\delta g_{\mu\nu}, \tag{1.12}$$

where $\eta_{\mu\nu} = \mathrm{diag}(-1,1,1,1)$ is the Minkowski metric and ϵ is the expansion parameter tracking the LSS. We expect that CMB temperature anisotropies are of the same order of magnitude of the metric perturbation, so that $\epsilon \sim 10^{-5}$. The FLRW background is symmetric under rotations in the 3D spatial hypersurfaces. One can exploit this fact and break down the metric perturbation $\delta g_{\mu\nu}$ into irreducible representations of the Euclidean rotations. This is the so-called *scalar-vector-tensor* decomposition. Due to the symmetry of FLRW, each subgroup decouples from the others to linear order, allowing an independent analysis of each type of modes [5, 34–38][1]. Considering the FLRW background fixed, then under an infinitesimal gauge transformation $x^\mu \rightarrow x^\mu + \epsilon\xi^\mu$, the metric perturbation transforms as

$$\delta g'_{\mu\nu} = \delta g_{\mu\nu} - \left(\bar{\nabla}_\mu \xi_\nu + \bar{\nabla}_\nu \xi_\mu\right), \tag{1.13}$$

where $\bar{\nabla}_\mu$ are the covariant derivatives built with the FLRW metric. The metric perturbation, $\delta g_{\mu\nu}$, being a 4 symmetric tensor, has 10 independent components. The gauge freedom fixes 4 of them, leaving 6 modes to be fixed with Einstein's equations. A common gauge choice is the so-called Poisson's gauge [34, 39], in which the line element takes the form

$$ds^2 = a^2(\tau)\left[-(1+2\epsilon\Phi)d\tau^2 + 2\epsilon\omega_i d\tau dx^i + (1-2\epsilon\Psi)d\mathbf{x}^2 + 2\epsilon\gamma_{ij}dx^i dx^j\right], \tag{1.14}$$

where

1. Φ and Ψ are two scalar gravitational potentials (2 modes),

2. ω_i is the vector potential, such that $\partial^i\omega_i = 0$ (2 modes),

3. γ_{ij} is the transverse and traceless tensor mode, such that $\eta^{ij}\gamma_{ij} = \partial^i\gamma_{ij} = 0$ (2 modes),

with the convention that spatial indices are raised and lowered with the Minkowski metric, η_{ij}. In Poisson's gauge, the two gravitational potentials Φ and Ψ correspond to the gauge invariant Bardeen's potentials [40] and they describe the perturbation of the time direction and of the spatial hypersurfaces' curvature. Note that the tensor mode γ_{ij} *does not* coincide with our definition of GWs, which will be given later.

---

[1]There are many references for cosmological perturbation theory. This section is based on [34]. However, we do change notation to be consistent with the rest of this Thesis, e.g. the two scalar gravitational potentials have exchanged names $\Phi \rightarrow \Psi$ and $\Psi \rightarrow \Phi$, we call $\mathcal{H}$ the conformal Hubble parameter instead of η.

Similarly to the metric, also the matter stress-energy tensor is decomposed as $T^\mu_\nu = \bar{T}^\mu_\nu + \epsilon \delta T^\mu_\nu$, or expliciting the components out, as

$$
\begin{align}
T^0_0 &= -\bar{\rho} - \epsilon \delta \rho \tag{1.15}\\
T^i_0 &= -\epsilon (\bar{\rho} + \bar{P}) \, v^i \tag{1.16}\\
T^0_i &= +\epsilon (\bar{\rho} + \bar{P}) \, [v_i + \omega_i] \tag{1.17}\\
T^i_j &= +\bar{P} \delta^i_j + \epsilon \left(\delta P \delta^i_j + \Sigma^i_j \right) \tag{1.18}
\end{align}
$$

where $\bar{\rho} = \bar{\rho}(\tau)$ and $\bar{P} = \bar{P}(\tau)$ are the background energy density and the isotropic pressure, only time dependent. The anisotropic stress, Σ^i_j, accounts for velocity gradients related to irreversible processes, and we assume it is traceless by reabsorbing any bulk contribution in the definition of the pressure. Also, in the expression above, v^i is the peculiar velocity, whose definition is

$$
u^\mu = \frac{1}{a} \left[(1 - \epsilon \Phi), \, \epsilon v^i \right]. \tag{1.19}
$$

An important quantity is the energy density contrast

$$
\delta \equiv \frac{\delta \rho}{\bar{\rho}}, \tag{1.20}
$$

sourcing the gravitational potential wells. The peculiar velocity and Σ^i_j can be decomposed into irreducible representations with respect to the spatial rotation as well

$$
v_i = v^T_i + \partial_i v, \qquad \Sigma_{ij} = \mathcal{D}_{ij} \Sigma + \partial_{(i} \Sigma_{j)} + \Sigma^{TT}_{ij}, \tag{1.21}
$$

with $\partial^i v^T_i = 0$ and $\partial^i \Sigma^{TT}_{ij} = 0$ and

$$
\mathcal{D}_{ij} \Sigma \equiv \left(\partial_i \partial_j - \frac{1}{3} \delta_{ij} \Delta \right) \Sigma, \qquad \partial_{(i} \Sigma_{j)} \equiv \frac{1}{2} \left(\partial_i \Sigma_j + \partial_j \Sigma_i \right), \tag{1.22}
$$

and we called $\Delta = \partial_k \partial^k$. In the decomposition of the velocity, v is called *velocity gradient*, and it will play an important role later. All these expressions are then plugged in Einstein Eqs. (1.3), yielding the linearized equations

$$
\begin{align}
\left[G^0_0 \right]: \quad & -k^2 \Psi_k - 3\mathcal{H}(\Psi'_k + \mathcal{H}\Phi_k) = 4\pi G a^2 \, \bar{\rho} \, \delta_k, \tag{1.23}\\
\left[G^0_i \right]_\parallel: \quad & -\left(\Psi'_k + \mathcal{H}\Phi_k \right) = 4\pi G a^2 (\bar{\rho} + \bar{P}) \, v_k, \tag{1.24}\\
\left[G^0_i \right]_\perp: \quad & -k^2 \omega_{k,i} = 16\pi G a^2 (\bar{\rho} + \bar{P}) \left[v^T_{k,i} + \omega_{k,i} \right], \tag{1.25}\\
\left[G^i_i \right]: \quad & \Psi''_k + \mathcal{H} \left(\Phi'_k + 2\Psi'_k \right) + (2\mathcal{H}' + \mathcal{H}^2)\Phi_k - \frac{k^2}{3} \left(\Phi_k - \Psi_k \right) = 4\pi G a^2 \delta P_k, \tag{1.26}\\
\left[G^i_{j \neq i} \right]_\parallel: \quad & (\Psi_k - \Phi_k) = 8\pi G a^2 \, \Sigma_k, \tag{1.27}\\
\left[G^i_j \right]_\perp: \quad & -(\partial_\tau + \mathcal{H}) \, k_{(i} \omega_{k,j)} = 8\pi G a^2 k_{(i} \Sigma_{k,j)}, \tag{1.28}\\
\left[G^i_j \right]_{TT}: \quad & (\partial^2_\tau + 2\mathcal{H}\partial_\tau + k^2)\gamma_{ij} = 8\pi G a^2 \Sigma^{TT}_{k,ij}, \tag{1.29}
\end{align}
$$

in Fourier space (see Eq. (1.115) for notation). Note that k^i is a 3D spatial vector and $k^2 \equiv \eta^{ij} k_i k_j$. The isotropy of the FLRW background guarantees that each perturbed quantity is exclusively a function of (τ, k) and, in particular, does not depend on the direction of the wave-vector. This point will become crucial in Chapter 6, and will come back into the discussion. As usual, using Eq. (1.24) into (1.23), one finds the Poisson's equation

$$\Psi_k = -\frac{3H_0^2 \Omega_m^0}{2ak^2} \delta_m^C(a, k), \qquad \delta_m^C(a, k) \equiv \delta_k - 3\mathcal{H}(\bar{\rho} + \bar{P}) v_k \qquad (1.30)$$

where we have defined the gauge-invariant density contrast, $\delta_m^C(a, k)$. Eq. (1.30) clearly shows that Ψ_k is affected by the instantaneous variations of its source (contrary to the retarded time for solutions of wave-like equations). Crucially, some equations among (1.23) - (1.29) are of first or zero order in time derivative. These are called *constraint equations*, and their role is to enforce particular relations between the field variables, such as the one between the scalar gravitational potential and the density contrast in Eq. (1.30).

In the ΛCDM model and in the late time Universe, we neglect the contribution to the stress-energy tensor given by radiation and focus only on baryons, cold dark matter and the cosmological constant. The former two are given in terms of a collisionless, non-relativistic gas of particles, with null adiabatic sound speed so that $\delta P = 0$ and negligible anisotropic stress, $\Sigma_{ij} = 0$. Not clustering, the cosmological constant only affects the background dynamics and does not contribute to the perturbation of stress-energy tensor. In this case, Eq. (1.27) becomes sourceless as the right-hand side vanishes in absence of anisotropic stress, so that

$$\Psi_k(\tau) = \Phi_k(\tau). \qquad (1.31)$$

As far as vector modes go, we note that also Eq. (1.25) is a Poisson equation, like (1.30), and that Eq. (1.28) shows that vector modes are redshifted away by the Hubble expansion unless supported by the anisotropic stress [37]. Hence, relying on the assumption $\Sigma_{ij} = 0$, one can set $\omega_i = v_i^T = 0$. The matter equations (continuity and Euler equations) can be found either via the conservation of the stress-energy tensor $\delta_\epsilon [\nabla_\mu T^\mu{}_\nu = 0]$, or via suitable combinations of the linearized Einstein equations (and their time derivatives) and using also the background Friedmann's Eq. (1.1.1). Overall, in a ΛCDM late time Universe, the geometry of the spacetime and of the energy-momentum density, at first order in ϵ, is governed by the set of equations

$$\delta_k' - k^2 v_k = 3\Phi_k', \qquad (1.32)$$

$$v_k' + \mathcal{H} v_k = -\Phi_k, \qquad (1.33)$$

$$\Phi_k' + \mathcal{H}\Phi_k = -\frac{3H_0^2 \Omega_m^0}{2a} v_k, \qquad (1.34)$$

$$\Phi_k'' + 3\mathcal{H}\Phi_k' + (\mathcal{H}^2 + 2\mathcal{H}')\Phi_k = 0, \qquad (1.35)$$

together with Eqs. (1.30), (1.31) and (1.29). An important consequence of these equations comes from evaluating the last one during matter domination. In this case, we neglect Ω_Λ in Friedmann Eq. (1.7), so that

$$\mathcal{H}^2 + 2\mathcal{H}' = \mathcal{H}^2 + H_0^2 \left(2a^2\mathcal{H}\Omega_m + a^2\Omega_m'\right) = 3\mathcal{H}^2 - 3\mathcal{H}^2 = 0, \tag{1.36}$$

using also Eq. (1.6). Because of this, Eq. (1.35) becomes $\Phi_k'' + 3\mathcal{H}\Phi_k' = 0$, which admits as a solution

$$\Phi_k(\tau) \sim \frac{\mathcal{C}_k}{a^2} + \Phi_k^m, \tag{1.37}$$

meaning that the gravitational potential is supported by one decaying and one constant solution in matter domination. Neglecting the decaying branch, this leads to the important results that $\Phi_k(\tau) = \Phi_k^m$, i.e. the gravitational potential wells are constant and do not grow during matter domination. Since we take δ_m^C, v and Φ to be solutions of Einstein's equation, we can relate them in a more compact form. To this end, we define the *matter transfer function, $T_m(k)$*, describing the behavior of the matter density contrast through the equality between radiation and matter dominated epochs, and the *matter growth factor, $D_m(a)$*, accounting for its late time evolution [5]. We write the field perturbations in terms of these two as

$$\delta_m^C(a, k) = -\frac{9}{10} T_m(k)\mathcal{G}_m(a,k)\Psi_k^{in}, \tag{1.38}$$

$$v(a, k) = -\frac{9}{10} T_m(k)\,\mathcal{G}_v(a,k)\Psi_k^{in}, \tag{1.39}$$

$$\Phi(a, k) = \frac{9}{10} T_m(k)\frac{\mathcal{G}_\Phi(a,k)}{a}\Psi_k^{in}. \tag{1.40}$$

where Ψ_k^{in} is the primordial value of the gravitational potential and

$$\mathcal{G}_\phi = D_m, \qquad \mathcal{G}_m = \frac{2k^2}{3H_0^2\Omega_m^0} D_m, \qquad \mathcal{G}_v = f(a)\frac{\mathcal{H}}{k^2}\mathcal{G}_m. \tag{1.41}$$

In the expression above $f \equiv d\ln D_m/d\ln a$ is the growth rate. Ideally, one uses these forms of the density contrast, velocity gradient and gravitational potential into the linearized Einstein's equations, to find the evolution equation for $T_m(k)$ and $D_m(a)$. These are normally integrated numerically with Einstein-Boltzmann solvers codes, such as CAMB, CLASS (see [41, 42]). This in particular means that the form of $\{\mathcal{G}_\phi, \mathcal{G}_m, \mathcal{G}_v\}$ depends on the gravitational theory. Alternatively, one can use suitable fitting formulas for them [5, 43–45]. Since we are interested in the late time Universe, well after the end of the radiation epoch, the transfer function is nearly constant [5, 43, 44], while the growth factor for modes inside the horizon ($k \gg \mathcal{H}$) can be approximated as [5, 35, 46]

$$D_m(a) = \frac{5H_0^2\Omega_m^0}{2}\frac{\mathcal{H}(a)}{a}\int_0^a \frac{da}{[\mathcal{H}(a)]^3}. \tag{1.42}$$

Note that in our notations we use $\mathcal{H} = (a'/a)(\tau)$ as the Hubble parameter in conformal time, while in [5] they use $H = (\dot{a}/a)(\tau)$, and the dot stands for derivative with respect to the cosmic time $dt = ad\tau$. A more handy fitting formula given in [35, 46] is

$$D_m(a) = \frac{5\Omega_m^0}{2a^2 E^2(a)} \left[\left(\frac{\Omega_m^0}{a^3 E^2(a)} \right)^{4/7} - \frac{\Omega_\Lambda^0}{E^2(a)} + \left(1 + \frac{\Omega_m^0}{2a^3 E^2(a)} \right) \left(1 + \frac{\Omega_\Lambda^0}{70 E^2(a)} \right) \right], \quad (1.43)$$

with $E^2(a) = \mathcal{H}^2/(a^2 H_0^2) = (\Omega_m^0/a^3 + \Omega_\Lambda^0)$. A quantity that will be used later in the text, is the *gravitational potential transfer function*, which is given by

$$\mathcal{T}_k^\Phi(a) = \frac{9}{10} T_m(k) \frac{\mathcal{G}_\Phi(a, k)}{a}, \quad (1.44)$$

as it can be understood from Eq. (1.40).

1.1.3. Statistical description of the large-scale structures

Describing the cosmic web is intrinsically a statistical task: we are interested in describing its average properties, rather than the exact shape and position of each gravitational potential's well or tensor perturbation.[2] Accordingly, we will treat $\delta g_{\mu\nu}(x)$ and $\delta T_\nu^\mu(x)$ as random fields with zero mean, and their observed configurations are a specific realization of the stochastic process, i.e. a particular member of the statistical ensemble. These random fields inhabit the cosmological Universe which, on large-scales, is homogeneous and isotropic, suggesting the idea of promoting these properties to a statistical level for the description of the cosmic inhomogeneities. Hence, given any cosmological perturbation, $\delta A(\tau, \mathbf{x})$, we will assume that it is *statistically homogeneous*, so that its mean and variance are independent of position, and *statistically isotropic*, implying that there is no preferred direction. Assuming also that the fields at large distances are uncorrelated [48], we get that these random fields are *Ergodic*, in the sense that we can exchange

$$\text{ensemble average} \quad \longleftrightarrow \quad \text{volume average}$$

since, in sufficiently far away portions of the Universe, $\delta A(\tau, \mathbf{x})$ and $\delta A(\tau', \mathbf{y})$ should be causally disconnected, making them two independent representative realizations of the stochastic process. In this sense, ensemble expectation values of field dependent observables are well approximated by volume averages, provided that the volume is large enough. A quantity which plays a major role in the description of LSS, is the *two-point autocorrelation function* of the random field

$$\xi^A(\tau, \mathbf{x}; \tau', \mathbf{x}') \equiv \langle \delta A(\tau, \mathbf{x}) \delta A(\tau', \mathbf{x}') \rangle, \quad (1.45)$$

---

[2]This section takes inspiration form [47].

where the average $\langle\ldots\rangle$ is the ensemble average, or the volume one. For a statistically homogeneous and isotropic field, the two-point function must be translation and rotation invariant, therefore

$$\xi^A(\tau,\mathbf{x};\tau',\mathbf{x}') = \xi^A(\tau,\tau',|\mathbf{x}-\mathbf{x}'|). \tag{1.46}$$

Another important quantity is the *power spectrum*, namely the autocorrelation function in Fourier space

$$P^A(\tau,\mathbf{k};\tau',\mathbf{k}') \equiv \big\langle \delta A(\tau,\mathbf{k})\,\delta A(\tau',\mathbf{k}') \big\rangle = \int d^3x\,d^3x'\,\xi_A(\tau,\mathbf{x};\tau',\mathbf{x}')\,e^{-i\mathbf{k}\cdot\mathbf{x}-i\mathbf{k}\cdot\mathbf{x}'}. \tag{1.47}$$

When the real-space 2-point function depends only on $|\mathbf{x}-\mathbf{x}'|$, also the power spectrum takes a simplified form

$$P^A(\tau,\mathbf{k};\tau',\mathbf{k}') = \int d^3x\,d^3x'\,\xi_A(\tau,\tau',|\mathbf{x}-\mathbf{x}'|)\,e^{-i\mathbf{k}\cdot\mathbf{x}-i\mathbf{k}\cdot\mathbf{x}'} =$$
$$= (2\pi)^3\,\delta^3(\mathbf{k}+\mathbf{k}') \int_0^{+\infty} dr\,4\pi\,\frac{\sin(kr)}{kr}\,r^2\,\xi_A(\tau,\tau',r) \tag{1.48}$$

from which we read that, in the case of statistically homogeneous and isotropic random fields the power spectrum is such that

$$P^A(\tau,\mathbf{k};\tau',\mathbf{k}') = (2\pi)^3\,\delta^3(\mathbf{k}+\mathbf{k}')P^A(k,\tau,\tau'). \tag{1.49}$$

In particular, the assumption of homogeneity results into a diagonal power spectrum, so that the different Fourier modes are independent, while isotropy implies that it depends only on the modulus $k=|\mathbf{k}|$, of the wave-vector.

But what is the physical meaning of these quantities? This is best understood looking at the case of *Gaussian Random Fields*: fields whose probability density functional, dictating the stochastic properties, is given by

$$\mathscr{P}\big[\delta A(\tau,\mathbf{k})\big] = \prod_{\mathbf{k}} \frac{1}{\sqrt{2\pi}P(k,\tau)}\,\exp\left[-\frac{|\delta A(\tau,\mathbf{k})|^2}{2P(k,\tau)}\right]. \tag{1.50}$$

Therefore, for a Gaussian random field: each Fourier component is statistically independent of the others and follows a Gaussian distribution with variance given by the power spectrum (at equal time). $\mathscr{P}\big[\delta A(\tau,\mathbf{k})\big]$ can then be understood as the joint probability of having a specific realization for $\delta A(\tau,\mathbf{k})$ at each $\mathbf{k}$. Since the Fourier mode $\delta A(\tau,\mathbf{k})$ is complex, it is easy to understand that Eq. (1.50) actually implies that the *real amplitudes* of each mode are gaussian distributed, while the *phases* are drawn from a uniform distribution. Finally, in the case of Gaussian Random fields, all odd-number correlation functions vanish.

If the random field $\delta A(\tau,\mathbf{x})$ is defined on the sphere, it is convenient to work in harmonic space, rather than Fourier. This is the typical case, for instance, where we observe an incoming GW or photon: we are interested in the direction of arrival, while

its comoving distance and time are related by the geodesic equation. In these cases, it is more convenient to decompose the field on the spherical harmonics basis, rather than the Fourier one, as

$$\delta A(\tau, \chi, \hat{n}) = \sum_{\ell=0}^{+\infty} \sum_{m=-\ell}^{\ell} a_{\ell m}^A(\tau, \chi) Y_{\ell m}(\hat{n}), \tag{1.51}$$

where χ is the comoving distance and $\hat{n} = (\theta, \varphi)$ the coordinates on the unit 2-sphere, such that $\mathbf{x} = \chi \hat{n}$. By using the properties of the spherical harmonics (see Appendix A), we can relate $a_{\ell m}^A$ with the Fourier component of the field as

$$a_{\ell m}^A(\tau, \chi) = 4\pi i^\ell \int \frac{d^3 k}{(2\pi)^3} \, \delta A(\tau, \mathbf{k}) \, j_\ell(k\chi) \, Y_{\ell m}^*(\hat{n}), \tag{1.52}$$

$$\left[a_{\ell m}^A(\tau, \chi) \right]^* = 4\pi (-i)^\ell \int \frac{d^3 k}{(2\pi)^3} \, [\delta A(\tau, \mathbf{k})]^* \, j_\ell(k\chi) \, Y_{\ell m}(\hat{n}) \tag{1.53}$$

where $k = |\mathbf{k}|$ and $j_\ell(k\chi)$ is the spherical Bessel function. With these expressions, we can define the *angular power spectrum*

$$C_{\ell m; \ell' m'}^A(\tau, \chi; \tau', \chi') = \left\langle a_{\ell m}^A(\tau, \chi) \, a_{\ell' m'}^A(\tau', \chi') \right\rangle, \tag{1.54}$$

and relate it to the power spectrum. In the case of statistically homogeneous and isotropic fields, it is easy to compute that

$$C_{\ell m; \ell' m'}^A(\tau, \chi; \tau', \chi') = 4\pi \, \delta_{\ell \ell'} \delta_{mm'} \int_0^{+\infty} \frac{dk}{k} \, j_\ell(k\chi) \, j_\ell(k\chi') \left[\frac{k^3 P(k, \tau, \tau')}{2\pi^2} \right], \tag{1.55}$$

from which we understand that the angular power spectrum, in this case, is given by

$$C_{\ell m; \ell' m'}^A(\tau, \chi; \tau', \chi') = \delta_{\ell \ell'} \delta_{mm'} \, C_\ell^A(\tau, \chi; \tau', \chi'). \tag{1.56}$$

With these definitions, we can understand the advantage of having introduced the transfer functions in Eqs. (1.38) - (1.40): they allow describing three random fields at the price of one. Let's take the example of the gauge invariant density contrast, $\delta_m^C(a, k)$. We promote it to a Gaussian random field, and its two point function in Fourier space will be the *matter power spectrum*, $P_m(k)$. This quantity is the target of multiple observational campaigns, ranging from those targeting redshift-space-distortions and galaxy clustering or weak lensing surveys. Using Eq. (1.38), we can write it as

$$P_m(a, k) = \left[\frac{9}{10} T_m(k) \mathcal{G}_m(a, k) \right]^2 P_{in}^\Psi(k), \tag{1.57}$$

because the transfer functions and growth factor incorporate only deterministic processes, and similarly for $\nu(a, k)$ and $\Phi(a, k)$. This means that we can describe the statistical properties of the three fields characterizing the LSS all in terms of one single power spectrum, $P_{in}^\Psi(k)$. In the expression above, $P_{in}^\Psi(k)$ is the *primordial scalar*
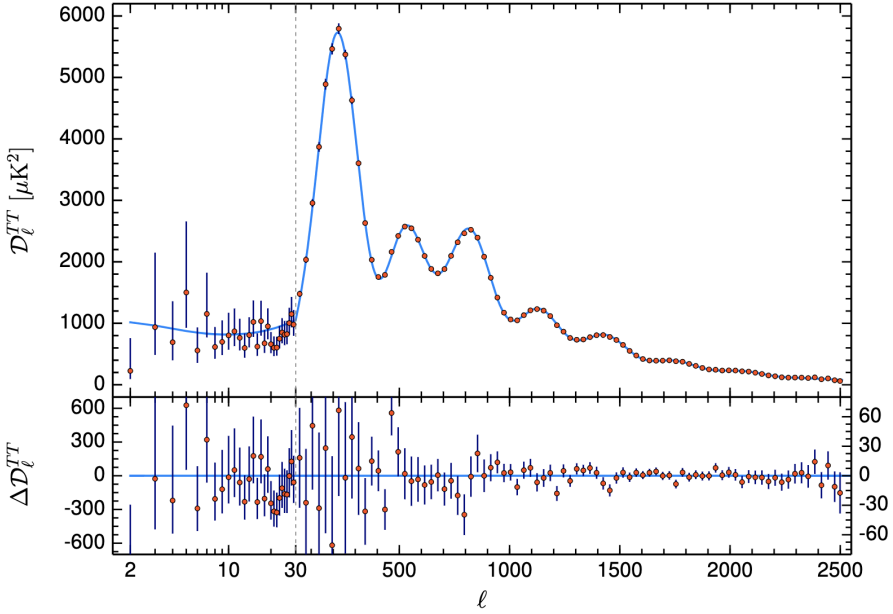
Figure 1.1: The angular power spectrum of the CMB temperature anisotropies, displaying the acoustic peaks of the photon-baryon fluid, from [4]. On the y-axis $\mathcal{D}_\ell = \ell(\ell+1)C_\ell$. The blue line is the prediction of ΛCDM with the best fit values of its parameters, while the red dots corresponds to data. The lower panel shows the residuals with respect to this model. For small ℓ, the plateau corresponds to the integrated Sachs Wolfe effect (ISW), an effect that depends on the integrated time dependence of the gravitational potentials (see e.g. Eq. (1.114)). Since these are constant during matter domination, the ISW switches on during dark energy domination. In this region, though, the error is dominated by the irreducible cosmic variance.

power spectrum: it contains information about the initial conditions of the linear scalar perturbations. In the standard theory, these are set by the *inflaton*, a primordial spin-0 field which guides the Universe through an exponentially accelerated phase of expansion before the particles of the standard model were produced [5, 47]. The simplest inflationary theory predicts an almost scale-invariant primordial power spectrum

$$P_{in}^{\Psi}(k) = A_s \left[\frac{k}{k_*} \right]^{n_s - 1} , \tag{1.58}$$

with k_* a pivot scale, A_s the amplitude of the scalar power spectrum and $n_s = 0.9649 \pm 0.0042$ the spectral index, both measured through observations of the CMB by the Planck satellite at the % precision [3]. So, from the matter power spectrum, by knowing the gravitational theory, we can extract information about the initial stages of the Universe in what would seem a remarkably straightforward way, at least on linear scales. This seemingly simple task is then complicated by the fact that we do not directly observe all the matter, as the majority of this is in the form of dark mat-

ter, which does not emit electromagnetic radiation. This means that we do not have direct access to the full density contrast $\delta_m^C(a, k)$, but only to galaxies which should be located in the peaks of the CDM distribution. To account for this, cosmologist introduce the time-dependent *linear galaxy bias* as

$$\delta_g(z, k) = b(z)\,\delta_m^C(z, k)\,, \tag{1.59}$$

where z is the redshift and δ_g is the galaxy overdensity field, to which we have direct access from a galaxy survey. Therefore, we can measure its power spectrum, and relate it to the one of matter as $P_g(z, k) = [b(z)]^2 P_m(z, k)$ [5, 47]. To further complicate the matter, one has to keep into account the so-called *Redshift Space distortions* (RSD): the peculiar velocity of the galaxy falling into the gravitational potential well adds a contribution to the measured redshift [49]. This contribution introduces a dependence on the cosine of the angle between the line-of-sight and the peculiar velocity, μ, such that

$$P_g(z, k) = \left[\, b(z) + b_v f(z)\mu_k^2 \,\right]^2 P_m(z, k)\,, \tag{1.60}$$

where b_v is the bias between the galaxy and matter velocity distributions and f the growth rate already introduced.
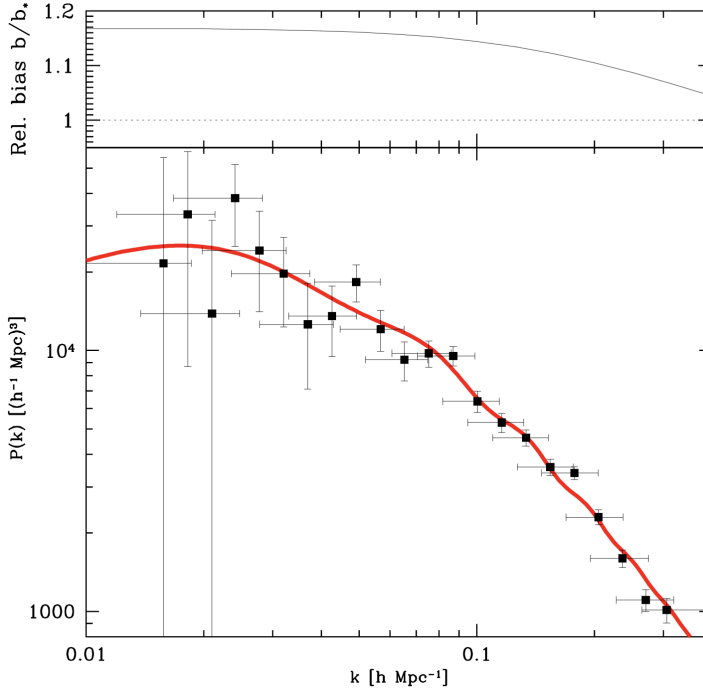
Figure 1.2: The galaxy power spectrum from [50]. The solid curve is the best fit linear ΛCDM model.

All of these considerations can be generalized to the case of more random fields. For instance, with two of them we can consider their correlation matrix

$$\xi^{AB}(\tau,\mathbf{x};\tau',\mathbf{x}') \equiv \left\langle \delta A(\tau,\mathbf{x})\, \delta B(\tau',\mathbf{x}') \right\rangle, \tag{1.61}$$

which allows defining the cross power spectrum $P^{AB}(k)$ through its 3D Fourier transform, or the angular cross correlations $C^{AB}(\ell)$ through its decomposition on the spherical harmonics basis. Once again, we can appreciate the great value of Eqs. (1.38) - (1.40): they clearly show that the different scalar tracers (δ_m^C, v, Φ) actually have the same statistical properties, and hence it is worth considering their correlations. This possibility is very powerful as the measurements of the different fields are, in general, independent, therefore less subject to systematic errors. Additionally, since the growth factors $\{\mathcal{G}_m, \mathcal{G}_v, \mathcal{G}_\Phi\}$ in Eq. (1.41) depend differently on the cosmological model parameters, the mixed estimators ξ^{AB}, can feature a greater constraining power on the cosmological parameters, due to the breaking of degeneracies. As we will show in Section 1.4.3, also GWs and SNe can be used to trace the underlying dark matter distribution, in a way that depends on the background cosmology too. We will use GWs to build estimators to constrain the parameters of scalar-tensor theories in Chapter 2 in combination with SNe, and in Chapter 3 in combination with galaxy and weak lensing surveys.

1.2. Alternative models for the late time Universe

General Relativity is the unique theory for an interacting, massless, spin-2 field in 4 dimensions [51]. It is based on the assumptions of diffeomorphism invariance as symmetry, the metric being the only field entering the gravitational action and that the latter must lead to equations of motion at most of second order. Any alternative to General Relativity, then, will in general introduce new degrees of freedom by abandoning any of these assumptions. This is true even if no new fields are explicitly added to the gravitational action. For example, having higher order equations of motion leads to more propagating degrees of freedom, requiring additional initial conditions. In such cases, one constraint equation of General Relativity could be promoted to a dynamical one [52]. Dropping diffeomorphism invariance also introduces new degrees of freedom as symmetries can be restored by adding new fields with suitable transformation laws under the broken generators, the so-called *"Stuckelberg fields"* [53]. In the simplest scenario, compatibly also with the broken time-translation of the expanding homogeneous and isotropic Universe, is to add one additional degree of freedom. This field can, eventually, drive the late time cosmic acceleration on large scales [52, 54]. For this reason, we address it generically as the "DE field". In order to satisfy some minimal stability requirements, *scalar-tensor theories* must lead to second order equations of motion for the propagating degrees of freedom, one massless tensor and one scalar. Scalar-tensor theories have a long

1

history, and many famous gravitational theories belong to this class. Among them, for instance, we account Quintessence theories [55], Brans-Dicke gravity [56], Covariant Galileon cosmologies [57] and K-essence theories [58]. Covariant Galileons attracted much attention in cosmology because of the existence of a tracking solution which evolves into a de Sitter fixed point [59]. All of these theories belong to the so-called *Horndeski family* [60–62]. Initially considered the most general action of a scalar-tensor theory leading to a stable dynamics, this class of theories was subsequently enlarged in the beyond-Horndeski theories [63, 64], and then DHOST [65–70]. General Relativity, plus Λ, corresponds to the trivial case in which the DE field is constant, hence ΛCDM is always contained in the class of scalar-tensor gravities.

To be able to source the cosmic exponentially accelerated expansion, the DE field must have a mass of the order of magnitude of the Hubble scale, i.e. $\sim 10^{-33}$ eV. As a result, its Compton wavelength is large, and the field mediates a long range interaction. Because of this extra force, the laws of gravity appear modified above this scale [71–73]. Typically, this shows into a modification of the Poisson Eq. (1.30). Cosmological observables can be altered even below the scale of the Compton wavelength, since the DE field can still influence the dynamics of the homogeneous and isotropic Universe [74]. Another characteristic features of all scalar-tensor theories regards their small-scale behavior. If the DE field exists, it must hide itself in high-density region environments, such as the Solar System, where General Relativity has passed all tests performed so far. Thus, viable scalar-tensor theories must be equipped with a dynamical mechanism that make manifest the presence of the DE field only on large-scales (low density), such as the linear scales of cosmological perturbations, and suppresses otherwise. This *screening* can be achieved through non-linear interactions, which become prominent at small scales, with the result of effectively decoupling the DE field from matter (see [51] for a review).

1.2.1. The Horndeski subclass with luminal gravitational waves

The power of scalar-tensor theories, lies in the fact that they are a class. Practically, this means that one can treat many different alternatives at the same time, simply by leaving their coupling functions unspecified, rather than going on a one-to-one basis. Because of this, they are suited to build tests: instead of computing the phenomenology of each specific theory, we will have a continuous parametrized class of them, which we can constrain after gathering the necessary data. For instance, we have already commented that surveys mapping the galaxies' distribution have access to the growth of the linear gravitational potentials, through $P_g(a, k) = [b(a)]^2 P_m(a, k)$, and that how matter inhomogeneities grow depends on the theory of gravity, as it is shown in Eq. (1.57). In a dynamical dark energy scenario describing the late-time cosmic expansion, the initial condition set by P_{in}^{Ψ} will be the same, but the transfer function and the growth factor will be changed, $T_m \rightarrow T_m^{DE}$ and

$\mathcal{G}_m \to \mathcal{G}_m^{DE}$, in a way that depends on the free coupling functions of the scalar-tensor theory. Another example comes from the tensor sector, as the amplitude, the propagation speed and the polarization content of the GWs can, in principle, be modified in a way which depends on the free scalar-tensor couplings.

For simplicity, in this Thesis we restrict our study to Horndeski models in which tensor modes propagate luminally [75–78] at all redshifts, satisfying the bound from GW170817 [79]. Therefore, we consider the action

$$S = \mathcal{S}_G[g_{\mu\nu}, \varphi] + \mathcal{S}_M[g_{\mu\nu}, \chi_i], \tag{1.62}$$

with the gravitational part given by

$$\mathcal{S}_G = \int d^4x \sqrt{-g} \left(\frac{M_P^2[\varphi]}{2} R + G[\varphi, X] \Box \varphi + K[\varphi, X] \right), \tag{1.63}$$

where φ is the DE field, $X \equiv -\partial^\mu \varphi \partial_\mu \varphi / 2$ its kinetic term, and M_P, G, K are free functions encoding possible self-couplings of DE field, and interactions with the space-time metric. We assume that the matter action, $\mathcal{S}_M[g_{\mu\nu}, \chi_i]$, is universally coupled with the *Jordan frame* metric $g_{\mu\nu}$. This means that photons are not directly coupled to the DE field, and they interact with it only indirectly through gravitational interaction. This observation is crucial as it is the starting point for all the *multi - messenger* tests: the difference in the couplings between gravitational and electromagnetic waves to the DE field produced different phenomenologies in these two sectors, even when these two have similar frequencies. Because of the very different typical wavelength, though, it could be that photons and GWs are in different optical regimes and in this case DE effects can be degenerate with wave optics ones [80]. Note that sometimes it is convenient to perform a conformal transformation $g_{\mu\nu} = \Omega^2(\varphi) \tilde{g}_{\mu\nu}$, to remove the non-minimal coupling between the metric and the DE field. In this frame, also known as *Einstein frame*, one fixes $\Omega^2(\varphi)$ such that $M_P^2[\varphi] R[g_{\mu\nu}] \to m_0^2 R[\tilde{g}_{\mu\nu}]$ to remove the minimal coupling, and where $m_0^2 = (8\pi G)^{-1}$ is the Planck's mass. As a result $\mathcal{S}_M[g_{\mu\nu}, \chi_i] \to \mathcal{S}_M[\Omega^2(\varphi) \tilde{g}_{\mu\nu}, \chi_i]$, and the matter action becomes explicitly dependent on the DE field. This kind of description is useful in the context of screening scenarios (see e.g. [51]) and we use it in Chapter 5.

Starting from (1.62), one can derive the gravitational and scalar field equations by varying it with respect to $g_{\mu\nu}$ and φ. Effectively, the former can be recast in the form (1.3) with a particular stress-energy tensor,

$$G_{\mu\nu} = 8\pi G \left[T_{\mu\nu}^{(\text{DE})} \left[g_{\alpha\beta}, \varphi \right] + T_{\mu\nu} \left[g_{\alpha\beta}, \chi_i \right] \right], \tag{1.64}$$

where the explicit form of $T_{\mu\nu}^{(\text{DE})}$ depends on the Horndeski functions: M_P, K, G.

1.2.2. Cosmology in alternative scenarios

Starting from Eq. (1.64), one can work out how cosmology is changed in the chosen extended theory. The presence of the DE field does not affect the cosmological principle, or the fact that the Universe is expanding, nor that matter is in the form of clumped structures on large scales. The effect of its presence is to, possibly, alter the dynamics of the scale factor and of the growth of LSS. Therefore, the approach to tackle the problem is the same as before: we choose the metric as in Eq. (1.12), and solve Eq. (1.64) perturbatively, instead of Eq. (1.3). The result is a set of equations similar to Eq. (1.7) and Eqs. (1.23) - (1.29), but with additional terms originating from $T_{\mu\nu}^{(\mathrm{DE})}$. The system of equations is also supplemented by the DE field equation of motion, both at the level of the homogeneous and isotropic configuration and its linear perturbations. Analogously to the metric and the matter stress-energy tensor, the DE field is decomposed as

$$\varphi(x) = \varphi_0(\tau) + \epsilon\delta\varphi(x), \qquad (1.65)$$

where we have chosen as background $\bar{\phi} = \varphi_0(\tau)$, namely a field configuration compatible with the symmetries of FLRW. Although conceptually simple, the exercise of working out cosmology in these extended theories is rather long and tedious, unless one chooses some specific form for the Horndeski functions M_P, K, G. Instead of choosing a specific model, one can opt for more agnostic explorations [81]. A powerful approach proposed in literature is the so-called Effective Field Theory of Dark Energy (EFT) [82–87]: a unifying framework able to give predictions about the expansion of the Universe and the growth of LSS.

At the center of the EFT approach is the idea that the observed time evolving profile of the expanding Universe is the result of a spontaneous symmetry breaking of time-translation. The Goldstone boson of the symmetry breaking, $\pi(x)$, is identified with the DE field via $\pi(x) = \delta\varphi(x)/\varphi_0'$, since the background expansion assures $\varphi_0' \neq 0$. Using then techniques of the effective approaches in quantum field theory, one can then write the most general action for the linear perturbations around the symmetry-breaking background. The EFT, then, starts by considering the gauge transformation of the perturbation of the DE field

$$\epsilon\delta\varphi' = \epsilon\delta\varphi - \xi^0\,\varphi_0', \qquad (1.66)$$

since φ_0 is exclusively time dependent, and choosing the *unitary gauge* : $\delta\varphi' = 0$. This way, the slices of constant time are identified with the hypersurfaces of uniform scalar field. As a result, one is left exclusively with the metric perturbation to construct the operators entering the second order action dictating the LSS linear dynamics, and they can be organized in power of derivatives. Since LSS are large-scale fluctuations, the most relevant operators dictating their dynamics contain fewer derivatives. The unitary gauge breaks time translation invariance, so that explicit functions of time are allowed in the EFT action. Additionally, the normalized vector orthogonal

to the constant time hypersurfaces, in unitary gauge reads

$$n_\mu \equiv -\frac{\partial_\mu \varphi}{\sqrt{-(\partial \varphi)^2}} \to -\frac{\delta_\mu^0}{\sqrt{-g^{00}}}, \tag{1.67}$$

since $\partial_\mu \varphi = \delta_\mu^0$ if φ is used as time coordinates. This means that, when building the EFT action we can contract tensors with n_μ, terms with 0 free upper indices are allowed, such as g^{00} or R^{00}. For more details on the construction of the EFT action, see [82, 85, 86, 88]. Imposing second-order equations of motion, and additionally a luminal speed of propagation for tensors, the resulting quadratic action reads

$$S = \int d^4 x \sqrt{-g} \left\{ \frac{m_0^2}{2} \left[1 + \Omega(\tau) \right] R + \Lambda(\tau) - c(\tau) a^2 \delta g^{00} + \right.$$
$$\left. + \gamma_1(\tau) \frac{m_0^2 H_0^2}{2} (a^2 \delta g^{00})^2 - \gamma_2(\tau) \frac{m_0^2 H_0}{2} (a^2 \delta g^{00}) \delta K_\mu^\mu \right\} + S_m[g_{\mu\nu}, \chi_i]. \tag{1.68}$$

where $m_0^2 = (8\pi G)^{-1}$ and $\delta g^{00}, \delta K_\mu^\mu$ are, respectively, the reduced Planck mass, the perturbations of the time-time component of the inverse metric, and the trace of the perturbations to the extrinsic curvature of constant-time hypersurfaces. The free functions of time $\Omega(a), \Lambda(a), c(a)$ and $\gamma_1(a), \gamma_2(a)$ are the EFT functions; the first three affect the dynamics both of the background and linear cosmological perturbations, while the latter two affect only perturbations. ΛCDM is included in this framework, and it corresponds to the choice $\Lambda(a) = const$, with the rest of EFT functions being zero. Different EFT functions correspond to different characteristics of the theory: the non-minimal coupling $\Omega(a)$, leads to a running Planck mass; the kineticity $\gamma_1(a)$, quantifies the independent dynamics of the scalar field; the braiding $\gamma_2(a)$, broadly signals a coupling between the metric and the scalar degree of freedom. Notice that we adopt the convention of [89, 90] for the EFT functions. The matter action is assumed to be universally coupled to the Jordan frame metric, as discussed previously.

The spirit of the EFT is to assign parametrization for the time dependency of the EFT functions, without relying on information coming from having chosen a specific model. Nonetheless, if one is interested in one specific realization of a scalar-tensor theories, the gravity model included in the EFT approach can be translated into the EFT language via particular mapping procedures. For reference: non-minimally coupled quintessence, f(R) gravity and Brans-Dicke theories would be characterized by non-trivial background EFT functions, while having $\gamma_1 = \gamma_2 = 0$; k-essence would further have $\gamma_1 \neq 0$ and k-mouflage correspond to all functions being non-zero. Alternative conventions are found in the literature, most commonly the so-called α_i parametrization [91, 92] in terms of $\{\alpha_M, \alpha_K, \alpha_B\}$ (while $\alpha_T = c_T^2 - 1$ is zero for our case) for which there is a simple direct correspondence with $\{\Omega, \gamma_1, \gamma_2\}$ (see e.g. [90, 93]). A typical feature of EFT of DE is that it allows to formulate a set of conditions that the EFT functions need to satisfy among them in order for the resulting

1

theory to be viable and do not develop instabilities [86, 88, 92–95]. These can be quite powerful in restricting the parameter space of the EFT functions for which it makes sense to explore the phenomenology [96, 97] purely on theoretical grounds.

The modified equations of motion that follow from the EFT action are implemented in the code `EFTCAMB` [89, 90]: the extension of `CAMB` to scalar-tensor theories based on the EFT action (1.68). While we use this code to solve such equations numerically, it is still enlightening to understand how DE field modifies the equations of the cosmological model. For a thorough review of the EFT formalism and its applications to cosmological tests of gravity, we refer the reader to [93] and references therein.

Modifications to the expansion history

From Eq. (1.68), it is clear that only $\Omega(a), \Lambda(a), c(a)$ can affect the expansion history of the Universe, as their presence in the EFT action results in a modification of Friedmann's equation (1.7). In order to deal with more familiar quantities, one can opt to work in the *designer* approach [85, 86, 90], and reverse the problem. In this approach, the expansion history is a given, and the two Friedmann equations are used to fix two of three EFT functions, in terms of the third one and $\mathcal{H}(a)$. To fix the expansion $\mathcal{H}(a)$, one can choose the equation of state of the DE field, w_{DE}, since the background metric and DE field equations of motion can be rearranged to obtain

$$\mathcal{H}^2 = a^2 H_0^2 \left(\Omega_m + \Omega_\Lambda + \frac{\rho_{\mathrm{DE}}(a)}{\rho_{crit}} \right), \qquad \rho'_{\mathrm{DE}} + 3\mathcal{H}\rho_{\mathrm{DE}}(1 + w_{\mathrm{DE}}(a)) = 0, \qquad (1.69)$$

and also two constraint equations giving Λ and c in terms of $\mathcal{H}(a)$ and the non-minimal coupling, $\Omega(a)$. Therefore, a model in the designer approach is fully specified by a choice $\Omega(a)$ and $w_{\mathrm{DE}}(a)$. While there is no preferred parametrization for their time dependency, a very common choice for the DE equation of state is the so-called "Chevallier-Polarski-Linder" (CPL) [98, 99] parametrization,

$$w_{\mathrm{DE}}(a) = w_0 + w_a(1 - a), \qquad (1.70)$$

where w_0 and w_a are two constants. Choosing a parametrization has the effect of reducing the problem from constraining a time dependent function, throughout the entire history of the Universe, to constraining just a few constant parameters. Figure 1.3 shows an example of such constraints coming from the Planck mission [4], observing CMB temperature and polarization anisotropies, and the galaxy and weak lensing survey DES [100].

Modifications to the growth of structures

By varying the second order EFT action (1.68) with respect to the metric perturbation, one can find the equations of motion governing the linear growth of the cosmic structures. The results are implemented in the code EFTCAMB, which we use
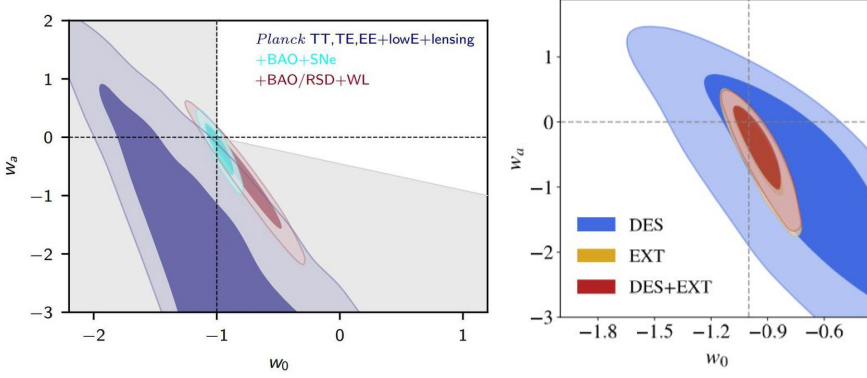
Figure 1.3: Marginalized constraints on $\{w_0, w_a\}$ from CMB observation [4] (left panel) and the galaxy survey DES [100] (right panel) alone or in combination with other probes. ΛCDM corresponds to $w_0 = -1$ and $w_a = 0$.

to compute the modified transfer functions and growth factors when needed. Despite the vast range of possibilities, including the DE field comes with some generic features, which can help in understanding the modified phenomenology of the linear scales. Typically, a dynamical dark energy field sources a scalar anisotropic shear stress, invalidating Eq. (1.31), and modifies the Poisson's Eq. (1.30). Detecting such deviations is the goal of galaxy and weak lensing surveys, such as DES [101, 102] and KiDS [103, 104], already delivering data, or the Stage IV missions: *Euclid* [105], the Vera C. Rubin Observatory [12, 106, 107] and Nancy Grace Roman Space Telescope [108]. All of these instruments are able to map LSS by analyzing properties of some tracers of it: the distribution of galaxies on large scales follows the gravitational potential, and the weak lensing induced distortions of their shapes depend on the foreground matter distribution (weak lensing is a typical propagation effect, as we will also see later). If one is not interested in the specific footprint of each operator in the EFT action (1.68) into the final observable, then it is also possible to opt to parametrize *directly* the gravitational field equations. Focusing only on the scalar sector, we rewrite Eqs. (1.31) and (1.30) as [109–111]

$$\Psi_k = \eta(a, k)\, \Phi_k \tag{1.71}$$

$$\Phi_k = -4\pi G a^2 \mu(a, k)\, \bar{\rho}\, \delta_m^C(a, k), \tag{1.72}$$

$$\Phi_k + \Psi_k = -8\pi G a^2 \Sigma(a, k)\, \bar{\rho}\, \delta_m^C(a, k), \tag{1.73}$$

and it is easy to prove the relation $\eta = 2\Sigma/\mu - 1$. These parametrizations are valid in the absence of shear anisotropic stress, otherwise the left-hand-side of the last two equations must be generalized [4, 109, 110]. The two functions $\eta(a, k)$ and $\Sigma(a, k)$ have specific physical interpretations[3]. The factor $\eta(a, k)$, signifying a difference be-

---

[3]We use notations of [4] and call $\eta(a, k)$ the slip parameters. In other references, such as [110] the slip is also referred to as $\gamma(a, k)$.

1

tween the two gravitational potential, is called *gravitational slip*. μ parametrizes modifications to the Newtonian gravitational potential, while Σ regulates variations of the Weyl potential, $\Psi_W \equiv (\Phi + \Psi)/2$, affecting the geodesic equations of photons. While η is not directly linked to an observable, μ and Σ are, therefore, they can be probed with future observations [112–114]. A modified growth pattern of LSS, also causes changes in the velocities at which galaxies fall inside the gravitational potential wells, opening also *redshift space distortions* as another investigation channel for μ, to be combined with weak lensing surveys probing Σ [115, 116]. While the parametrizations in Eqs. (1.72) and (1.73) are incredibly handy to make contact with observations, their embedding into the theoretically motivated EFT functions is highly non-trivial. This fact is not to be underestimated: when dealing with the EFT functions (or equally the Horndeski functions), it is straightforward to formulate the stability conditions and explore viable theories, while it is not the case for $\mu(a, k), \Sigma(a, k)$. It is possible, to some extent, to translate these theoretical priors onto the phenomenologically motivated $\mu(a, k), \Sigma(a, k)$, and reduce the parameter space to investigate [95, 97, 117]. The parametrizations Eqs. (1.72) and (1.73) are also employed in parameterized approaches to cosmological perturbation theories, such as the Post-Friedmann Framework [52, 118–121].
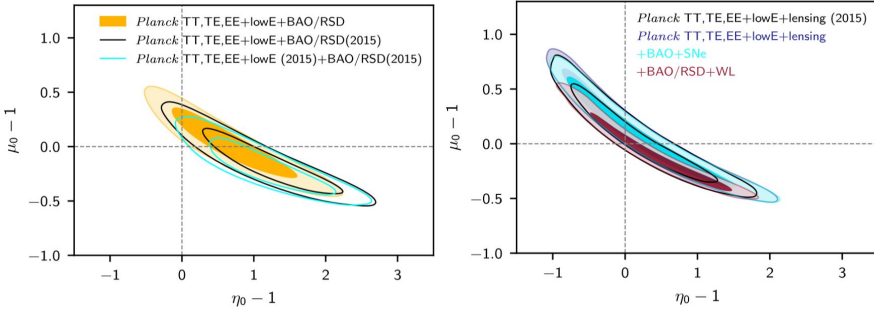
Figure 1.4: Marginalized posterior distributions of the values of μ and η today from [4], from Planck alone or in combination with additional external data, neglecting any scale dependence. The CMB photons are sensitive to modifications of the cosmic structures' growth both through the integrated Sachs Wolfe effect, and the lensing inducing secondary anisotropies.

The dynamics of the tensor perturbations is, in general, affected by the DE field as well. Since we are considering theories where the tensor modes propagate luminally, Eq. (1.29) can only be modified as (see e.g. [122–124])

$$\gamma_{ij}'' + 2\mathcal{H}(1 - \delta(\tau))\gamma_{ij}' + k^2 \gamma_{ij} = 0. \tag{1.74}$$

One can understand this as follows: being the DE field a scalar, it cannot produce a source for the linear order tensor modes. Therefore, the only way it can enter in their equation is through a modification of the time dependent coefficients already present in Eq. (1.29). Since we are requiring a luminal propagation speed, the ratio

between the coefficients with the second derivatives must remain 1 (in our units $c = 1$), so that, effectively, the only term that is allowed to gain extra contribution is the damping one. For theories described by the action (1.68), it can be checked that

$$\delta(\tau) = -\frac{\partial \log M_P[\varphi_0]}{\partial \log a} = -\frac{M_P'[\varphi_0]}{\mathcal{H} M_P[\varphi_0]}, \qquad (1.75)$$

where $M_P'[\varphi_0]$ is the time derivative of the running Planck's mass. This factor is commonly found in literature also under the name α_M [91]. As in the case of the scalar perturbations, one can opt for a phenomenological approach also in the case of GWs, instead of relating $\delta(\tau)$ to a specific theory, similarly to μ and Σ. In this case, deviations from General Relativity are usually parametrized by $\{\Xi_0, n\}$, as we will show in Eq. (1.108).

The fact that the DE field affects both scalars and tensors is a reflection of the assumption of having one, unique underlying theory describing the LSS: the same set of parameters enters the dynamics of all the perturbation modes. For this reason, it is possible to combine the information coming from *scalar sector probes*, such as galaxy clustering and lensing or the CMB angular power spectrum, with those from *tensor sector probes*, and exploit their joint power to pin down the effects of the DE field. GW170817 [125] is an example of such synergy: with one GW detection, the parameter space of the full Hordenski action has been restricted to three free functions, M_P, K, G^4, and the EFT functions to four, $\Omega(a), w_{DE}(a), \gamma_1(a), \gamma_2(a)$ [76, 127, 128]. This is understandable since the equations of the tensor modes and of the gravitational slip both come from the spatial, traceless part of the gravitational field equations [124]. This drastic reduction of the parameter space, naturally, has caveats and loopholes [129, 130]. Other signatures of the DE field which affect both scalar and tensor modes have been investigated, for instance, in [110] and a more general review can be found in [78].

1.3. Gravitational waves

In Section 1.1.2 we have introduced large-scale structures and decomposed them into irreducible representations of the Euclidean spatial rotations. Among them, there was a tensor contribution, γ_{ij}, but we claimed that this is not what we identify as GWs in this Thesis. So what are GWs in our description? We define a GW, $h_{\mu\nu}$, as a linear perturbation, around a background configuration, $\bar{g}_{\mu\nu}$, of the spacetime metric

$$g_{\mu\nu} = \bar{g}_{\mu\nu}(x) + \alpha \, h_{\mu\nu}, \qquad \text{with} \qquad \alpha \ll 1, \qquad (1.76)$$

where α is the expansion parameter used to keep track of the order of magnitude of the GW. Naturally, if one is considering scalar-tensor theories, also the DE field must

---

[4]See [126] for generalization to beyond Horndeski theories.

be expanded as

$$\varphi = \bar{\varphi}(x) + \alpha\delta\phi. \tag{1.77}$$

In analogy with $h_{\mu\nu}$ being called GW, $\delta\phi$ is usually named *scalar wave* (SW)[5]. Note that in Eqs. (1.76) and (1.77), the background configurations are not necessarily homogeneous and isotropic and, as such, they can depend on the four spacetime coordinates, as indicated. If one takes a closer look at these two definitions and Eqs. (1.12) and (1.65) for LSS, it is easy to realize that these are formally the same, and the only difference is the background spacetime: in the case of LSS $\{\bar{g}_{\mu\nu}, \bar{\varphi}(x)\} = \{a^2(\tau)\eta_{\mu\nu}, \varphi_0(\tau)\}$, while these two can assume different forms in the case of GWs and SWs. This consideration, which might be argued a subtlety, has substantial consequences, both at the computational and interpretation level. Therefore, according to our definition, GWs are more similar to the whole LSS, $\delta g_{\mu\nu}$, rather than just its tensor subgroup and the study of their propagation is, in some way, similar to the study of the growth of cosmic structures. Note that we use two different expansion parameters to count the expansion in powers of the GW and the LSS: in the first case we use α, while in the second ϵ. This notation will be kept consistent throughout the entire Thesis, and can always be used as a guideline to understand which quantity is being used.

The linear dynamics of a GW, in the general theory of Eq. (1.64), can be found by considering

$$\delta_\alpha\left[G_{\mu\nu} - 8\pi G\, T^{(DE)}_{\mu\nu}\left[g_{\alpha\beta}, \varphi\right] - 8\pi G T_{\mu\nu}\left[g_{\alpha\beta}, \chi_i\right]\right] = 0\,, \tag{1.78}$$

where δ_α means linearization to first order in α. The case of General Relativity is contained in these equations if one chooses $K = G = 0$ and $M_P(\varphi) = (8\pi G)^{-2}$ as forms of the Horndeski functions. As in the case of LSS, from the general coordinate covariance of the full theory, the linear metric perturbation inherits the gauge freedom

$$\alpha\, h'_{\mu\nu} = \alpha\, h'_{\mu\nu} - \left(\bar{\nabla}_\mu \xi_\nu + \bar{\nabla}_\nu \xi_\mu\right), \tag{1.79}$$

with $\bar{\nabla}_\mu$ the covariant derivatives with respect to $\bar{g}_{\mu\nu}$. So, we are free to choose a gauge for $\alpha\, h_{\mu\nu}$, in the same way as we choose the Poisson's one to describe the cosmic structures in Eq. (1.14). Poisson's gauge was convenient in the case of LSS, because the symmetries of the FLRW background guaranteed the decoupling of the linear scalar, vector and tensor modes, as it can be clearly seen in Eqs. (1.23) - (1.29). In the case of a GW, where $\bar{g}_{\mu\nu}$ is, usually, either treated as unknown, or less symmetric than FLRW, the typical gauge choices performed in the context of LSS are not particularly convenient, and one usually opts for different ones. Nonetheless, one can already start appreciating the difficulty of the problem at hand: in cosmology it is clear which part of $\epsilon g_{\mu\nu}$ propagates ($\epsilon\gamma_{ij}$ in Eq. (1.29)) and which part corresponds

---

[5]Note that we are using the symbol $\alpha\delta\phi$ for the scalar wave and $\epsilon\delta\varphi$ for the DE clustering participating in the LSS.

to the gravitational potential ($\epsilon\Psi$ in Eq. (1.30)). What about $\alpha h_{\mu\nu}$? How can we separate, in the far zone, the static potential from the propagating modes (i.e. those modes which remain even when setting the sources to zero) when the background spacetime is highly non-symmetric? Engineering ways to go tackle this problem is the main focus of Chapter 6. As a general rule, when the background does not display any particular symmetry, it is convenient to go for a covariant gauge choice, such as the de-Donder gauge,

$$\bar{\nabla}^\mu \hat{h}_{\mu\nu} = 0, \tag{1.80}$$

where $\hat{h}_{\mu\nu} = h_{\mu\nu} - h\bar{g}_{\mu\nu}/2$ is the trace-reversed metric perturbation. In this gauge, the first order Einstein tensor reads

$$\delta_\alpha G_{\mu\nu} = -\frac{\alpha}{2}\left[\bar{\Box}\hat{h}_{\mu\nu} + 2\bar{R}_{\lambda\mu\alpha\nu}h^{\lambda\alpha} - h_\nu^\lambda \bar{R}_{\lambda\mu} - h_\mu^\lambda \bar{R}_{\lambda\nu} + h_{\mu\nu}\bar{R} - \bar{g}_{\mu\nu}h^{\alpha\beta}\bar{R}_{\alpha\beta}\right], \tag{1.81}$$

where all the barred quantities are computed with the background metric. Assuming also that the background fields are on-shell, namely satisfying the field equations (1.64), we rewrite equation (1.78) as

$$\bar{\Box}\hat{h}_{\mu\nu} + 2\bar{R}_{\lambda\mu\alpha\nu}h^{\lambda\alpha} - \bar{g}_{\mu\nu}h^{\alpha\beta}\bar{R}_{\alpha\beta} + 8\pi G\left[\delta_\alpha\Theta_{\mu\nu} + \delta_\alpha\Theta_{\mu\nu}^{\mathrm{DE}}\right] = 0, \tag{1.82}$$

where

$$\delta_\alpha\Theta_{\mu\nu} \equiv \frac{1}{2\alpha}\left[\bar{g}_{\mu\sigma}\left(\delta_\alpha T_\nu^\sigma\right) + \bar{g}_{\nu\sigma}\left(\delta_\alpha T_\mu^\sigma\right)\right], \tag{1.83}$$

and $\delta_\alpha\Theta_{\mu\nu}^{\mathrm{DE}}$ the same for $T_{\mu\nu}^{(\mathrm{DE})}$. These equations constitute the starting point for studying the propagation of GWs through the background spacetime, $\bar{g}_{\mu\nu}$.

1.3.1. Sources and wavelengths of GWs

Although it might look like GWs and electromagnetic waves are similar, there are some essential differences between the two. For instance, astronomical electromagnetic signals are usually an incoherent superposition of photons emitted from individual sources, while GWs can also be produced by coherent bulk motions of mass-energy or by nonlinear spacetime curvature features [131]. Moreover, the photon's wavelength is usually much smaller than the dimension of the source, allowing us to make pictures of the source and to treat them in *the ray-optics* limit. For GWs the situation is the opposite, and their frequency spectrum ranges from $\sim 10^3$ Hz downward for roughly 20 orders of magnitude, almost complementary to the range typical of astronomical electromagnetic radiation (from 10^7 Hz upward) [132]. Even the low energy CMB photons have frequencies of the order of 160 GHz. Because of the variety of frequencies that GWs might have, they cannot always be treated in the ray (or geometrical) optics limit, as often it is necessary to opt for a treatment able to include *wave effects*.

Broadly speaking, GWs sources are divided into two main categories: astrophysical or cosmological. Among the first class, we include: continuous sources (rotating

1

pulsars with intrinsic asymmetry from crust deformations), burst events (collapses of stars) and inspirals of compact objects binaries, by far the most famous as they are the sources of the GWs detected by LIGO-Virgo. The frequencies of these events depend on properties of the astrophysical sources, such as the masses of the black holes and neutron stars composing the binaries, and are typically in the high frequency side of the GW spectrum (>mHz). Belonging to the second class, instead, we find waves normally generated in the early Universe, such as the inflationary tensor modes [22–24, 133], or by quadrupolar collapse of large cosmic structures [134]. Various mechanisms can source GWs in the primordial Universe: cosmic strings and phase transitions [135–139], or second order scalar perturbation [140–148] are the most widely investigated. These waves are spread in a broad band of the frequency spectrum and are expected to form a stochastic background.

Regardless of the specifics of their source, we want to stress the vast range of frequencies characterizing GWs, contrary to the typical high ones for photons. This unique feature makes them the perfect test ground to probe some particular assumptions usually made in the context of wave propagation over curved spacetimes, well justified for the highly energetic electromagnetic signals but not necessarily for GWs. These assumptions are necessary in order to solve Maxwell's equations in curved spacetime (see e.g. [149]), or Eq. (1.82) in the case of GWs, otherwise too complicated. According to the frequency, different simplifying approaches are more or less convenient, as we will see.

1.3.2. Definition of a gravitational wave: optical regimes

Assuming that the theory we are working with admits general coordinate invariance, then its linearized version inherits the invariance under infinitesimal gauge transformations, such as in Eq. (1.79) for the metric perturbation. In the context of scalar-tensor theories, one also has the freedom to gauge the DE field according to

$$\alpha\delta\phi' = \alpha\delta\phi - \xi^\mu\partial_\mu\bar{\varphi}(x)\,. \tag{1.84}$$

The background $\bar{\varphi}(x^\mu)$ is generic, and it can depend on all the four spacetime coordinates, in contrast to the LSS expansion and transformation in Eqs. (1.65) and (1.84). Due to this gauge freedom, it can soon be realized that the expansions in Eqs. (1.76) and (1.77) are easier said than done, and the problem of the *definition* of the GW and SW arises right away. Considering that the numerical components of a tensor can be made large or small by means of coordinate transformation, using the smallness of α as a criterion to distinguish the linear perturbation from the background spacetime, is not sufficient [150]. In other words, the splittings in Eqs. (1.76) and (1.77) are unambiguous only if supplemented by an additional coordinate independent criterion to distinguish $\bar{g}_{\mu\nu}$ from $h_{\mu\nu}$, and $\bar{\varphi}$ from $\delta\phi$. There are two main approaches to tackle this problem,

1. linking the additional criterion to properties of the GWs and SWs such as their frequency: when these are much higher than the typical background time variation scale, the splitting in Eqs. (1.76) and (1.77) can be achieved by means of suitable averaging procedures.

2. assigning a priori a background $\{\bar{g}_{\mu\nu}, \bar{\varphi}\}$ and assuming it to be gauge invariant.

Note that the second avenue is the one adopted in standard cosmological perturbation theory for LSS, which suffers from the same problematics. In this case the FLRW background configuration of the metric, $\bar{g}_{\mu\nu} = a^2(\tau)\eta_{\mu\nu}$, and scalar field, $\bar{\varphi} = \varphi_0(\tau)$, are considered fixed and gauge independent.

According to the specific situation, one approach is more suitable than the other. We take the problem of the definition of the GW and SW at the heart of our discussion, and use this initial bifurcation to set up the two different *optical regimes* for GWs and SWs: *ray-optics*, where these two are defined according to the first method, and the *wave-optics* when using the second criterion. This assumption is going to be questioned and revisited throughout this entire dissertation, especially in Chapters 4, 5 and 6.

Ray-optics definition

We can separate clearly what is « wave » from what is background when these two vary on two distinguishable scales. The literature of GWs in *ray-optics*, alternatively called *geometric optics* regime, starts from the pioneering works of Isaacson [151, 152], and then proceeds in many other papers, such as [153–155].
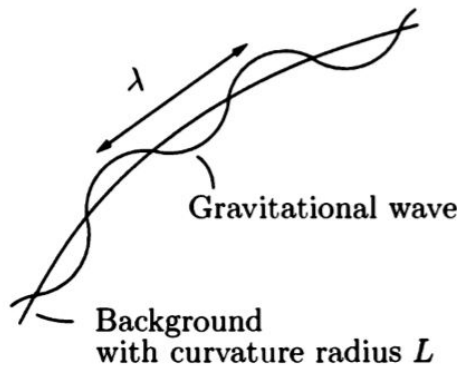
Figure 1.5: GW wavelength λ compared to background curvature radius L. A GW can be distinguished from an unknown background when $\lambda \ll L$.

1

In the geometric optics picture, one starts by introducing the parameter

$$\frac{1}{\omega} \equiv \frac{\lambda}{L} \ll 1\,, \tag{1.85}$$

where λ is the wavelength of the GW and L the typical scale of spatial variation of the background metric (see Figure 1.5). In the case where the background still varies on length scales smaller than the GW frequency, but it is practically static, one can use the different time profiles to separate GW and background, as in

$$\frac{1}{\omega} \equiv \frac{f_B}{f_{gw}} \ll 1\,, \tag{1.86}$$

where $f_{gw} = c/\lambda$ and f_B is the frequency of the background. This is the typical situation in a GW detection through ground-based detectors: the size of their arms are smaller than the wavelength of the GW itself ($\lambda \simeq 500 - 50$ km corresponding to frequencies of $10^2 - 10^3$ Hz for typical waves detected by those interferometers) making the short-wave expansion as in Eq. (1.85) useless. Moreover, the variations of the gravitational field around the Earth due to its in-homogeneities are greater than the amplitude of the wave and occurs on small scales with respect to λ, but it is almost static [150]. Given this separation of scales (spatial or temporal), one can perform the splitting in Eq. (1.76) in a coordinate independent fashion, by defining an average $\langle \dots \rangle$ such that the background metric is the "mean" metric: $\bar{g}_{\mu\nu} \equiv \langle g_{\mu\nu} \rangle$, and $h_{\mu\nu}$ is defined via $\langle h_{\mu\nu} \rangle = 0$. For scalar-tensor theories, the same goes for the SW and the background DE field profile. The description is completed by assigning a prescription on how to perform the averaging, and this is where the high-frequency nature of the GWs (and SWs) comes into play. The most widely used technique, also described in [151, 152], is the *ADM scheme*: we perform a space (or temporal) averages over volumes containing many periods of the GW, so that oscillatory perturbations average out to zero. Additionally, when the condition (1.85) is met, the background spacetime is practically constant in a wavelength and an almost plane-wave ansatz

$$h_{\mu\nu} \quad = \quad \text{Re}\left[\mathcal{A}_{\mu\nu}\, e^{i\,\omega\,\theta} \right]\,, \tag{1.87}$$

$$\delta\phi \quad = \quad \text{Re}\left[\Xi\, e^{i\,\omega\,\vartheta} \right] \tag{1.88}$$

can be chosen. In the expressions above, Re is the real part, $\mathcal{A}_{\mu\nu}$ is the amplitude (tensorial) of the GW and Ξ the one of the SW, θ and ϑ the phases of the waves. Note that the high frequency character is encoded in the $\omega \gg 1$. The amplitudes and the phases are assumed to be varying slowly, so they are almost constant within a period. Alternative names which can be found in literature for the ansatz above are: eikonal, geometric optics ansatz or WKB ansatz. The gradients of the metric perturbations chosen as in Eqs. (1.87) and (1.88) are enhanced by a factor ω, coming from a derivative acting on the exponential: $\partial h_{\mu\nu}$, $\partial \delta\phi \sim 1/\omega \gg 1$.

Given these expressions, one proceeds in plugging them into the differential Eq. (1.82) which, then, can be organized in powers of ω. Being second order, the

equation has the schematic form

$$\omega^2 \left[\dots \right] + \omega \left[\dots \right] + \left[\dots \right] = 0, \tag{1.89}$$

since each derivative acting on the exponential brings down a factor ω. Because $\omega \gg 1$, in order for this equation to be satisfied, the coefficients of each term in the ω expansion must vanish independently. From setting the coefficient of ω^2 equal to zero, one finds the dispersion relation of the GW, while the first order gives an evolution equation for the amplitude of the wave. Additionally, it is usually assumed that the standard matter content does not have high frequency excitations [38]: $\delta_\alpha \Theta_{\mu\nu}[\chi_i] = 0$. This assumption will be widely commented and explored in Chapter 6, where we dubbed it *Classical Matter approximation*. In theories in which the DE field is dynamical, the situation is slightly more complicated (one has to decouple the kinetic terms of the degrees of freedom by performing a diagonalization), but conceptually analogous.

The ray-optics description is well suited to describe GWs in the bands observed by the ground- and space- based interferometers, considering their propagation through the large-scale structures of the Universe. These waves have frequencies $\gtrsim 10^{-3}$Hz, while the typical frequency associated to the linear matter structures lies in the CMB band, $\sim 10^{-16}$ Hz so that $\omega \lesssim 10^{-13}$. Nevertheless, the power of the geometric optics approximation is that it allows to draw general conclusions *regardless* of the spacetime of propagation, as long as Eq. (1.85) remains valid. Let us make an example in General Relativity. We plug the WKB ansatz in Eq. (1.87), into Eq.(1.82) with the choice $M_P = (8\pi G)^{-2}$ and $K = G = 0$, and find

$$\omega^2 \quad : \quad \bar{g}_{\mu\nu} \, k^\mu \, k^\nu = 0, \tag{1.90}$$

$$\omega^1 \quad : \quad \bar{\nabla}_\mu \left(\mathcal{A}^2 \, k^\mu \right) = 0, \tag{1.91}$$

where $\mathcal{A}^2 \equiv \mathcal{A}_{\mu\nu} \mathcal{A}^{\mu\nu}$ and

$$k_\mu \equiv \partial_\mu \theta, \tag{1.92}$$

is the GW wave vector, or equally defined in terms of the covariant derivative. These equations allow the effective interpretation of a GW as a collection of particles, the *gravitons*, propagating with a wave vector k^μ, which according to Eq. (1.90) is a null vector, and the wave's amplitude satisfies the continuity Eq. (1.91). The wave vector k^μ identifies the *rays* via $k^\mu = dx^\mu/d\lambda$, with λ the affine parameter, which are geodesics of the background spacetime, since

$$k^\mu \bar{\nabla}_\mu k_\nu = k^\mu \bar{\nabla}_\mu (\partial_\nu \theta) = k^\mu \bar{\nabla}_\nu (\bar{\nabla}_\mu \theta) = \frac{1}{2} \bar{\nabla}_\nu (k^\mu k_\mu) = 0. \tag{1.93}$$

Note that Eqs. (1.90) and (1.91) are valid regardless of the form of $\bar{g}_{\mu\nu}$, as previously claimed. In this picture, the physical nature of the GW clearly arises (as opposed to

1

gauge modes), with the possibility of defining a GW stress-energy tensor [152], ac-
counting for the energy and momentum transport by the waves (more details can
be found in Chapter 4). One can also understand this by making the following con-
sideration: within a wavelength λ, space appears locally flat, and so the Riemann
tensor describing curvature is gauge invariant. As long as $1/\omega \ll 1$, GWs do not have
long wavelengths modes and the gauge invariant local behavior carries over the en-
tire spacetime. Not only, because of the particle interpretation, one can adopt the
techniques typical of photons, to treat GWs as well. Two relevant examples are: the
Cosmic Rulers formalism [156–158], to describe projection effects induced by cosmic
structures on the propagating GWs, and the Boltzmann equation [159], to describe
the stochastic gravitational wave background (SGWB) similarly to the CMB.

Finally, the parameter ω is sometimes used to set up an expansion of the high-
frequency perturbations' amplitudes. These additional terms are called the *beyond
geometric optics corrections*, and they take the form

$$h_{\mu\nu} \quad = \quad \text{Re}\left[\left(\mathcal{A}_{\mu\nu} + \omega^{-1}\mathcal{A}^1_{\mu\nu} + \omega^{-2}\mathcal{A}^2_{\mu\nu} + \cdots\right)e^{i\omega\theta}\right], \qquad (1.94)$$

$$\delta\phi \quad = \quad \text{Re}\left[\left(\Xi + \omega^{-1}\Xi^1 + \omega^{-2}\Xi^2 + \cdots\right)e^{i\omega\vartheta}\right]. \qquad (1.95)$$

The beyond geometric optics order can contain valuable information and their role
in lensing of GWs, in General Relativity, has been intensively investigated, e.g. in [154,
155, 160, 161].

Wave-optics definition

Whenever Eq. (1.85) is not satisfied, the eikonal approximation cannot be cho-
sen. This is the case, for instance, of stochastic backgrounds of gravitational waves
(SGWB): it contains arbitrarily low frequencies, so it is preferable to have a descrip-
tion for it valid across its entire spectrum. In this case, we are forced to use the
second approach to define waves: one must specify a fixed background fields con-
figuration, and the field perturbations are simply defined as $\alpha h_{\mu\nu} = g_{\mu\nu} - \bar{g}_{\mu\nu}$ or
$\alpha\delta\phi = \varphi - \bar{\varphi}$, in every gauge. We will use this approach in Chapter 6, to describe the
SGWB without employing techniques which rely on the eikonal ansatz, typical of the
ray-optics limit. This way, our formalism will be valid in every frequency range and
can accommodate wave optics effects: interference and diffraction of the waves in-
duced by masses situated along the path of the GW. These types of problems have
been addressed for the first time in [162], and proceeded with many subsequent
works [149, 163–166], showing that these become important when the mass of the
lens is such that

$$M_L \lesssim 10^5 M_\odot \left(\frac{f}{Hz}\right)^{-1}, \qquad (1.96)$$

where f is the frequency of the GW. Such papers were then generalized to the case
of multi-lens systems [167], or lenses composed of binary objects [168] and expand-

ing backgrounds [169], and they are all in General Relativity. Wave-optics phenomena are expected to occur, for instance, in micro-lensing events due to substructures [170, 171] for GWs in the LIGO-Virgo frequency band [16]. Interestingly, it was proposed to use such events to discover unknown objects, such as intermediate mass black holes [172], more exotic forms of compact dark matter [173], or low-mass dark matter halos [174] and primordial black holes [175]. In the case of resolved GW events observed by LISA, it has been assessed that over $(0.1 - 1.6)\%$ of massive black hole binaries in the range of $10^5 - 10^{6.5}$ solar masses will display wave-optics effects [176, 177], while, in the frequency band of the ground-based detectors, it is expected that such events will be visible for sources up to redshift $z_s = 2 - 4$ with third generation observatories [178]. The condition in Eq. (1.96) can also be rewritten in terms of λ, the GW wavelength, and L, the background variation scale, as $\lambda \gtrsim L$: it is the opposite regime compared to the one of Eq. (1.85). Not surprisingly, wave-optics effects become important away from the regime where the effective description of a wave in terms of a stream of particles holds.

When choosing the wave-optics definition for the GW, there is no simplifying ansatz for the waves and one has to attempt solving Eq. (1.82) with the chosen background configuration (changing gauge for the GW if needed). Recalling that this approach is also the one used in the context of LSS, whenever we take $\{\bar{g}_{\mu\nu}, \bar{\varphi}\}$ to be compatible with FLRW and its symmetries, then studying the propagation of GWs and SWs is formally equivalent to doing cosmological perturbation theory, and the only difference is the name of the actors: α plays the role of ϵ, $\alpha h_{\mu\nu}$ the one of $\epsilon \delta g_{\mu\nu}$ and $\alpha \delta \phi$ the one of $\epsilon \delta \varphi$. Any other situation, must be evaluated case by case. For instance, in the literature of wave-optics effects in gravitational lensing [179], addressed in General Relativity ($\delta_\alpha \Theta^{DE}_{\mu\nu} = 0$), the chosen background is the one describing a static, Newtonian source,

$$d\bar{s}^2 = -\Big(1 + 2\epsilon U(\boldsymbol{x})\Big) d\bar{t}^2 + \Big(1 - 2\epsilon U(\boldsymbol{x})\Big) d\boldsymbol{x}^2, \qquad (1.97)$$

where U represent the gravitational potential well of the lens. In this case, Eq. (1.82) reduces simply to $\bar{\Box} \hat{h}_{\mu\nu} = 0$, outside the lens[6]. Then, usually one proceeds by neglecting polarization effects on the GW [179]. To this end, the GW is decomposed as $h_{\mu\nu} = h e_{\mu\nu}$, where h is the amplitude and $e_{\mu\nu}$ the polarization tensor which is considered constant. This way, the wave equation is transformed into an equation only for the amplitude: $\partial_\mu(\sqrt{-\bar{g}} \bar{g}^{\mu\nu} \partial_\nu h)$, where $\bar{g}_{\mu\nu}$ is given by Eq. (1.97). Expanding it to first order in U one finds [179]

$$\Big(\Delta + \omega^2\Big) h(\omega, \boldsymbol{x}) = 4\omega^2 \epsilon U(\boldsymbol{x}) h(\omega, \boldsymbol{x}), \qquad (1.98)$$

where $h(t, \boldsymbol{x}) = e^{-i\omega t} h(\omega, \boldsymbol{x})$ and Δ is the Laplacian operator in spherical coordinates (r, θ, φ) with $r \equiv \sqrt{x^2 + y^2 + z^2}$. Without the lens ($U = 0$), the amplitude of the wave would fall inversely proportional to the distance as $h^{NL} = A e^{i\omega r}/r$. At this

---

[6]The authors also neglect the contribution proportional to the Riemann tensor by assumption.

1

point, there are two main strategies to solve Eq. (1.98): the first involving the so-called *Diffraction Integral* (see e.g. [179]) while the second using the *Green's function method* (see e.g. [165]). We review only the second one because we will use a similar method in Chapter 6. In the Green's function method, one sets up a solution of Eq. (1.98) by considering that the effect of the gravitational potential must be small, since ϵ is a small parameter. Therefore, the full solution must be similar to the unlensed ($U = 0$) wave

$$h(\omega, \boldsymbol{x}) = h^{(0)}(\omega, \boldsymbol{x}) + \epsilon h^{(1)}(\omega, \boldsymbol{x}). \qquad (1.99)$$

Then, one plugs this expansion into Eq. (1.98) and matches order by order in ϵ. This way $h^{(0)}$ is a solution of Eq. (1.98) with $U = 0$ and $h^{(1)}$ satisfies

$$\left(\Delta + \omega^2\right) h^{(1)}(\omega, \boldsymbol{x}) = 4\omega^2 \, U(\boldsymbol{x}) \, h^{(0)}(\omega, \boldsymbol{x}). \qquad (1.100)$$

As in [165], we solve this equation Using the Green's function of the Helmholtz equation, $e^{i\omega|\mathbf{x}-\mathbf{x}'|}/|\mathbf{x}-\mathbf{x}'|$, and obtain

$$h^{(1)}(\omega, \boldsymbol{x}) = -\frac{\omega^2}{\pi} \int d^3 x' \, \frac{e^{i\omega|\mathbf{x}-\mathbf{x}'|}}{|\mathbf{x}-\mathbf{x}'|} \, U(\boldsymbol{x}') \, h^{(0)}(\omega, \boldsymbol{x}'). \qquad (1.101)$$

The solution of $h^{(1)}$ encodes the diffraction and interference pattern typical of the wave-optics regime, which are frequency dependent. Moreover, since the frequency of a GW produced during the inspiral of a compact object binary increases while going toward the merger, monitoring in time a lensed GW event will allow observing the change in the diffraction pattern. This frequency dependecy of the observed lens pattern can be used to break degeneracies between the lens parameters and infer properties of the lens objects with an increased level of detail and precision [180, 181]. For instance, the so-called *mass-sheet* degeneracy can be lifted [149].

1.4. GWs in ray-optics limit: relativistic effects

We have seen that the ray-optics definition of a GW allows for a treatment which is independent of the background spacetime metric. This is clearly visible in Eqs. (1.90) and (1.91), which are valid for any $\bar{g}_{\mu\nu}$, as long as $\omega^{-1} \ll 1$. In this Section, we merge all the knowledge gained from the three previous ones. First, we generalize Eqs. (1.90) and (1.91) in the case of the Horndeski theory (1.62), promoting again φ to a dynamical variable. Then we choose as background field configuration $\{\bar{g}_{\mu\nu}, \bar{\varphi}\}$ the cosmological perturbed solution, namely Eq. (1.14) for the metric and Eq. (1.65) for the DE field. This means that we will have a double parameter expansion: α keeping track of the GW and SW, as in Eqs. (1.76) and (1.77), and ϵ for the LSS included in the background field profiles. We will show that GWs propagating on such spacetimes are damped (their amplitude is inversely proportional to the luminosity distance) and that LSS source the so-called *Relativistic effects*, modulating the amplitude of the signals.

1.4.1. Ray-optics with a DE field

When considering the Horndeski action (1.62), the linearized gravitational field equations become (1.82), with $\delta_\alpha \Theta^{\text{DE}}_{\mu\nu} \neq 0$. If one plugs the geometric optics ansatz into the equation of motion, then Eqs. (1.90) and (1.91) result modified. Since the action (1.62) is tailored to have GWs propagating at the speed of light, then the dispersion relation remains unchanged, and the wave vector k^μ, defined as the gradient of the phase of the WKB ansatz in Eq. (1.92), satisfies

$$\bar{g}_{\mu\nu} k^\mu k^\nu = 0. \tag{1.102}$$

In these extended gravitational theories, GWs are still described in terms of gravitons propagating along null geodesics of $\bar{g}_{\mu\nu}$. It has been shown in [158, 182][7], that the amplitude of the tensor modes of the GW, $\mathcal{A}^T$, satisfies

$$\bar{\nabla}_\rho \left[k^\rho (\mathcal{A}^T)^2 \ln M_P^2[\bar{\varphi}(x)] \right] = 0, \tag{1.103}$$

in the Horndeski theory (1.62) and with $\bar{\varphi}$ the generic, background DE field configuration. Eq. (1.91) follows simply by choosing $M_P[\bar{\varphi}] = (8\pi G)^{-2}$. The result of having promoted the cosmological constant to a dynamical scalar field described by the action (1.62), is encoded in a modification to the GW tensor modes amplitude's conservation equation. This is clear from the extra factor $\ln M_P^2[\bar{\varphi}(x)]$ in Eq. (1.103).

1.4.2. Standard sirens: the GW luminosity distance

The cosmological background is an expanding spacetime. Because of this, propagating waves are damped. This is the so-called *Hubble friction*, encoded in the factor $\mathcal{H}$ of Eq. (1.29) or the modified one $\mathcal{H}(1-\delta(\tau))$ in Eq. (1.74). Naturally, these considerations are contained also in Eq. (1.103). Indeed, it is easy to check that, if one chooses $\{\bar{g}_{\mu\nu}, \bar{\varphi}\} = \{a^2(\tau)\eta_{\mu\nu}, \varphi_0(\tau)\}$, then Eq. (1.103) is compatible with Eq. (1.74).

In case of a homogeneous and isotropic background, the amplitude evolution Eq. (1.103) can be integrated [158] to give

$$\mathcal{A}^T(z) = \frac{\mathcal{Q}^T (1+z)^2}{\bar{d}_L^{\text{GW}}(z)} \tag{1.104}$$

where $\mathcal{Q}^T$ is an integration constant that depends on the properties of the source, z is the redshift, related to the scale factor as $1+z = a^{-1}$. In the solution above, we have introduced the *gravitational wave's luminosity distance*, $\bar{d}_L^{\text{GW}}(z)$, defined as

$$\bar{d}_L^{\text{GW}}(z) \equiv \frac{M_P(z)}{M_P(0)} \bar{d}_L^{\text{EM}}(z), \tag{1.105}$$

[7]The procedure is actually slightly different, and we do not report it here. In particular, it requires decomposing the GW on a polarization basis, and focusing only on its tensor modes (in our definition, the GW $\alpha h_{\mu\nu}$ is more similar to the LSS, $\epsilon \delta g_{\mu\nu}$, rather than only its tensor modes $\epsilon \gamma_{ij}$). In the equation, $\mathcal{A}^T$ is the amplitude of the tensorial part of $\alpha h_{\mu\nu}$.

1

where the *electromagnetic luminosity distance* is

$$\bar{d}_L^{\text{EM}}(z) = (1+z)\bar{\chi}(z) = \frac{(1+z)}{H_0} \int_0^z \frac{dz'}{E(z')}, \tag{1.106}$$

with $\bar{\chi}(z)$ the comoving distance and $E(z) \equiv \mathcal{H}(z)/(a^2 H_0) = \Omega_m + \Omega_\Lambda + \rho_{\text{DE}}(a)/\rho_{crit}$ as in Friedmann's equation (1.69). Eq. (1.104) is a fundamental result in the literature of GWs in scalar-tensor theories. From it, together with Eq. (1.105), we see that the effect of the modification to the Hubble friction in the GW's tensor modes equation, is to produce a difference between the luminosity distances as inferred from electromagnetic signals and those from the amplitude of GWs. Since photons are contained in the universally coupled matter action, $\mathcal{S}_M[g, \chi]$, they are not directly affected by the DE field, and the Hubble drag they feel is not modified. The presence of a dynamical DE field, in this case, enters only implicitly the expansion rate $E(z)$. This different behavior between the GW and EM sector is a golden resource for testing scalar-tensor theories aimed at describing the late-time accelerated expansion. It allows to directly investigate the non-minimal coupling between the DE field and the curvature, also known as running Planck's mass, $M_P(\varphi)$ (see e.g. [183–192]). Eq. (1.105) is also renowned in literature with different notations, especially in terms of $\delta(\tau) = -\partial \ln M_P/\partial \ln a$, or $\alpha_M = -\delta(\tau)$. In this case

$$\frac{M_P(z)}{M_P(0)} = \exp\left[\int_0^z dz' \frac{\delta(z')}{1+z'}\right]. \tag{1.107}$$

This expression has two clear behaviors: when $z \to 0$, the integral becomes trivial and no modification of the luminosity distance occur. On the other hand, when $z \gg 1$ then, we enter matter domination, and we expect $\delta(z) \to 0$ since the DE field becomes very subdominant, and the results of General Relativity should be recovered. In this case, the ratio $M_P(z)/M_P(0)$ reaches a constant. Another very common parametrization for Eq. (1.105), more similar in spirit to the phenomenological approach, can be found in [122, 183, 184] and sees the introduction of the two parameters Ξ_0 and n as

$$\frac{\bar{d}_L^{\text{GW}}(z)}{\bar{d}_L^{\text{EM}}(z)} = \Xi_0 + \frac{1 - \Xi_0}{(1+z)^n}. \tag{1.108}$$

Such parametrization reproduces the two expected behaviors: when $z \to 0$ the ratio goes to 1 and when $z \gg 1$, the second term can be neglected and the same ratio approaches the constant value Ξ_0. Up to now, we do not have tight constraints on the value of Ξ_0 [193–195] and large deviations are still allowed by the data, possibly making its effect dominant over the one due to a modified expansion history [183, 184]. Interestingly, it has been proposed to use strongly lensed GW observations to put constraints on Ξ_0, confirming that we will be able to put constraints at the percent level with ~ 4600 events [196].

Before moving on to the relativistic corrections, we wish to stress one last point. The results of this Section are of utmost importance even when the prefactor

$M_P(z)/M_P(0) = 1$. Eq. (1.104) leads in any case to the important observational fact that a GW detection provides a direct measurement of the luminosity distance of their source. These events are, thus, standard distance indicator, dubbed *Standard Sirens* [197], similarly to SNe, also known as *Standard Candles*. Because of this, one can perform, with GW observations, the same distance-redshift tests which allowed the discovery of the late time accelerated expansion with SNe observations [195, 198, 199]. In this type of tests, one uses the knowledge of both the luminosity distance and redshift to pin down the only unknown left in Eq. (1.106): $H_0 E(z)$. Thus, in this way we constrain the expansion history and the Hubble parameter today, H_0 [200–202], the latter being one of the two parameters of the standard cosmological model under the spotlight. Indeed, there is a discrepancy of about $\sim 5\sigma$ between the measurements of H_0 inferred from the CMB anisotropies power spectrum (assuming ΛCDM) and the one from SNe (see [15] for a review and references therein). Standard sirens, thus, provide a third and independent way, affected by entirely different systematics, to constrain such parameter and could prove to be crucial into breaking the tie between the various determinations of H_0 [203]. Unfortunately, standard sirens come with a catch: GW observations carry information exclusively about the luminosity distance, and the redshift determination has to be obtained either through a direct detection of an electromagnetic counterpart [197, 198, 204], as it was for GW170817 [205], or via the individualization of the host galaxy of the source or through statistical methods [188, 206–210].

1.4.3. Relativistic corrections

After having described the solution of Eq. (1.103) on FLRW Universe, we can include the effect of LSS. We further simplify the situation, considering the so-called *restricted Poisson's gauge*, a subcase of Eq. (1.14) where $\epsilon\, w_i = \epsilon\, \gamma_{ij} = 0$. This choice is suitable in the late time Universe if there are no free tensor modes [39] and it is compatible with having a scalar dynamical DE field: being a scalar, it cannot source vector and tensor modes at linear order. With this assumption, the background field's configurations are

$$d\bar{s}^2 \;=\; a^2(\tau)\Big[-(1+2\epsilon\Phi)d\tau^2+(1-2\epsilon\Psi)d\mathbf{x}^2\Big], \tag{1.109}$$
$$\bar{\varphi}(x) \;=\; \varphi_0(\tau)+\epsilon\,\delta\varphi(x), \tag{1.110}$$

where Φ, Ψ are the two gravitational potentials in Poisson's gauge and $\delta\varphi$ is the DE field fluctuation.

Before getting into the details of the computation, let us sketch what we expect to find. On the homogeneous and isotropic background, the luminosity distances depend only on redshift, leading to the standard distance-redshift relation. Because the LSS break the rotational symmetry in the 3D spatial slices, we expect inhomogeneities in the Universe to induce a dependence also on the direction of observa-
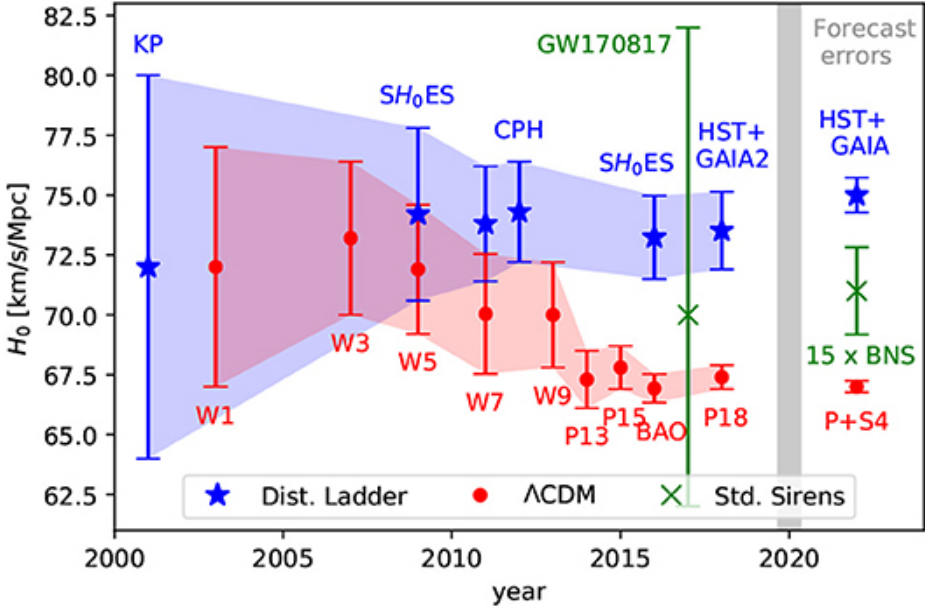
Figure 1.6: From [211]. Determinations of the Hubble constant H_0 from local Universe measurements (blue), and from CMB assuming ΛCDM (red). The green line corresponds to its measurement from the bright event GW170817 [205].

tion

$$d_L(\hat{\theta}, z) = \bar{d}_L(z) + \epsilon \, \Delta d_L(\hat{n}, z). \tag{1.111}$$

The average luminosity distance, $\bar{d}_L(z)$, in the equation above, theoretically corresponds to Eq. (1.106) for photons and Eq (1.105) for GWs, since $\epsilon \delta g_{\mu\nu}$ has zero mean. Fluctuations in the electromagnetic luminosity distance Δd_L, which we introduced in Eq. (1.114), constitute an important probe for linear cosmology and have been well studied [212–216], while the case of GWs has been addressed in General Relativity in [217–223]. Relativistic effects, thus, can be used to probe the linear structures of the Universe. If one is not interested in them, and only wish to use standard distance-redshift tests, they must still be accounted for as they introduce irreducible errors in the determinations of the parameters [224–226]. Including relativistic effects can also have impact in the searches for the electromagnetic counterparts [218].

Mathematically, the problem at hand requires plugging Eqs. (1.109) and (1.110) into Eq. (1.103) and solve for $\mathcal{A}^T$. Naturally, this turns out to be very complicated and one resorts to perturbative schemes to solve the equations. Such methods were first developed in the context of photon propagations, and in particular go under the name of *Cosmic Rulers* [156, 227, 228] or also *line-of-sight approaches* [216, 229, 230]. Indeed, starting from Maxwell's equations, an evolution law identical to (1.91) can be found also for the amplitude of an electromagnetic signal [149, 212]. These

types of computations were then generalized to the case of GWs in geometric optics in [157, 217] in General Relativity, and in [158] in the Horndeski theories of the form (1.62). This is the principal reason why we restrict our studies to scalar-tensor theories with luminal GWs: the form of the relativistic effects is not known otherwise. The Cosmic Rulers formalism also accounts for the projections effects induced by the fact that we observe in the *observer-frame*, different from the *real-frame* because, when observing, we use coordinates that flatten the past light-cone of the GW. Regardless of the method, the general philosophy is to expand (1.103) up to first order in LSS (ϵ) and define $\mathcal{A}^T = \bar{\mathcal{A}}^T(1 + \epsilon \Delta \ln \mathcal{A}^T)$, where $\bar{\mathcal{A}}^T$ satisfies the equations at order ϵ^0, while $\Delta \ln \mathcal{A}^T$ those at order ϵ^1 (or equivalently in terms of the luminosity distance knowing that $\mathcal{A}^T \propto (d_L^{\text{GW}})^{-1}$). The logic is very similar to what we have done to find the wave-optics solution in Eq. (1.101), but starting from (1.103) and using Eqs. (1.109) and (1.110) instead of a background representing a static Newtonian lens.

In [158], it can be found that the relativistic effects on GW's amplitude, induced by propagation effects through the cosmic web, in the theory (1.62), are

$$
\frac{\Delta d_L^{\text{GW}}(\hat{n}, z)}{\bar{d}_L^{\text{GW}}(z)} = - \kappa - (\Phi + \Psi) + \frac{1}{\chi} \int_0^\chi d\tilde{\chi} \, (\Phi + \Psi) + \Phi \left(\frac{1}{\mathcal{H}\chi} - \frac{M_P'[\varphi_0]}{\mathcal{H} M_P[\varphi_0]} \right)
$$
$$
+ \left(1 - \frac{1}{\mathcal{H}\chi} + \frac{M_P'[\varphi_0]}{\mathcal{H} M_P[\varphi_0]} \right) \left[v_\parallel - \int_0^\chi d\tilde{\chi} \, (\Phi' + \Psi') \right] + \frac{M_{P,\varphi}[\varphi_0]}{M_P[\varphi_0]} \delta\varphi,
$$
$$
(1.112)
$$

where a prime indicates differentiation w.r.t. conformal time, κ denotes the weak lensing convergence, χ the comoving distance to the source, Φ the Newtonian potential, Ψ the intrinsic spatial curvature potential, $v_\parallel$ the component along the line of sight of the peculiar velocity of the source, and $M_{P,\varphi}$ is the derivative with respect to the scalar field: all in the restricted Poisson gauge and following the conventions of [158]. The physical effects contributing to Δd_L^{GW}, in order, are: weak lensing convergence, volume dilation and a Shapiro time delay, that are only indirectly influenced by the DE field; Sachs-Wolfe (SW), Doppler shifts, and Integrated Sachs-Wolfe (ISW), showing an additional explicit decay that depends on the time evolution of $M_P[\varphi_0(\tau)]$; damping due to DE field inhomogeneities, $\epsilon \delta\varphi(x)$. The weak lensing convergence field, namely κ in Eq. (1.112), is given by

$$
\kappa(\hat{n}) = -\frac{1}{2} \nabla_\theta^2 \Phi_L(\hat{n}) = - \int_0^\chi \frac{d\chi'}{\chi'} \int_{\chi'}^\infty d\chi_* \left(\frac{\chi_* - \chi'}{\chi_*} \right) \nabla_\theta^2 \Psi_W(\chi' \hat{n}, z') \qquad (1.113)
$$

where Ψ_W is the Weyl potential and ∇_θ^2 indicates the 2D Laplacian with respect to the angle between the image and optical axis [149, 231]. Note that we are neglecting the shear deformations of the signal since these are subdominant in linear perturbation theory where WL mainly affects the magnification of the GWs.

1

In presence of the DE field, the GW luminosity distance generally differs from the one traced by electromagnetic signals. This is clear at the unperturbed level from Eq. (1.105). Not surprisingly, this is also true for their large-scale fluctuations as GWs follows Eq. (1.103), where the Horndeski function M_P is explicitly present, while photons are not directly affected by the DE field. As already mentioned, it is possible to find a WKB solution for Maxwell's equation, and this would look like Eq. (1.91) also in the presence of a dynamical DE field. Therefore, the luminosity distance fluctuations as inferred from an EM detection, in the Horndeski theory (1.62), are given by

$$\frac{\Delta d_L^{\text{EM}}(\hat{n}, z)}{\bar{d}_L^{\text{EM}}(z)} = -\kappa - (\Phi + \Psi) + \frac{1}{\chi}\int_0^\chi d\tilde{\chi}\,(\Phi + \Psi) + \frac{\Phi}{\mathcal{H}\chi} + \left(1 - \frac{1}{\mathcal{H}\chi}\right)\left[v_\parallel - \int_0^\chi d\tilde{\chi}\,(\Phi' + \Psi')\right],$$
$$(1.114)$$

as it can be derived also by taking Eq. (1.112) and discarding terms in which $M_P[\varphi_0]$ appears explicitly. We clarify that Eqs. (1.114) and (1.112) carry an implicit dependence on all the Horndeski functions M_P, K, G, as the expansion history of the Universe and the growth of cosmic structures obey the modified equations described in Section 1.2.2. In a parametrized approach, these would correspond to Eqs. (1.69), (1.72) and (1.73) (see e.g. [232] for an explicit example). When opting for this kind of approach, though, one must be careful that the forms chosen for $w_{\text{DE}}, \mu(a, k)$ and $\Sigma(a, k)$ are compatible with having started from the Horndeski theory in action (1.62), namely with luminal tensor modes speed [233].

Therefore, the luminosity distance fluctuations provide direct access to the linear structures of the Universe. In non-minimally coupled scalar-tensor theories, some of the effects building these signals are different for distances inferred from GWs or from electromagnetic signals, offering a new way to directly probe the effects of a dynamical DE field. The way that this information can be used is similar to what done in Section 1.1.3: promoting the field fluctuations to random variables, one computes their correlation functions. Thanks to Eqs. (1.114) and (1.112), we can relate the power spectra of the luminosity distance fluctuations, which we can obtain through GW and SNe observations, to those of the gravitational potentials, Φ and Ψ, and DE clustering $\epsilon\delta\varphi$, and investigate them.

1.5. This Thesis

This dissertation is divided in three parts, each of which tackles a specific aspect of the main theme: the propagation of GWs through cosmic structures. In the first two parts, we will use GWs in the ray optics regime to test scalar-tensor models of gravity aimed at describing the late time cosmic expansion. In the last part, we will demote the DE field back to a cosmological constant and address the matter of wave-optics effects. Each Chapter picks up the thread of thoughts from the previous one, investigating the extent of the assumptions made and possibly generalizing them. Keeping

the detection prospect in high regard, the goal is not only to produce testable predic-
tions, but also to understand various aspects of gravitational wave propagation that
are yet to be fully grasped.

Part I: Ray-optics limit: beyond the homogeneous and isotropic Universe

We dedicate this part to the exploration of the potentialities of the luminosity dis-
tance fluctuations in Eqs. (1.112) and (1.114) in constraining cosmological param-
eters of various scalar-tensor models contained within the action (1.62). This part
aims, therefore, at building tests using the *amplitude* of the GWs as signal. In partic-
ular,

- **Chapter 2**: we will investigate the power spectrum of the luminosity distance
  fluctuations of GWs observations, in two scalar-tensor models. After a first ex-
  ploration, we will build an estimator which combines GWs and SNe observa-
  tions with the goal of picking up the *dark energy clustering* contribution to the
  covariance of the observation. In other words, we attempt at singling out the
  contribution of $\epsilon\delta\varphi$ in Eq. (1.112), by comparing GW and electromagnetic ob-
  servations. This signal is otherwise buried under the dominant contribution
  of the weak lensing convergence κ. We will conclude that, although picking up
  the DE clustering signal is very challenging, the estimator we built still provides
  a smoking gun proof for theories with a running Planck's Mass $M_P[\varphi]$, which
  can be used after gathering enough GWs and SNe data.

  Based on: *Detecting Dark Energy Fluctuations with Gravitational Waves*
  A. Garoffolo, M. Raveri, A. Silvestri, G. Tasinato, C. Carbone, D. Bertacca, S.
  Matarrese,
  Phys.Rev.D 103 (2021) 8, 083506, e-Print: 2007.13722 [astro-ph.CO]

- **Chapter 3**: considering that weak lensing gives the greatest contribution to
  the GW luminosity distance fluctuations, we investigate its role in constraining
  cosmological parameters. Hence, in this Chapter we focus on the contribution
  from κ in Eq. (1.112), and study its potentialities both alone and in combina-
  tion with galaxy surveys (both clustering and weak lensing). Without choosing
  a specific GW mission, we assess the number of GW events and the precision
  with which the luminosity distance must be determined, in order for GW ob-
  servations to become competitive with galaxies in constraining cosmological
  parameters.

  Based on: *Prospects of testing late-time cosmology with weak lensing of gravi-
  tational waves and galaxy surveys*
  A. Balaudo, A. Garoffolo, M. Martinelli, S. Mukherjee, A. Silvestri,
  e-Print: 2210.06398 [astro-ph.CO]

1

Part II: Ray-optics limit: distance duality relation and polarization tests

After having investigated the potentialities of Eqs. (1.112), in this part we turn to other possible tests, always in the ray-optics limit. Indeed, from a GW detection, one receives more information than only its luminosity distance. In particular, we will take a step back and asks which other quantities related to their amplitude are modified in scalar-tensor theories, and then we will start looking at the polarization content.

- **Chapter 4**: distance measures have always played a prime role in building tests for the cosmological model. The fact that the luminosity distance, as inferred from a GW detection, can be modified compared to the electromagnetic one, is a golden opportunity to tests non-minimally coupled scalar-tensor theories. Nevertheless, in cosmology there are multiple notions of distances which can play an equivalently important role to d_L^{GW} in producing tests for the gravitational theory. In this Chapter, after deriving the equations of motion of a GW in a scalar-tensor set-up where these propagate at the speed of light, we take a proper look at the definition of *GW cosmological distances*, showing that, in the ray-optics regime, on top of d_L^{GW}, one can also define an angular diameter distance, $d_A^{\mathrm{GW}}(z)$. To achieve this, we derive from a general principle the GW stress-energy tensor, under the assumption that the GW and SW propagate at different speeds. We will prove the validity of the *Etherington's reciprocity law*, namely $d_L^{\mathrm{GW}}(z) = (1+z)^2 d_A^{\mathrm{GW}}(z)$, implying that also the GW angular diameter distance is modified compared to the electromagnetic one. Finally, we investigate the implications of our findings in the context of strong lensing time delays.

  Based on: *Gravitational-wave cosmological distances in scalar-tensor theories of gravity*
  G. Tasinato, A. Garoffolo, D. Bertacca, S. Matarrese
  JCAP 06 (2021) 050, e-Print: 2103.00155 [gr-qc]

- **Chapter 5**: in order to derive the equations of motion of the GW and SW, in the previous Chapter we assumed that the amplitude of the SW was a factor ω^{-1} smaller than the GW. We justified this assumption by asking that at the moment of emission the SW is not sourced, so that it is produced by propagation effects only. In this Chapter, we elaborate on this assumption and thoroughly revisit the two definitions of GW given: as in geometric-optics and in wave-optics. We will see that, depending on the assumptions, different conclusions can be drawn about the amplitude of the SW. We investigate, then, whether the SW can be directly detected in light of screening mechanisms. In the context of two of them, we show that this should not be the case regardless of the definition used for the GW.

  Based on: *Unifying gravitational waves and dark energy*

A. Garoffolo, O. Contigiani,
e-Print:2110.14689 [astro-ph.CO]

Part III: Wave-optics limit: the stochastic background and its polarization:

In this last part, we assume that dark energy is described by the cosmological constant, Λ, as in the standard model of cosmology. We also switch the definition of the GW and opt to investigate the wave-optics limit, showing that the interaction with matter structures during propagation, in this limit, can produce scalar and vector polarization modes.

- **Chapter 6**: we study the propagation of GWs in a perturbed cosmological Universe without relying on tools typical of ray-optics techniques. This way, we can easily account for wave-optics effects. Similarly to Eq. (1.101), we obtain a perturbed solution for the waves, though accounting carefully for their polarization content instead of treating them as scalar fields. We work under the *classical matter approximation*, namely that the effect of the waves on the matter inhomogeneities is negligible. Our result shows that the interaction with matter structures can produce scalar and vector components in the GW, on top of tensor ones. We build the two point correlation function of the tensor modes, and introduce the Stokes parameters. In the case of an unpolarized, Gaussian, statistically homogeneous and isotropic initial background, we show that the interaction with matter does not generate a net difference between left- and right- helicity tensor modes, as expected, but it also does not produce Q- and U- polarization modes.

  Based on: *Wave-optics limit of the stochastic gravitational wave background*
  A. Garoffolo,
  e-Print: 2210.05718 [astro-ph.CO]

1

Appendices

A. Special functions, Fourier and Harmonic transformations

In our convention, the 3D Fourier transform and anti-transform are given by

$$f(\tau, \mathbf{x}) \;=\; \int \frac{d^3 k}{(2\pi)^3} \, e^{i\mathbf{k}\cdot\mathbf{x}} f_{\mathbf{k}}(\tau), \tag{1.115}$$

$$f(\tau, \mathbf{k}) \;=\; \int d^3 x \, e^{-i\mathbf{k}\cdot\mathbf{x}} f(\tau, \mathbf{x}). \tag{1.116}$$

Similarly, a function can be expanded on a spherical harmonics basis using

$$f(\tau, \chi, \hat{n}) \;=\; \sum_{\ell=0}^{+\infty} \sum_{m=-\ell}^{\ell} a_{\ell m}(\tau, \chi) Y_{\ell m}(\hat{n}), \tag{1.117}$$

$$a_{\ell m}(\tau, \chi) \;=\; \int_{\mathcal{S}^2} d^2 \hat{n} \, f(\tau, \chi, \hat{n}) Y_{\ell m}^*(\hat{n}), \tag{1.118}$$

with $\mathbf{x} = \chi \hat{n}$, where $\hat{n}$ is the vector on the unit sphere, i.e. $\hat{n} = (\theta, \phi)$ represents the angular coordinates. The spherical harmonics $Y_{\ell m}(\hat{n})$ are eigenfunctions of the angular part of the Laplacian

$$\left[\frac{1}{\sin\theta} \frac{\partial}{\partial\theta} \left(\sin\theta \frac{\partial}{\partial\theta} \right) + \frac{1}{\sin^2\theta} \frac{\partial^2}{\partial\varphi^2} \right] Y_{\ell m}(\theta, \varphi) = -\ell(\ell+1) Y_{\ell m}(\theta, \varphi) \tag{1.119}$$

and their explicit expression takes the form

$$Y_{\ell m}(\hat{n}) = \sqrt{\frac{2\ell+1}{4\pi} \frac{(\ell-|m|)!}{(\ell+|m|)!}} \, P_{\ell m}(\cos\theta) \, e^{im\varphi} \times \begin{cases} (-1)^m & m \geq 0 \\ 1 & m < 0 \end{cases}, \tag{1.120}$$

where $P_{\ell m}(\mu)$ are the associated Legendre functions, satisfying

$$P_{\ell m}(\mu) = (-1)^m (1-\mu^2)^{m/2} \frac{d^2}{d\mu^2} P_{\ell}(\mu), \tag{1.121}$$

and $P_{\ell}(\mu)$ is the Legendre polynomial. These are ℓth-order polynomials in $\mu \in [-1, 1]$. The first polynomials are

$$P_0(\mu) = 1, \qquad P_1(\mu) = \mu, \qquad P_2(\mu) = \frac{3\mu^2 - 1}{2}, \tag{1.122}$$

while the higher ones can be found by using the recursion relation

$$(\ell+1) P_{\ell+1}(\mu) = (2\ell+1) \mu P_{\ell}(\mu) - \ell P_{\ell-1}(\mu). \tag{1.123}$$

The spherical harmonics satisfy the orthonormality relations

$$\int_{\mathcal{S}^2} d^2 \hat{n} \, Y_{\ell m}^*(\hat{n}) \, Y_{\ell' m'}(\hat{n}) \;=\; \delta_{\ell\ell'} \delta_{mm'} \tag{1.124}$$

and they are related to Legendre polynomials via

$$P_\ell(\hat{n} \cdot \hat{n}') \quad = \quad \frac{4\pi}{2\ell + 1} \sum_{m=-\ell}^{\ell} Y_{\ell m}^*(\hat{n}) \, Y_{\ell m}(\hat{n}').$$

(1.125)

Another class of important special functions are the spherical Bessel functions, $j_\ell(x)$, solutions of the differential equation

$$\frac{d^2 j_\ell}{dx^2} + \frac{2}{x} \frac{d j_\ell}{dx} + \left[1 - \frac{\ell(\ell + 1)}{x^2} \right] j_\ell = 0.$$

(1.126)

They cover a relevant role because of the relation

$$e^{i\mathbf{k} \cdot \mathbf{x}} \quad = \quad \sum_{\ell=0}^{\infty} i^\ell \, (2\ell + 1) \, j_\ell(k\chi) \, P_\ell(\hat{k} \cdot \hat{n}),$$

(1.127)

where we used again $\mathbf{x} = \chi \hat{n}$ and similarly $\mathbf{k} = k \hat{k}$.

Part I

Ray-optics limit: beyond the homogeneous and isotropic Universe

2

Detecting the clustering of Dark Energy

Luminosity distance estimates from electromagnetic and gravitational wave sources are generally different in models of gravity where dark energy is a dynamical field beyond the standard cosmological scenario. This leaves a unique imprint on the angular power-spectrum of fluctuations of the luminosity distance of gravitational-wave observations, which tracks inhomogeneities in the dark energy field. Exploiting the synergy between supernovae and gravitational wave distance measurements, in this Chapter we build a joint estimator that directly probes dark energy fluctuations, providing a conclusive evidence for their existence in case of detection. Moreover, such measurement would also allow probing the running of the Planck mass. We discuss experimental requirements to detect these signals.

2.1. Introduction

Any theory attempting at providing a cosmological model must include predictions for the large-scale structures' dynamics. As a result, the dispositions of galaxies and the one of other tracers of the cosmic web, should contain footprints of any modification of the standard pictures. Scientific missions trying to characterize the spacetime always rely on the detection of a messenger: whether an electromagnetic (EMW) or a gravitational wave (GW). Therefore, the first detection of GWs has guaranteed a new observational window onto our Universe, promising to offer complementary probes to shed light on the dynamics of the Universe on cosmological scales. As described in Section 1.4.2, GW events at cosmological distances, in the geometric optics regime, can be used as *Standard Sirens* [197, 225, 234] for measuring the expansion rate of the Universe. This recent approach is complementary to measuring the luminosity distance of *Standard Candles*, like Type-Ia Supernovae (SNe): one of the two principal probes for the recent exponential expansion of the Universe [6, 7]. On the homogeneous and isotropic background, the luminosity distances depend only on redshift, leading to the standard distance-redshift relation tests as described in Section 1.4.2. After their emission, photons and gravitons travel through the dark matter gravitational potential wells, with the effect of spoiling the FLRW results regarding their luminosity distances to the sources. Inhomogeneities in the Universe induce a dependence of the distances also on the direction of observation in addition to redshift, $\Delta d_L(z, \hat{n})$, as described in Section 1.4.3. This additional dependence must be kept into account to perform accurate tests: distance measurements are reaching an unprecedented the level of precision, such that neglecting relativistic effects can bias our cosmological parameter inference. However, fluctuations in the luminosity distance do not only constitute a source of error: they give us direct access to the LSS. The possibility of having multi-messenger observations opened the powerful possibility of testing theoretical proposals which break the degeneracy between the GW and the electromagnetic sector. This is exactly the case for scalar-tensor theories of gravity described in Section 1.2, where photons, contrary to GWs, are not coupled directly to the DE scalar field. In presence of a dynamical DE field, the GW luminosity distance generally differs from the one traced by electromagnetic signals, both at the unperturbed, background level [183–190] and in its large-scale fluctuations [158, 235]. Importantly, fluctuations in the electromagnetic luminosity distance, Δd_L^{EM}, are affected by the DE field only indirectly, as it can be seen in Eq (1.114), while the GW one, Δd_L^{GW}, contains contributions directly proportional to the running Planck's mass, M_P and the clustering of the DE field, $\delta\varphi$, as it can be seen in Eq. (1.112). In this Chapter, we combine two standard distance indicators, SNe and GWs, and combine their luminosity distance fluctuations into a novel estimator to *directly* detect the signal of DE clustering. This signal can not be mimicked by other effects and would provide convincing evidence for the existence of the DE field. If DE does not directly couple to known particles through non-gravitational

interactions, the one proposed here is a promising method to pursue its direct detection, on cosmological scales, far from sources that can hide its presence by means of screening mechanisms (see e.g. [51, 236, 237]).

2.2. The GW luminosity distance power-spectrum

The luminosity distance, as inferred by an EM or GW signal propagating through a Universe with structures, depends on the observed redshift, z, and on the direction of arrival in the sky, $\hat{\theta}$. We decompose the observed luminosity distance of a source as a sum of its background and fluctuation components, as in Eq. (1.111). We use Eq. (1.112) to build the angular power-spectrum of GW luminosity distance fluctuations averaged over a given redshift distribution of the sources

$$C_\ell^{\mathrm{GW}} = 4\pi \int d\ln k \left(\frac{\Delta d_L^{\mathrm{GW}}}{\bar{d}_L^{\mathrm{GW}}}\right)_{k\ell}^W \left(\frac{\Delta d_L^{\mathrm{GW}}}{\bar{d}_L^{\mathrm{GW}}}\right)_{k\ell}^W , \tag{2.1}$$

where we work in Fourier space for the perturbations, k being the momentum, and

$$\left(\frac{\Delta d_L^{\mathrm{GW}}}{\bar{d}_L^{\mathrm{GW}}}\right)_{k\ell}^W = \int_0^\infty dz\, j_\ell(k\chi)\, W(z) \left(\frac{\Delta d_L^{\mathrm{GW}}}{\bar{d}_L^{\mathrm{GW}}}\right), \tag{2.2}$$

and $j_\ell(x)$ is the spherical Bessel function and $W(z)$ is the source window function, normalized to 1. The effect of each term in Eq. (1.112) on the angular power-spectrum can be studied independently in terms of the different sources, highlighting each relativistic or modified gravity effect,

$$\left(\frac{\Delta d_L^{\mathrm{GW}}}{\bar{d}_L^{\mathrm{GW}}}\right)_{k\ell}^W = \int_0^{\tau_A} d\tau\, j_\ell(k\chi)\Big\{S_\kappa^{\mathrm{GW}} + S_{vol}^{\mathrm{GW}} + S_{Sh}^{\mathrm{GW}} + S_{SW}^{\mathrm{GW}} + S_{Dop}^{\mathrm{GW}} + S_{ISW}^{\mathrm{GW}} + S_{\delta\varphi}^{\mathrm{GW}}\Big\}, \tag{2.3}$$

with τ_A is the conformal time corresponding to $z = +\infty$ and

$$S_\kappa^{\mathrm{GW}}(\tau) = (\Phi_k + \Psi_k)\int_0^\tau d\tilde{\tau}\, \frac{\ell(\ell+1)}{2}\frac{(\tilde{\chi}-\chi)}{\tilde{\chi}\chi} W(\tilde{\tau}) \tag{2.4}$$

$$S_{vol}^{\mathrm{GW}}(\tau) = -W(\tau)(\Phi_k + \Psi_k), \tag{2.5}$$

$$S_{Sh}^{\mathrm{GW}}(\tau) = (\Phi_k + \Psi_k)\int_0^\tau d\tilde{\tau}\, \frac{W(\tilde{\tau})}{\tilde{\chi}} \tag{2.6}$$

$$S_{SW}^{\mathrm{GW}}(\tau) = W(\tau)\Big(\frac{1}{\chi\mathcal{H}} - \frac{M_P'}{\mathcal{H}M_P}\Big)\Psi_k, \tag{2.7}$$

$$S_{Dop}^{\mathrm{GW}}(\tau) = -\partial_\tau\Big[W(\tau)\Big(1 - \frac{1}{\mathcal{H}\chi} + \frac{M_P'}{\mathcal{H}M_P}\Big)v\Big] \tag{2.8}$$

$$S_{ISW}^{\mathrm{GW}}(\tau) = (\Phi_k' + \Psi_k')\int_0^\tau d\tilde{\tau}\, W(\tilde{\tau})\Big(1 + \frac{M_P'}{\mathcal{H}M_P} - \frac{1}{\chi\mathcal{H}}\Big), \tag{2.9}$$

$$S_{\delta\varphi}^{\mathrm{GW}}(\tau) = W(\tau)\frac{M_{P,\varphi}}{M_P}\delta\varphi \tag{2.10}$$

where $W(\tau) = (1 + z)\,\mathcal{H}\,W(z)$. In (2.4) we assumed $v^i(k, \tau) = i\,k^i\,v(\tau)$, namely that the peculiar velocity field is irrotational. The reason why we introduced this notation is that it is more suitable for direct implementation of the calculation of C_ℓ^{GW} in EFTCAMB [90]: the Einstein-Boltzmann solver code, described in Section 1.2.2, allowing us to study this quantity for a broad host of DE models. Note also that EFTCAMB evolves the perturbed gravitational field equations in terms of the rescaled DE field $\pi(x) = \frac{\delta\varphi(x)}{\varphi_0'(\tau)}$, assuming that $\varphi_0'(\tau) \neq 0$, as it is in a cosmological setting. Therefore, the last source among the ones above can be rewritten as

$$S_{\delta\varphi}^{\text{GW}}(\tau) = W(\tau)\,\frac{M_{P,\varphi}}{M_P}\,\varphi_0'(\tau)\,\pi(x) = W(\tau)\,\frac{M_P'}{M_P}\,\pi(x)\,. \tag{2.11}$$

In order to explore in detail the impact of the DE field on C_ℓ^{GW} we focus for a
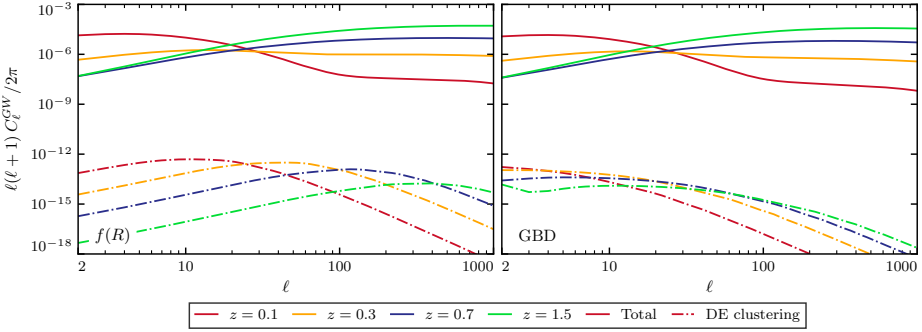
Figure 2.1: Angular power-spectrum of gravitational-wave luminosity distance fluctuations. Solid lines show the total power-spectrum, dashed lines the scalar field clustering component.
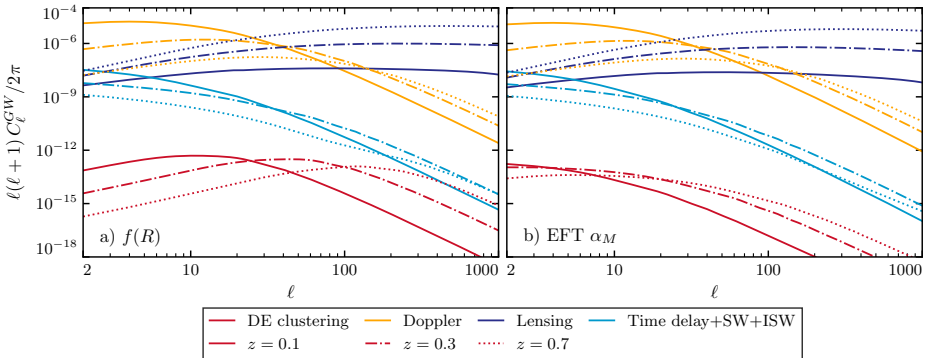
Figure 2.2: Various contributions to the angular power-spectrum of gravitational-wave luminosity distance fluctuations according to Eqs. (2.4)-(2.10). Solid, dashed and dotted contributions stand for increasing redshifts bins.

moment on two representative models. First, a designer $f(R)$ model on a ΛCDM

background [238], with the only model parameter set to $B_0 = 10^{-4}$ which is compatible with current constraints [239]. Second, an agnostic parametrization of M_P, such that the ratio (M'_P/M_P) is a linear function of the scale-factor, $a(z)$, $M'_P/M_P \equiv (M'_P/M_P)|_o \, a$, where $(M'_P/M_P)|_o$ is the value of the ratio today, which we set to 0.05. This minimal parametrization, implemented on a ΛCDM background, is representative of the Generalized Brans-Dicke (GBD) [240–242] family of theories. In both these models, the Planck mass M_P depends on the scalar field value alone, $\varphi_0(\tau)$.

Figures 2.1 and 2.2 show the angular power-spectrum, C_ℓ^{GW}, for the two scenarios described above. To highlight redshift dependencies, we choose a Gaussian distribution for the GW sources centered in various redshifts z_i, with width $\Delta z = 0.01$, i.e. $W(z) = \mathcal{N} \exp[-(z-z_i)^2/(2\Delta z^2)]$ where $\mathcal{N}$ is the normalization constant. The total signal significantly changes shape with increasing redshift. At low redshifts and large scales, the signal is dominated by the Doppler effect, encoded in $S_{Dop}^{\mathrm{GW}}(\tau)$, due to the bulk-flow of the environment in which the GW sources are embedded. The Doppler contribution then decays for growing ℓ, and the angular power-spectrum at small scales is dominated by lensing convergence, described in $S_\kappa^{\mathrm{GW}}(\tau)$; the Doppler term also decays in redshift, while lensing grows and eventually dominates the high-redshift part of the signal. This is a standard behavior: as lensing is an integrated effect, it accumulates throughout the propagation. These behaviors can be observed in Figure 2.2. For both models considered, the relative behavior between Doppler and lensing convergence is qualitatively unaltered with respect to the General Relativistic results [157]. Figure 2.1 also shows the direct contribution of $\delta\varphi$ to the total signal, i.e. $S_{\delta\varphi}^{\mathrm{GW}}$ of Eq. (2.10). This is of the same order of magnitude in both scenarios, and results largely subdominant compared to the total signal. For the $f(R)$ model, the scalar field contribution has a noticeable scale-dependent feature that evolves in time as the Compton wavelength of the model. At higher redshift, the Compton scale of the scalar field is smaller and, correspondingly, the feature in the power-spectrum moves to smaller scales. In the GBD case, on the other hand, any feature in the shape of the power-spectrum is less pronounced, as it only leads to the decay of DE fluctuations below the horizon.

2.3. The joint SNe/GW estimator

The direct contributions of DE fluctuations to C_ℓ^{GW} are very small compared to other effects, making it impossible to detect their presence in the angular correlations using GW data only. Interestingly, since photons are not affected directly by DE or MG, Δd_L^{EM} is structurally unchanged w.r.t. the results of General Relativity, hence is obtained by neglecting all the explicit DE terms present in Eq. (1.112). The EM luminosity distance fluctuations, then, formally follow Eq. (1.114), with the gravitational potentials following the modified laws as described in Sections 1.2.2. We can single

out the distinctive DE field contributions, by combining standard sirens and standard candles: assuming that we have measurements of both SN and GW at the same redshifts and positions and subtract the two luminosity distances fluctuations as

$$\Delta_\varphi(\hat{n}, z) \equiv \frac{\Delta d_L^{\text{EM}}(\hat{n}, z)}{\bar{d}_L^{\text{EM}}} - \frac{\Delta d_L^{\text{GW}}(\hat{n}, z)}{\bar{d}_L^{\text{GW}}}, \qquad (2.12)$$

where the average luminosity distances are given in Eqs. (1.106) and (1.105). In what follows, we will use the estimator above in a statistical fashion. For this, we will need populations of GW and SN in overlapping regions of the sky and redshift bin, instead of having both events exactly in the same position and at the same redshift. For the theories considered here, Eq. (2.12) takes the form

$$\Delta_\varphi(\hat{\theta}, z) = \frac{M_P'}{\mathcal{H} M_P} \left(\Phi - v_\parallel + \int_0^\chi d\tilde{\chi} (\Phi' + \Psi') \right) - \frac{M_{P,\varphi}}{M_P} \delta\varphi, \qquad (2.13)$$

where only the explicit DE-dependent effects are present. In addition to the DE clustering contribution, only three effects contribute to Δ_φ: a residual Doppler, SW and ISW effects. Most importantly, lensing convergence, which is the dominant contribution to luminosity distance anisotropies, cancels out. Similarly as before, for the joint estimator Δ_φ we find the set of sources

$$
\begin{aligned}
S_{SW}^{\Delta_\varphi}(\tau) &= W(\tau) \frac{M_P'}{\mathcal{H} M_P} \Psi \\
S_{Dop}^{\Delta_\varphi}(\tau) &= \partial_\tau \left[W(\tau) \frac{M_P'}{\mathcal{H} M_P} v \right] \\
S_{ISW}^{\Delta_\varphi}(\tau) &= -\left(\Phi_k' + \Psi_k' \right) \int_0^\tau d\tilde{\tau} \, W(\tilde{\tau}) \left(\frac{M_P'}{\mathcal{H} M_P} \right), \\
S_{\delta\varphi}^{\Delta_\varphi}(\tau) &= -W(\tau) \frac{M_{P,\varphi}}{M_P} \delta\varphi
\end{aligned}
\qquad (2.14)
$$

For particular classes of events, Eq. (2.12) could be directly evaluated for pairs of sources at the same position and redshift. In our analysis we require this to hold only statistically, by integrating Eq. (2.12) over a joint redshift distribution and computing its angular power-spectrum:

$$C_\ell^{\Delta_\varphi} = C_\ell^{\text{SN}} + C_\ell^{\text{GW}} - 2 C_\ell^{\text{SN-GW}}, \qquad (2.15)$$

where C_ℓ^{SN} (C_ℓ^{GW}) are the SN (GW) luminosity distance angular power-spectra, and $C_\ell^{\text{SN-GW}}$ the cross-spectrum between the two. In this form we need the redshift and position of GW/SNe sources to be the same only on average, i.e. same redshift distributions and overlapping regions in the sky. In Fig. 2.3 we show $C_\ell^{\Delta_\varphi}$ as a function of the source redshift for the two representative DE models. We consider the case of localized SN/GWs sources to study the redshift dependence of $C_\ell^{\Delta_\varphi}$. In $f(R)$, the DE clustering component is dominating the total angular power-spectrum, making its
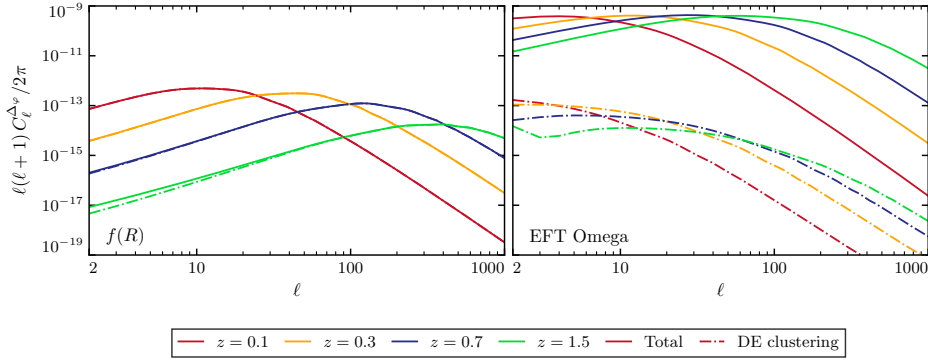
Figure 2.3: The angular power-spectrum of the difference between GW and SN luminosity distance fluctuations. Solid lines show the total power-spectrum, dashed lines the scalar field clustering component.

features manifest. In the GBD model, instead, the total signal is dominated by the Doppler effect. Nevertheless, a detection of this signal still constitutes a direct proof of the DE field's presence.

2.4. Observational prospects

We next investigate the detection prospects for the fluctuations of the GW luminosity distance via C_ℓ^{GW}, and DE clustering via $C_\ell^{\Delta_\varphi}$. We consider the noise power-spectrum for both SN and GW, as given by only a shot-noise contribution [243, 244]:

$$N_\ell^i = \frac{4\pi f_{\text{sky}}}{N_i} \left(\frac{\sigma_{d_L}^i}{d_L^i} \right)^2 \equiv \frac{4\pi f_{\text{sky}}}{N_i^{\text{eff}}} \,, \tag{2.16}$$

where $i = \{\text{SN}, \text{GW}\}$ and f_{sky} is the sky fraction covered by observations, which we assume to be $f_{\text{sky}} = 1$ for simplicity. We also define the effective number of sources, N_i^{eff}, as the product of the number of events, N_i, in a given redshift bin and the ratio $\sigma_{d_L}^i / d_L^i$ related to the relative uncertainty on the luminosity distance which is proportional to the magnitude uncertainty. In this way N_i^{eff}, which sets the overall noise levels, takes into account the number of events detected and the precision of each measurement. As the signal decays in scale faster than $\propto \ell^{-2}$, we expect to have the best chance of measuring it from large-scale observations. For this reason we assume that future localization uncertainties can be neglected [245].

The noise for the joint estimator of Eq. (2.15) is given by the sum of the two noise power-spectra for GW and SN, since we assume that any stochastic contribution is uncorrelated. Consequently, the number of effective events needed for a detection

of $C_\ell^{\Delta_\varphi}$ is given by the harmonic mean of the two single ones

$$N_{\Delta_\varphi}^{\text{eff}} = \left[\frac{1}{N_{\text{SN}}^{\text{eff}}} + \frac{1}{N_{\text{GW}}^{\text{eff}}} \right]^{-1}. \tag{2.17}$$

The error on a power-spectrum measurement is given by

$$\sigma(C_\ell) = \sqrt{2/(2\ell+1)f_{\text{sky}}}\,[C_\ell + N_\ell]\,, \tag{2.18}$$

and the corresponding signal-to-noise ratio is

$$\frac{S}{N} = \sqrt{\sum_\ell \left(\frac{C_\ell}{\sigma(C_\ell)} \right)^2}. \tag{2.19}$$

In the case of C_ℓ^{GW} this applies directly, while for $C_\ell^{\Delta_\varphi}$ one needs to do full error propagation on Eq. (2.15): the final result is the same, provided one uses for $N_{\Delta_\varphi}^{\text{eff}}$ the harmonic mean given above. The noise power-spectrum in Eq. (2.16) is scale-independent so we can solve the inverse problem of determining the number of effective events needed to measure the power-spectra with a desired statistical significance. In practice, we fix a target $S/N = 5$, and solve the equation of S/N for N^{eff} both in the case of GW sources alone and Δ_φ. Finally, we investigate the scenario where the GW source redshift is unknown. In this case we assume the shape of the GW redshift distribution as given in [220], while the SN one as in [246]. Since the SN and GW redshift distributions need to match for our estimator to work, we take the product of the two and build the joint probability of measuring both SN and GW at the same redshift. In particular, we consider

$$\frac{dN^{\text{GW}}(z)}{dz} = \mathcal{N}_{\text{GW}} \frac{\chi^2(z)}{(1+z)^2 \mathcal{H}}\,, \qquad \frac{dN^{\text{SN}}(z)}{dz} = \mathcal{N}_{\text{SN}} \times \begin{cases} 2.5\, \dfrac{\chi^3(z)}{(1+z)^{1.5}} & z < 1 \\[2mm] 9.7\, \dfrac{\chi^3(z)}{(1+z)^{3.5}} & z \geq 1 \end{cases}, \tag{2.20}$$

where $\mathcal{N}_{\text{GW}}$ and $\mathcal{N}_{\text{SN}}$ are suitable normalization. Even if such redshift distributions depend on the cosmological model (for instance through $\mathcal{H}(z)$), we use their ΛCDM expressions, as we have checked that this dependency is negligible. Intermediate cases in which the EM counterpart is not available, but estimates of the redshift distributions are obtained via statistical methods [207, 209, 247, 248], would fall in between the two extreme cases examined here.

Table 2.1 summarizes the results reporting the number of effective sources for a 5σ detection of the angular power-spectra C_ℓ^{GW} and $C_\ell^{\Delta_\varphi}$, both in the case of GW events with known as well as unknown redshifts (the latter designated as "w/o z"). We also indicate the value of $N_{\text{GW}}^{\text{eff}}$ in General Relativity, for comparison. The detection threshold for GW luminosity distance fluctuations, $N_{\text{GW}}^{\text{eff}}$, does not change appreciably for the different scenarios, since we selected representative models sufficiently

	GR	$f(R)$		GBD	
	$N_{\mathrm{GW}}^{\mathrm{eff}}$	$N_{\mathrm{GW}}^{\mathrm{eff}}$	$N_{\Delta_\varphi}^{\mathrm{eff}}$	$N_{\mathrm{GW}}^{\mathrm{eff}}$	$N_{\Delta_\varphi}^{\mathrm{eff}}$
$z = 0.1$	10^7	10^7	10^{14}	10^7	10^{12}
$z = 0.3$	10^8	10^8	10^{15}	10^8	10^{11}
$z = 0.7$	10^8	10^8	10^{16}	10^8	10^{12}
$z = 1.5$	10^7	10^7	10^{17}	10^7	10^{12}
w/o z	10^7	10^7	10^{19}	10^7	10^{14}

Table 2.1: Effective number of events for a 5-σ detection of C_ℓ^{GW} and $C_\ell^{\Delta_\varphi}$.

close to ΛCDM to satisfy current constraints. In fact, as shown in Fig. 2.1, C_ℓ^{GW} is dominated by lensing convergence at high redshifts and by Doppler shift at low redshifts. The former is *indirectly* modified by DE, while the latter is also sensitive to the background configuration of the DE field: both these effects are small in the considered models. Since lensing convergence and Doppler effect dominate the angular correlations of GW sources, it is not possible to distinguish the DE clustering contribution in C_ℓ^{GW} within the total signal.

As far as $N_{\Delta_\varphi}^{\mathrm{eff}}$ is concerned, the results show that it is possible to detect the signal of the joint estimator in both cases of known and unknown redshifts. In $f(R)$, this signal is dominated by the DE field fluctuations, as shown in Fig. 2.3, hence allowing for its direct detection. In the GBD model, the signal of the joint estimator is dominated by Doppler shift, easier to detect, explaining the lower number of effective events compared to $f(R)$. In this case, one would not be able to distinguish directly the DE field inhomogeneities, but its detection is still a proof of a time-dependent Planck mass. Comparing the two scenarios of known and unknown GW source's redshift, we see that the number of effective events is larger in the latter case because a broader redshift range weakens the signal. However, in this situation the events are not restricted to a redshift bin, hence one can use the whole population of SN/GW sources provided that they are both present. Nonetheless, the number of effective events required is very high, suggesting that the detection precision per source has to improve to eventually measure such signal. In fact, we remark that N_i^{eff} is the effective number of sources, *the real number of events can be lowered by having smaller statistical errors on the single detection.* As an example, in order to measure the DE signal, the detection of a population of about 10^6 GW sources and about the same number of SN events in a redshift bin at $z > 1$, would require a precision, per event, of about $\sigma_{d_L}/d_L \sim 10^{-6}$ in the case of $f(R)$, and $\sim 10^{-3}$ for the GBD model. Since the required effective number of events scales quadratically with per-event precision, σ_{d_L}/d_L, but

only linearly with number of events, increasing precision is likely a better strategy.

2.5. Discussion and Conclusions

Fluctuations in the DE field can distinctively alter the propagation of GWs with respect to light. In this Chapter, by combining the luminosity distance measurements from GW and SN sources, we proposed the new estimator Δ_φ for the *direct* detection of the imprint of the DE fluctuations, that does not rely on non-gravitational interactions between DE and known particles. This signal cannot be mimicked by other effects and, as such, it provides a distinctive evidence for a dynamical DE model. Even in the case of a DE clustering signal below cosmic variance, any detection of our joint estimator would be a convincing proof of a running Planck mass, as we showed for two specific models. Reversely, it can be used to place complementary bounds on theories of dynamical dark energy non-minimally coupled to gravity, along similar lines of recent forecasts as in [161, 249] for the case of standard sirens. Since we exploit angular correlations at large scales, we expect our method not to be affected by screening mechanisms nearby sources.

Since the required effective number of source is quite large, one should leverage as much as possible on the precision of the measurement; for instance, given the number of SN/GW events (of order 10^6, at least in the higher redshift bins) that can be observed with future SN surveys [12, 250] and space-based interferometers [251, 252], a detection would be possible, if one decreases the statistical error on each measure according to table 2.1. Notice also that for our estimates we considered an ideal case: the number of events needed for a detection might be higher to deal with possible systematic effects. This suggests that future facilities might have to develop new technologies and observational strategies to meet these detection goals. We leave it to future work to determine whether a detection of the signal we propose can be aided by studying additional DE models, synergies with large scale structure surveys or considering different sources of GW/EM signals. For example, future experiments will detect large numbers of binary white dwarfs [253] on galactic scales and much beyond [254, 255]. These events are supposed to be progenitors of Type-Ia SN in the so-called double degenerate scenario [256], offering a common source for GW and SN signals (see e.g. [257]). In this case, Eq. (2.12) holds locally and Δ_φ could be directly reconstructed in configuration space, provided that non-linearities and DE screening effects can be properly taken into account.

Note: My contribution to the paper this Chapter is based on regards all the scientific aspects, both theoretical and numerical, and the writing.

3

Synergies with galaxy surveys

We investigate the synergy of upcoming galaxy surveys and gravitational wave (GW) experiments in constraining late-time cosmology, examining the cross-correlations between the weak lensing of gravitational waves (GW-WL) and the galaxy fields. Without focusing on any specific GW detector configuration, we benchmark the requirements for the high precision measurement of cosmological parameters by considering several scenarios, both in ΛCDM and alternative DE theories. We find that, in some of the explored setups, GW-WL contributes to the galaxy signal by doubling the accuracy on non-ΛCDM parameters. Though the most extreme cases presented here are likely beyond the observational capabilities, we show nonetheless that – provided that enough statistics of events can be accumulated – GW-WL offers the potential to become a cosmological probe complementary to large-scale structure surveys.

3.1. Introduction

The historical direct detection of a gravitational wave (GW) by the LIGO-Virgo collaboration in 2015 [1], marked the beginning of a series of observing campaigns that led to the detection of around one hundred sources [16, 258, 259]. In the near future, the KAGRA interferometer [260] will join LIGO-Virgo in their observing runs, while the space-based interferometer LISA [25] is expected to launch in the late '30s. The third generation of ground-based GW detectors will see light with the network of Einstein Telescope (ET) [18] and Cosmic Explorer (CE) [19], drastically improving the sensitivity to GW signals and measure hundreds of thousands of events over 10 years of observations. While GW170817 led the way, allowing the first GW measurement of the Hubble constant [205], multi-band GW observations will open a new promising window in observational cosmology, which can be used both to trace different GW sources populations, and to investigate the matter structures along the line of sight. Meanwhile, the intense worldwide effort towards mapping the Universe via galaxy and weak lensing surveys has started to deliver large-scale structure (LSS) data of unprecedented precision, such as those provided by KiDS [103, 104] and DES [101, 102] collaborations. With Stage IV missions (*Euclid* [105], the Vera C. Rubin Observatory [12, 106, 107] and Nancy Grace Roman Space Telescope [108]) we will see a paradigm shift in the volume of data available. This will lead to a new level of scrutiny of the standard model of cosmology: ΛCDM, introduced in Section 1.1. This model successfully describes the Universe in terms of few parameters, yet the rise of precision cosmology has seen the emergence of some tensions between datasets when interpreted within it [13, 14], which could signal the first cracks in ΛCDM as we are achieving a new level of precision in the measurement of its parameters [15].

With the ongoing/upcoming cosmological surveys, we have the opportunity to probe gravity on cosmological scales, and shed light, for instance, on the nature of dark energy. We focus on extensions of ΛCDM that address the phenomenon of cosmic acceleration by means of a scalar dynamical dark energy component or modifying the laws of gravity on large scales [52, 54], as in Section 1.2. In order to further tighten the constraints coming from wide surveys that combine galaxy clustering (GC) and weak lensing (WL) on the cosmological parameters, it will be crucial to bring in new probes able to provide independent measurements and also break degeneracies between the various effects participating in the growth of cosmic structures. Multi-band GW observations are very interesting to this extent, as they offer complementary probes, characterized by a different set of systematics with respect to galaxy surveys.

The dynamics of GWs depends on the extended parameters on two level: explicitly, if they enter directly their propagation equation (e.g. Eq. (1.103)), and implicitly, via a different expansion rate of the Universe and growth of gravitational potentials (see discussion after Eq. (1.114)). On the contrary, the dynamics of photons is not explicitly modified in DE theories such as (1.62), opening the possibility of gaining con-

straining power through probes that combine electromagnetic and GW signals. One example of such degeneracy breaking is the cosmological friction term, the *Hubble drag*, which gets modified for GWs (see, e.g. Eqs. (1.74) or (1.103)) when the theory displays a running Planck's Mass, but not for photons. This results in a difference between the luminosity distance inferred from electromagnetic sources and the one inferred from the amplitude of GWs, as stated in Eq. (1.105), and widely addressed in literature as a mean to test the theory of gravity [122, 123, 183–191].

In this Chapter, we focus on the weak lensing (GW-WL) contribution to the GW's luminosity distance fluctuations (Eq. (1.112)) and explore its potentialities in constraining cosmological parameters. For high enough redshift sources ($z \gtrsim 1.5$), GW-WL can cause up to ~ 5% distortion in the GW strain, posing a serious limitation to the precision with which the true luminosity distance of the sources is measured [157, 225, 261]. More interestingly, and similarly to what done in Chapter 2, it can also be exploited as signal [262], especially when cross-correlated with galaxies [177, 223, 263], CMB lensing [222], HI intensity mapping [264, 265] and other GW probes [266, 267], since both messengers span the same large-scale structures when propagating. We introduce a lensing convergence estimator for GWs, which contains explicitly a contribution from the conformal coupling, $M_P[\varphi]$, characteristic of scalar-tensor theories, thus maximizing the constraining power on cosmological parameters when cross correlating GW-WL with the galaxy fields (GC and WL). Without focusing on a specific GW detector, with its noise and sensitivity, we investigate the requirements, in terms of number of sources and detection precision, for GW-WL to contribute significantly to the GC+WL signal of galaxies.

3.2. Gravitational waves observation

As already discussed in Section 1.4.2, in the DE theories described by the action (1.62), the non-minimal coupling $M_P[\varphi]$ induces an additional dissipation term in the equation for propagation of GWs on the cosmological background [91, 122, 183]. Because of this reason, the amplitude of a GW can be damped differently compared to the one of an electromagnetic wave, leading to the relation Eq. (1.105), for the two luminosity distances. For later convenience, we rewrite such relation in terms of the EFT function $\Omega(a)$, as

$$\bar{d}_L^{\text{GW}}(z) = \sqrt{1 + \Omega(z)} \, \bar{d}_L^{\text{EM}}(z), \tag{3.1}$$

since, comparing the actions (1.62) and (1.68), it is clear that $M_P[\varphi_0(\tau)] = m_0\sqrt{1 + \Omega(\tau)}$.

As the GW strain can be parameterized in terms of the redshifted masses of the binary objects, GW sources cannot probe independently the redshift of the source unless there is a known mass-scale or physical scale which can be used to break the degener-

acy between mass and redshift [206, 268–271]. For some GW sources, such as binary neutron stars (NS) [200, 203, 204, 272, 273], NS-BH [274, 275], stellar and intermediate mass binary black holes (BH) [276] and massive binary BHs [277–279] embedded in accretion disks, a detectable electromagnetic counterpart can potentially be observed and used to measure its redshift directly with a spectroscopic (or photometric) follow-up of the host galaxy. These sources are typically dubbed 'bright' sirens and are the ones we consider here.

3.2.1. Convergence estimators for Gravitational Waves

On their journey through the expanding Universe, photons and GWs encounter clumped matter structures which induces scale-dependent corrections to their luminosity distance, Δd_L^{GW} in Eq. (1.112). Depending on the angular scale and redshift, some of the relativistic effects can be dominant. For instance, in [280] it was shown that for GW sources at redshifts higher than ~ 0.5 WL convergence is the dominant correction, that can reach $\sim 5\%$ of the measured strain. This qualitative result was then confirmed in [281], as discussed in Chapter 2 (see Figure 2.1). Given its substantial magnitude, WL is also a valuable signal to be exploited, rather than only a source of error, to probe the growth history and pattern of the LSS in the Universe. As it can be observed from Eq. (1.113), WL convergence is an integrated effect, it builds up during the propagation. For this reason, we focus on GW sources at high redshift, reaching up to $z \simeq 2.5$, for which we approximate Eq. (1.112) to

$$\frac{\Delta d_L^{\mathrm{GW}}}{\bar{d}_L^{\mathrm{GW}}} \simeq -\kappa_{\mathrm{GW}}, \tag{3.2}$$

where κ_{GW} is the lensing convergence field of GWs, that for a population of sources reads

$$\kappa_{\mathrm{GW}}(\hat{n}) = -\frac{1}{2}\nabla_\theta^2 \phi_L(\hat{n}) = -\int_0^\chi \frac{d\chi'}{\chi'} \int_{\chi'}^\infty d\chi_* \left(\frac{\chi_* - \chi'}{\chi_*}\right) \frac{dn_{\mathrm{GW}}}{d\chi_*} \nabla_\theta^2 \Psi_W(\chi'\hat{n}, z'), \tag{3.3}$$

where $dn_{\mathrm{GW}}/d\chi_*$ is the distribution of the GW sources, Ψ_W is the Weyl potential, related to the matter overdensity as in Eq. (1.73), and ∇_θ^2 indicates the 2D Laplacian with respect to the angle between the image and optical axis. Note that we are neglecting the shear deformations of the signal since these are subdominant in linear perturbation theory where WL mainly affects the magnification of the GWs. In the case of bright events, we construct an estimator to extract the WL convergence from GW data as follows

$$\hat{\kappa}_{\mathrm{GW}}(z, \hat{n}) \equiv 1 - \frac{d_L^{\mathrm{GW}}(z, \hat{n})}{\bar{d}_L^{\mathrm{EM}}(z)}, \tag{3.4}$$

namely as the fractional difference between the GW luminosity distance $d_L^{\mathrm{GW}}(z, \hat{n})$, inferred from the measurement of the GW strain, and the electromagnetic background luminosity distance $\bar{d}_L^{\mathrm{EM}}(z)$. Here, we take the latter as defined via Eq. (1.106)

by choosing a fiducial cosmological model for $E(z)$. Such an estimator can be biased in three ways: the experimental error on the $d_L^{GW}(z, \hat{n})$ measurement, the error on the source redshift, or by a wrong choice of the cosmological model (i.e. biased values of the parameters in $E(z)$). To account for all the effects above we introduce three parameters ϵ_{GW}, ϵ_z and ϵ_c, and modify the convergence estimator as

$$
\hat{\kappa}_{GW} = 1 - \frac{\sqrt{1 + \Omega(z)}\,(1 - \kappa_{GW} + \epsilon_{GW})}{(1 + \epsilon_z + \epsilon_c)}
$$

$$
\sim 1 - \sqrt{1 + \Omega(z)}\,(1 - \kappa_{GW} + \epsilon_{GW} - \epsilon_z - \epsilon_c + \kappa_{GW}\epsilon_z + \kappa_{GW}\epsilon_c)\,,
$$

(3.5)

where we linearized to first order in ϵ_{GW}, ϵ_z, and ϵ_c assuming they are all small. The estimator in (3.4) relies on the availability of source's redshift information, reason why we are limiting this analysis to bright GW events.

3.3. Tomographic Observables

We consider cross-correlations between the density field of galaxies, δ_g, the weak lensing convergence fields as measured by galaxies, κ_g, and the weak lensing convergence field as measured by GW, κ_{GW}. The angular power spectrum for the cross-correlations is (see Section 1.1.3)

$$
C_\ell^{X_i Y_j} = \int_0^{z_{max}} \frac{dz}{\chi^2(z) H(z)} W_{X_i}(k(\ell, z), z) W_{Y_j}(k(\ell, z), z) P_P(k(\ell, z), z)\,,
$$

(3.6)

where $X_i, Y_j = [\delta_g, \kappa_g, \kappa_{GW}]$ at the ith and j-th tomographic bin, $P_p(k) \propto A_s(k/k_*)^{n_s - 1}$ is the primordial power spectrum, with A_s and n_s its amplitude and spectral index and k_* a pivot scale [3, 4]. We applied the Limber and flat-sky approximations [282–287], which sets $k(\ell, z) = (\ell + 1)/\chi(z)$, which we call simply k. $W_{X_i}(k, z)$ is the window function for the observable X in the i-th tomographic bin. For galaxies, the window function can be written as

$$
W_{\delta_g}^i(k, z) = \mathcal{T}_\delta(k, z) b_g^i(z) n_g^i(z) H(z)\,,
$$

(3.7)

where $\mathcal{T}_\delta(k, z)$ is the matter transfer function, evolving the primordial power spectrum such that $P_\delta(k, z) = \mathcal{T}_\delta^2(k, z) P_p(k)$. In Eq. (3.7), $n_g^i(z)$ and $b_g^i(z)$ are, respectively, the galaxy redshift distribution and the linear galaxy bias in the i-th redshift bin which we model following [288]. The window function of the GW lensing convergence is

$$
W_{\kappa_{GW}}^i(k, z) = \mathcal{T}_{\Psi_W}(k, z) \int_z^\infty dz' \frac{\chi(z') - \chi(z)}{\chi(z')} n_{GW}^i(z')\,,
$$

(3.8)

where $n_{GW}^i(z)$ is the redshift distribution of GW sources in the i-th bin, and $\mathcal{T}_{\Psi_W}(k, z)$ is the Weyl potential transfer function, which allows to get its power spectrum

$P_{\Psi_W}(k, z) = T^2_{\Psi_W}(k, z)P_{\rm p}(k)$. The galaxy WL convergence window function is

$$W^i_{\kappa_{\rm g}}(k, z) = \mathcal{T}_{\Psi_W}(k, z) \int_z^\infty {\rm d}z' \frac{\chi(z') - \chi(z)}{\chi(z')} n^i_{\rm g}(z') + W^i_{\rm IA}(k, z), \qquad (3.9)$$

where, with respect to Eq. (3.8) we introduce an extra term $W^i_{\rm IA}(k, z)$ to include the Intrinsic Alignment (IA) systematic effect that we model following [288], *i.e.*

$$W^i_{\rm IA}(k, z) = -\mathcal{T}_\delta(k, z)\frac{A_{\rm IA}C_{\rm IA}\Omega_{\rm m,0}F_{\rm IA}(z)}{D(z)} n^i_{\rm g}(z)H(z), \qquad (3.10)$$

where $D(z)$ is the growth factor, $\Omega_{\rm m,0}$ the current matter density, and the subscript IA highlights the terms including the nuisance parameters $A_{\rm IA}$, $\beta_{\rm IA}$ and $\eta_{\rm IA}$, the last two being contained in the $F_{\rm IA}$ function, while $C_{\rm IA} = 0.0134$ is a fixed constant.

Scalar-tensor theories modify the growth pattern of perturbations, affecting differently the different observables. The window functions just described will be correspondingly modified, mainly through the transfer functions $\mathcal{T}_\delta(k, z)$ and $\mathcal{T}_{\Psi_W}(k, z)$, which encode the evolution of density perturbation and lensing potential, respectively. Modifications of the growth also affect the growth factor $D(z)$ entering the IA contribution to the power spectra. As discussed in Section 1.2.2, their analytic forms are too complicated to give explicitly, so that they are computed, once again, through the Einstein-Boltzmann solver code EFTCAMB [89, 90]. We also use the same code to produce the angular power spectra described in this section.

Finally, we model the distribution of sources (src) in each redshift bin as

$$n^i_{\rm src}(z) = \frac{dn_{\rm src}}{dz}\left[{\rm Erf}\left(\frac{z - z^i_-}{\sqrt{2}\sigma^{\rm src}_z(z)}\right) - {\rm Erf}\left(\frac{z - z^i_+}{\sqrt{2}\sigma^{\rm src}_z(z)}\right) \right], \qquad (3.11)$$

with src $= [{\rm g}, {\rm GW}]$, z^i_- and z^i_+ the lower and upper limits of the i-th bin, $\sigma^{\rm src}_z(z)$ the error on the redshift measurement for the considered source, and $dn_{\rm src}/dz$ is parameterised as

$$\frac{dn_{\rm src}}{dz} \propto \left(\frac{z}{z_0}\right)^2 \exp\left[-\left(\frac{z}{z_0}\right)^{3/2} \right]. \qquad (3.12)$$

The parameter z_0 entering Eq. (3.12), as well as the redshift error $\sigma^{\rm src}_z$ of Eq. (3.11), are survey dependent and we will specify them in the following Section (Sec. 3.4) where we introduce the surveys considered in this study.

In this Chapter, we focus on the GW lensing auto-correlation, $C^{\kappa_{\rm GW}\kappa_{\rm GW}}_\ell$, and its cross-correlations with galaxies, $C^{\kappa_{\rm GW}\delta}_\ell$ and $C^{\kappa_{\rm GW}\kappa_{\rm g}}_\ell$. Using the estimator in Eq. (3.5), we can see that

$$\langle \hat{\kappa}_{\rm GW}\delta_{\rm g} \rangle \simeq \sqrt{1+\Omega}\langle \kappa_{\rm GW}\delta_{\rm g} \rangle, \qquad (3.13)$$

$$\langle \hat{\kappa}_{\rm GW}\kappa_{\rm g} \rangle \simeq \sqrt{1+\Omega}\langle \kappa_{\rm GW}\kappa_{\rm g} \rangle, \qquad (3.14)$$

$$\langle \hat{\kappa}_{\rm GW}\hat{\kappa}_{\rm GW} \rangle \simeq (1+\Omega)\langle \kappa_{\rm GW}\kappa_{\rm GW} \rangle + N_{\rm GW} + N_z, \qquad (3.15)$$

where we have considered that the three sources of error $\{\epsilon_{\mathrm{GW}}, \epsilon_z, \epsilon_c\}$ are not correlated between themselves or with either the convergence or the contrast density field. To derive the equations above, we have neglected terms of third order or higher in the perturbations, introduced the noise's power spectra $N_{\mathrm{GW}} = \langle \epsilon_{\mathrm{GW}} \epsilon_{\mathrm{GW}} \rangle$ and $N_z = \langle \epsilon_z \epsilon_z \rangle$, and used that $\langle \epsilon_{\mathrm{GW}} \rangle = \langle \epsilon_z \rangle = 0$ when the average is performed over large volumes. Contrary, in general $\langle \epsilon_c \rangle \neq 0$, hence in a complete analysis the term should be included. However, this correction is typically small, and we will assume the noise to be dominated by other terms, that we model in Sec. 3.4.

3.4. Models, methodology and surveys specifications

This section provides details of the gravitational models on which we forecast constraints, as well as the details on the analysis we performed to obtain them.

3.4.1. Models

We forecast the constraining power of GW-WL, alone and in combination with galaxy clustering and WL, on the cosmological parameters. We investigate gravitational models belonging to the Horndeski class of theories and described by the action of Eq. (1.68). We work in the *designer* approach [90], by fixing the background expansion history to a choice for the DE equation of state w_{DE} as explained in Section 1.2.2, so that any EFT model is fully specified after assigning the EFT functions $\{w_{\mathrm{DE}}, \Omega, \gamma_1, \gamma_2\}$. We model the dark energy equation of state using the CPL parametrization [98, 99]

$$w_{\mathrm{DE}}(a) = w_0 + w_a(1-a) \tag{3.16}$$

as in Eq. (1.70). With this prescription, the continuity equation in Eq. (1.69), dictates that the background DE density evolves as

$$\rho_{\mathrm{DE}}(a) = \rho_{\mathrm{DE}}^0 \, a^{-3(1+w_0+w_a)} e^{-3w_a(1-a)}, \tag{3.17}$$

with $\rho_{\mathrm{DE}}^0 = \rho_{\mathrm{DE}}(a=1)$ its value today.

Then, we choose to parameterize the time dependencies of $\Omega(a)$ and $\gamma_2(a)$ as

$$\Omega(a) = \Omega_0 \frac{\rho_{\mathrm{DE}}}{\rho_{\mathrm{DE}}^0}, \qquad \gamma_2(a) = \gamma_2^0 \frac{\rho_{\mathrm{DE}}}{\rho_{\mathrm{DE}}^0}, \tag{3.18}$$

linking the modifications to ΛCDM to the DE energy density. This way, the effects of having $\Omega(a), \gamma_2(a) \neq 0$ become small in the early Universe, when matter or radiation are driving its expansion. Additionally, we set $\gamma_1 = 0$ for all models, given that it affects only negligibly linear perturbations in the range of our observables (see e.g. [289]). Based on these assumptions, we consider three scenarios:
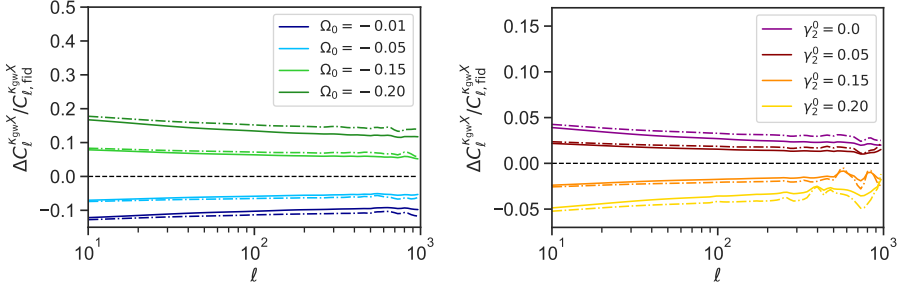
Figure 3.1: Relative deviations of the angular power spectrum, as a function of multipole ℓ for model M2. We plot in the left (right) panel how C_ℓ vary for different values of Ω_0 (γ_2^0), while keeping the remaining parameters fixed to their fiducial values in Table 3.1. The solid lines correspond to auto-correlations of GW-WL ($X = \kappa_{\mathrm{GW}}$), while the dashed lines is the cross-correlations of GW-WL with galaxy WL ($X = \kappa_g$).

- **ΛCDM:** we consider the EFT parameters fixed to reproduce the standard model, i.e. $w_0 = -1$ and $w_a = \Omega_0 = \gamma_2^0 = 0$. Consequently, the set of free parameters consists of $\{\Omega_{\mathrm{CDM}}^0, \Omega_{\mathrm{b}}^0, h, n_{\mathrm{s}}, \sigma_8\}$: the CDM and baryonic relative energy densities at present time, the reduced Hubble constant $h = H_0/100$, the spectral index of the primordial power spectrum, and the amplitude of the linear matter power spectrum measured at $8/h\,\mathrm{Mpc}$, respectively.

- **Model I (M1):** we fix $\gamma_2^0 = 0$; thus, the cosmology is specified by the parameters of ΛCDM plus $\{w_0, w_a, \Omega_0\}$. This model is representative of the Generalized Brans-Dicke class: with a non-minimal coupling, but no derivative interaction ($\gamma_2^0 = 0$).

- **Model II (M2):** we fix $w_0 = -1.05$ and $w_a = 0$; thus, the cosmology is specified by the parameters of ΛCDM and $\{\Omega_0, \gamma_2^0\}$. This model is representative of the class of kinetic gravity braiding models [290], where the conformal coupling and the derivative coupling are both allowed ($\Omega \neq 0$, $\gamma_2 \neq 0$).

We sketch the impact of the EFT parameters on the $C^{XY}(\ell)$ in Figure 3.1, where we plot the relative difference $(C_\ell^{\kappa_{\mathrm{GW}}X} - C_{\ell,\mathrm{fid}}^{\kappa_{\mathrm{GW}}X})/C_{\ell,\mathrm{fid}}^{\kappa_{\mathrm{GW}}X}$ adopting model M2 and choosing as baseline the cross-correlation computed in the fiducial cosmology. We plot curves for $X = \kappa_{\mathrm{GW}}$ (solid lines) and $X = \kappa_g$ (dashed lines) varying the value of Ω_0 in the left panel and γ_2^0 in the right panel, while all other parameters are kept fixed at the fiducial value (see Tab. 3.1). We observe that taking Ω_0 lower than the fiducial value acts to strengthen the signal, while values closer to zero (and hence, to the LCDM value for Ω_0) diminish the signal. On the contrary, higher values of γ_2^0 tend to dampen the signal, while values closer to 0 enhance it. We notice, however, that the correlations react more strongly to small variations in Ω_0 than to changes in γ_2^0. Indeed, the values chosen for the right panel of Figure 3.1 span the full range available to γ_2^0 in this model to ensure a stable theory, while causing only variations in the

cross-correlations of, at most, 5%.

3.4.2. Analysis method

To compute forecasts, we adopt the Fisher matrix formalism [288, 291], which allows us to obtain bounds on the free parameters of the analysis from the information matrix $\mathcal{F}_{\alpha\beta}$. Following [288], we define the Fisher matrix as

$$
\mathcal{F}_{\alpha\beta} = \sum_{\ell=\ell_{\min}}^{\ell_{\max}} \frac{2\ell+1}{2} \sum_{i,j,m,n} \sum_{A,B,C,D} \frac{\partial C_{ij}^{AB}(\ell)}{\partial\theta_\alpha} \left[K^{-1}(\ell)\right]_{jm}^{BC} \frac{\partial C_{mn}^{CD}}{\partial\theta_\beta} \left[K^{-1}(\ell)\right]_{ni}^{DA}, \tag{3.19}
$$

where α and β run over the set of free cosmological parameters θ, while A, B, C and D run over the density and convergence fields $[\delta_g, \kappa_g, \hat{\kappa}_{GW}]$ and finally i, j, m and n run over all unique pairs of tomographic bins. By the Cramer-Rao inequality, the lower bound on the standard deviation for the parameter θ_α is

$$
\sigma_\alpha = \sqrt{\Sigma_{\alpha\alpha}} \quad \text{with} \quad \Sigma_{\alpha\alpha} \equiv [\mathcal{F}^{-1}]_{\alpha\alpha}. \tag{3.20}
$$

To compute our matrices we use `CosmicFish` [292, 293][1], that we extended to include GW weak lensing. The covariance matrix K is defined as

$$
K^{A_i B_j}(\ell) = \frac{C^{A_i B_j}(\ell) + N^{A_i B_j}(\ell)}{\sqrt[4]{f_{\text{sky}}^A f_{\text{sky}}^B}}, \tag{3.21}
$$

where f_{sky}^A is the sky fraction covered by the detector measuring the observable A, and N_{ij}^{AB} the noise of the correlation considered, which we model as

$$
N^{\delta_i \delta_j}(\ell) = \frac{1}{\bar{n}_g^i} \delta_{ij}, \tag{3.22}
$$

$$
N^{\kappa_g^i \kappa_g^j}(\ell) = \frac{\sigma_\epsilon^2}{\bar{n}_{\kappa_g}^i} \delta_{ij}, \tag{3.23}
$$

$$
N^{\kappa_{GW}^i \kappa_{GW}^j}(\ell) = \frac{1}{\bar{n}_{GW}^i} \left(\frac{\sigma_{d_L}^2}{d_L^2} + \frac{\sigma_s^2}{d_L^2}\right) e^{\frac{\ell^2 \theta_{\min}^2}{8\ln 2}} \delta_{ij}, \tag{3.24}
$$

where δ_{ij} is the Kronecker delta and $\bar{n}_A^i$ is the number of sources in the i-th redshift bin for the probe A. We assume also that the noises of different probes are uncorrelated. In the equations above, σ_ϵ represents the intrinsic ellipticity affecting shear measurements, σ_{d_L} represents the average experimental error on the luminosity distance of the GW sources, while $\sigma_s = (\partial d_L/\partial z)\sigma_z^{GW}$ is the contribution to the luminosity distance error brought by the uncertainty on the merger redshift σ_z^{GW}, where the propagation is obtained assuming a fiducial cosmology. Lastly, $\theta_{\min}$ is the sky-localization area of the GW event, which also dictates the maximum available multipole for the analysis.

---

[1]`CosmicFish` is publicly available at https://cosmicfish.github.io/.

Model	h	$\Omega_{m,0}$	$\Omega_{b,0}$	n_s	σ_8	w_0	w_a	Ω_0	γ_2^0
ΛCDM	0.6774	0.31	0.05	0.9667	0.8159	(-1.0)	(0.0)	(0.0)	(0.0)
Model I	0.6774	0.31	0.05	0.9667	0.8159	-1.1	-0.05	-0.1	(0.0)
Model II	0.6774	0.31	0.05	0.9667	0.8159	(-1.05)	(0.0)	-0.1	0.1

Table 3.1: Fiducial values for the parameters of the cosmological models considered. Round brackets around a value mean that the corresponding parameter is kept fixed during the Fisher analysis, while the remaining are constrained simultaneously. In addition, we also let the galaxy bias in each bin and the IA parameters free to vary, for which we use the same fiducial values as [288].
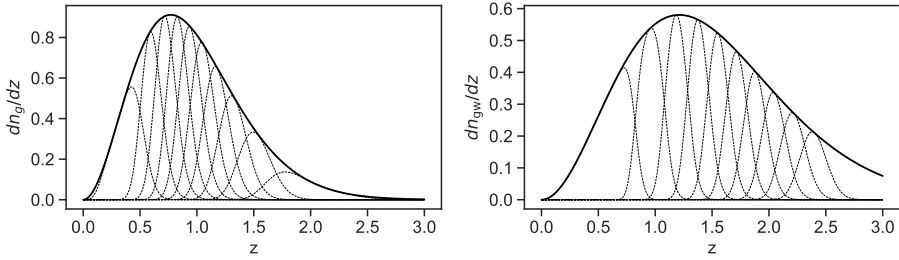
Figure 3.2: Normalized redshift distribution of galaxies and bright GW sources (left and right panel respectively). The dashed lines illustrate the redshift binning applied in our analysis.

3.4.3. Galaxy and GW surveys

We use the specifications of [288], as representative of a Stage IV galaxy survey, for the galaxy distribution in Eq. (3.12), and the fraction of sky observed. We instead take a simpler approach for the photometric redshift error, using Eq. (3.11) with $\sigma_z^{\mathrm{g}} = 0.03(1 + z)$, from which we obtain the distribution of sources in ten equipopulated redshift bins with $z \in [0, 2.5]$. We use a minimum multipole $\ell_{\min} = 10$ for both galaxy clustering and weak lensing, while fix the maximum multipole to $\ell_{\max}^{\mathrm{GC}} = 750$ for the former and $\ell_{\max}^{\mathrm{WL}} = 1000$ for the latter, in line with the "pessimistic" scenario of [288], but with the further limitation in the weak lensing multipoles because of the lack of a consolidated recipe to deal with non-linearities in the Horndeski theory (1.62).

Concerning the GW survey, we opt for $z_0 = 1.5$ for the GW source distribution in Eq. (3.12): this way Eq. (3.12) is compatible with both the forecasts of [277] for LISA luminous massive black hole binaries, and of [273] for the binary neutron stars observed by a network of ET in combination with two CE detectors. The reason for choosing this parametrization is the attempt of remaining as detector a-specific as possible, while still modeling the sources' distribution to mimic forecasted future observations. As we match it to distributions of mock observed events, our source distribution automatically accounts for possible selection effects of both GW and EM detectors. As in the case of galaxies, we consider $z \in [0, 2.5]$ and bin the GW sources

in ten equipopulated redshift bins. We also explore different binning choices: we consider the cases with only eight and six equipopulated bins. We observe a very small deterioration in the cosmological constraints when decreasing the number of tomographic bins, as larger bins tend to smooth out the lensing signal, as we show in Section 3.5.3. However, our conclusions on the impact of GW-WL on the constraining power remains the same regardless of binning, thus in what follows we will report results only for the most favorable choice of 10 bins.

The main quantities that can impact the weak lensing estimation from bright GW sources are the uncertainty on the luminosity distance, the error on the source redshift and the total number of bright GW events. The peculiar velocity correction for sources at high redshift are going to be a less significant contamination [224]. We consider several possibilities for the total number of detected GW events, $N_{\rm GW}$, ranging from 10^3 to 10^6, while we vary the average precision on the luminosity distance, σ_{d_L}/d_L, from 10% down to 0.5%. We assume that the GW sources have an electromagnetic counterpart (or an identifiable host galaxy), whose redshift is measured either photometrically, with error $\sigma_z^{\rm GW} = 0.03(1+z)$, or spectroscopically, with error $\sigma_z^{\rm GW} = 0.0005(1+z)$ [79, 125]. In Figure 3.2 we show the normalized source distribution of galaxies (left panel) and bright GW events (right panel) adopted in this analysis, together with a representation of the redshift binning that is applied, and we summarize the specifications considered for galaxy and GW surveys in Table 3.2.

Since we are focusing on bright sirens, in Eq. (3.24) we set $\theta_{\rm min} = 0$, thus implying that the event is perfectly localized by identifying the EM counterpart. On the other hand, in our analysis we truncate the summation in Eq. (3.19) at $\ell_{\rm max} = 1000$ to match the limiting multipoles of the galaxy survey, which is equivalent to limit angular scales to $\theta_{\rm min} \sim 11\,{\rm arcmin}$. Going up to larger $\ell_{\rm max}$ would result in an enhancement of the signal-to-noise ratio. This on one hand would imply tighter constraints on cosmological parameters when all sources are combined. At the same time, though, the GC and WL signal themselves would benefit from the accessibility of higher multipoles, resulting in tighter galaxy-only constraints to begin with. Thus, we can expect that, qualitatively, the impact of GW on the galaxy bounds remains similar even if higher multipoles are accessible.

3.5. Results

Using the specifications, models and methodology described in Sec. 3.4, we include in the Fisher matrix the contributions from all correlators C_ℓ^{XY} with X and Y in $[\delta_{\rm g}, \kappa_g, \hat{\kappa}_{\rm GW}]$, to explore the joint constraining power of GW-WL and galaxy surveys over cosmological parameters. We collect the fiducial values chosen for the parameters of the different models in Tab. 3.1, which are compatible with current bounds [4, 289]. Additionally, we choose the fiducial cosmology in such a way that

Galaxy Clustering						
$f_{\text{sky}}^{\text{g}}$	σ_z^{g}	-	z_0	$\bar{n}_g$ [arcmin^{-2}]	$\ell_{\min}$	$\ell_{\max}$
0.35	$0.03(1+z)$		$0.9/\sqrt{2}$	30	10	750
Galaxy Weak Lensing						
$f_{\text{sky}}^{\kappa_{\text{g}}}$	σ_z^{g}	σ_ϵ	z_0	$\bar{n}_{\kappa_{\text{g}}}$ [arcmin^{-2}]	$\ell_{\min}$	$\ell_{\max}$
0.35	$0.03(1+z)$	0.3	$0.9/\sqrt{2}$	30	10	1000
Bright GW Weak Lensing						
$f_{\text{sky}}^{\kappa_{\text{GW}}}$	σ_z^{GW}	$\sigma_{d_L}/d_L(\%)$	z_0	N_{GW}	$\ell_{\min}$	$\ell_{\max}$
1	$0.03(1+z)$ $0.0005(1+z)$	$\in [0.5,10]$	1.5	$\in [10^2, 10^6]$	10	1000

Table 3.2: Parameters of the noises (Eqs. (3.22), (3.23) and (3.24)) and binned source distributions (Eq. (3.11)) of the probes considered.

the parameters' values fall within the stable region of the models considered (identified via the stability sampler of EFTCAMB) and that the numerical derivatives, needed to obtain the Fisher matrices (3.19), can be performed without exiting this region.

To account for degeneracies, we vary all together the highest number of parameters possible, in each model, as described in Table 3.1. If a probe is not particularly sensitive to a certain parameter, if it is let free to vary, we marginalize over it instead of considering it fixed to its fiducial value. This is the case, for instance, of weak lensing: it is mostly sensitive to Ω_{CDM} and σ_8, and doesn't depend much on other parameters such as the baryons' abundance. In addition, we always let free to vary the galaxy bias in each bin b_{g}^i and the IA parameters A_{IA}, β_{IA} and η_{IA}, for which we use the same fiducial values as [288].

3.5.1. Lambda CDM

Let us start with the ΛCDM scenario. In Figure 3.3 we show the marginalized 1σ relative bounds obtained on Ω_{CDM}^0 and σ_8 varying the total number of GW observations, N_{GW}, and the luminosity distance precision σ_{d_L}/d_L. The first row shows the results considering photometric observations of the electromagnetic counterparts or of the GW host galaxy, while the second row assumes spectroscopic observations. For photometric observations, we notice that the bounds on both Ω_{CDM}^0 and σ_8 do not change for about half of the configurations considered (yellow regions in the plots), regardless of the choices made for the GW sector. In these regions, the bounds on cosmological parameters are strongly dominated by galaxies, contributing almost entirely to the constraining power. The black line marks the point
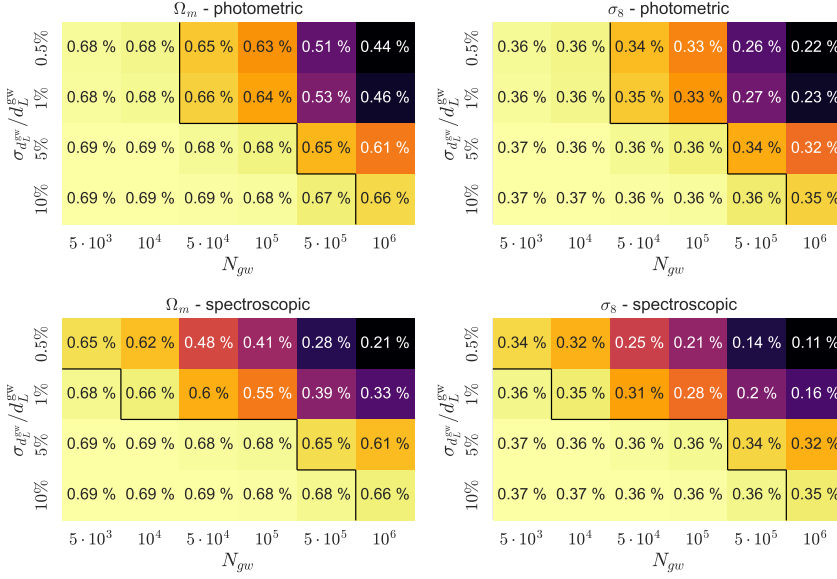
Ω_m - photometric

$\sigma_{d_L^{\mathrm{gw}}}/d_L^{\mathrm{gw}}$	$5\cdot10^3$	10^4	$5\cdot10^4$	10^5	$5\cdot10^5$	10^6
0.5%	0.68 %	0.68 %	0.65 %	0.63 %	0.51 %	0.44 %
1%	0.68 %	0.68 %	0.66 %	0.64 %	0.53 %	0.46 %
5%	0.69 %	0.69 %	0.68 %	0.68 %	0.65 %	0.61 %
10%	0.69 %	0.69 %	0.69 %	0.68 %	0.67 %	0.66 %

σ_8 - photometric

$\sigma_{d_L^{\mathrm{gw}}}/d_L^{\mathrm{gw}}$	$5\cdot10^3$	10^4	$5\cdot10^4$	10^5	$5\cdot10^5$	10^6
0.5%	0.36 %	0.36 %	0.34 %	0.33 %	0.26 %	0.22 %
1%	0.36 %	0.36 %	0.35 %	0.33 %	0.27 %	0.23 %
5%	0.37 %	0.36 %	0.36 %	0.36 %	0.34 %	0.32 %
10%	0.37 %	0.37 %	0.36 %	0.36 %	0.36 %	0.35 %

Ω_m - spectroscopic

$\sigma_{d_L^{\mathrm{gw}}}/d_L^{\mathrm{gw}}$	$5\cdot10^3$	10^4	$5\cdot10^4$	10^5	$5\cdot10^5$	10^6
0.5%	0.65 %	0.62 %	0.48 %	0.41 %	0.28 %	0.21 %
1%	0.68 %	0.66 %	0.6 %	0.55 %	0.39 %	0.33 %
5%	0.69 %	0.69 %	0.68 %	0.68 %	0.65 %	0.61 %
10%	0.69 %	0.69 %	0.69 %	0.68 %	0.68 %	0.66 %

σ_8 - spectroscopic

$\sigma_{d_L^{\mathrm{gw}}}/d_L^{\mathrm{gw}}$	$5\cdot10^3$	10^4	$5\cdot10^4$	10^5	$5\cdot10^5$	10^6
0.5%	0.34 %	0.32 %	0.25 %	0.21 %	0.14 %	0.11 %
1%	0.36 %	0.35 %	0.31 %	0.28 %	0.2 %	0.16 %
5%	0.37 %	0.36 %	0.36 %	0.36 %	0.34 %	0.32 %
10%	0.37 %	0.37 %	0.36 %	0.36 %	0.36 %	0.35 %

Figure 3.3: Marginalized 1σ relative confidence bounds for Ω_{CDM}^0 (left panel) and σ_8 (right panel) in ΛCDM. Top row: bright sirens with photometric redshift determination. Bottom row: similar with spectroscopic error. In all tables, bounds are derived from the combination of GW weak lensing, galaxies weak lensing and galaxy clustering, for different values of N_{GW} and $\sigma_{d_L^{\mathrm{GW}}}/d_L^{\mathrm{GW}}$.

at which GW events start to weight in significantly: about 5×10^5 bright sources with luminosity distance determined at least at 1% precision, or 10^6 sources with luminosity distance determined at 5% precision, or better, are necessary to witness a significant impact of GW-WL on the constraints already placed by galaxy probes. Similar considerations can be drawn for the spectroscopic case: GW becomes competitive with galaxies only for $N_{\mathrm{GW}} \geq 10^5$ for $\sigma_{d_L^{\mathrm{GW}}}/d_L^{\mathrm{GW}} \leq 1\%$ (or $N_{\mathrm{GW}} \geq 10^6$ for $\sigma_{d_L^{\mathrm{GW}}}/d_L^{\mathrm{GW}} \leq 5\%$). We can though recognize the reduced noise affecting GW lensing in the overall better performance of the spectroscopic sirens: for all configurations in which GW contributes significantly to the constraining power, spectroscopic sources always provide bounds up to 0.1% tighter than the photometric ones. For example, the 0.7% ($\sim 0.4\%$) bound placed on Ω_{CDM}^0 (σ_8) by galaxies can be reduced to 0.45% (0.2%) by factoring in the contribution of 10^6 photometric sirens measured with $\sigma_{d_L^{\mathrm{GW}}}/d_L^{\mathrm{GW}} = 1\%$, and further shrinked to $\sim 0.3\%$ (0.15%) considering instead the same number of spectroscopic events. Although we do not reproduce them here, we have performed the same analysis for the other free ΛCDM parameters, finding a similar behavior regarding the constraints on n_{s} (see also Figure 3.4). However, the impact of GW-WL on the constraints of h and Ω_b, remains mild for all configurations explored, since GW-WL is not particularly sensitive to those parameters.
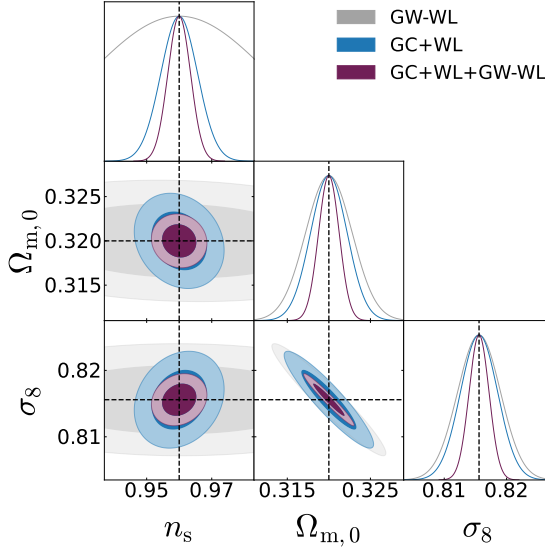
Figure 3.4: Marginalized forecasts for ΛCDM parameters. We fix $N_{\mathrm{GW}} = 5 \cdot 10^5$, $\sigma_{d_L^{\mathrm{GW}}}/d_L^{\mathrm{GW}} = 1\%$ and red-shift information with spectroscopic error. Constraints come from GW weak lensing only (grey), galaxies WL and clustering (blue), and their combination (dark red).

In Figure 3.4 we show the triangular plots for three free parameters of ΛCDM, after having marginalized over h and Ω_b. In order to understand the extent of the impact of GW-WL, we opt for the scenario in which $N_{\mathrm{GW}} = 5 \cdot 10^5$ are detected with a precision of 1% on their luminosity distance measure and with a spectroscopic determination of the redshift. We plot bounds obtained considering GW-WL only, GC and galaxies WL, and the joint contribution of galaxy surveys and GW-WL. In the spectroscopic case, the GW-WL constraints on $\Omega_{m,0}$ and σ_8 are comparable with those coming from galaxies, and they halve when all probes are combined, also thanks to the reduced impact of nuisance parameters. On the contrary, GW-WL alone is not able to constrain n_s. When considering the probes all together, the bounds on σ_8 and Ω_{CDM}^0 shrink, breaking also the mild degeneracy that exists in the galaxy-only constraints between the couple of parameters $(n_s, \Omega_{\mathrm{CDM}}^0)$ and (n_s, σ_8). The net result is a strong reduction also of the bound on n_s. The analysis performed above shows that GWs, valuable because they provide independent measurements of the cosmological parameters, can improve the constraints induced by the other galaxy-related probes only if their statistical power (in terms of number of events and detection precision), is comparable with those of a galaxy survey. Indeed, in ΛCDM where the non-minimal coupling $\Omega(a) = 0$, the estimator in Eq. (3.4) corresponds to the same convergence measured by galaxy surveys. Hence, GW-WL and its cross-correlations with galaxies contributes to the constraining power only by effectively strengthening the WL statistics, in the case of the standard cosmological model.
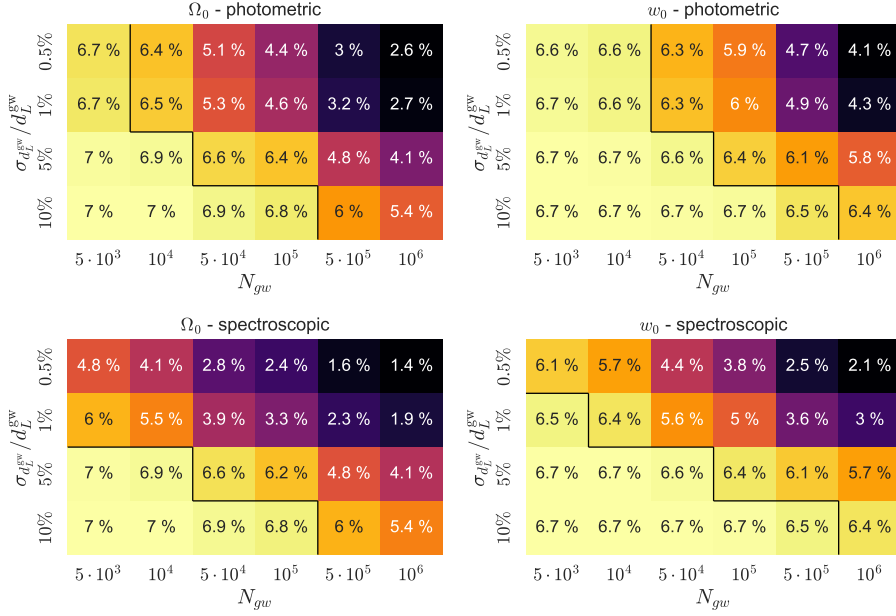
Figure 3.5: Marginalized 1σ confidence bounds on Ω_0 and w_0 parameters of Model I, obtained from combining GW weak lensing with galaxy weak lensing and clustering. We assume that all GW sources have a photometric (top panels) or spectroscopic (bottom panels) redshift determination.

3.5.2. Dark Energy models

We not turn our attention to Model I and Model II. In both cases, the estimator (3.4) receives explicit contributions from the conformal coupling $\Omega(a)$, making GW-WL effectively different from the corresponding galaxy probe. As before, we vary N_{GW}, $\sigma_{d_L^{\text{GW}}}/d_L^{\text{GW}}$ and the error on the sources' redshift determination σ_z. For each combination, we compute the Fisher forecasts on the cosmological parameters, including all options of the kind C_ℓ^{XY}, $X, Y \in [\delta_g, \kappa_g, \hat{\kappa}_{\text{GW}}]$.

In Figure 3.5 we show the marginalized 1σ bounds on Ω_0 and w_0 in M1, for the case of photometric (top row) and spectroscopic (bottom row) redshifts. Similarly to Figure 3.3, in the regions below the black line, the constraining power is mainly due to galaxy-probes. Contrary to ΛCDM, because of the definition of $\hat{\kappa}_{\text{GW}}$ in Eq. (3.4), GW become more impactful for less daring configurations of N_{GW} and $\sigma_{d_L^{\text{GW}}}/d_L^{\text{GW}}$. In the case of photometric redshift, 5×10^4 GW sources determined with $\sigma_{d_L^{\text{GW}}}/d_L^{\text{GW}} \leq 1\%$ are already sufficient to detect a tightening of the constraints on w_0 and Ω_0. In the case of spectroscopic redshift information, for every value of N_{GW}, there is at least one setup in which GWs improve the constraining power.

Figure 3.6 shows analogous tables for Ω_0 and γ_2^0 in the M2 case. Here, galaxy-
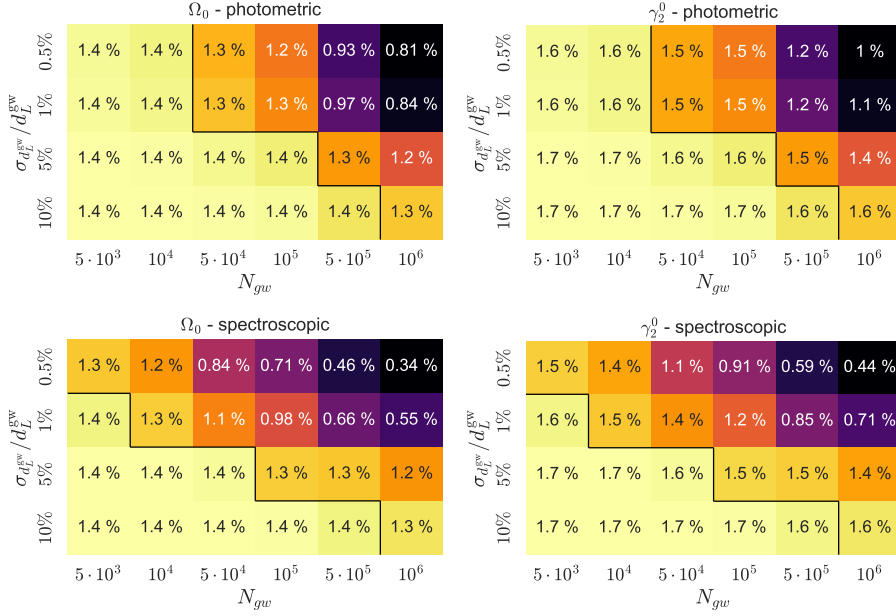
Figure 3.6: Marginalized 1σ confidence bounds on MG parameters obtained from combining GW weak lensing with galaxy weak lensing and clustering. We consider bright sirens and vary the number of GW detections N_{GW} and the precision on the luminosity distance determination σ_{d_L}. Bounds are reported for the parameters Ω_0 and γ_2^0 in our M2 model in the assumption that all GW sources will have a photometric (top panels) or spectroscopic (bottom panels) counterpart.

dominated constraints are tighter on the parameters than in the M1 case as $\{w_0, w_a\}$, affecting the background, are kept fixed. This allows for an overall easier determination of the value of the EFT functions today, which in turn requires higher N_{GW} for GW-WL to have an impact on cosmological bounds. In the photometric scenario, about $10^5 - 10^6$ sources are required to reach % and sub-% level precision on Ω_0, while the number drops to $N_{\mathrm{GW}} \sim 10^4 - 10^5$ in the spectroscopic case. In the photometric and spectroscopic cases, large enough statistics allows determining both parameters at the % and $\sim 0.4\%$ level.

In Figure 3.7 we report the triangular plots with marginalized constraints for some of the parameters of M1 (left panel) and M2 (right panel). We opt for the scenario in which $5 \cdot 10^5$ GW events are detected with a spectroscopic bright counterpart and their luminosity distance is determined at 1% accuracy. The left panel of Figure 3.7 highlights that the GW-only contours are still remarkably wide with respect to the galaxy ones. We show this more evidently in the left panel of Figure 3.8, where we plot the GW-WL only constraints in gray compared to the GC+WL constraints in blue.

The reason behind this, that GW-WL alone is not a good probe to constrain the DE
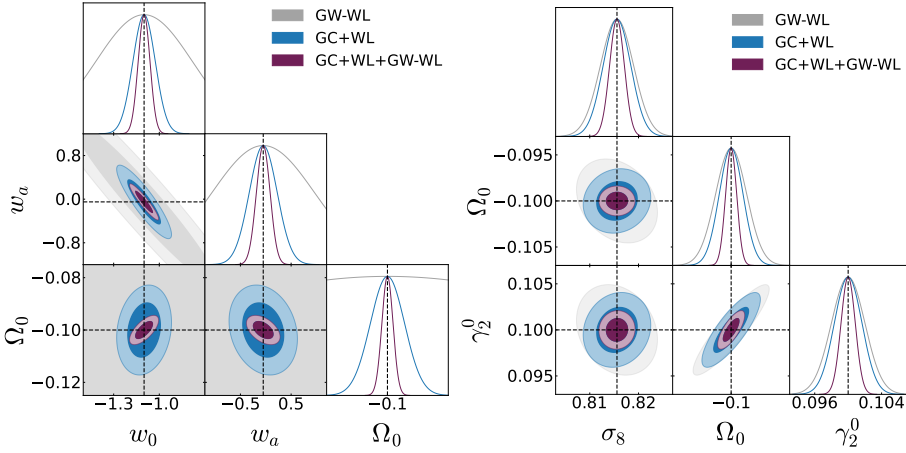
Figure 3.7: Marginalized forecasts for the MG parameters of model M1 (left panel) and M2 (right panel) in an idealistic scenario where $5 \cdot 10^5$ GWs events are detected with a bright counterpart measured spectroscopically, and luminosity distance measured with 1% precision. Constraints come from GW weak lensing only (gray), galaxies WL and clustering (blue), and GW and galaxy probes combined, including cross-correlations between the probes (purple).

equation of state, and the poor determination of w_{DE} leaves the coupling evolution unconstrained (see Eq. (3.18)), resulting in very loose bounds on Ω_0. Regardless of this, the combined GW+galaxy constraints (dark red contours in Figure 3.7) on the EFT parameters of M1 are narrower than the galaxy-only bounds. This increase of constraining power must come from the cross-correlations $C_\ell^{\kappa_{\mathrm{GW}}\delta}$ and $C_\ell^{\kappa_{\mathrm{GW}}\kappa_{\mathrm{g}}}$, as it can be seen in the right panel of Figure 3.8, where we compare the marginalized bounds of the galaxies with the contours obtained including only GW-WL and its two cross-correlations with the galaxy fields (GW-WL+XC, brown contours). The joint power of GW-WL with, in particular, GC is breaking (or mitigating) the degeneracies in the DE parameters sector, shrinking the constraints. This confirms the essential role that GW-WL cross-correlations can have in impacting cosmological bounds.

As for model M2 (right panel in Figure 3.7) we see that constraints from GW-WL alone are much tighter than in M1: here w_0 and w_a are fixed so that their degeneracies with others EFT parameters are canceled. As the bounds are comparable with those coming from galaxies, we conclude that the role of GW-WL cross-correlations in this case is less significant, and the GW-WL auto-correlation already concurs to the overall constraining power. GW-WL intervenes, though, to break the mild degeneracies present in the GC+WL bounds between (Ω_0, γ_2^0) and σ_8. Accordingly, bounds on σ_8 are narrowed thanks to the GW contribution.

Note that in model I and II, the ΛCDM parameters $\{h, \Omega_{m,0}, \Omega_{b,0}, n_s, \sigma_8\}$ are still present. In both cases we find similar results to those of Section 3.5.1, i.e. $\mathcal{O}(10^5)$
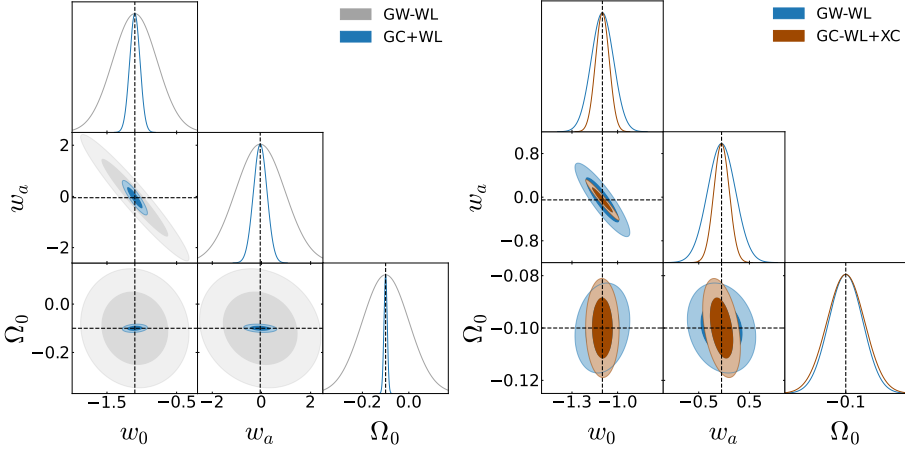
Figure 3.8: Comparison of the marginalized 1σ bounds on the MG parameters of M1. We consider the same setup of Figure 3.7, i.e. $N_{GW} = 5 \cdot 10^5$, $\sigma_{d_L} = 1\%$ and spectroscopic counterparts. In both panels, the blue contours represent bounds placed through GC+WL only, matching the same blue contours of the left panel of Figure 3.7. In the left panel, these are compared with GW-WL-only bounds, zooming out with respect to Figure 3.7 to include the full extent of the grey contours. In the right panel instead, the blue contours are confronted with bounds obtained considering only the auto-correlation of GW-WL and its cross-correlations with galaxies (brown regions), while not including GC+WL auto and cross-correlations.

or more GW sources are needed to even to impact significantly the bounds placed on those by galaxies alone, $\mathcal{O}(10^6)$ in the case of h and Ω_b. For a better comparison of the results obtained with different setups, we consider a Figure of Merit (FoM)

$$\text{FoM} = \det(\mathcal{F}_{\alpha,\beta})^{\frac{1}{2N}} \, , \tag{3.25}$$

where $\mathcal{F}_{\alpha,\beta}$ is the Fisher matrix of Eq. (3.19) marginalized over the bias and IA noise parameters, and N is the total number of parameters of the model [294]. The FoM is the 2N-th root of the product of the Fisher matrix eigenvalues, so it is inversely proportional to the volume of the N-dimensional ellipsoid delimiting the 1σ confidence region in the parameter space. The FoM thus allows us to investigate and quantify how the volume of the bounds in the parameter space is reduced when, for example, the statistics of the GW's event is increased. We compute the FoM (see Figure 3.9) for the Fisher matrices (3.19) of models M1 and M2, including all auto and cross-correlations of GW-WL, GC and galaxy WL and for all scenarios explored above in terms of N_{GW} and σ_{d_l}. We also considered separately the cases in which GW events redshifts are determined photometrically or spectroscopically. From Figure 3.9, considering the photometric cases (top row), we see that FoM start increasing significantly from $N_{GW} = 5 \times 10^4$ for all choices of σ_{d_L}, though it performs significantly better for $\sigma_{d_L} \leq 1\%$. The small difference between the curves for $\sigma_{d_L} \leq 1\%$ and $\sigma_{d_L} \leq 0.5\%$ suggests that the photometric redshift error is starting to dominate the correlation noise in Eq. (3.24): improving the d_L measurement of photometric
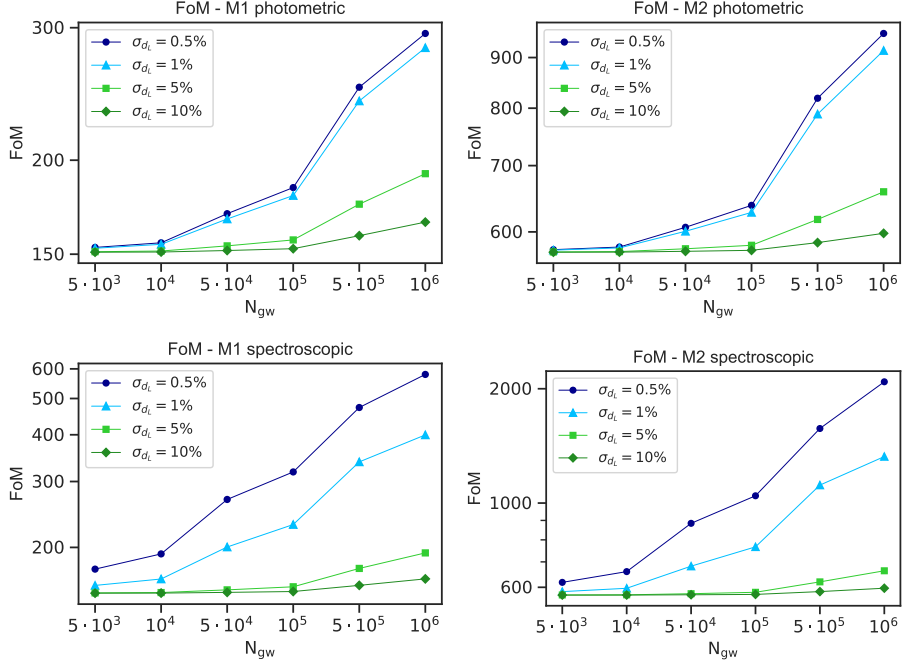
Figure 3.9: Figures of merit for different numbers of total detected events N_{GW} and several choices of $\sigma_{d_L^{\text{GW}}}/d_L^{\text{GW}}$. The top row displays results considering a spectroscopic redshift determination, while the bottom row those in case of photometric error. The left panels refer to M1, while the right panels to M2.

events beyond the 1% accuracy level only implies a minor increase in the GW-WL constraining power, and one should opt in maximizing the number of detections. On the contrary, because the redshift error is lower, for spectroscopic events the correlation noise remains dominated by σ_{d_L}, and improvements to the FoM happen for every choice of the latter. The FoM for model M1 are, in general, much lower than those of M2. This reflects our previous considerations on how placing tight constraints on model M1 is more difficult, because the EFT functions on M1 have higher freedom as their time evolution is not fixed, and there are higher degeneracies between the EFT parameters.

3.5.3. Impact of GW binning

To investigate the role of binning, we compare the FoM also for different configurations of their choice, for different values of N_{GW} and relative error on the luminosity distance measure. More in details, we consider 6, 8 and 10 equipopulated tomographic bins as described in Section 3.4.3. The results are reported in Figure 3.10, where we plot the ration of the FoM for all observational scenarios in the case of 6

bins (left panel), and 8 bins (right panel), over the configuration with 10 bins, i.e. FoM_n/FoM_{10}. Reducing the number of bins, in all cases, implies a lower FoM so a deterioration of the constraints on the cosmological parameters: decreasing the bins number, and thus increasing the bins size, has the effect of smoothing out the correlation signal in any given bin. This effect is compensated by a greater number of events falling in each bin, that attenuates the correlation noise of Eq. (3.24). In general, the FoM depends mildly on the number of bins. Higher deviations occur for higher numbers of detected events and better accuracy on the luminosity distance measurement, though we notice that even in the most extreme case of 6 tomographic bins and 10^6 GW events with d_L detected at 1% accuracy, FoM_6 is lower than FoM_{10} only of $\sim$ 1%. Therefore, our choice of 10 bins for the GW sources does not affect significantly the results presented previously.
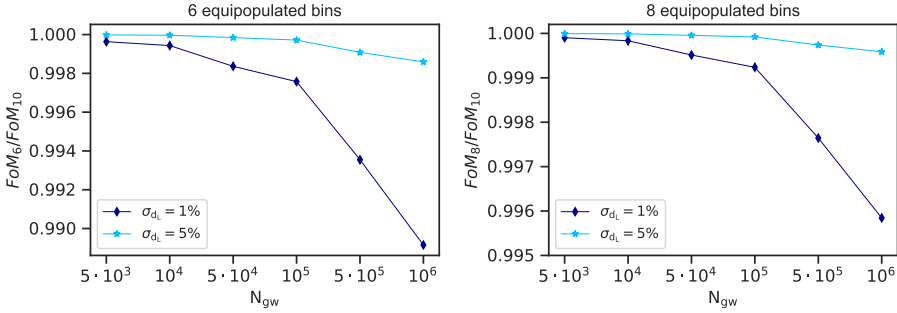
Figure 3.10: Ratio $FoM_{[6,8]}/FoM_{10}$ of the FoM computed binning the GW sources in 10 equipopulated tomographic bins and the FoM obtained for the same configurations in terms of number of GW sources N_{GW} and percentage uncertainty on the luminosity distance σ_{d_L}, but with a different number of bins (6 and 8 in the left and right panel respectively). The results regard the model M1.

3.6. Discussion and Conclusions

In this Chapter, we focused our attention to the weak-lensing signature on the estimates of the GW luminosity distances in Eq. (1.112), using it as a signal to investigate gravity on cosmological scales. We built the estimator $\hat{\kappa}_{GW}$ in Eq. (3.4), as a proxy for the GW-WL field, which we will be able to extract from detections of sources at high-enough redshift ($z \gtrsim 0.5$), where WL is the main relativist effect. This estimator, in the case of DE theories with a running Planck's mass, receives a contribution from the conformal coupling, making it even more interesting in the context of tests of the standard cosmological model. When focusing exclusively on ΛCDM, GW-WL can still provide an important information channel to constrain the cosmological parameters, as the contribution of GW increases the WL statistics. We have explored extensively the cross-correlations between $\hat{\kappa}_{GW}$ and standard galaxy density fields δ_g and galaxy weak lensing κ_g, providing the observational requirements, in terms

of number of detected events and precision of each measurement, for future GW detectors to make stringent constraints on late time cosmological models, reaching beyond the limits that will be placed by the next generation of galaxy surveys. Focusing only on observations with a redshift information, we also distinguished the cases for which this is known with a photometric or spectroscopic measure.

We find that in the ΛCDM case, GW-WL starts to improve on galaxy-only constraints on σ_8 and Ω_{CDM}^0 if at least $\mathcal{O}(10^5)$ events are detected. When the DE parameter space is included, the situation becomes model dependent, as different EFT parameters can break (or not) different degeneracies. This is the main difference between Model I and Model II: WL alone is not particularly sensitive to the late time expansion history, so that whenever w_{DE} is left free to vary (as in M1 compared to M2), the bounds on the conformal coupling today Ω_0 are very large, given also its parametrization in Eq. (3.18). Nevertheless, the degeneracy between $\{w_{\mathrm{DE}}, \Omega_0\}$ in WL is broken when introducing the cross-correlations with also galaxy WL and galaxy clustering. This means that the constraining power of M1 are boosted when considering these probes together, and more reasonable values of N_{GW} and $\sigma_{d_L^{\mathrm{GW}}}$ are needed, while those of M2 scale down in a less pronounced way only because of the increased statistics. The specific numbers of N_{GW} and $\sigma_{d_L^{\mathrm{GW}}}$ needed in order for the GWs to actively participate in the constraining power can be found in Tables 3.3, 3.5 and 3.6, for ΛCDM, M1 and M2 respectively. The forecasts presented in this Chapter can be improved, for instance, by considering the cross-correlation signal up to higher ℓ_{max}, provided that a solid method to treat non-linearities is available.

To put the presented numbers in perspective, the network detector network of Einstein Telescope and (one or two) Cosmic Explorer place the number of observed bright binary neutron stars at few thousands of events per year [18, 273, 295], with forecasted error on luminosity distance of about 10% [273, 295]. We must however remark that, according to the cited estimates, ET is not expected to reach the average $\sim 1\%$ accuracy on the luminosity distance determination required by our more promising setups (see e.g. Figs. 3.5 and 3.6), likely not even in combination with 2 CE detectors. An average accuracy over d_L of $\sim 10\%$ could still lead to improvements on the galaxy-only cosmological constraints, but in that case we found that, for this to happen, $O(10^6)$ GW sources are required. Stacking a large statistics of highly accurate GW events will be possible with proposed far future observatories like the space-based Big Bang Observer [26] and Advanced Laser Interferometer Antenna [245], expected to reach sub-percent precision in the determination of the luminosity distance and with a total number of detected events of several hundreds of thousands. These detectors are also expected to have a high angular resolution [26, 245], facilitating the task of finding an electromagnetic counterpart or the host galaxy, needed for the redshift.

In conclusion, we find that the cross-correlations of galaxies and GW-WL have the

potential to become, with time, crucial probes of cosmology, complementary to galaxy surveys and other cosmological observables. Where sufficient statistics is available, this new probe can both help tighten constraints and strongly reduce existing degeneracies between the EFT parameters.

Note: My scientific contribution to the work presented in this Chapter regards the theoretical aspects. I've also had a mentoring role, introducing the first author to EFTCAMB and writing the scripts employed in the first explorations of the work. In particular, we used the version of the code we updated for *Detecting Dark Energy Fluctuations with Gravitational Waves*, namely Chapter 2. I also contributed in writing the paper.

Part II

Ray-optics limit: distance duality relation and polarization tests

4

The gravitational waves' angular diameter distance

We analyze the propagation of high-frequency gravitational waves in scalar-tensor theories of gravity, with the aim of examining properties of cosmological distances as inferred from their measurements. By using symmetry principles, we first determine the most general structure of the GW linearized equations and of the GW energy momentum tensor, assuming that GW propagate at the speed of light. We then specialize to the case of GW propagating through a perturbed cosmological spacetime, deriving the expressions for the GW luminosity and angular diameters distances, proving the validity of the Etherington reciprocity law $d_L^{\mathrm{GW}} = (1+z)^2 d_A^{\mathrm{GW}}$. We find that, as in the case of the luminosity distance, also the GW angular diameter distance is explicitly modified compared to the electromagnetic one. We discuss implications of this result in the context of strong lensing time delay, showing that the effects of the scalar field representing dark energy compensate: lensed GW arrive at the same time as their lensed electromagnetic counterparts.

4.1. Introduction

Cosmologists use various different definitions of *distance* depending on the context and the observables they are interested in [296, 297]. While usually definitions make use of light detected from distant sources, GW offer new tools for measuring cosmological distances. We have already seen an example of GW distance in Section 1.4.2: using Eq. (1.104) one can infer the GW luminosity distance. This definition of $\bar{d}_L^{\text{GW}}(z)$ is simply given in analogy to the General Relativistic result (the GW's amplitude is inversely proportional to the luminosity distance), and it doesn't follow from rigorous definitions. The purpose of this Chapter is to formally derive the *gravitational waves cosmological distances*, in particular the *luminosity distance* in Section 4.5.2 and the *angular diameter distance* in Section 4.5.3, in a gravitational theory where dark energy is represented by a scalar field. Following early important works [197, 198, 204, 225, 234, 247], $d_L^{(\text{GW})}$ is being recognized as a key observable to independently measure cosmological parameters by means of GW, as well as testing scalar-tensor theories of gravity, as we have seen in Chapters 2 and 3. Here, we wish to draw some more general statements about GWs in scalar-tensor gravity models, relaxing also the cosmological background assumption, namely that the background metric is Eq. (1.14). To this extent, the high-frequency approximation is rather useful: as discussed in Section 1.3.2, we can define GWs without specifying the background line element. We use symmetries as a guiding principle, in particular generalized coordinate invariance, for characterizing the scalar-tensor system and the behavior of propagating degrees of freedom, without choosing a specific model. To disentangle tensor and scalar waves, generically coupled when the propagation is considered over arbitrary spacetimes, we assume that the properties of the GW at emission are identical to those of General Relativity, and we identify physically reasonable conditions to decouple the evolution equations of these different sectors. Focusing on the propagation of tensor modes, we work out their stress-energy tensor at second order, and define a covariant conservation of the *graviton number density current*, which we use to formally define the *Gravitational wave distances*, d_L^{GW} and d_A^{GW}, in scalar-tensor theories. The effects of a dynamical dark energy factorize into an overall multiplication factor.

Only after this general results, we focus on the case of cosmological perturbed spacetimes, and we prove the validity of the Etherington's reciprocity law

$$d_L^{\text{GW}} = (1+z)^2 \, d_A^{\text{GW}}, \tag{4.1}$$

within a scalar-tensor framework considered. Since this relation is at the basis for relating angular and luminosity distances in GW measurements, it is of crucial importance to understand whether it is valid or not in a general theory of gravity, for GW propagation on a general space-time. The definitions given in this Chapter are, of course, compatible with Eq. (1.104). Considering that d_L^{GW} can be modified

with respect to the distance inferred through an electromagnetic signal, as shown in Eq. (1.105), then the validity of Eq. (4.1) implies that also angular diameter distances are rescaled by the same factor, i.e.

$$d_A^{\text{GW}} = \frac{M_P(z)}{M_P(0)} \, d_A^{\text{EM}} \, . \tag{4.2}$$

Finally, we investigate our results about $d_A^{(\text{GW})}$ in the context of strong lensing of GWs and their time delay, which depends on a combination of angular diameter distances [149]. Strong lensing of GW can be important in the future for providing alternative ways for determining cosmological parameters (see e.g. [298]). Since we are considering theories where GWs travel at the speed of light, these follow null-geodesics as photons, and we do not expect any different time delay between GW and EM signals. We show explicitly that this is the case in Section 4.5.5, where we rewrite the time delay formula, which is given in terms of the modified $d_A^{(\text{GW})}$, all in terms of the geometrical comoving distances.

4.2. Tensor and scalar waves

Even though we do not restrict ourselves to a specific Horndeski theory, we assume that the physical system under consideration derives from an action of the form

$$\mathcal{S} = \int d^4 x \sqrt{-g} \left(\frac{M_p^2}{2} R - \mathcal{L}(g_{\mu\nu}, \varphi) \right) , \tag{4.3}$$

where φ is the DE field. In Section 1.3.2, we addressed the subtle issue of defining the metric perturbation. In scalar-tensor theories, this problematic extends similarly also to the definition of the scalar field fluctuations, which we address here. The approach taken in this Chapter follows the definition of the field fluctuations typical of geometric optics techniques.

We base our considerations on a double perturbative expansion for the metric and the scalar field around quantities solving the background equations, as in [151, 152]. We expand metric and scalar fields as[1]

$$g_{\mu\nu}(t, \mathbf{x}) = \bar{g}_{\mu\nu}(t, \mathbf{x}) + \alpha \, h_{\mu\nu}(t, \mathbf{x}) , \tag{4.4}$$
$$\phi(t, \mathbf{x}) = \bar{\varphi}(t, \mathbf{x}) + \alpha \, \delta\phi(t, \mathbf{x}) , \tag{4.5}$$

and we are interested to study the dynamics of the metric and scalar perturbations $h_{\mu\nu}$ and $\delta\varphi$. We adopt the geometric optics arguments to define the field fluctuations: $h_{\mu\nu}$ and φ are small high-frequency fluctuations whose gradients are enhanced by a factor of ω with respect to the background. This parameter, defined

---

[1] Please note the notation: $\delta\phi$ corresponds to the scalar wave, while $\delta\varphi$ in, e.g., Eq. (1.110) is the large scale structure contribution of the DE clustering. To make this difference more apparent, we use two different expansion parameters: α and ϵ.

for the first time in Eq. (1.85), is given by

$$\frac{1}{\omega} = \frac{\lambda}{L} \ll 1,\tag{4.6}$$

controlling the ratio among the typical (small) wavelength λ of the high-frequency fields versus the (large) scale L of spatial variation of slowly-varying background quantities.

The general topic of identifying the propagating scalar and tensor degrees of freedom in theories such as (4.3) started in the classic papers [299, 300], considering a Minkowski background. It was then reconsidered, using a variety of methods, in [158, 182, 235, 281, 301] attempting to go beyond the flat hypothesis. The problem, technically speaking, arises because the generic background configuration $\{\bar{g}_{\mu\nu}, \bar{\varphi}\}$ allows for coupling between tensor and scalar modes and, thus, correctly identify their roles in the evolution equations can be subtle. The issue can be even more subtle in theories where scalar and metric fluctuations propagate with different speed, a phenomenon associated with spontaneous breaking of global Lorentz invariance by means, for instance, of a non-vanishing time-like or space-like gradient of the DE field. Note that these situations are the most interesting: they include cosmological and screenings settings. Here we develop a covariant approach to address the problem, more similar in spirit to the original works of Isaacson [151, 152], and to the effective field theory of inflation [82] and dark energy [86] (see e.g. [87] for a comprehensive review).

In our set-up, we assume to have an action in Eq. (4.3), invariant under generalized coordinate transformations, and that the background fields profile break spontaneously Lorentz symmetry, providing the preferred vector

$$v_\mu \equiv \partial_\mu \bar{\varphi}.\tag{4.7}$$

Under an infinitesimal spacetime translation, $x^\mu \to x^\mu + \xi^\mu$, the linearized fluctuations transform as

$$\begin{aligned} h'_{\mu\nu} &= h_{\mu\nu} - (\bar{\nabla}_\mu \xi_\nu + \bar{\nabla}_\nu \xi_\mu), & (4.8)\\ \delta\phi' &= \delta\phi - v^\mu \xi_\mu, & (4.9) \end{aligned}$$

for infinitesimal vector ξ_μ and where $\bar{\nabla}_\mu$ is the covariant derivative associated to $\bar{g}_{\mu\nu}$. In order to actively apply the transformation in Eq. (4.8) and have that $h'_{\mu\nu}$ is still a small (first order in α) and high-frequency (its gradient of order ω), we assume that ξ_μ is a high-frequency field too and that its size is reduced by a factor of ω^{-1} with respect to $h_{\mu\nu}$ [150],

$$\mathcal{O}(\xi_\mu) \sim \frac{1}{\omega}\mathcal{O}(h_{\mu\nu}) \sim \frac{\alpha}{\omega}.\tag{4.10}$$

The gradients acting on the high-frequency ξ_μ in Eq. (4.8), enhance their contributions by a factor $\mathcal{O}(\omega)$, so that the result is of order $\alpha \times \mathcal{O}(\omega^{-1}) \times \mathcal{O}(\omega) = \alpha \times \mathcal{O}(\omega^0)$, i.e. of the same order of $h_{\mu\nu}$.

We note that, because of the spontaneously broken background, i.e. $v_\mu \neq 0$, the gauge transformations in Eqs. (4.8) and (4.9) mix the metric and scalar perturbations, in the sense that a gauge fixing on one will affect also the other and vice-versa. Even if DE fluctuations are not produced at the source as we are assuming here (for example thanks to some screening mechanism), they can be generated by metric fluctuations that are travelling from source to detection. We then expect that propagation effects are able to excite scalar modes with an amplitude suppressed by a factor of $\mathcal{O}(\epsilon)$ with respect to metric fluctuations:

$$\mathcal{O}(\varphi) \sim \omega^{-1} \, \mathcal{O}(h_{\mu\nu}). \tag{4.11}$$

This assumption makes compatible Eqs. (4.10) and (4.9) ($v^\mu \xi_\mu$ is of order α/ω). In any case, understanding the extent of the implications of such assumption, and providing more formal arguments for all the considerations just illustrated, is the topic of Chapter 5.

4.2.1. Decomposing the metric fluctuation

Assuming a time-like v_μ, we introduce the vector

$$X_\mu \equiv \frac{v_\mu}{\sqrt{2X}}, \qquad \text{such that} \qquad X^\mu X_\mu = -1, \tag{4.12}$$

where $X \equiv -(v^\mu v_\mu)/2$. We decompose the gauge vector ξ_μ into its orthogonal and parallel components with respect to v_μ,

$$\xi_\mu = \xi_\mu^{(T)} + X_\mu \xi^{(S)}, \qquad \text{with} \qquad X^\mu \xi_\mu^{(T)} = 0. \tag{4.13}$$

From this definition, and Eq. (4.9), it is clear that $\delta\phi$ transforms only under transformations generated by $\xi^{(S)}$. We also introduce the quantity

$$\tilde{h}_{\mu\nu} \equiv h_{\mu\nu} + \bar{\nabla}_\mu H_\nu + \bar{\nabla}_\nu H_\mu, \qquad \text{with} \qquad H_\mu \equiv \frac{X_\mu}{\sqrt{2X}} \delta\phi. \tag{4.14}$$

Because of Eq. (4.11), the contributions to $\tilde{h}_{\mu\nu}$ are of the same order in the gradient expansion ω^{-1}, and it is easy to show that $\tilde{h}_{\mu\nu}$, transforms only under transformations generated by $\xi_\mu^{(T)}$ as

$$\tilde{h}'_{\mu\nu} = \tilde{h}_{\mu\nu} - \bar{\nabla}_\mu \xi_\nu^{(T)} - \bar{\nabla}_\nu \xi_\mu^{(T)}, \tag{4.15}$$

so that we can choose gauges for $\tilde{h}_{\mu\nu}$ and $\delta\phi$ independently. This procedure is equivalent to performing a Stuckelberg trick [53]. We define the orthogonal projection operator relative to the vector X^μ,

$$\Lambda_{\mu\nu} \equiv \bar{g}_{\mu\nu} + X_\mu X_\nu, \tag{4.16}$$

and decompose $\tilde{h}_{\mu\nu}$ as,

$$\tilde{h}_{\mu\nu} = X_\mu X_\nu h^{(S)} - \left(X_\mu h_\nu^{(V)} + X_\nu h_\mu^{(V)} \right) + h_{\mu\nu}^{(T)}, \tag{4.17}$$

with $h^{(S)} \equiv X^\rho X^\sigma \tilde{h}_{\rho\sigma}$, $h_\mu^{(V)} \equiv X^\rho \Lambda_\mu^\sigma \tilde{h}_{\rho\sigma}$ and $h_{\mu\nu}^{(T)} \equiv \Lambda_\mu^\rho \Lambda_\nu^\sigma \tilde{h}_{\rho\sigma}$ Under a T-type transformation they transform as

$$h'^{(S)} = h^{(S)}, \tag{4.18}$$

$$h_\mu'^{(V)} = h_\mu^{(V)} - X^\rho \bar{\nabla}_\rho \xi_\mu^{(T)}, \tag{4.19}$$

$$h_{\mu\nu}'^{(T)} = h_{\mu\nu}^{(T)} - \left(\bar{\nabla}_\mu \xi_\nu^{(T)} + \bar{\nabla}_\nu \xi_\mu^{(T)} \right) - X^\rho \left(X_\mu \bar{\nabla}_\rho \xi_\nu^{(T)} + X_\nu \bar{\nabla}_\rho \xi_\mu^{(T)} \right), \tag{4.20}$$

up to order $\mathcal{O}(\omega^0)$. Indeed, the gauge transformation in Eq. (4.15), produces also terms at orders $\mathcal{O}(\omega^{-1})$, which we do not consider here as we focus only on the geometric optics orders $\mathcal{O}(\omega)$ and $\mathcal{O}(\omega^2)$ (see discussion about geometric optics in Section 1.3.2). We note that $h^{(S)}$ is both $S-$ and T-gauge invariant at order $\mathcal{O}(\omega^0)$. For later purposes, we further decompose $h_{\mu\nu}^{(T)}$ as

$$h_{\mu\nu}^{(T)} = \gamma_{\mu\nu} + \frac{1}{3} \Lambda_{\mu\nu} h^{(tr)} \tag{4.21}$$

with $h^{(tr)} \equiv \Lambda^{\mu\nu} h_{\mu\nu}^{(T)}$ and $\Lambda^{\mu\nu} \gamma_{\mu\nu} = \bar{g}^{\mu\nu} \gamma_{\mu\nu} = 0$, and whose transformation laws are,

$$h'^{(tr)} = h^{(tr)} - 2\Lambda^{\mu\nu} \bar{\nabla}_\nu \xi_\mu^{(T)}, \tag{4.22}$$

$$\gamma'_{\mu\nu} = \gamma_{\mu\nu} - \left(\bar{\nabla}_\mu \xi_\nu^{(T)} + \bar{\nabla}_\nu \xi_\mu^{(T)} \right) + \frac{2}{3} \Lambda_{\mu\nu} \bar{\nabla}^\rho \xi_\rho^{(T)} - X^\rho \left(X_\mu \bar{\nabla}_\rho \xi_\nu^{(T)} + X_\nu \bar{\nabla}_\rho \xi_\mu^{(T)} \right). \tag{4.23}$$

4.2.2. Gauge fixing

We first choose $\xi^{(S)}$ and $\xi_\mu^{(T)}$ such that

$$\delta\phi + \sqrt{2X} \xi^{(S)} = 0, \qquad \rightarrow \qquad \delta\phi' = 0, \tag{4.24}$$

$$h_\mu^{(V)} - X^\rho \bar{\nabla}_\rho \xi_\mu^{(T)} = 0 \qquad \rightarrow \qquad h_\mu'^{(V)} = 0. \tag{4.25}$$

The last condition is compatible, at order $\mathcal{O}(\omega^0)$, with the orthogonality requirement $X^\mu h_\mu^{(V)} = 0$ as it can be checked by contracting with X^μ both sides. Eq. (4.25) leaves the residual T-gauge freedom $X^\rho \nabla_\rho \zeta_\mu^{(T)} = 0$, which we use to fix

$$\bar{\nabla}^\mu \gamma'_{\mu\nu} = 0, \tag{4.26}$$

at order $\mathcal{O}(\omega^0)$, using Eq. (4.23). After such gauge choices, the quantity $\gamma'_{\mu\nu}$ is transverse and traceless; we identify it as the high-frequency GW and dub it

$$\gamma'_{\mu\nu} \equiv h_{\mu\nu}^{(TT)}. \tag{4.27}$$

We point out that is not possible to choose $h^{(\mathrm{tr})} = 0$, using the residual gauge freedom, left after the last transformation, if $h^{(\mathrm{tr})}$ depends on the coordinate in the direction of X_μ. For simplicity, we can exhaust the gauge freedom imposing $\nabla^\mu \xi_\mu^{(T)} = 0$, such that the trace $h^{(\mathrm{tr})}$ is gauge-invariant, while the transverse-traceless GW excitations $h_{\mu\nu}^{(TT)}$ are invariant under the residual transformation that can be read from Eq. (4.23):

$$h_{\mu\nu}^{(TT)} \rightarrow h_{\mu\nu}^{(TT)} - \bar{\nabla}_\mu \xi_\nu^{(T)} - \bar{\nabla}_\nu \xi_\mu^{(T)} . \tag{4.28}$$

After the gauge fixing procedure described, the metric perturbation reads

$$\tilde{h}_{\mu\nu} = X_\mu X_\nu h^{(S)} + \frac{1}{3} \Lambda_{\mu\nu} h^{(\mathrm{tr})} + h_{\mu\nu}^{(TT)} . \tag{4.29}$$

The quantity $\tilde{h}_{\mu\nu}$, before we make any gauge choice, has 10 non-vanishing components. Making gauge fixings as explained above, we imposed 6 conditions, since both $h_\mu^{(V)}$ and $h_{\mu\nu}^{(TT)}$ are by construction orthogonal to the vector X^μ. Hence, we are left with 4 independent metric components. In Section 4.3.1 we show that only 3 out of these 4 are independent propagating degree of freedom, while $h^{(S)}$ is a constrained field. We will decouple the evolution equations of The evolution equations of $h^{(\mathrm{tr})}$ and $h_{\mu\nu}^{(TT)}$ under physical assumptions on the velocities of the fields involved.

4.3. Equations of motion

Isaacson, working in the context of the geometric optics limit of General Relativity, showed that the original diffeomorphism invariance is preserved order-by-order in the gradient expansion [151, 152] in the equations of motion. In our scalar-tensor framework, we change perspective and *impose* the symmetry invariance at each order in the ω-expansion. This viewpoint allows us to write the most general structure for the equations governing the GW dynamics, and to encode the effects of the DE field in few physically transparent parameters.

4.3.1. Separating the evolution equations

We consider that the equations of motion of $\tilde{h}_{\mu\nu}$ in Eq. (4.29), can be obtained from the action (4.3). As usual in the context of geometric optics, we neglect the contribution of standard matter, considering that it does not have high-frequency excitations. The gravitational field equations can be expressed in terms of $\tilde{h}_{\mu\nu}$ as

$$G_{\mu\nu}^{(1)} \left[\tilde{h}_{\rho\sigma} \right] = T_{\mu\nu}^{(1)} \left[\tilde{h}_{\rho\sigma} \right] , \tag{4.30}$$

where $G_{\mu\nu}^{(1)} \left[\tilde{h}_{\rho\sigma} \right]$ is the linearized Einstein tensor, written in terms of $\tilde{h}_{\rho\sigma}$, and $T_{\mu\nu}^{(1)}$ represent any other contribution to the field equations. Note that we are choosing the gauge $\delta\phi = 0$, hence it does not appear in the equations above. Taking the trace

of Eq. (4.30), we find that the left-hand-side is given by (minus) the first order Ricci scalar

$$R^{(1)} = -\bar{\Box} h^{(\text{tr})} + \Lambda^{\alpha\beta} \bar{\nabla}_\alpha \bar{\nabla}_\beta \left(h^{(S)} + \frac{1}{3} h^{(\text{tr})} \right), \tag{4.31}$$

from which we see that, while the trace scalar $h^{(\text{tr})}$ receives a kinetic contribution controlled by the d'Alembert operator $\bar{\Box}$, second derivatives acting on the scalar $h^{(S)}$ are weighted by the projector operator $\Lambda_{\mu\nu}$. Let us consider, as an example, the case of a background field configuration which is homogeneous and isotropic. In this case, $\bar{g}_{\mu\nu}$ is the FLRW metric and $v_\mu \propto \delta_{\mu 0} \varphi_0'$ so that $\Lambda^{\alpha\beta} \bar{\nabla}_\alpha \bar{\nabla}_\beta h^{(S)} \propto \partial^i \partial_i h^{(S)}$. As a result, one finds that the kinetic contributions of $h^{(S)}$ coming from the Ricci scalar, are not sufficient for propagating this field. Indeed, $h^{(S)}$ plays a role analogous to the lapse function N in the ADM formalism (see e.g. [160]): not dynamical and whose equation of motion serves as a constraint equation. We also discuss in Appendix B an explicit, simple example where $h^{(S)}$ is manifestly non-dynamical. To proceed further, one has to understand whether the energy-momentum tensor in the right-hand-side of Eq. (4.30), can make $h^{(S)}$ dynamical by, for instance, containing a term such $\sim \bar{\Box} h^{(S)}$. If in the action (4.3), the couplings of dark energy scalar to the metric are expressed in a covariant form in terms of the metric, Riemann, and Ricci tensors, we claim this is not possible. Indeed, if this is the case, their contribution will have a form similar to the one of the Ricci in Eq. (4.31) and, consequently, the same considerations as above apply. We conclude that the role of $h^{(S)}$ is to fix certain conditions on the high-frequency modes.

Assuming that we have solved the equation of $h^{(S)}$, we are left with $h_{\mu\nu}^{(TT)}$ and $h^{(\text{tr})}$ as potentially propagating high-frequency degrees of freedom. The linearized gravitational field equations, can be decomposed as

$$G_{\mu\nu}^{(1)} \left[h_{\rho\sigma}^{(TT)} \right] + G_{\mu\nu}^{(1)} \left[h^{(\text{tr})} \right] = T_{\mu\nu}^{(T)} \left[h_{\rho\sigma}^{(TT)} \right] + T_{\mu\nu}^{(\text{tr})} \left[h^{(\text{tr})} \right]. \tag{4.32}$$

We expect that second derivatives contributions to the scalar sector have a rich structure, due to the presence of $v^\mu \neq 0$. As a consequence, tensor and scalar fluctuations normally propagate with different velocities. We set the speed of GW to the one of light, given the strong experimental bounds on the GW velocity associated with the GW170817 event [302], and make the ansatzs

$$h_{\mu\nu}^{(TT)} = \mathcal{A}_{\mu\nu}^{(T)} \exp\left[i \omega \psi^{(TT)} \right], \tag{4.33}$$

$$h^{(\text{tr})} = \mathcal{A}^{(\text{tr})} \exp\left[i \omega \psi^{(\text{tr})} \right]. \tag{4.34}$$

The amplitudes of both modes are slowly varying, while the phases are rapidly varying thanks to the factors of ω in the exponent. When plugging Eqs. (4.33) and (4.34) into Eq. (4.32), one gets a linear combination of terms with rapidly oscillating phases and slowly varying overall coefficients, with structure

$$\left(\ldots \,_{|\omega^2, \omega^1} \right) \exp\left[i \omega \psi^{(TT)} \right] + \left(\ldots \,_{|\omega^2, \omega^1} \right) \exp\left[i \omega \psi^{(\text{tr})} \right] = 0 \tag{4.35}$$

where within the parenthesis we collect slowly varying contributions at order ω^2 and ω^1 in a gradient expansion. The ω^2 contributions depend on the derivative of the phases $\psi^{(TT)}$ and $\psi^{(\text{tr})}$: they control the dispersion relations for the two species of excitations, scalar and GW. Since in general $h_{\mu\nu}^{(TT)}$ and $h^{(\text{tr})}$ propagate with different speed, they are characterized by distinct dispersion relations, hence the phases $\psi^{(TT)}$ and $\psi^{(\text{tr})}$ are different. Eq. (4.35) is a linear combination of two contributions weighted by two distinct phases which rapidly oscillate over space and time: in order to satisfy it, we need to impose that the coefficients of each of these two terms separately vanish. Within the geometric optics limit, this procedure effectively separates the evolution of scalar modes (characterized by the phase $\psi^{(\text{tr})}$) and GW modes (characterized by the phase $\psi^{(TT)}$). Under all these assumptions illustrated, we consider Eq. (4.32) satisfied if

$$G_{\mu\nu}^{(1)}\left[h^{(\text{tr})}\right] \;=\; T_{\mu\nu}^{(\text{tr})}\left[h^{(\text{tr})}\right], \tag{4.36}$$

$$G_{\mu\nu}^{(1)}\left[h_{\rho\sigma}^{(TT)}\right] \;=\; T_{\mu\nu}^{(T)}\left[h_{\rho\sigma}^{(TT)}\right], \tag{4.37}$$

namely the two sectors solve individually their respective equations. As a result, the GW sector is decoupled from the scalar one at the linearized level.

4.3.2. The tensor mode equation

We now investigate the tensor mode equation in Eq. (4.37). The left-hand-side corresponds to the linearized Einstein tensor, evaluated in $h_{\rho\sigma}^{(TT)}$. Since the latter is transverse and traceless, we have that

$$G_{\mu\nu}^{(1)}\left[h_{\rho\sigma}^{(TT)}\right]\Big|_{\omega^2,\,\omega^1} = -\frac{1}{2}\bar{\Box}h_{\mu\nu}^{(TT)}\Big|_{\omega^2,\,\omega^1}. \tag{4.38}$$

The right-hand-side of Eq. (4.37) is theory dependent, nevertheless, symmetry considerations allow us to determine the general structure of $T_{\mu\nu}^{(1)}[h_{\rho\sigma}^{(TT)}]$, without relying on specific models. Considering Eq. (4.38) as left-hand-side of Eq. (4.37), and the invariance under residual $T-$ types gauge transformations, we see that the right-hand-side should be:

1. transverse and traceless,

2. orthogonal to v^μ at orders ω^2 and ω^1,

3. invariant under the transformation (4.28),

4. conserved at order ω^2: $\left[\nabla^\mu T_{\mu\nu}^{(T)}\right]_{\omega^2} = 0$,

5. containing at most second derivatives of $h_{\rho\sigma}^{(TT)}$: since we are considering an action of the form (4.3), stability requires that the corresponding equations of

motion are at most second order[2].

Additionally, we demand that it ensures that GW propagate at the speed of light, to be compatible with GW170817 [125]. The only allowed structure of the linearized $T_{\mu\nu}^{(T)}(h_{\rho\sigma})$ that satisfies all of these requirements at orders ω^2, ω is

$$T_{\mu\nu}^{(T)} \quad = \quad \tau_A \bar{\Box} h_{\mu\nu}^{(TT)} + \tau_B \, v^\rho \, \bar{\nabla}_\rho \, h_{\mu\nu}^{(TT)} , \tag{4.39}$$

where $\tau_{A,B}$ depend only on slowly varying fields. Calling the combination

$$\mathcal{T} = -\frac{2\tau_B}{1+2\tau_A} , \tag{4.40}$$

we can rewrite the GW evolution equation as

$$\left(\bar{\Box} h_{\mu\nu}^{(TT)} \right)_{|\omega^2, \omega^1} = \mathcal{T} \times \left(v^\rho \bar{\nabla}_\rho \, h_{\mu\nu}^{(TT)} \right)_{|\omega^1} . \tag{4.41}$$

The deviations from GR on the propagation of high-frequency GW only appear as a first-order gradient of the GW high-frequency fluctuation, proportional to the parameter $\mathcal{T}$ depending on slowly-varying fields. Such contribution can be thought as a 'friction term' for the GW, and is common in scalar-tensor theories with non-minimal couplings between scalar and metric degrees of freedom. In the context of gravitational wave cosmology, several groups explored the consequences of such term in specific cosmological models [114, 123, 124, 161, 183, 184, 186, 191, 211, 222, 223, 303–308], as we did in Chapters 2 and 3.

4.3.3. Amplitude evolution equation

We consider the eikonal anstaz in Eq. (4.34) where the gradient of the phase defines the GW 4-momentum as

$$k_\mu = \bar{\nabla}_\mu \psi^{(TT)} , \tag{4.42}$$

and plug it into the equation of motion (4.41). As usual in the context of geometric optics, we organize the equation obtained in this way in power of ω

$$\left[\dots \right] \omega^2 + \left[\dots \right] \omega + \dots = 0 , \tag{4.43}$$

and, since $\omega \gg 1$, we require that the coefficient of each order vanishes, in order to satisfy the equation. At order ω^2 we obtain,

$$k^\mu k_\mu = 0 , \qquad k^\rho \bar{\nabla}_\rho k^\mu = 0 , \tag{4.44}$$

---

[2]It could be possible that the equations of motion become second order only after having used specific constraint relations. This should be the case of DHOST theories, for instance.

which states that the GW 4-momentum is a null vector, propagating along null geodesics. Calling λ the affine parameter of the geodesics, we have that for any function f, the derivative along the geodesics is $df/d\lambda = k^\rho \bar{\nabla}_\rho f$. At order ω, we find the evolution equation for the amplitude

$$\left[2 k^\rho \bar{\nabla}_\rho \mathcal{A}^{(T)} + (\bar{\nabla}_\rho k^\rho) \mathcal{A}^{(T)} \right] = \mathcal{T} k^\rho v_\rho \mathcal{A}^{(T)}, \tag{4.45}$$

where we defined $\mathcal{A}^{(T)}$ as $\mathcal{A}^{(T)} = \sqrt{\mathcal{A}_{\mu\nu}^{(T)} (\mathcal{A}^{(T)})^{\mu\nu}}$. Recalling that $v_\mu = \bar{\nabla}_\mu \bar{\varphi}$, the previous equation can be 'integrated' to

$$\bar{\nabla}_\rho \left(e^{-\int \mathcal{T}} k^\rho \left[\mathcal{A}^{(T)} \right]^2 \right) = 0, \tag{4.46}$$

where the schematic expression $\int \mathcal{T}$ denotes the following integral

$$\int \mathcal{T} \equiv \int_{\lambda_s}^{\lambda} \mathcal{T} \frac{d\bar{\varphi}}{d\lambda'} d\lambda'. \tag{4.47}$$

In the equation above, λ_s corresponds to the value of the affine parameter at the source position. The quantity in Eq. (4.47) represents a cumulative integration of the friction term in Eq. (4.41) over the GW geodesic's affine parameter. In integrating Eq. (4.45) we have chosen boundary conditions such that there are no scalar field effects at the source position $\lambda = \lambda_s$, as assumed throughout the work. Importantly, we do not need to demand that $\mathcal{T}$ is 'small' for writing Eq. (4.46).

4.4. Conservation laws

Eq. (4.45) shows that the DE field can introduce an additional damping term. However, the fact that this can be integrated, lead us to Eq. (4.46), giving us reasons to believe that we can actually still formulate a conservation law.

4.4.1. The energy momentum of GW

The presence of GWs can back-react on the background curvature. These effects were quantified, in the geometric optics limit and in General Relativity, by Isaacson [152], introducing the GW stress-energy tensor, which is at second order in the amplitude expansion regulated by α. Focusing only on the tensor modes $h_{\mu\nu}^{(TT)}$, we derive their associated stress-energy tensor in the generalized gravitational set-up outlined in the previous Sections. Again, we do so by changing perspective: we build the stress tensor bottom-up by using symmetry arguments, namely finding the only possible second-order tensor which is gauge invariant under the residual transformation in Eq. (4.28). Indeed, also Isaacson in [152] showed that the GW stress tensor in General Relativity is gauge invariant, at the geometric optics order, and here we use this symmetry property as a guiding principle to build $T_{\mu\nu}^{(2),\text{ST}}$.

We start by that the stress-energy tensor must be quadratic in $h^{(TT)}_{\mu\nu}$, and contain two derivatives acting on the transverse-traceless GW excitations (by 'integration by parts', we can place one derivative per field). Given this information, the most general structure that $T^{(2)}_{\mu\nu}$ can have is

$$T^{(2),\text{ST}}_{\mu\nu} = \frac{1}{32\pi\omega^2} \langle \bar{\nabla}_\mu h^{(TT)}_{\alpha\beta} \bar{\nabla}_\nu h^{(TT)}_{\gamma\delta} \rangle \mathcal{C}^{\alpha\beta\gamma\delta}, \qquad (4.48)$$

where $\mathcal{C}^{\alpha\beta\gamma\delta}$ depends on slowly-varying fields and the symbol $\langle \ldots \rangle$ denotes the so-called Brill-Hartle spatial average [152, 160]. Being $h^{(TT)}_{\gamma\delta}$ traceless, we have that $\mathcal{C}^{\alpha\beta\gamma\delta} \not\propto \bar{g}^{\gamma\delta}$, otherwise the stress-energy tensor would vanish. Also, because $T^{(2),\text{ST}}_{\mu\nu}$ is conserved at order ω^2 and $h^{(TT)}_{\gamma\delta}$ is transverse and traceless, the only way to arrange the free indices μ, ν is the one in Eq. (4.48). After fixing the gauge as discussed in Section 4.2.2, we are left with invariance under the transformation in Eq. (4.28). We select $\mathcal{C}^{\alpha\beta\gamma\delta}$ in Eq. (4.48) such that the stress-energy tensor is invariant under the same gauge transformations. Using Eq. (4.28), we see that the latter transforms as $T^{(2),\text{ST}}_{\mu\nu} \rightarrow T^{(2),\text{ST}}_{\mu\nu} + \delta T^{(2),\text{ST}}_{\mu\nu}$ where

$$\delta T^{(2),\text{ST}}_{\mu\nu} = -\frac{1}{16\pi\omega^2} \langle \bar{\nabla}_\mu \bar{\nabla}_\alpha \xi^{(T)}_\beta \bar{\nabla}_\nu h^{(TT)}_{\gamma\delta} \rangle \mathcal{C}^{\alpha\beta\gamma\delta}, \qquad (4.49)$$

$$= \frac{1}{16\pi\omega^2} \langle \bar{\nabla}_\mu \xi^{(T)}_\beta \bar{\nabla}_\nu \bar{\nabla}_\alpha h^{(TT)}_{\gamma\delta} \rangle \mathcal{C}^{\alpha\beta\gamma\delta}, \qquad (4.50)$$

which must vanish for any $\xi^{(T)}_\beta$, and for any choice of μ, ν. This can be achieved by choosing $\mathcal{C}^{\alpha\beta\gamma\delta} = \mathcal{C} \delta^{\alpha\gamma} C^{\beta\delta}$, for some function C and tensor $C^{\beta\delta}$ and upon using the transversality of the GW. Plugging this result in Eq. (4.48) we obtain

$$T^{(2),\text{ST}}_{\mu\nu} = \frac{\mathcal{C}}{32\pi\omega^2} \langle \bar{\nabla}_\mu h^{(TT),\alpha}_\beta \bar{\nabla}_\nu h^{(TT)}_{\alpha\delta} \rangle C^{\beta\delta}. \qquad (4.51)$$

Since the EMT is symmetric in the indexes, the quantity $C^{\beta\delta}$ is symmetric. Applying again the transformation (4.28), and integrating by parts, we find that the invariance of the stress-energy tensor also imposes $C^{\beta\delta} \propto \delta^{\beta\delta}$. Therefore, symmetry arguments fixed the form of the GW stress-energy tensor, up to a multiplicative function, to

$$T^{(2),\text{ST}}_{\mu\nu} = \frac{\mathcal{C}}{32\pi\omega^2} \langle \bar{\nabla}_\mu h^{(TT)}_{\alpha\beta} \bar{\nabla}_\nu h^{(TT)\alpha\beta} \rangle. \qquad (4.52)$$

This result would be identical to the General Relativistic one in [152], is the function $\mathcal{C}$ of the slowly varying fields was = 1. In our case, we fix it by using the conservation equation[3].

$$\nabla^\mu T^{(2),\text{ST}}_{\mu\nu} = 0, \qquad (4.53)$$

---

[3]The GW stress-energy tensor enters the background gravitational field equations, of the form $G^{(0)}_{\mu\nu} = T^{(2),\text{ST}}_{\mu\nu}[h^{(TT)}] + T^{(2),\text{ST}}_{\mu\nu}[h^{(tr)}]$. Bianchi's identities guarantee the conservation of the right-hand-side of the latter equations. The assumption of having independent scalar and tensor sector guarantees that the two stress-energy tensors are conserved separately.

which, together with Eqs. (4.46) and (4.44) for the amplitude of the tensor modes, fixes $\mathcal{C}$ to the value $e^{-\int \mathcal{T}}$. Hence, we find that the second order GW energy-momentum tensor, in the geometric optics limit and at leading order, reads

$$T_{\mu\nu}^{(2),\text{ST}} = \frac{e^{-\int \mathcal{T}}}{32\,\pi} \left[\mathcal{A}^{(T)}\right]^2 k_\mu k_\nu . \tag{4.54}$$

4.4.2. Conservation of the graviton number density current

The results of geometric optics of Section 4.3.3, allow us to interpret the GW stress-energy tensor in Eq. (4.54) and its conservation in terms of a graviton number density 4-current. We identify the quantity

$$\mathcal{N}_\mu \equiv k_\mu \left[\mathcal{A}^{(T)}\right]^2 e^{-\int \mathcal{T}} \qquad \rightarrow \qquad \bar{\nabla}_\mu \mathcal{N}^\mu = 0, \tag{4.55}$$

as the *graviton number density 4-current*, which is conserved by virtue of Eq. (4.46), and all the assumptions it is based on. We can express the GW stress-energy tensor in terms of the graviton number density as,

$$T_{\mu\nu}^{(2),\text{ST}} = \frac{1}{16\,\pi} k_{(\nu} \mathcal{N}_{\mu)} , \tag{4.56}$$

where the parenthesis stands for the symmetrization in the μ, ν indices. Being able to express the GW stress-energy tensor as in Eq. (4.56), supports its definition found through only symmetry arguments: it's tensor whose components are related to the flux of the $\mu - th$ component of the energy-momentum density through a surface with x^ν constant coordinate (the vector k_ν is the wave-vector of the GW). This interpretation relies on the possibility of defining the rays, identified by the wave-vector k^μ, which make clear the concept of a *trajectory* for a gravitational wave.

We can give a further interpretation of these results in terms of the geometry of the cross-sectional area of the GW's ray bundle, $S(\lambda)$ in Figure 4.1, to further support the identification of $\mathcal{N}^\mu$ as the graviton number density 4-current. If λ is the affine parameter associated to the GW rays with 4-momentum k^μ, a geometric optics theorem (see [160], exercise 22.13) states that,

$$\frac{d\,S(\lambda)}{d\lambda} - \bar{\nabla}_\mu k^\mu \, S(\lambda) = 0 , \tag{4.57}$$

which combined with Eq. (4.55) implies

$$\frac{d}{d\lambda} \left\{ e^{-\int \mathcal{T}} \left[\mathcal{A}^{(T)}\right]^2 S(\lambda) \right\} = 0 , \tag{4.58}$$

clearly showing that the combination $e^{-\int \mathcal{T}} \left[\mathcal{A}^{(T)}\right]^2$ is inversely proportional to the bundle's cross-sectional area, rather than only $\left[\mathcal{A}^{(T)}\right]^2$ as in General Relativity.
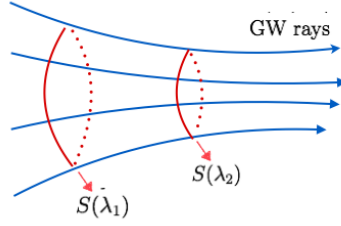
Figure 4.1: *Geometric optics representation of graviton number conservation. The flux of a stream of gravitons crossing the S-areas is conserved along the GW affine parameter. See Eq.* (4.58).

4.5. Gravitational wave distances and duality relation

In this Section we give the definitions of the *gravitational waves distances* by generalizing to the case of GWs in scalar-tensor theories the works [157, 213–217, 309] about fluctuations of the luminosity and angular diameter distances, both of photons and GWs. All of these works descend from the one done by Sasaki in [212] regarding photons, which we follow very closely in this Section. After giving these definitions, we prove the validity of *Etherington's reciprocity law*, also known as *distance duality relation*, between GW luminosity and angular distances, also in the scalar-tensor theories considered in this Chapter[4]. This law states that, in General Relativity, between the electromagnetic luminosity and angular diameter distance the following relation holds

$$d_L = (1+z)^2 \, d_A \, , \tag{4.59}$$

if: the spacetime is described by a pseudo-Riemannian manifold, photons propagate along null geodesics of the spacetime and their number density is conserved [149, 310, 311]. Such relation has been tested from several electromagnetic observations [312–316] and its role in the context of multi-messenger observation was explored as well in [185]. Etherington's reciprocity law, because it relies on very minimal assumptions, it provides a perfect playground to test the theory of gravity or the cosmological model [317], so one might wonder if we should expect a similar relation also for the GWs distances

$$d_L^{(\text{GW})} = (1+z)^2 \, d_A^{(\text{GW})} \, , \tag{4.60}$$

in light of the results obtained in Sections 4.3.3 and 4.4.1.

---

[4]We study the propagation of GW over a perturbed cosmological background and prove its validity up to first order in the perturbations

4.5.1. Raychaudhuri equation

Before giving the definitions of the GW distances, we perform some preliminary steps into further characterizing the GW's rays, which will become useful later. Our starting equations are the GW stress-energy tensor of Eq. (4.54), the amplitude evolution equation in Eq. (4.46) and the geodesic equation (4.44).

We perform a conformal transformation, defining the metric $\hat{g}_{\mu\nu} \equiv \bar{g}_{\mu\nu}/a^2$ and $\hat{g}^{\mu\nu} \equiv \bar{g}^{\mu\nu}/a^{-2}$ [5], mapping a null GW geodesics in $\bar{g}_{\mu\nu}$ into null geodesics in $\hat{g}_{\mu\nu}$ with rescaled affine parameter [32]

$$d\hat{\lambda} = a^{-2}\, d\lambda. \tag{4.61}$$

The amplitude evolution equation in the comoving frame then results

$$\frac{d}{d\hat{\lambda}}\left(e^{-\frac{1}{2}\int \mathcal{T}}\mathcal{A}^{(T)}\,a\right) + \frac{1}{2}\left(e^{-\frac{1}{2}\int \mathcal{T}}\mathcal{A}^{(T)}\,a\right)\hat{\theta} = 0 \qquad \text{with} \qquad \hat{\nabla}_\mu \hat{k}^\mu = \hat{\theta}, \tag{4.62}$$

where $\hat{\nabla}_\mu$ is the covariant derivative associated to the conformal metric and $\hat{k}_\mu \equiv k_\mu$, while $\hat{k}^\mu \equiv \hat{g}^{\mu\nu}\hat{k}_\nu$. The *expansion parameter* θ, satisfies the *Raychaudhuri equation,* which can be determined from Eq. (4.44), is

$$\frac{d\hat{\theta}}{d\hat{\lambda}} = -\hat{R}_{\mu\nu}\hat{k}^\mu\hat{k}^\nu - \frac{\hat{\theta}^2}{2} - 2\hat{\sigma}^2, \tag{4.63}$$

where $\hat{\sigma}^2 \equiv \hat{k}_{(\alpha;\beta)}\hat{k}^{(\alpha;\beta)}/2 - \hat{\theta}^2/4$ is the shear of the GW ray's bundle, and $\hat{R}_{\mu\nu}$ the conformal spacetime Ricci tensor [212]. The graviton number conservation (4.58) remains unchanged and reads

$$\frac{d}{d\hat{\lambda}}\left\{e^{-\int \mathcal{T}}\mathcal{A}^{(T)\,2}\,S(\hat{\lambda})\right\} = 0. \tag{4.64}$$

4.5.2. Gravitational wave luminosity distance

In the physical frame, we introduce an observer the 4-velocity u^μ, which measures the GW's energy flux given by

$$\mathcal{F}^\alpha \quad = \quad -\left[T^{(2),\mathrm{ST}}\right]^\mu{}_\nu\,\mathcal{P}^\alpha{}_\mu\,u^\nu, \tag{4.65}$$

$$\quad = \quad \mathcal{F}\,n^\alpha, \tag{4.66}$$

with the GW flux amplitude and frequency measured by the observer are

$$\mathcal{F} = \frac{e^{-\int \mathcal{T}}}{32\,\pi}\left[\mathcal{A}^{(T)}\right]^2 \nu^2, \qquad \nu = -k_\mu u^\mu, \tag{4.67}$$

and also

$$\mathcal{P}^\alpha_\mu = \delta^\alpha_\mu + u^\alpha\,u_\mu, \qquad n^\alpha = \frac{1}{\nu}\left(k^\alpha - \nu u^\alpha\right). \tag{4.68}$$

---

[5]From now onward, quantities in conformal frame are denoted with a hat

The notion of GW frequency allows us to define the redshift z at the value $\hat{\lambda}$ of the comoving GW geodesics affine parameter as

$$1 + z(\hat{\lambda}) = \frac{\nu(\hat{\lambda})}{\nu(0)} . \tag{4.69}$$

We assume that GW are emitted by an approximately spherically symmetric system, with characteristic radius R_s, see left panel of Figure 4.2, which we will $\to 0$ at the end of the computation. The flux amplitude $\mathcal{F}$ measured at the source position is related with the intrinsic source luminosity by the relation

$$\mathcal{F}(\hat{\lambda}_s) = \frac{\mathscr{L}_{GW}}{4\pi R_s^2} , \tag{4.70}$$

with $\hat{\lambda}_s$ the conformal affine parameter at the source. We define *GW luminosity distance* $d_L^{(GW)}$ as the ratio of GW power emitted at source position (intrinsic GW luminosity), versus the GW flux at detector location [212]

$$d_L^{(GW)} \equiv \left[\frac{\mathscr{L}_{GW}}{4\pi \mathcal{F}(0)} \right]^{\frac{1}{2}} = \sqrt{\frac{\mathcal{F}(\hat{\lambda}_s)}{\mathcal{F}(0)}} \, R_s . \tag{4.71}$$

Substituting relation (4.67), we find the following expression

$$d_L^{(GW)} = \exp\left[-\frac{1}{2} \int_0^{\hat{\lambda}_s} \mathcal{T} \right] \times \frac{\mathcal{A}^{(T)}(\hat{\lambda}_s)}{\mathcal{A}^{(T)}(0)} \times \left[1 + z(\hat{\lambda}_s) \right] \times R_s . \tag{4.72}$$

Note the role of the scalar field-induced friction term in the overall exponential factor, that encodes the interesting phenomenology of these theories, providing interesting observation prospects in case of multi-messenger events. By taking the definition of EM luminosity distance in [212], we find the ration between the two distances

$$\frac{d_L^{(GW)}}{d_L^{(EM)}} = \exp\left[-\frac{1}{2} \int_0^{\hat{\lambda}_s} \mathcal{T} \frac{d\bar{\phi}}{d\lambda'} \, d\lambda' \right] , \tag{4.73}$$

singling out the modified gravity contribution as an integral from $\lambda = 0$ (the position of the observer) to the source at $\hat{\lambda} = \hat{\lambda}_S$. This factor reduces to the effective Planck's mass of Eq. (1.105) for specific choices of $\mathcal{T}$, as we show explicitly in Appendix A.

4.5.3. Gravitational wave angular distance

The *GW angular distance* $d_A^{(GW)}$ is defined in terms of the ratio between the angular diameter d_s of the source located at conformal affine parameter $\hat{\lambda}_s$, and the source apparent angular size $\Delta\phi$ as measured by an observer at $\hat{\lambda} = 0$,

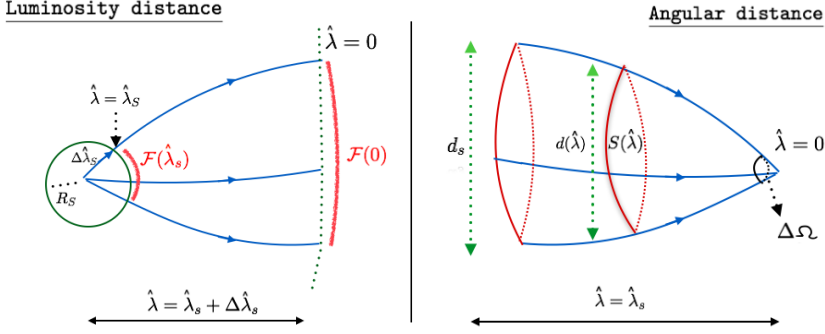$$d_A^{(GW)} \quad \equiv \quad \frac{d_s}{\Delta\Omega} . \tag{4.74}$$

Figure 4.2: *Representative plot of the GW/photon rays from source to detector position. The path of the ray bundle in blue is parameterized by the affine parameter $\hat{\lambda}$. **Left panel**: quantities entering the luminosity distance are associated with a bundle diverging from source to detector. **Right panel**: quantities entering the angular distance are associated with a bundle converging from source to detector. See text for definitions.*

Following [212], it is convenient to reexpress $d_A^{(GW)}$ as

$$d_A^{(GW)} = \left(\frac{S(\hat{\lambda}_s)}{S(\Delta\hat{\lambda}_o)} \right)^{1/2} \frac{\mathbf{d}(\Delta\hat{\lambda}_o)}{\Delta\Omega}, \qquad (4.75)$$

with $S(\hat{\lambda})$ and $\mathbf{d}(\hat{\lambda})$ the cross-section area and the diameter of the GW's ray bundle at $\hat{\lambda}$, and $\Delta\hat{\lambda}_o$ is the affine parameter in proximity of the observer (see Figure 4.2, right panel). In [212], it is shown that

$$\frac{\mathbf{d}(\Delta\hat{\lambda}_o)}{\Delta\Omega} = \frac{a^2[\tau(0)]\,\Delta\hat{\lambda}_o}{(1 + z(\hat{\lambda}_s))\,a[\tau(\hat{\lambda}_s)]}, \qquad (4.76)$$

connecting the ratio $\mathbf{d}(\Delta\hat{\lambda})/\Delta\Omega$ with $\Delta\hat{\lambda}_o$. Thanks to Eq. (4.64), relating the amplitude of the GW with the area of the cross-section of the ray bundle, we can rewrite Eq. (4.75) as

$$d_A^{(GW)} = \exp\left[\frac{1}{2} \int_{\Delta\hat{\lambda}_o}^{\hat{\lambda}_s} \mathcal{T} \right] \times \left(\frac{\mathcal{A}^{(T)}(\Delta\hat{\lambda}_o)}{\mathcal{A}^{(T)}(\hat{\lambda}_s)} \right) \times \frac{\mathbf{d}(\Delta\hat{\lambda}_o)}{\Delta\Omega}. \qquad (4.77)$$

4.5.4. Etherington's reciprocity law

We now prove the validity of Etherington's reciprocity law, connecting luminosity and angular GW distances. In the case of photons, the Etherington reciprocity law takes the form in Eq. (4.59) and it descends from very generic hypothesis: the spacetime is described by a Riemannian manifold, photons propagate along null geodesics of the spacetime and their number density is conserved [149, 310]. Among them, and in the case of GWs in geometric optics, our scalar-tensor scenario only affects the conservation of the graviton number density, via the $e^{-\int \mathcal{T}}$ in Eq. (4.64), standing

for the friction induced by the DE scalar field. Nonetheless, we derived a modified conservation law, namely Eq. (4.55), hence there are good reasons to believe that the reciprocity law still holds for the GW distances, as defined in Sections 4.5.2 and 4.5.3.

Our findings and definitions so far are valid in any background spacetime, provided that the background scalar field assumes a non-trivial profile and $v_\mu \neq 0$. Here we choose a perturbed cosmological background

$$\bar{g}_{\mu\nu} \;=\; a^2(\tau)\left[\eta_{\mu\nu} + \epsilon\,\delta\hat{g}_{\mu\nu}\right], \tag{4.78}$$

$$\bar{\varphi} \;=\; \varphi_0(\tau) + \epsilon\,\delta\varphi(x), \tag{4.79}$$

and derive the Etherington's relation up to first order in cosmological perturbations as in [212]. In the expressions above, $\eta_{\mu\nu}$ is the Minkowski metric, and we have introduced again ϵ as the parameter keeping track of the order of magnitude of the long wavelength metric and scalar field perturbations, describing the large-scale structures, opposed to α for the high-frequency fluctuations. Therefore, even if we chose the unitary gauge for the high-frequency scalar field $\alpha\,\delta\phi(x)$, the long wavelength DE field perturbation, $\epsilon\,\delta\varphi(x)$, is still present. Recalling that we defined the comoving wave-vector as $\hat{k}^\mu \equiv \hat{g}^{\mu\nu}k_\nu$, we introduce a null vector

$$\hat{K}^\mu \equiv -\frac{\hat{k}^\mu}{v(\hat{\lambda}_s)\,a[\tau(\hat{\lambda}_s)]}\,, \tag{4.80}$$

and, from now onward, $\hat{\lambda}$ will be the affine parameter associated to it. This vector is normalized such that $\left(\hat{g}_{\mu\nu}\hat{K}^\mu\hat{u}^\nu\right)_{\hat{\lambda}_s} = 1$, where $\hat{u}^\mu$ is the observer 4-velocity in the conformal frame. The introduction of the vector $\hat{K}^\mu$ is convenient to easily relate the physical size of the source with the affine parameter along the GW geodesics. In fact, as shown in [212], the characteristic size R_s of the source can be expressed as

$$R_s = a(\tau(\lambda_s))\,\Delta\hat{\lambda}_s\,, \tag{4.81}$$

with $\Delta\hat{\lambda}_s$ the infinitesimal affine parameter associated with the source size (see Figure 4.2, left panel).

We prove the distance duality relation by taking the following steps:

i. We use Raychaudhuri equation (4.63), to relate the expansion parameter, $\hat{\theta}$, to the comoving affine parameter, $\hat{\lambda}$. The integration in $\hat{\lambda}$ requires the choice of boundary conditions; these will be different between luminosity and angular diameter distance because of the different geometry of the ray's bundle, as shown in Figure 4.2.

ii. We use Eq. (4.62) to relate the GW's amplitude to $\hat{\theta}$ and, using the result of the previous step, to the comoving affine parameter. We plug these relations in

Eqs. (4.72) and (4.77), written in terms of the GW's amplitude, to have $d_L^{(GW)}$ and $d_A^{(GW)}$ in terms of the comoving affine parameter (and the perturbation of the expansion rate).

iii. We combined the expressions obtained and arrive to Eq. (4.60).

Step i.

We solve Raychaudhuri equation (4.63) perturbatively in ϵ, the expansion parameter which tracks the large-scale structures in Eq. (4.78). We expand the expansion parameter as

$$\hat{\theta}(\hat{\lambda}) = \hat{\theta}_0(\hat{\lambda}) + \epsilon \delta\hat{\theta}(\hat{\lambda}), \tag{4.82}$$

so that $\hat{\theta}_0(\hat{\lambda})$ would represent its value on a Minkowski spacetime (remember we have performed a conformal transformation). The affine parameter $\hat{\lambda}$ still has contributions at linear order in ϵ [156, 157]. By expanding Eq. (4.63) in ϵ, and solving it at each order (see also [212, 318] for details), it can be checked that $\hat{\theta}_0$ and $\delta\hat{\theta}$ are given by,

$$\hat{\theta}_0(\hat{\lambda}) - \hat{\theta}_0(\hat{\lambda}_b) = \frac{2}{\hat{\lambda} - \hat{\lambda}_b}, \tag{4.83}$$

$$\delta\hat{\theta}(\hat{\lambda}) - \delta\hat{\theta}(\hat{\lambda}_b) = -[\hat{\theta}_0(\hat{\lambda})]^2 \int_{\hat{\lambda}_b}^{\hat{\lambda}} d\lambda' \frac{1}{[\hat{\theta}_0(\lambda')]^2} \times \delta(\hat{R}_{\mu\nu}\hat{K}^\mu\hat{K}^\nu)(\lambda'), \tag{4.84}$$

where $\hat{\theta}_0(\hat{\lambda}_b)$, $\delta\hat{\theta}(\hat{\lambda}_b)$ are boundary conditions to be fixed at $\hat{\lambda}_b$. We choose different boundary conditions in the case of the luminosity or the angular diameter distance. Looking at the left panel of Figure 4.2, it is clear that, in the first case, the expansion parameter $\hat{\theta}$ is zero at the source position $\hat{\lambda}_s + \Delta\hat{\lambda}_s$, while from the right panel of Figure 4.2, we see that $\hat{\theta} = 0$ at $\hat{\lambda} = \Delta\hat{\lambda}_o$, namely the observer position, in the case of angular distances. The main difference between the two situations is the direction the GW ray's bundle is diverging: toward or away from the observer. Therefore, for the luminosity distance boundary conditions we have

$$\hat{\theta}_0^L(\hat{\lambda}) = \frac{2}{\hat{\lambda} - \hat{\lambda}_s - \Delta\hat{\lambda}_s}, \tag{4.85}$$

$$\delta\hat{\theta}^L(\hat{\lambda}) = \frac{1}{[\hat{\lambda} - \hat{\lambda}_s - \Delta\hat{\lambda}_s]^2} \int_{\hat{\lambda}}^{\hat{\lambda}_s} d\lambda' [\lambda' - \hat{\lambda}_s - \Delta\hat{\lambda}_s]^2 \times \delta(\hat{R}_{\mu\nu}\hat{K}^\mu\hat{K}^\nu), \tag{4.86}$$

while for the angular diameter distance boundary conditions

$$\hat{\theta}_0^A(\hat{\lambda}) = \frac{2}{\hat{\lambda} - \Delta\hat{\lambda}_o}, \tag{4.87}$$

$$\delta\hat{\theta}^A(\hat{\lambda}) = -\frac{1}{[\hat{\lambda} - \Delta\hat{\lambda}_o]^2} \int_{\Delta\hat{\lambda}_o}^{\hat{\lambda}} d\lambda' [\lambda' - \Delta\hat{\lambda}_o]^2 \times \delta(\hat{R}_{\mu\nu}\hat{K}^\mu\hat{K}^\nu). \tag{4.88}$$

Step ii.

As in [212], we can use the results above to integrate Eq. (4.62) and obtain the relation

$$\exp\left[-\frac{1}{2}\int_0^{\hat{\lambda}_s}\mathcal{T}\right]\times\frac{\mathcal{A}^{(T)}(\lambda_s)\,a(\tau(\lambda_s))}{\mathcal{A}^{(T)}(0)\,a(\tau(0))}=\frac{\lambda_s+\Delta\hat{\lambda}_s}{\Delta\hat{\lambda}_s}\exp\left[-\frac{1}{2}\int_0^{\hat{\lambda}_s}d\lambda\,\delta\theta_L(\lambda)\right].\quad(4.89)$$

in the case of the luminosity distance boundary conditions, while

$$\exp\left[-\frac{1}{2}\int_0^{\hat{\lambda}_s}\mathcal{T}\right]\times\frac{\mathcal{A}^{(T)}(\lambda_s)\,a(\tau(\lambda_s))}{\mathcal{A}^{(T)}(0)\,a(\tau(0))}=\frac{\Delta\lambda_o}{\hat{\lambda}_s}\exp\left[-\frac{1}{2}\int_{\Delta\lambda_o}^{\hat{\lambda}_s}d\lambda\,\delta\theta_A(\lambda)\right]\quad(4.90)$$

in the case of the angular diameter distance ones. We plug these two results into Eqs. (4.72) for d_L^{GW} and (4.77) for d_A^{GW}, and obtain

$$d_L^{(\text{GW})}(\hat{\lambda}_s)\quad=\quad a[\tau(0)]\left[1+z(\hat{\lambda}_s)\right]\hat{\lambda}_s\times\exp\left[-\frac{1}{2}\int_0^{\hat{\lambda}_s}d\lambda\,\delta\theta_L(\lambda)\right],\quad(4.91)$$

$$d_A^{(\text{GW})}(\hat{\lambda}_s)\quad=\quad\frac{a[\tau(0)]}{1+z(\hat{\lambda}_s)}\hat{\lambda}_s\times\exp\left[\frac{1}{2}\int_0^{\hat{\lambda}_s}d\lambda\,\delta\theta_A(\lambda)\right],\quad(4.92)$$

where we have used also the relation in Eq. (4.76) and sent $\Delta\hat{\lambda}_s,\Delta\hat{\lambda}_o\to0$.

Notice that all the effects of scalar field-induced friction, are implicitly included in the expressions (4.89) and (4.90), which relate the affine parameter at the source position, $\hat{\lambda}_s$, with the remaining quantities. The compact expressions in Eqs. (4.91) and (4.92) (accompanied by relations (4.89) and (4.90)) include the effects of cosmological fluctuations implicitly. These can be made explicit by following the same procedure of [212]. Another possible approach is to use the *Cosmic Rulers* formalism, first developed in the context of photon propagation [156], then for GWs in General Relativity [157] and eventually in a scalar-tensor theory set up in [158]. This approach explicitly identifies contributions from peculiar velocities, weak lensing, Sachs-Wolfe effects, volume effects, and Shapiro time delay, and allows appreciating the contributions due to presence of the DE field, as in Eq. (1.112) of the Introduction. For the purpose of proving the validity of Etherington reciprocity law, Eqs. (4.91) and (4.92) are sufficient.

Step iii.

Combine Eqs. (4.91) and (4.92), we get

$$\tilde{d}_A^{(\text{GW})}\quad=\quad\frac{\tilde{d}_L^{(\text{GW})}}{(1+\tilde{z})^2}\exp\left[\frac{1}{2}\int_0^{\hat{\lambda}_s}(\delta\theta_A(\lambda)+\delta\theta_L(\lambda))\,d\lambda\right],\quad(4.93)$$

$$=\quad\frac{\tilde{d}_L^{(\text{GW})}}{(1+\tilde{z})^2}.\quad(4.94)$$

The explicit computational steps between Eqs. (4.93) and (4.94) can be found in [212]: since Eqs. (4.86) and (4.88) do not contain explicit DE-modifications, they are the same of the analogous computation for photons in General Relativity. The second line, Eq. (4.94), is the desired Etherington's relation, valid including first order perturbations.

Hence, we have proved that in the scalar-tensor framework discussed in this work, with the modified conservation of graviton number density in Eq. (4.55), luminosity and angular distances for GW are connected by the classic Etherington's law (4.94). A straightforward consequence of this result is that also the GW angular diameter distance satisfies an analogous relation to Eq. (4.73), namely

$$
\frac{d_A^{(GW)}}{d_A^{(EM)}} = \exp\left[-\frac{1}{2} \int_0^{\hat{\lambda}_s} \mathcal{T} \frac{d\bar{\phi}}{d\lambda} \, d\lambda \right].
\tag{4.95}
$$

Given the relevance of Eq. (4.73) in the context of multi-messenger events to test DE, Eq. (4.95) states that the same important role can be played by the angular diameter distances.

4.5.5. Implications for GW lensing

We discuss the implications of our findings for GW strong lensing: when a massive object is located between a source, emitting photon or GWs, and the observer, its gravitational field bends the messenger's path, resulting in a remapping of the source into multiple images. By comparing the arrival time between the images, it is possible to derive another distance measure, the so-called *time delay distance*, defined as

$$
D_{\Delta t} = (1 + z_l) \frac{d_{OL}^A d_{SO}^A}{d_{SL}^A},
\tag{4.96}
$$

where z_l is the lens redshift and $d_{OL}^A, d_{SO}^A d_{SL}^A$ are the angular diameter distances between observer-lens, source-observer and source-lens [149]. The time delay distance can be used to trace the distance-redshift relation and infer cosmological parameters [319, 320], similarly to what is done with the luminosity and angular diameter distances, or test the GW propagation properties [190]. Determining the value of the Hubble parameter today, H_0, through the observations of multi-lens system is a very promising avenue, and a great effort is being dedicated into making this tool more efficient and competitive [321]. Strong lensing of GWs hasn't been observed yet, however future interferometers such as LISA will likely detect lensed events [322], since it is able to probe high redshifts, so the literature of this topic is quite broad [164, 171, 178, 179, 226, 301, 322, 322–349]. One very promising application of these types of events is exactly that they can be used to test the distance duality relation: strong lensing events of standard distance indicators (SN [350] or

GWs [351]) can give us access both to luminosity distance and angular diameter distance.

We consider strong GW lensing from point-like lens in the geometric optics limit, valid when the GW wavelength is well shorter than the Schwarzschild radius of the lens. In this limit, we do not need to discuss interference effects, that will be the topic of Chapter 6. The goal of this section is to understand whether, in the scalar-tensor theory of gravity considered in this Chapter, the time delay between "light images" can differ from the time delay between "GW images", in a multi-messenger detection. Indeed, multi-messenger time delay can prove to be a powerful test for cosmology [333, 347]. The works [346, 348] show conclusively that GW and EM lensed signals arrive at the same time at the detector, provided that both waves propagate at the same speed and are emitted at the same time. In the geometric optics limit, this is expected when photons and GW travel through null geodesics, since by definition both sectors cover the minimal possible distance from source to detector. Causality arguments based on Fermat principle allow one to prove this statement in full generality and [348] also argues that the same result should be valid in any theory of gravity.

As for photons, the GW time delay $\Delta t^{(\mathrm{GW})}$ can be expressed as [149]

$$\Delta t^{(\mathrm{GW})} = (1 + z_l) \frac{d_{OL}^{(\mathrm{GW})} d_{SO}^{(\mathrm{GW})}}{2 d_{SL}^{(\mathrm{GW})}} |\theta - \theta_S|^2 + t_{\Phi}^{(\mathrm{GW})}, \qquad (4.97)$$

where z is the lens's redshift, $d_{OL}^{(\mathrm{GW})}$ the GW angular distance as measured from the observer to the lens, $d_{SO}^{(\mathrm{GW})}$ the one from source to the observer, and $d_{SL}^{(\mathrm{GW})}$ from source to lens. In Eq. (4.97), θ is the observed angular position of the source, θ_S the would-be angular position of the source in absence of the lens. The first contribution in Eq. (4.97) is the *geometrical time delay*, and its derivation can be found in Appendix C, while the second contribution, t_{Φ}, is the *Shapiro time delay*, due to the due to the gravitational field of the lens. This contribution is similar to the one found in Eq. (1.112), and it is the same for GW and EM observations in a scalar-tensor framework, as it can be checked by also considering the same term in Eq. (1.114). In other words $t_{\Phi}^{(\mathrm{GW})} = t_{\Phi}^{(\mathrm{EM})}$. The geometrical contribution to Eq. (4.97), though, depends on the GW angular diameter distance, which can be modified compared to the EM ones, as Eq. (4.95) states. The corresponding EM-time delay, $\Delta t^{(\mathrm{EM})}$, can be found by substituting $d_A^{(\mathrm{EM})}$ in the same time delay expression [149]. Hence, even if apparently $\Delta t^{(\mathrm{GW})} \neq \Delta t^{(\mathrm{EM})}$, because of the different angular diameter distances, we will prove that the two time delay coincides, in line with the causality arguments

previously mentioned. Using Eq. (4.95), we can write

$$
\begin{aligned}
\Delta t_{\text{geo}}^{(\text{GW})} &= (1+z)\,\frac{d_{OL}^{(\text{GW})}\,d_{SO}^{(\text{GW})}}{2\,d_{SL}^{(\text{GW})}}\,|\theta-\theta_S|^2, \\
&= \left(\frac{d_{OL}^{(\text{GW})}}{d_{OL}^{(\text{EM})}}\right)\left(\frac{d_{SO}^{(\text{GW})}}{d_{SO}^{(\text{EM})}}\right)\left(\frac{d_{SL}^{(\text{EM})}}{d_{SL}^{(\text{GW})}}\right)\Delta t_{\text{geo}}^{(\text{EM})}, \\
&= \left(\exp\left[-\frac{1}{2}\int_{\lambda_O}^{\lambda_L}\mathcal{T}\frac{d\bar\phi}{d\lambda}\,d\lambda-\frac{1}{2}\int_{\lambda_S}^{\lambda_O}\mathcal{T}\frac{d\bar\phi}{d\lambda}\,d\lambda+\frac{1}{2}\int_{\lambda_S}^{\lambda_L}\mathcal{T}\frac{d\bar\phi}{d\lambda}\,d\lambda\right]\right)\Delta t_{\text{geo}}^{(\text{EM})}, \\
&= \Delta t_{\text{geo}}^{(\text{EM})}. \qquad\qquad (4.98)
\end{aligned}
$$

We can see that integrals in the exponential carefully compensate, so that the geometric part of the time delays are equal, $\Delta t_{\text{geo}}^{(\text{GW})} = \Delta t_{\text{geo}}^{(\text{EM})}$. Together with the fact that the Shapiro contribution is the same for photons and GWs, the result extends to the full time delay, as in Eq. (4.97).

4.6. Discussion and Conclusions

In this Chapter, we studied the propagation of high-frequency gravitational waves in scalar-tensor theories of gravity, with the aim of examining properties of cosmological distances as inferred from GW measurements. We first developed a bottom-up, covariant approach to describe the dynamics of the high-frequency perturbations, based on the principle of coordinate invariance. Symmetry considerations allowed us to extract transverse-traceless components of the high-frequency scalar-tensor fluctuations, identified with GW. In scenarios where scalar and tensor components propagate at different speeds, we argued that the two sectors decouple at the linearized level around an arbitrary background, and the evolution of high-frequency GW and scalar modes can be studied independently. We then determined the most general structure of the GW linearized equations, namely Eq. (4.41) and of the GW energy momentum tensor in Eq. (4.48), where the presence of a dynamical DE scalar field is encoded in the slowly varying factor $\int \mathcal{T}$. Following the guide of [212], we defined the *gravitational waves distances*, d_L^{GW} and d_A^{GW}, which descend from the GW's stress-energy tensor, obtainable exclusively because of the geometric optics assumption which allows for a simultaneous definition of wave-vector, k^μ, and trajectory via $k^\mu = dx^\mu/d\lambda$. Both GW luminosity and angular distances can be modified with respect to General Relativity, as shown in Eqs. (4.73) and (4.95), in a way that Etherington's reciprocity law (4.60) still holds, in a perturbed universe and within a scalar-tensor framework. We discussed implications of this result for gravitational lensing, focussing on time-delays of lensed GW. Compatibly with causality arguments, we showed that the time delay between EM images, $\Delta t^{(\text{EM})}$, corresponds to the same in terms of GW images, $\Delta t^{(\text{GW})}$, because we assumed that these were traveling on null geodesics.

Appendices

A. Comparison with the literature

To make contact with literature, here we show that Eq. (4.73), when specialized for a FLRW Universe, coincides with the standard expression. We choose $ds^2 = a^2(\tau)\eta_{\mu\nu}dx^\mu dx^\nu$ and $\bar\varphi = \varphi_0(\tau)$, so that $v_\mu = (\bar\varphi'_0, 0, 0, 0)$. For definiteness, we compare our results with the notation of [249], in which the evolution of the amplitude of high-frequency tensor modes is given by

$$h'' + 2\mathcal{H}\,(1 - \delta(\tau))\,h' - \nabla^2 h = 0, \tag{4.99}$$

where $\nabla^2 = \partial^i \partial_i$ and the ratio of the luminosity distances is written as

$$\frac{d_L^{(GW)}}{d_L^{(EM)}} = \exp\left[-\int_0^z \frac{\delta(z')}{1+z'}\,dz'\right]. \tag{4.100}$$

Evaluating Eq. (4.41) on the homogeneous and isotropic gives

$$h'' + 2\mathcal{H}\left(1 - \frac{\mathcal{T}\,\varphi'_0}{2\mathcal{H}}\right)h' - \nabla^2 h = 0. \tag{4.101}$$

Comparing this equation with Eq. (4.99), we identify

$$\delta(\tau) = \frac{\mathcal{T}\,\varphi'_0}{2\mathcal{H}}, \tag{4.102}$$

so that

$$\begin{aligned}
\frac{d_L^{(GW)}}{d_L^{(EM)}} &= \exp\left[-\int_0^{z_s} \frac{\delta(z)}{1+z}\,dz\right] = \exp\left[-\int_{t_0}^{t_s} \delta(t)\,H\,dt\right] = \exp\left[-\int_{\tau_0}^{\tau_s} \delta(\tau)\,\mathcal{H}\,d\tau\right] \\
&= \exp\left[-\int_{\tau_0}^{\tau_s} \frac{\mathcal{T}\,\bar\phi'}{2\mathcal{H}}\,\mathcal{H}\,d\tau\right] = \exp\left[-\frac{1}{2}\int_{\tau_0}^{\tau_s} \mathcal{T}\,\bar\phi'\,d\tau\right] \\
&= \exp\left[-\frac{1}{2}\int_0^{\lambda_s} \mathcal{T}\,\frac{d\bar\phi}{d\lambda}\,d\lambda\right],
\end{aligned} \tag{4.103}$$

which is Eq. (4.73). In the derivation above, we also used $d\tau/dt = 1/a$, $\mathcal{H} = H/a$, $1 + z = a(0)/a(t)$. Using the relation between $\delta(\tau)$ and the running Planck's mass [122]

$$\delta(\tau) = \frac{\partial \ln M_P[\varphi_0(\tau)]}{\partial \ln a} \tag{4.104}$$

it is also straightforward to check that

$$\frac{d_L^{(GW)}}{d_L^{(EM)}} = \exp\left[-\frac{1}{2}\int_0^{\lambda_s} \mathcal{T}\,\frac{d\bar\phi}{d\lambda}\,d\lambda\right] = \exp\left[-\int_0^{z_s} \frac{\delta(z)}{1+z}\,dz\right] = \frac{M_P(z)}{M_P(0)}, \tag{4.105}$$

recovering Eq. (1.105).

B. A simple example: $F(\varphi) R$

Let us make a specific, simple example of the friction-term contributions found in our general formula of Eq. (4.41), which arises in models characterized by a time-varying Planck mass controlled by the dark energy scalar field φ. We consider the following non-minimal kinetic coupling between scalar φ and metric

$$\mathcal{L} = F(\varphi)R, \tag{4.106}$$

which can be considered a part of the classic Brans-Dicke action [56]. We linearize the gravitational field equations following this action and decompose them in terms of the high-energy fluctuations, focusing on orders ω^2 and ω^1 in the gradient expansion, as described in Section 4.3.1. We find that GW modes, as defined in Eq. (4.27), obey the equation

$$\Box h_{\mu\nu}^{(TT)} = \frac{2F_{,\varphi}}{F} v^\lambda \bar{\nabla}_\lambda h_{\mu\nu}^{(TT)}, \tag{4.107}$$

where $F_{,\varphi} = \partial F/\partial\varphi$. An evolution equation governing scalar modes can be determined by taking the trace of the Einstein equations

$$\bar{\Box} h^{(\text{tr})} - \Lambda_{\alpha\beta} \bar{\nabla}^\alpha \bar{\nabla}^\beta \left(h^{(S)} + \frac{1}{3} h^{(\text{tr})} \right) = - \frac{3\sqrt{2X}F_{,\varphi}}{F} X^\lambda \bar{\nabla}_\lambda \left(h^{(S)} + h^{(\text{tr})} \right), \tag{4.108}$$

where the vector X_μ is defined in Eq. (4.12), and the projector $\Lambda_{\mu\nu}$ in Eq. (4.16). These equations have the structure described in Section 4.3.1. Comparing the GW evolution equation (4.107), with the general expression in Eq. (4.41), we notice that the former has a friction term $\mathcal{T} = 2F_{,\phi}/F$. Upon renaming $F[\varphi] = M_P^2[\varphi]/2$, one can realize that this is the usual friction term. Using the results of section 4.4.1, we find that the stress-energy tensor at second order in the transverse-traceless fluctuations reads

$$\begin{aligned} T_{\mu\nu}^{(2),\text{ST}} &= \epsilon^2 \frac{e^{-\int \mathcal{T}}}{32\pi} \langle \nabla_\mu h_{\rho\sigma}^{(TT)} \nabla_\nu h^{(TT)\,\rho\sigma} \rangle \\ &= \epsilon^2 \frac{1}{32\pi} \exp\left[\int_{\varphi_{\text{in}}}^\varphi \frac{d\ln F}{d\tilde\varphi} d\tilde\varphi \right] \langle \nabla_\mu h_{\rho\sigma}^{(TT)} \nabla_\nu h^{(TT)\,\rho\sigma} \rangle \\ &= \epsilon^2 \frac{F(\varphi)}{32\pi} \langle \nabla_\mu h_{\rho\sigma}^{(TT)} \nabla_\nu h^{(TT)\,\rho\sigma} \rangle, \end{aligned} \tag{4.109}$$

where we chose the extreme of integration φ_{in} such that $F(\varphi_{\text{in}}) = 1$. This tensor has the expected structure associated with the Lagrangian density of Eq. (4.106). We can apply these findings to cosmology, and consider the case of GW propagating through a FLRW Universe, with metric $ds^2 = a^2(\tau)\eta_{\mu\nu}dx^\mu dx^\nu$, and for a homogeneous scalar field $\bar\varphi = \varphi_0(\tau)$. Then Eq (4.107) turns into

$$h_{\mu\nu}^{(TT)''} + 2\mathcal{H}\left(1 - \frac{F_{,\varphi}\varphi_0'}{F\mathcal{H}}\right) h_{\mu\nu}^{(TT)'} - \nabla^2 h_{\mu\nu}^{(TT)} = 0, \tag{4.110}$$

where $\mathcal{H}$ is the conformal Hubble parameter. The effect of the friction term due to the non-minimal scalar-tensor couplings has the expected structure and is manifest within the parenthesis of the previous expression.

C. The geometric time-delay
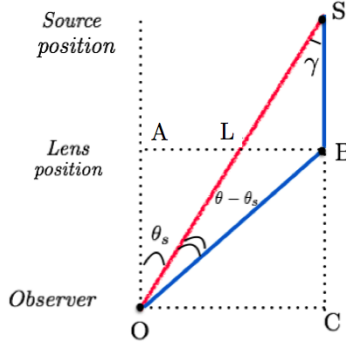
Figure C.3: *The configuration we consider.*

We derive the expression for the geometric time delay, i.e. the first term in Eq. (4.97). Since we are considering GWs propagating at the speed of light, these follow null geodesics whose affine parameter is the comoving distance, which we denote ℓ. For example, ℓ_{AL} is the length of the line that joins point A with point L in Figure C.3. Angular distances are defined as ratios between lengths and angles they subtend with respect to who observes them (which we write as the first letter, remember the definition of d^A using Figure 4.2, right panel). We will have

$$D_{OL} \;=\; \ell_{AL}/\theta_s, \qquad\qquad D_{SL} = \ell_{LB}/\gamma, \qquad\qquad D_{SO} = \ell_{OC}/\gamma. \quad (4.111)$$

We work in the limit of infinitesimal angles, so that

$$\ell_{OL}\sin\theta_s \;=\; \ell_{AL} \qquad\qquad \Rightarrow \qquad\qquad \ell_{OL} \sim D_{OL}, \qquad (4.112)$$
$$\ell_{OB}\cos\theta \;=\; \ell_{OL}\cos\theta_s \qquad\qquad \Rightarrow \qquad\qquad \ell_{OB} \sim \ell_{OL} \sim D_{OL} \qquad (4.113)$$

Considering GWs traveling at the speed of light, the geometrical time delay can be computed as

$$\Delta t = \ell_{SB} + \ell_{OB} - \ell_{SO}. \qquad (4.114)$$

Since the triangles LSB and OSC are similar, we can write the equality

$$\frac{\ell_{LS}}{\ell_{OS}} = \frac{\ell_{LB}}{\ell_{OC}} = \frac{D_{SL}}{D_{SO}}, \qquad (4.115)$$

so that

$$\ell_{OS} = \ell_{OL} + \ell_{LS} = \ell_{OL} + \ell_{OS} \frac{D_{SL}}{D_{SO}}.$$ (4.116)

implying

$$\ell_{OS} = D_{OL} \left(1 - \frac{D_{SL}}{D_{SO}}\right)^{-1} = \frac{D_{OL}D_{SO}}{D_{SO} - D_{SL}}.$$ (4.117)

Moreover, the law of cosines ensures that

$$\ell_{SB}^2 = \ell_{OB}^2 + \ell_{OS}^2 - 2\ell_{OB}\ell_{OS}\cos(\theta - \theta_s).$$ (4.118)

Expanding the cosine for small angles, we can reassemble the previous formula as

$$\ell_{SB} \simeq (\ell_{OS} - \ell_{OB})\sqrt{1 + \frac{\ell_{OB}\ell_{OS}}{(\ell_{OB} - \ell_{OS})^2}|\theta - \theta_s|^2},$$ (4.119)

$$\simeq (\ell_{OS} - \ell_{OB})\left(1 + \frac{\ell_{OB}\ell_{OS}}{2(\ell_{OB} - \ell_{OS})^2}|\theta - \theta_s|^2\right).$$ (4.120)

Then the time delay reads

$$\Delta t = \frac{\ell_{OB}\ell_{OS}}{2(\ell_{OS} - \ell_{OB})}|\theta - \theta_s|^2 = \frac{D_{OL}}{2}\frac{D_{OL}D_{SO}}{D_{SO} - D_{SL}}\frac{1}{\frac{D_{OL}D_{SO}}{D_{SO}-D_{SL}} - D_{OL}}|\theta - \theta_s|^2,$$

$$= \frac{D_{OL}D_{SO}}{2D_{SL}}|\theta - \theta_s|^2,$$ (4.121)

which is the formula used in Eq.(4.97) of the main text, with the GW angular diameter distance.

Note: My contribution to the paper this Chapter is based on regards all the scientific aspects, especially, but not only, the theoretical computations of the first part. I also had an active role in writing.

5

Polarization tests: direct detection of the scalar wave

In scalar-tensor theory of gravity, gravitational waves can have a modified dynamics and an enriched polarization content, supported by the dark energy scalar field. In this Chapter, we address the possibility of a direct detection of the extra scalar polarization, as a new probe to test the theory of gravity. We do so in light of two screening mechanisms, chameleon and symmetron, showing that the scalar waves, in every frequency range, are not directly detectable. This implies that a detection of the scalar polarization in the gravitational wave sector would disprove the scalar-tensor theories considered, rather than be a smoking gun for.

5.1. Introduction

Since the discovery of the late time accelerated expansion of the Universe, an incredible effort has been dedicated into understanding the nature of its origin. The simplest extension to the cosmological constant consists of a scalar field, φ, coupled to the metric, $g_{\mu\nu}$, in various ways, provided that some stability and symmetry requirements are met. Because of this additional gravitational force, in these scalar-tensor theories both the growth of matter perturbations and the propagation of GWs are modified. Detecting ϕ via the former is a key goal of the next galaxy surveys [9, 11, 352, 353] while the observation of GWs by LIGO-Virgo [1] has opened the possibility of using the latter. The evolution of matter perturbations is mainly studied at large scales and low energies, where linear perturbation theory holds. One can therefore investigate the modification of the growth of structures by performing a study of the linear perturbation around the homogeneous and isotropic cosmological background, which is given a priori. Another powerful alternative in this regard is the Effective Field Theory of Dark Energy (EFT) [86, 88, 354], which allows a joint treatment of all scalar-tensor with second order equations of motion and which is implemented in Einstein-Boltzmann solver codes to produce predictions for the modified observables and produce constraints [89, 96, 186, 355]. In both of these descriptions, since the background configuration is assumed as the starting point, perturbations are defined as the difference between the full fields and their background counterparts. On the other hand, GWs in scalar-tensor theories are addressed in the high energy limit [158, 182], since this is the regime corresponding to the observed waves so far. The sources of these waves are also located close enough to the observer for the spacetime geometry not to be homogeneous and isotropic in the region of propagation. If this was the case, then one cannot start with the assumption of a cosmological background. The strategy in this case is to exploit the wave's highly oscillatory behavior by introducing an expansion in derivatives of high-frequency perturbations [151, 152]. This way it is possible to study the propagation of GWs over slowly-varying, but otherwise unknown, backgrounds. In these approaches, field perturbations are then defined through particular averaging schemes. The separation of variation scales between perturbation and background can be regarded as a symmetry breaking, and helps identify the true degrees of freedom of the theory [150, 356]. In scalar-tensor theories, on top of the standard two tensor modes composing a GW, there is also a propagating scalar wave [300, 357], representing the dark energy scalar field. As seen in the previous Chapters, the tensor modes dynamics can be altered with extra damping terms [122, 183, 184] or different propagation speed [358]. Assuming that the same theory is responsible for the modifications in both the tensor and scalar sector, combining the information obtained via these two independent probes is a compelling task in light of the future scientific missions, though non-trivial because of the differences in energy scales and formalism used to describe them [359]. For instance, the combined detection

of GW170817 and GRB170817A [125] set the speed of GW to the one of light. However, its source was located at very low redshift, $z \lesssim 0.001$, and it frequency very close to the EFT cutoff, so that using the information gathered from its detection to reduce the EFT parameter spaces is dubious [129]. Therefore, in the first part of this Chapter we further elaborate on the definitions of metric perturbation à la *ray-optics* versus the *wave-optics* one, given in Section 1.3.2, to fully understand how deep their differences can make the two descriptions diverge. We will show that these two definitions restrict the allowed class of diffeomorphisms, characterizing the linear gauge transformations, in two different ways. The arguments presented in this first part of the Chapter, place themselves in the middle of the existing literature of GWs in the high-frequency regime: the geometric optics limit of GWs is well understood in General Relativity [150–152, 155], while the propagation of tensor and scalar linear perturbations in scalar-tensor theories is historically addressed on a flat background [299, 300] or a FLRW one, under the mask of cosmological perturbation theory and the EFT. Initial efforts to merge these two sectors can be found in more recent works [158, 182, 301, 360].

These initial results, set up the stage for the discussion about the detection prospects of the dark energy scalar wave as a test for the gravitational theory. We study this in light of the so-called *screening mechanism*: a feature of all viable scalar-tensor theories aimed at suppressing the force carried by scalar field in high density regions such as the Solar System, where all the tests performed exclude its presence [361]. The role of screening in shaping the distribution of matter in the Universe has been studied extensively [51, 362–364], but such mechanisms have never been discussed in the context of GWs and in light of the high-frequency expansion. Indeed, it is still not understood whether a scalar wave would be able to pass through a screened region and be detectable on Earth, nor if GWs in these extended theories are affected by it. We address such question by studying the geodesic deviation equation and conclude that the scalar wave, in every frequency range and in the theories considered here, should be screened and, consequently, not detectable.

5.2. Origin of differences: definition of the field's perturbations

We consider those scalar-tensor theories for which the action in Einstein frame can be written as the canonical action for a scalar field, φ, coupled to the matter fields, Ψ_i, through a conformal transformation:

$$\mathcal{S} = \int \mathrm{d}^4 x \sqrt{-g} \left[\frac{M_p^2}{2} R - \frac{1}{2} g^{\mu\nu} \nabla_\mu \varphi \nabla_\nu \varphi - V(\varphi) \right] + \mathcal{S}_m(\Omega^2(\varphi) g_{\mu\nu}, \Psi_i), \qquad (5.1)$$

where $g_{\mu\nu}$ is the metric, R is the Ricci scalar and $V(\varphi), \Omega(\varphi)$ two arbitrary functions modelling the field potential and the conformal coupling. Because matter couples to the Jordan frame metric, $\tilde{g}_{\mu\nu} = \Omega^2(\varphi) g_{\mu\nu}$, this theory is sometimes studied by performing a conformal transformation, where it takes the form of a Generalized Brans-Dicke theory. In this case, the scalar field action of Eq. (5.1) loses its canonical form and a modified Planck mass appears in front of R. We study the dynamics of perturbations in vacuum. This assumption is justified in cosmological settings when the scalar field drives the expansion of the Universe and in screening scenarios outside the localized matter sources.

Once an action is given, one is interested in studying the dynamics of the field or of their linear perturbations. To be able to study the latter, one has to decide how to distinguish the field perturbations from their respective background configurations. As discussed in Section 1.3.2 of the Introduction, a notation as

$$g_{\mu\nu} = \bar{g}_{\mu\nu} + \alpha\, h_{\mu\nu}\,, \quad \varphi = \bar{\varphi} + \alpha\delta\phi\,, \tag{5.2}$$

is rather uninformative unless a criterion to distinguish $\{h_{\mu\nu}, \delta\varphi\}$ from $\{\bar{g}_{\mu\nu}, \bar{\phi}\}$ is given. Here we revisit again the two main approaches, which in Section 1.3.2 we used to define the GW in the *ray-optics* regime versus the one in *wave-optics* limit, and extend the discussion also to the scalar wave (SW), represented by $\alpha\delta\phi$. We already gave a taste of the line of thoughts which we will follow in Eqs. (4.10) and (4.11) of Chapter 4. Here we pick it up again, and try to understand it even further. We assume that the amplitude of the perturbations is smaller than their background counterparts. This is quantified by the parameter α such that $|h_{\mu\nu}|/|\bar{g}_{\mu\nu}|, |\delta\varphi|/|\bar{\phi}| \sim \alpha \ll 1$.

• *Approach 1:* The first approach is the one adopted by standard perturbation theory. In this case, the splitting between background and perturbation is done by choosing a priori a background configuration. For instance, in a cosmological setting the quantities $\{\bar{g}_{\mu\nu}, \bar{\phi}\}$ are fixed to the homogeneous and isotropic Universe and consequently, perturbations are uniquely defined as $h_{\mu\nu} = g_{\mu\nu} - \bar{g}_{\mu\nu}$ and $\delta\varphi = \phi - \bar{\phi}$. An additional assumption is that $\{\bar{g}_{\mu\nu}, \bar{\phi}\}$ are considered gauge invariant. Taking again the example of the unperturbed cosmological background, after performing this procedure one usually separates the field perturbations in scalar-vector and tensor modes and identifies GWs as the latter. We point out that a similar approach is adopted in the EFT though the assigned action is built from symmetry arguments, rather than given as Eq. (5.1). This approach is also the one opted for in the literature of wave-optics limit for gravitational waves and photons [149, 179].

• *Approach 2:* In the second approach, typical of the high-frequency expansion, one assumes that the field perturbations can be separated from the background by means of suitable averaging procedures. In this case, the field background configu-

rations are the smooth mean quantities

$$\langle g_{\mu\nu}\rangle = \bar{g}_{\mu\nu}, \quad \langle\varphi\rangle = \bar{\varphi}, \tag{5.3}$$

and the perturbations are defined implicitly via $\langle h_{\mu\nu}\rangle = \langle\delta\varphi\rangle = 0$. We require $\bar{\phi}$ to be a function of the spacetime coordinates, so that

$$v_\mu \equiv \partial_\mu\bar{\varphi} \neq 0 \tag{5.4}$$

and we introduce the parameter L, measuring the variation length scale of $\bar{\varphi}$, so that

$$|v_\mu| \sim \bar{\varphi}/L. \tag{5.5}$$

We also assume that $\{\bar{g}_{\mu\nu}, \bar{\varphi}\}$ vary on the same length scale. The excluded case in which $\bar{\varphi} = const$ is trivial, because in this case the background is known. Indeed, $\bar{\varphi} = const$ contains the maximally symmetric Minkowski, de Sitter and anti-de Sitter solutions. Then, one needs to give prescriptions on how to perform the averages in Eq. (5.3). One of the most widely used, which also justifies the name high-frequency expansion, is the *ADM averaging scheme* [151, 152]. In this case, assuming that the field perturbations $\{h_{\mu\nu}, \delta\phi\}$ have shorter variation scales compared to their background counterpart, the averages in Eq. (5.3) can be taken as an average over a spacetime volume containing many periods of the high-frequency perturbations. As done before in the Introduction and Chapter 4, in this approach, one also defines the quantity

$$\frac{1}{\omega} \equiv \frac{\lambda}{L} \ll 1, \tag{5.6}$$

where λ is the order of magnitude of the derivatives of the perturbations: $|\partial h_{\mu\nu}| \sim h/\lambda$ and $|\partial\delta\phi| \sim \delta\phi/\lambda$. This parameter allows us to formally evaluate the $\langle\ldots\rangle$: oscillatory perturbations average out to zero after integrating over volumes larger than λ but small enough to be independent of ω. As already mentioned in the Introduction, the parameter ω can also be defined through the frequencies of the wave and the background, i.e. $1/\omega = f_B/f_{gw}$ and the averages become time averages over multiple periods of the wave, rather than spatial ones. In practice, ω is used to separate between the so-called *low-frequency modes*, i.e. the background, and the *high-frequency modes*, i.e. the oscillatory perturbations.

5.2.1. Consequences on the gauge transformation

As discussed in Section 1.3.2, in order to make Eq. (5.2), we need to assign an extra criterion to uniquely distinguish $\{\bar{g}_{\mu\nu}, \bar{\varphi}\}$ from $\{h_{\mu\nu}, \delta\varphi\}$, otherwise they can be mixed via the linearized gauge transformation. Under the transformation

$$x^\mu \to x^\mu + \xi^\mu \tag{5.7}$$

because of the symmetries of the action (5.1), the fields transform as

$$g'_{\mu\nu}(x') \;=\; g_{\rho\sigma}(x)\,\frac{\partial x^\rho}{\partial x'^\mu}\frac{\partial x^\sigma}{\partial x'^\nu}\,. \tag{5.8}$$

$$\varphi'(x') \;=\; \varphi(x)\,. \tag{5.9}$$

Considering now an infinitesimal generator, $\xi^\mu = \alpha\delta\xi^\mu$, we can straightforwardly find the linearized versions of the symmetry transformations

$$\bar{g}'_{\mu\nu}(x) + \alpha\,h'_{\mu\nu}(x) \;=\; \bar{g}_{\mu\nu}(x) + \alpha\,h_{\mu\nu}(x) - \alpha\,(\bar{\nabla}_\mu\delta\xi_\nu + \bar{\nabla}_\nu\delta\xi_\mu)\,, \tag{5.10}$$

$$\bar{\varphi}'(x) + \alpha\,\delta\phi'(x) \;=\; \bar{\varphi}(x) + \alpha\,\delta\phi(x) - \alpha\,v^\mu\,\delta\xi_\mu\,, \tag{5.11}$$

where $\bar{\nabla}_\mu$ is the covariant derivative associated to $\bar{g}_{\mu\nu}$. From the expressions above we understand that the requirement $\alpha \ll 1$ is not enough to define the GW and SW, as nothing forbids the background field's configurations, $\{\bar{g}'_{\mu\nu}(x), \bar{\varphi}'(x)\}$ to acquire also a small (order α) part. In order to have a well-defined $h'_{\mu\nu}(x)$ and $\delta\phi'(x)$ after the transformation, one must also decide how to assign the extra terms coming from the part in the transformation's laws which depend on $\delta\xi$. Moreover, even if we required ξ to be infinitesimal, its derivative could be large. This more transparent way of stating the problem at hand, makes clear how the two approaches solve it in different ways.

• *Approach 1:* In this case, one simply opt to have a fixed background. So that, by definition

$$\bar{g}'_{\mu\nu}(x) = \bar{g}_{\mu\nu}(x)\,, \qquad \text{and} \qquad \bar{\varphi}'(x) = \bar{\varphi}(x)\,. \tag{5.12}$$

Indeed, in standard cosmological perturbation theory, as the one presented in Sections 1.1.2 and 1.2.2, the FLRW metric is considered fixed [37]. Upon using Eq. (5.12) into the linearized gauge transformation, we find the standard transformation laws

$$h'_{\mu\nu}(x) \;=\; h_{\mu\nu}(x) - (\bar{\nabla}_\mu\delta\xi_\nu + \bar{\nabla}_\nu\delta\xi_\mu)\,, \tag{5.13}$$

$$\delta\varphi'(x) \;=\; \delta\varphi(x) - v^\mu\delta\xi_\mu\,, . \tag{5.14}$$

• *Approach 2:* In this approach, one assumes that the field perturbations vary on a smaller length-scale compared to that one of their background counterparts. Another way of stating this is that the GW and SW only contain frequency modes above a certain value, decided by ω (if it was possible to decouple the modes in Fourier space, the waves would contain modes only from a certain k onward). The linearized symmetry generator, $\alpha\delta\xi^\mu$, while it might be infinitesimal, in general it contains in principle every frequency mode. Using the averaging $\langle\ldots\rangle$, we split it as

$$\delta\xi^\mu = \delta\xi^\mu_{\text{low}} + \delta\xi^\mu_{\text{high}}\,, \qquad \text{with} \qquad \delta\xi^\mu_{\text{low}} \equiv \langle\delta\xi^\mu\rangle\,. \tag{5.15}$$

This way we are assuming that $\delta\xi^\mu_{\text{high}}$ varies on the same scales of the high-frequency GW and SW, namely $\{h_{\mu\nu}, \delta\phi\}$, and its gradients are enhanced by a factor ω as well.

By averaging, then, Eqs. (5.10) and (5.11), one would find that

$$h'_{\mu\nu}(x) \quad = \quad h_{\mu\nu}(x) - (\bar{\nabla}_\mu \delta\xi_\nu^{\text{high}} + \bar{\nabla}_\nu \delta\xi_\mu^{\text{high}}), \tag{5.16}$$

$$\delta\varphi'(x) \quad = \quad \delta\varphi(x) - v^\mu \delta\xi_\mu^{\text{high}}, . \tag{5.17}$$

while $\delta\xi_{\text{low}}$ would transform $\bar{g}_{\mu\nu}(x)$ into $\bar{g}'_{\mu\nu}(x)$. In other words, if we want the high-frequency behavior of the metric perturbation to be preserved by the gauge transformation (i.e. $|\partial h'_{\mu\nu}(x)| \sim \alpha/\lambda$), we need to restrict the class of allowed infinitesimal diffeomorphisms ($\alpha\delta\xi$) to those which have a highly oscillatory character as well ($\alpha\delta\xi_{\text{high}}^\mu$). However, this is not enough. From Eq. (5.16) we see that $\bar{\nabla}_\mu \delta\xi_\nu^{\text{high}} \sim \omega\alpha$, so that, in order to have $h'_{\mu\nu}(x)$ still a small perturbation, we need to lower its amplitude. We impose the condition

$$|\bar{\nabla}_\mu \delta\xi_\nu^{\text{high}}| \lesssim \alpha, \tag{5.18}$$

which leads to

$$|\partial_\mu \delta\xi_\nu^{\text{high}}| \sim \frac{|\delta\xi^{\text{high}}|}{\lambda} \lesssim \alpha \quad \rightarrow \quad |\delta\xi^{\text{high}}| \lesssim \frac{\alpha L}{\omega}. \tag{5.19}$$

Eq. (5.19) shows that, according to the value of ω, not every linearized diffeomorphism is allowed [150, 356]. Note that this requirement, based on the separation of ξ^μ of Eq. (5.15), is not imposed in *Approach 1* leading to subtleties in the gauge choices, as it will be shown later, which must be understood in order to relate GWs described in the two formalisms.

5.2.2. High-frequency expansion and gauge subtleties

In this section, we investigate the consequences of assuming Eq. (5.19) in *Approach 2*. We start by using ω to set up the expansions

$$h_{\mu\nu} = h_{\mu\nu}^0 + \omega^{-1} b_{\mu\nu}, \qquad b_{\mu\nu} = h_{\mu\nu}^1 + \omega^{-1} h_{\mu\nu}^2 + \dots \tag{5.20}$$

$$\delta\varphi = \delta\varphi^0 + \omega^{-1}\delta\psi, \qquad \delta\psi = \delta\varphi^1 + \omega^{-1}\delta\varphi^2 + \dots \tag{5.21}$$

$$\delta\xi_\mu^{\text{high}} = \delta\xi_\mu^0 + \omega^{-1}\delta\zeta_\mu, \qquad \delta\zeta_\mu = \delta\xi_\mu^1 + \omega^{-1}\delta\xi_\mu^2 + \dots, \tag{5.22}$$

as when studying beyond geometric optics corrections. When $\omega^{-1} \ll 1$, these are meaningful perturbative expansions, and Eqs. (5.19) and (5.22) lead to

$$\delta\xi_\mu^0 = 0. \tag{5.23}$$

This implies that the generator of linear, high-frequency diffeomorphisms vanishes in its geometric optics order. We can then reorganize the gauge transformations in Eqs. (5.16) and (5.17) in powers of ω as

$$h'_{\mu\nu} \quad = \quad h_{\mu\nu} - \omega^{-1}(\bar{\nabla}_\mu \delta\zeta_\nu + \bar{\nabla}_\nu \delta\zeta_\mu), \tag{5.24}$$

$$(\delta\varphi^0)' \quad = \quad \delta\varphi^0, \tag{5.25}$$

$$\delta\psi' \quad = \quad \delta\psi - v^\mu \delta\zeta_\mu, \tag{5.26}$$

from which we see that $\delta\varphi^0$ is gauge invariant and that whenever $v_\mu \neq 0$, the transformation above mixes $h_{\mu\nu}$ and $\delta\psi$, in the sense that gauge fixing one field modifies also the other and vice-versa. Moreover, the leading order terms transform as

$$(h^0_{\mu\nu})' = (h^0_{\mu\nu}) - \omega^{-1}(\partial_\mu \delta\xi^1_\nu + \partial_\nu \delta\xi^1_\mu), \qquad (\delta\varphi^0)' = \delta\varphi^0, \tag{5.27}$$

i.e., as if they lived on a flat background. This is not surprising, since covariant derivatives commute when acting on perturbations approximated at leading order in ω [151]. To arrive to the first equation above, one can expand the covariant derivatives in Eq. (5.24) and neglect the terms proportional to the Christoffel symbols: they are of order ω^{-1} since no derivative act on a highly oscillating field. From Eq. (5.25), it is clear that $\delta\varphi^0$ cannot be gauged away, and one must invoke other reasoning to, in case, discard it. For instance, in Chapter 4, we assumed that, at the source location, General Relativity holds. What we implicitly did, was to assume that $\delta\varphi^0$ is the part of the scalar wave generated by, e.g., an astrophysical source, while $\delta\psi$ the one related to propagation effects. With this notion in mind, assuming that the generation mechanisms does not produce the scalar field, means that $\delta\varphi^0$ is not sourced, hence we set it to zero in Chapter 4. Here we try to relax this assumption in what follows and investigate the complementary situation: instead of the production moment, the detection one. We will also show that regardless of this different interpretation of $\delta\varphi^0$ and $\delta\psi$, the number of degrees of freedom is still, in total, three.

Our discussion shows that there are gauges choices that are not suitable to describe perturbations across different energy scales, i.e. values of ω. For instance, unitary gauge, $\delta\phi = 0$, is not allowed in the language of the high-frequency expansion when $\omega^{-1} \ll 1$. This is not the case in *Approach 1*, that does not impose the condition in Eq. (5.18). We comment that, these subtleties in the gauge choices are not a problem per se, but one must be aware of them.

5.3. Gauge fixing and equations of motion

In this Section, we derive the equations of motion of the field perturbations. To obtain equations which are valid according to both definitions for them, we opt for gauge fixings that can be performed in both cases. In particular, we will avoid choosing the unitary gauge ($\delta\phi = 0$). Assuming $v^\mu v_\mu > 0$ we define the orthogonal projector

$$\Lambda_{\mu\nu} \equiv \bar{g}_{\mu\nu} - n_\mu n_\nu, \quad n_\mu \equiv \frac{v_\mu}{L}, \tag{5.28}$$

and decompose the metric perturbation as

$$h_{\mu\nu} = n_\mu n_\nu A + (n_\mu B_\nu + n_\nu B_\mu) + C_{\mu\nu}, \tag{5.29}$$

with $A \equiv n^\rho n^\sigma h_{\rho\sigma}$, $B_\mu \equiv n^\rho \Lambda^\sigma_\mu h_{\rho\sigma}$ and $C_{\mu\nu} \equiv \Lambda^\rho_\mu \Lambda^\sigma_\nu h_{\rho\sigma}$ [365]. The choice $v^\mu v_\mu > 0$ is suitable to investigate screening scenarios where the spacetime assumes a radial

profile, and in the last Section we address the detectability of the waves. In cosmological settings, on the other hand, $v^\mu v_\mu < 0$ and consequently one should construct the projector as $\Lambda_{\mu\nu} \equiv \bar{g}_{\mu\nu} + n_\mu n_\nu$. We impose the conditions

$$A = 0, \qquad B_\mu = 0. \tag{5.30}$$

Then, using the residual gauge freedom, we also fix:

$$C = \bar{g}^{\mu\nu} C_{\mu\nu} = 0, \qquad \bar{\nabla}^\mu C_{\mu\nu} = 0. \tag{5.31}$$

Note that we have exhausted the gauge freedom since Eqs. (5.30) and (5.31) amount to 4 conditions each. B_μ only has 3 independent components because it is orthogonal to n^μ and the condition $C = 0$ implies $n^\mu \bar{\nabla}^\nu C_{\mu\nu} = 0$, in fact

$$n^\mu \bar{\nabla}^\nu C_{\mu\nu} = -C_{\mu\nu}(K^{\mu\nu} - n^\mu a^\nu) = -C_{\mu\nu} K^{\mu\nu} \propto C, \tag{5.32}$$

where $K_{\mu\nu} \equiv \Lambda_\mu^\rho \bar{\nabla}_\rho n_\nu$ is the extrinsic curvature of the hypersurfaces orthogonal to n, and $a_\mu \equiv n^\rho \bar{\nabla}_\rho n_\mu$ the acceleration vector. In the last step, we used the fact that scalars can be computed in any coordinate system and that choosing $\bar{\phi}$ as a coordinate implies $K_{\mu\nu} \propto \Lambda_{\mu\nu}$. Using the background equations of motion,

$$\bar{R}_{\mu\nu} = \frac{1}{2}\left(v_\mu v_\nu + \bar{g}_{\mu\nu}\bar{V}\right), \qquad \bar{\Box}\bar{\varphi} = \bar{V}', \tag{5.33}$$

where $\bar{V} = V(\bar{\varphi})$ and $\bar{V}' = (\partial V/\partial\varphi)|_{\bar{\varphi}}$, one can show that the combination

$$\left(\bar{\Box}\delta\phi - \delta\phi\,\bar{V}''\right) + \bar{\nabla}^\mu[v^\nu h_{\mu\nu}] - \frac{1}{2}v^\mu\bar{\nabla}_\mu h, \tag{5.34}$$

is gauge invariant, where $\bar{V}'' = (\partial^2 V/\partial^2\phi)|_{\bar{\phi}}$, and h is the trace of $h_{\mu\nu}$. The last two quantities in the equation above vanish in the chosen gauge, hence $\delta\varphi$ is invariant under the residual gauge freedom and different from zero. In the high-frequency limit, being $\delta\varphi^0$ invariant, this result would regard $\delta\psi$.

To find the evolution equations of the field perturbations can be found by linearizing the equations of motion which descend from the action (5.1). Regardless of the choice for their definition, whether *Approach 1* or *Approach 2*, these are

$$\bar{\Box}\gamma_{\mu\nu} + 2\bar{R}_{\lambda\mu\alpha\nu}\gamma^{\lambda\alpha} = 0, \tag{5.35}$$

$$\bar{\Box}\delta\phi - \delta\phi\,\bar{V}'' = 0, \tag{5.36}$$

where we renamed the metric perturbation, after the gauge fixings, $\gamma_{\mu\nu}$. As usual, the system of equations represents a spin 2 wave, $\gamma_{\mu\nu}$, and a spin 0 wave, $\delta\varphi$. If $\delta\phi$ is a high-frequency field, then $\delta\varphi = \delta\varphi^0 + \omega^{-1}\delta\psi$ and Eq. (5.36) clearly shows that $\delta\varphi^0$ and $\delta\psi$ are not independent degrees of freedom. These equations do not display the additional damping term, typical of non-minimally coupled scalar-tensor theories [122], because they describe the perturbation in Einstein's frame. This factor can

be recovered by going to Jordan Frame through a conformal transformation, where matter is coupled to the metric $\tilde{g}_{\mu\nu} \equiv \Omega^2(\varphi)\, g_{\mu\nu}$. We also point out that we do not find modifications in the propagation speed of these modes because this effect is not predicted in scalar-tensor theories considered.

5.4. Observables in the high frequency limit

We study the $\omega^{-1} \ll 1$ limit of the evolution equations. Hence, we assume that we have derived Eqs. (5.35) and (5.36) by choosing the definition of the field's perturbation as in *Approach 2*. Since all the ingredients satisfy a wave equation, we make the following WKB ansatz

$$\gamma_{\mu\nu} = \Upsilon_{\mu\nu}\, e^{i\omega\theta}\,, \quad \delta\phi^0 = \delta\Phi\, e^{i\omega\theta}\,, \quad \delta\psi = \delta\Psi\, e^{i\omega\theta}\,, \tag{5.37}$$

where $\Upsilon_{\mu\nu}, \Phi, \Psi$ are complex, θ is real, and they are all slowly varying functions of the spacetime coordinates. In the expressions above, it is also understood that the fields corresponds to the Real Parts of the ansatzs, since $\{\gamma_{\mu\nu}, \delta\phi\}$ are real. We insert Eq. (5.37) into Eqs. (5.35), (5.36). Because a derivative acting on the exponential brings down a ω factor, we can separate the equations of motion into their ω^2, ω^1 and ω^0 orders. The leading order gives

$$\bar{g}^{\mu\nu}\, k_\nu\, k_\mu = 0\,, \tag{5.38}$$

where $k_\mu \equiv \partial_\mu\theta$ is the wave vector and $k^\mu \equiv \bar{g}^{\mu\nu} k_\nu$. Therefore, k_μ is a null vector tangent to a null geodesic, $k^\mu \bar{\nabla}_\mu k_\nu = 0$ which are interpreted as the rays of the graviton and scalar bundles [151, 152]. At orders ω^1 and ω^0 we find

$$2k^\rho\, \bar{\nabla}_\rho \Upsilon_{\mu\nu} + \Upsilon_{\mu\nu}\bar{\nabla}_\rho k^\rho = 0\,, \tag{5.39}$$

$$2k^\rho\, \bar{\nabla}_\rho \delta\Phi + \delta\Phi\, \bar{\nabla}_\rho k^\rho = 0\,, \tag{5.40}$$

$$2k^\rho\, \bar{\nabla}_\rho \delta\Psi + \delta\Psi\, \bar{\nabla}_\rho k^\rho = i(\bar{\Box}\Phi - \Phi\, \bar{V}'')\,. \tag{5.41}$$

The equations above imply that the squared amplitudes of $(\Upsilon_{\mu\nu}, \delta\Phi)$ scale with the inverse cross-sectional area of the particle's bundle (see Eqs. (4.57) and (4.58) of Chapter 4), while $\delta\Psi$ has an additional source/sink term.

5.4.1. Geodesic Deviation equation: polarization content

We can understand the effect of the gravitational and scalar waves on test particles by looking at the geodesic deviation equation in Jordan frame, namely in the frame where matter is exclusively coupled to the metric $\tilde{g}_{\mu\nu}$[1]. Since this equation describes the relative acceleration of two nearby geodesics, we can use them to describe the

---

[1]We use a tilde to denote a quantity in Jordan frame

polarization content of the GWs, and we will show that this is composed by both the tensor and scalar modes. In literature, these polarization modes are commonly classified via the Newmann-Penrose scalars [300]. However, this classification relies on the local Lorentz symmetry of the theory, which is spontaneously broken in our setting (we assumed $v_\mu \neq 0$), questioning its applicability. Indeed, the freedom of gauging away $\delta\Psi$, in favor of new components of $\Upsilon_{\mu\nu}$, is the manifestation of this fact. Even if this classification isn't suitable anymore, the relative acceleration between observers is related to the whole Riemann tensor perturbation, gauge invariant up $\mathcal{O}(\omega^1)$, and not its individual components.

From its definition, namely $\tilde{g}_{\mu\nu} = \Omega^2(\varphi)g_{\mu\nu}$, we can find the perturbation of the Jordan frame metric

$$\delta\tilde{g}_{\mu\nu} = \Omega^2(\bar{\varphi})\left[h_{\mu\nu} + 2\bar{g}_{\mu\nu}\frac{\Omega'(\bar{\varphi})}{\Omega(\bar{\varphi})}\delta\varphi\right]. \tag{5.42}$$

We note that the Eq. (5.42) is often used as a field redefinition aimed at decoupling the kinetic terms of the tensor and scalar perturbations in Jordan frame [300, 357]. As shown in Eqs (5.35) and (5.36), in Einstein frame the kinetic terms are indeed decoupled. In the $\omega^{-1} \ll 1$ limit, we write the WKB ansatz $\delta\tilde{g}_{\mu\nu} \equiv \tilde{H}_{\mu\nu}e^{i\omega\theta}$ so that, combining Eqs. (5.42) and (5.37) yields

$$\tilde{H}_{\mu\nu} = \Omega^2(\bar{\varphi})\left[\Upsilon_{\mu\nu} + 2\bar{g}_{\mu\nu}\frac{\Omega'(\bar{\varphi})}{\Omega(\bar{\varphi})}(\delta\Phi + \omega^{-1}\delta\Psi)\right]. \tag{5.43}$$

The factor $\Omega^2(\bar{\varphi})$ in front of the parenthesis of Eq. (5.42) encodes the extra damping term of GW and scalar wave found typically in Jordan frame (related to the factor $\int \mathcal{T}$ of Chapter 4, for instance). Using the result above, one can show that the perturbed Riemann tensor in Jordan frame is given by

$$\delta\tilde{R}_{\mu\nu\rho\sigma} = -2\omega^2 k_{[\rho}k_{[\nu}\tilde{H}_{\mu]\sigma]}e^{i\omega\theta} +$$
$$+ 2i\omega\left[k_{[\rho}\tilde{\nabla}_{[\nu}\tilde{H}_{\mu]\sigma]} + k_{[\nu}\tilde{\nabla}_{[\rho}\tilde{H}_{\sigma]\mu]} + \tilde{H}_{[\mu[\sigma}\tilde{\nabla}_{\rho]}k_{\nu]}\right]e^{i\omega\theta}, \tag{5.44}$$

where square brackets stand for antisymmetrization and $\tilde{\nabla}_\mu$ is the covariant derivative associated to the background Jordan frame metric, namely $\bar{\tilde{g}}_{\mu\nu} = \Omega^2(\bar{\varphi})\bar{g}_{\mu\nu}$. By looking at Eq. (5.43), we see that Eq. (5.44) receives contributions from both the tensor and the scalar modes, hence test particles responds also to the presence of the scalar field, though the strength of this interaction is modulated by the prefactor Ω'/Ω.

We point out that $\delta\tilde{R}_{\mu\nu\rho\sigma}$ is gauge invariant under gauge transformation in both Jordan and Einstein frames up to order $\mathcal{O}(\omega)$. Indeed, the transformations in Eqs. (5.16) and (5.17) are frame dependent: covariant derivatives and indices contractions are performed with the use of the Einstein frame metric. By using $\tilde{g}_{\mu\nu} = \Omega^2(\varphi)g_{\mu\nu}$ in the gauge transformation laws, it can be shown that a diffeomorphism with generator

ξ^μ, acting on a quantity defined in Einstein frame, corresponds to the same transformation in Jordan frame with the new generator $\tilde{\xi}^\mu = \Omega^2(\bar{\varphi})\xi^\mu$. As a consequence, the Riemann tensor perturbation in Jordan frame transforms as

$$\delta \tilde{R}'_{\mu\nu\rho\sigma} = \delta \tilde{R}_{\mu\nu\rho\sigma} - \mathcal{L}_{\tilde{\xi}} \tilde{R}_{\mu\nu\rho\sigma}\,, \tag{5.45}$$

under a gauge transformation in Einstein frame, which are the ones we performed in the beginning of this work. The last term in the equation above is of order $\mathcal{O}(\omega^0)$ since it does not contain derivatives of the high-frequency fields. This way we have proved the gauge invariance of the Jordan frame Riemann tensor, under gauge transformations in Einstein frame, up to order $\mathcal{O}(\omega)$.

Note that all $\{\Upsilon_{\mu\nu}, \delta\Phi, \delta\Psi\}$ enter the perturbed Riemann tensor in Eq. (5.44). From the equation above and Eq. (5.42) it is clear that the geometric optics orders $\Upsilon_{\mu\nu}$ and $\delta\Phi$ contribute up to $\mathcal{O}(\omega^2)$ in Eq. (5.44), while $\delta\Psi$ contributes at best at $\mathcal{O}(\omega)$ order. It is easy to check that, even when choosing the gauge $\delta\Psi' = 0$, the additional components which $\Upsilon'_{\mu\nu}$ picks up via the gauge transformation contribute at the same order of $\delta\Phi$ in the geodesic deviation equation, namely $\mathcal{O}(\omega)$, rather than $\mathcal{O}(\omega^2)$ as $\Upsilon_{\mu\nu}$. Indeed, we can gauge away $\delta\psi$ using Eq. (5.26) by choosing

$$\delta\zeta_\mu = \frac{v_\mu}{L^2}\delta\psi = \frac{v_\mu}{L^2}\delta\Psi\, e^{i\omega\theta} \tag{5.46}$$

where we also used the geometric optics ansatz in Eq. (5.37). Using this into Eq. (5.24) gives

$$\left[\Upsilon_{\mu\nu}\, e^{i\omega\theta}\right]' = \Upsilon_{\mu\nu}\, e^{i\omega\theta} - i\,\frac{\delta\Psi\, e^{i\omega\theta}}{L^2}\left[k_\mu v_\nu + k_\nu v_\mu\right] - \\ -\omega^{-1}\left[\bar{\nabla}_\mu\left(\frac{v_\nu\,\delta\Psi}{L^2}\right) + \bar{\nabla}_\nu\left(\frac{v_\mu\,\delta\Psi}{L^2}\right)\right]e^{i\omega\theta} \tag{5.47}$$

where we have used $k_\mu = \partial_\mu\theta$. By plugging this expression in Eq. (5.44), it is easy to realize that its contribution at order ω^2 vanishes, which would come from plugging the term at order ω^0 of the equation above, into the term at order ω^2 in Eq. (5.44). Using also Eq. (5.43), we find that

$$2\omega^2\, k_{[\rho} k_{[\nu} \tilde{H}'_{\mu]\sigma]}\, e^{i\omega\theta} = 2\omega^2\, k_{[\rho} k_{[\nu} \tilde{H}_{\mu]\sigma]}\, e^{i\omega\theta} - \\ -2\omega^2\, i\,\frac{\delta\Psi\, e^{i\omega\theta}}{L^2}\left[k_{[\rho} k_{[\nu} k_{\mu]}\, v_{\sigma]} + k_{[\rho} k_{[\nu} k_{\sigma]}\, v_{\mu]}\right]e^{i\omega\theta} + \mathcal{O}(\omega) = \\ = 2\omega^2\, k_{[\rho} k_{[\nu} \tilde{H}_{\mu]\sigma]}\, e^{i\omega\theta} \tag{5.48}$$

because the antisymmetrization of three copies of the same vector is null.

Therefore, we conclude that, regardless of the gauge choice, $\{\Upsilon_{\mu\nu}, \delta\Phi\}$ contribute to the highest order in the geodesics deviation equation, which drives the acceleration between tests particles, while the effects of $\delta\Psi$ are subdominant and suppressed by

a factor $\omega^{-1} \ll 1$. Moreover, the contribution of $\{\delta\Phi, \delta\Psi\}$ depends on the profile of the background scalar field and the conformal coupling, through the multiplicative factor $\Omega'(\bar{\varphi})/\Omega(\bar{\varphi})$ in Eq. (5.43).

Finally, we also comment that the acceleration between two nearby geodesics is given by the contraction of Eq. (5.44) with $\bar{u}^\mu \bar{u}^\rho$, the four-velocity of a Jordan frame observer. Being $\Upsilon_{\mu\nu}$ orthogonal to v_μ and not $\bar{u}^\mu$, it could be that the polarization content seen by the observer is different from the standard case. Investigating this possibility will be the topic of further works.

5.5. Screening: implications for polarization tests

We investigate the role of screening in the possibility of detecting directly the DE scalar field, in the theories considered in this Chapter. We consider two types of such mechanisms, compatibly with the choice of the action (5.1), namely chameleon and symmetron. The term V'' in Eq. (5.36) represents the mass squared of the background scalar field. In the presence of matter, the scalar field is governed instead by an effective potential given by

$$V'_{\text{eff}}(\bar{\varphi}) = V'(\bar{\varphi}) - \Omega^3(\bar{\varphi})\Omega'(\bar{\varphi})\tilde{T}, \tag{5.49}$$

where $\tilde{T}$ is the trace of the matter energy momentum tensor in Jordan frame. For a pressureless fluid, this corresponds to the matter density ρ. The interplay between the two terms in V_{eff} leads to the realization of a particular screening mechanism. For a spherical matter density, both exhibit the following behaviors:

- V''_{eff} increases: the field becomes more massive and the coupling to matter dominates over the vacuum mass.

- $\bar{\varphi} \to 0$: the field relaxes into the minimum of the effective potential, which is pushed towards 0. If the spherical distribution is massive enough, the field might satisfy $\bar{\varphi} \equiv 0$ inside the source.

- $\partial\bar{\varphi} = 0$ at the center, this is simply a spherical boundary condition required for continuity.

These conditions apply only inside the region dominated by matter, but their trends are also valid in the empty area surrounding a spherically symmetric object because the outside profile is smoothly joined to the constant low-value of the field inside the dense region [51, 366]. Therefore, we assume that these behaviors are valid also in our treatment, where we neglected the matter content. Broadly speaking, the chameleon mechanism relies on the larger mass to cancel the effect of a force by

reducing its range of action, while the symemtron relies on the suppression of the scalar field to cancel the conformal coupling $\Omega(\varphi)$.

In the low-frequency regime ($\omega^2 \ll V''$), Eq. (5.36) describes a damped wave [367]. This suppression is similar to the background result $\bar{\varphi} \to 0$ inside screened regions. This is not surprising, as the low-frequency limit corresponds to a breakdown of the background-perturbation dichotomy. Hence, waves in this energy range are screened.

More interesting is the high-frequency case. As shown in Eqs. (5.39) and (5.40), the amplitude of the waves at leading order, namely $\Upsilon_{\mu\nu}$ and $\delta\Phi$, are not affected by the field's background configurations, therefore one would expect to be able to detect a scalar wave. More specifically, neither of these equations do not show a sink term on their left-hand-sides, so one expects that if it is possible to detect the tensor mode, $\Upsilon_{\mu\nu}$, then the same conclusion holds also for, at least the leading order, scalar mode, $\delta\Phi$. In Jordan frame, however, it is clear that the detectability of the waves through the motion of test particles is a local effect that depends on the form of $\Omega(\bar{\varphi})$ evaluated on the background solution, see Eqs. (5.42) and (5.44). Therefore, even if the scalar wave amplitude is not suppressed, its coupling to matter might be. Looking at specific realizations of the theory, in the case of chameleon screening [368] we have $\Omega'/\Omega \sim 1/M$ in high-density regions,

$$\frac{\Omega'(\bar{\varphi})}{\Omega(\bar{\varphi})} \sim \frac{1}{M} \tag{5.50}$$

where M is the large mass scale of the coupling, constrained by laboratory experiments to be $M \gtrsim 10^{-5} \, M_{\rm pl}$, where $M_{\rm pl}$ is the Planck mass [237]. In the case of symmetron gravity [369], we have $\Omega'/\Omega \sim 0$,

$$\frac{\Omega'(\bar{\varphi})}{\Omega(\bar{\varphi})} \sim 0 \,, \tag{5.51}$$

implying that the effects of a high-frequency scalar wave are not visible on test particles.

5.6. Discussion and Conclusions

The growth of matter perturbations and the propagation of GWs are two key probes of the source of the late time cosmic accelerated expansion. With the current and future galaxy surveys and gravitational waves observatories, we will be able to use jointly the information coming from these two observationally independent sectors. However, the theoretical tools employed to describe their phenomenology are not always compatible as the assumptions they rely on are, in general, different. The first goal of this Chapter, was to show that their difference arise already at the level of the

definition of the field's perturbations: in the former as the difference between the fields and an assigned background as in *Approach 1*, in the latter via suitable averaging procedures as in *Approach 2*. We illustrated the consequence of the assumptions of *Approach 2* on the allowed gauge transformations, which are essentially summarized in Eq. (5.19), and we claimed that the gauge transformations couples the leading order GW, $h^0_{\mu\nu}$, with the next-to-leading order scalar field, $\delta\psi$.

Taking the theory in Eq. (5.1) as a working example, we derived the equations of motion of the field perturbations, namely Eqs. (5.35) and (5.36), opting a gauge choice which is allowed in both approaches. We then moved to the discussion of the detectability of the additional scalar wave in light of two screening mechanisms, chameleon and symmetron, and concluded that scalar waves are not detectable no matter their wavelength. In the low-frequency limit, when $\omega^2 \ll V''$, the scalar wave is damped when approaching a screened region because the amplitude of the scalar wave is affected by the non-trivial background profile. Rhis is not true when $\omega^{-1} \ll 1$, as the geometric optics leading order $\delta\Phi$ doesn't feel the features of $\bar{\varphi}$. Nevertheless, we showed that in this case screening suppresses the interactions between the scalar wave and matter via the multiplicative factor $\Omega'(\bar{\phi})/\Omega(\bar{\phi})$ in Eq. (5.44), making the scalar wave undetectable.

Note: I actively worked on every aspect of the paper this Chapter is based on. Note that this work is still under review, reason why the topics presented in this Chapter do not exactly overlap with the version of the paper on arXiv.

Part III

Wave-optics limit: the stochastic background and its polarization

6

Gravitational waves in the wave-optics limit

The stochastic gravitational wave background is a rich resource of cosmological information, encoded in its source statistics and anisotropies induced by propagation effects. We provide a theoretical description of it, without employing theoretical tools relying on the geometric-optics assumption. The formalism is based on the classical matter approximation, and it is able to capture wave-optics effects, such as interference and diffraction. We show that the interaction between the gravitational waves and the cosmic structures along the line-of-sight produce observable scalar and vector polarization modes. We build the two point correlation function of the tensor modes, and introduce the Stokes parameters. In the case of an unpolarized, Gaussian, statistically homogeneous and isotropic initial background, we show that the interaction with matter does not generate a net difference between left- and right- helicity tensor modes, as expected, but it also does not produce Q- and U- polarization modes

6.1. Introduction

The incoherent superposition of many gravitational waves builds up the so-called stochastic gravitational wave background (SGWB). The stochastic nature of the background can be traced back to its source (e.g. inflationary tensor modes [22–24, 133], cosmic strings and phase transitions [135–139], scalar induced GW [140–148]) or to limitations of specific instruments employed to detect GWs (e.g. cumulative signal from unresolved astrophysical sources as: compact objects binaries [370–373], stellar core collapse events [374]). The search for the stochastic background [375, 376] is already ongoing with the online GW observatories [377–379]. Exactly as the Cosmic Microwave Background (CMB), the SGWB contains a formidable amount of cosmological information, both in its frequency profile and in the angular power spectrum describing its anisotropies [177], justifying the importance of having different technologies to probe it [370, 380–382]. As the GW spectrum spans more than 20 orders of magnitude in frequency, multi-band GW observations will start a new observational phase for cosmology: the different behaviors in each energy regime can be used to break degeneracies between intrinsic and induced properties of the SGWB [383], or track different source populations [20, 384–391] or investigate dark energy [392]. The SGWB carries cosmological information on two levels: in its sources and through propagation effects, deforming the observed signal as the GWs travel through the inhomogeneous matter distribution. In case of the astrophysical background, the sources are additionally tracers of the underlying dark matter distribution, while large primordial non-Gaussianities in the squeezed limit can imprint anisotropies in the primordial SGWB [393–395].

The main goal of this Chapter, is to describe the interactions between the propagating GWs and the matter structures present in the Universe, going beyond the standard treatments and, hence, providing a novel and interesting cosmological probe. The current state of the art, describes the SGWB through the characterization of the *GW energy density spectrum*, $\Omega_{GW}(f)$, which can either be directly related to properties of the GW's sources [396–398], or computed through a Boltzmann equation approaches [159, 399, 400]. Line-of-sight effects are then accounted for by analyzing the propagation of GWs through the cosmic web. These include, e.g. Doppler, volume and weak gravitational lensing [136, 386, 396–403], and numerical tools to compute them are already being developed [404]. These effects are the same as those described in Section 1.4.3 generating the luminosity distance fluctuations. Both the Boltzmann equation and the line-of-sight treatments, rely on the possibility of describing effectively the GWs as particles, with a well-defined momentum and position at each time, a condition which is met only in the high-frequency limit [151, 152, 155]. As a drawback, the wave nature of the GWs is neglected and no polarization effects can be included. Additionally, in this regime, the frequency dependence of the interaction of the SGWB and the cosmological structures is washed

away. When addressing the opposite situation, namely the *wave-optics limit*, the oscillatory nature of the GWs is fully taken into account and frequency dependent interference or diffraction effects may arise. The possibility of capturing these effects is interesting for two main reasons: a resonantly positive interference can boost the GW signal, making the detection possibly more feasible, and the interaction between the waves and the matter structures, in this limit, can polarize the stochastic background.

The literature of wave-optics effects in gravitational lensing of gravitational waves started to flourish after their first detection, and it is starting to draw much attention. The interference and diffraction induced by a static lens has been addressed starting from the pioneering work [162], and proceeding with [149, 163–166], showing that these become important when the mass of the lens is such that

$$M_L \lesssim 10^8 M_\odot \left(\frac{f}{mHz} \right)^{-1} , \tag{6.1}$$

where f is the frequency of the GW, as described in Section 1.3.2 of the Introduction. In the case of resolved GW events observed by LISA, it has been assessed that over $(0.1 - 1.6)\%$ of massive black hole binaries in the range of $10^5 - 10^{6.5}$ solar masses will display wave-optics effects [176, 177], while, in the frequency band of the ground-based detectors, it is expected that such events will be visible for sources up to redshift $z_s = 2 - 4$ with third generation observatories [178]. Since the SGWB contains all the possible frequencies, the probability of having a wave-optics event is 1. Contrary to lensing in geometric optics, wave-optics effects are frequency dependent and induce non-trivial deformation in the GWs amplitude, making these events very promising candidates to infer properties of lenses [180]. Despite the exciting prospects, all of these works rely on the major assumption of treating the GWs as scalar waves, hence neglecting their tensorial nature, as shown explicitly in Section 1.3.2.

Leveraging on a parallelism with the CMB, we expect secondary effects to introduce a polarization pattern on the SGWB, tracking the profile of the gravitational potential wells along the line-of-sight [231, 405–407]. Similar effects have been investigated in the case of high-frequency GWs [408], where the authors claim that, already at the first order away from the geometric optics limit, new components in the GWs content arise. Following this logic, we expect that in the wave-optics regime, the polarization content of the SGWB should become a powerful resource of cosmological information, already in General Relativity. Still, it is generally believed that the detection of a non-trivial GW's polarization content is a sign of breaking of the standard gravitational theory; either because of the presence of parity violating GW sources [409–412] or of extra propagating degrees of freedom [413–415]. However, the direct detectability of the additional mediator has already been questioned in light of the screening mechanisms characterizing these theories, as we have shown

in Chapter 5. It then becomes imperative to disentangle the polarization content arising from new physics from the one simply due to secondary anisotropies, especially because efforts in extracting physics from the SGWB polarization content [416] and in characterizing its detection prospects [409, 417, 418] are already taking place.

Given all of these considerations, the aim of this Chapter is to provide a formalism describing the SGWB across the entire frequency spectrum, thus without relying on the geometric optics approximation. Attempts to go in this direction can be found in [419, 420], though the authors still employ a Boltzmann equation formalism and account for the wave effects by introducing suitable collision terms [421–425]. On the contrary, here we follow closely the logic of [165], and work directly at the level of the linearized Einstein's equations, finding an explicit solution for the GWs. In order to do so, we introduce the so-called *classical matter approximation*, which consist in neglecting the response of matter to the presence of the SGWB. The GW solution found this way contains scalar and vector modes, on top of the tensor ones, incorporating the induced polarization content of the SGWB. From this result, we build the two point function for the GW's tensor modes and draw conclusions on the statistics of the intensity and polarization of the SGWB.

6.2. Equations of motion of the metric perturbation

We consider a Universe whose geometry is described by the metric $\bar{g}_{\mu\nu}$, and the propagation of GWs on top of it. For our purposes, we assume that the background geometry entirely fixed by the matter content of the Universe. Eventually, we will choose $\bar{g}_{\mu\nu}$ to represent a perturbed cosmological background, therefore including also matter structures. These structures are not necessarily on large-scales, such as the LSS previously investigated, as our formalism is also able to account for gravitational potential wells generated by compact lenses. As in the rest of the Thesis, we work in a two parameter expansion: α, tracking the perturbation order of the gravitational wave around $\bar{g}_{\mu\nu}$, and ϵ, accounting for the matter structures around the homogeneous and isotropic spacetime. We will make use of ϵ only from Section 6.3 onward.

6.2.1. Perturbed Einstein's equations

As done in the Introduction, we start by the metric expansion in Eq. (1.76), namely

$$g_{\mu\nu} = \bar{g}_{\mu\nu} + \alpha\, h_{\mu\nu},\tag{6.2}$$

and find the linearized gravitational field Eq. (1.64). Since we work in General Relativity in this Chapter, we only consider the standard matter content and write

$$\delta_\alpha\left[G_{\mu\nu} - 8\pi G\, T_{\mu\nu} \right] = 0\,.\tag{6.3}$$

In (6.3), $T_{\mu\nu}$ is the matter stress-energy tensor and δ_α means linearization to first order in α. Choosing the de-Donder gauge (1.80), namely

$$\bar{\nabla}^\mu \tilde{h}_{\mu\nu} = 0, \tag{6.4}$$

where $\tilde{h}_{\mu\nu} = h_{\mu\nu} - h\bar{g}_{\mu\nu}/2$, the perturbation of the Einstein tensor reads

$$\delta_\alpha G_{\mu\nu} = -\frac{\alpha}{2}\left[\bar{\Box}\tilde{h}_{\mu\nu} + 2\bar{R}_{\lambda\mu\alpha\nu}h^{\lambda\alpha} - h_\nu^\lambda\bar{R}_{\lambda\mu} - h_\mu^\lambda\bar{R}_{\lambda\nu} + h_{\mu\nu}\bar{R} - \bar{g}_{\mu\nu}h^{\alpha\beta}\bar{R}_{\alpha\beta}\right]. \tag{6.5}$$

Assuming that the background fields are on-shell, $\bar{G}_{\mu\nu} = 8\pi G\,\bar{T}_{\mu\nu}$, we rewrite Eq. (6.3) as

$$\bar{\Box}\tilde{h}_{\mu\nu} + 2\bar{R}_{\lambda\mu\alpha\nu}h^{\lambda\alpha} - \bar{g}_{\mu\nu}h^{\alpha\beta}\bar{R}_{\alpha\beta} + 8\pi G\delta_\alpha\Theta_{\mu\nu} = 0, \tag{6.6}$$

where $\delta_\alpha\Theta_{\mu\nu}$, defined in Eq. (1.83), is

$$\delta_\alpha\Theta_{\mu\nu} \equiv \frac{1}{2\alpha}\left[\bar{g}_{\mu\sigma}\left(\delta_\alpha T_\nu^\sigma\right) + \bar{g}_{\nu\sigma}\left(\delta_\alpha T_\mu^\sigma\right)\right]. \tag{6.7}$$

6.2.2. Classical matter approximation

We regard matter as an external field whose role is *exclusively* to curve the background spacetime and unresponsive to the passage of the GWs. Indeed, we are interested in describing the propagation effects on the GW properties (such as strain, polarization and frequency) due to the structures in the Universe, and not how cosmic structures are affected by them. This assumption, which we dub *the classical matter approximation* (CM), explicitly consists of choosing,

$$\delta_\alpha\Theta_{\mu\nu} = 0, \tag{6.8}$$

so that Einstein's equations (6.6) become sourceless. If one thinks of $\bar{g}_{\mu\nu}$ as a perturbed FLRW spacetime, Eq. (6.8) can be also understood as assuming that the fluctuations in the matter sector induced by the GWs are negligible compared to the already present matter structures. Under this light, it becomes clear that the classical matter approximation is well suited to describe the late time Universe where relativistic species, which might have a non-negligible anisotropic shear stress, are subdominant. Compatibly with Eq. (6.8), we also expand the observer's 4-velocity to liner order in α as

$$u^\mu = \bar{u}^\mu + \delta_\alpha u^\mu \tag{6.9}$$

and require

$$\delta_\alpha u^\mu = 0. \tag{6.10}$$

This approximation implies immediately that the contraction of $h_{\mu\nu}$ with the unperturbed velocity vanishes. This can be checked using

$$u^\mu u_\mu = -1 \qquad \rightarrow \qquad h_{\mu\nu}\bar{u}^\mu\bar{u}^\nu = 0, \tag{6.11}$$

which we interpret as a compatibility condition of our approximation scheme. Note that Eq. (6.8) is not equivalent to neglecting the back-reaction of the waves on the spacetime, which is a second order contributions ($\sim h^2$) to the equations of motion of the background $\bar{g}_{\mu\nu}$. Rather, it means neglecting the interaction between the GWs and the matter species: the term $\delta_\alpha \Theta_{\mu\nu}$ in Eq. (6.6) descends from quadratic terms of the form $\propto h^{\mu\nu} \delta_\alpha \Theta_{\mu\nu}$ in the second order action.

6.2.3. Physical meaning of the CM approximation

In this Section, we illustrate the meaning of the assumption in Eq. (6.8) by considering the simplified case where $\bar{g}_{\mu\nu}$ is a homogeneous and isotropic spacetime.

Since we haven't characterized the metric perturbation as a gravitational wave yet, at this stage $h_{\mu\nu}$ includes also scalar and vector modes. Indeed, one of the main themes of this entire Thesis is: there is no formal difference between a GW defined in the *wave-optics limit*, as described in Section 1.3.2, and doing cosmological perturbation theory as in Section 1.1.2, apart from the choice of the background. In this Section, we choose $\bar{g}_{\mu\nu} = a^2(\tau)\eta_{\mu\nu}$, so there is really no formal difference between what we are about to present and what done and Section 1.1.2, except for the name of the players. Having said this, in the previous Section we opted for the de-Donder gauge choice, but in principle we could change it, decompose $h_{\mu\nu}$ into scalars - vectors - tensors subgroups and opt for Poisson's gauge, as we did for $\delta g_{\mu\nu}$ in Section 1.1.2.

By choosing $h_{\mu\nu}$ in Poisson's gauge, the perturbed line element takes the form

$$
\begin{aligned}
\mathrm{d}s^2 &= (\bar{g}_{\mu\nu} + \alpha h_{\mu\nu})\mathrm{d}x^\mu \mathrm{d}x^\nu = \\
&= a^2(\eta)\left\{-(1 + 2\alpha H_{00})d\eta^2 + 2\alpha H_{0i}\,d\eta\,dx^i + [(1 - 2\alpha H)\delta_{ij} + \alpha\gamma_{ij}]dx^i dx^j\right\},
\end{aligned}
\tag{6.12}
$$

where we have factored out an $a^2(\eta)$, so that $h_{00} = -2a^2 H_{00}$, $h_{0i} = -2a^2 H_{0i}$ and similarly for the spatial trace, $\bar{g}^{ij}h_{ij} = -2a^2 H$. It is known that in Eq. (6.12) there are: two scalar potentials, H_{00} and H, one transverse vector potential, H_{0i} such that $\partial^i H_{0i} = 0$, and one transverse-traceless tensor potential, γ_{ij} such that $\partial^i \gamma_{ij} = 0$ and $\gamma^i_i = 0$[1]. These potentials are decoupled at linear order, and they satisfy [34]

$$
\nabla^2 H = 4\pi G a^2 (\delta_\alpha T^0_0 + 3\mathcal{H}H_f), \qquad -\partial_i H_f = [\delta_\alpha T^0{}_i]_\parallel, \tag{6.13}
$$

$$
\nabla^2 H_{0i} = 16\pi G a^2 [\delta_\alpha T^0{}_i]_\perp, \tag{6.14}
$$

$$
(\partial_\tau^2 + 2\mathcal{H}\partial_\tau - \Delta)\gamma_{ij} = 8\pi G a^2 \,\delta_{ik}(\delta_\alpha T^k{}_j)_T, \tag{6.15}
$$

where $\delta_\alpha T^0{}_i = (\bar{\rho} + \bar{P})(\delta_\alpha u_i + H_{0i})$ and with $(\delta_\alpha T^k{}_j)_T$ we mean the tensor part of $\delta_\alpha T^i{}_j$. By imposing Eqs. (6.8) and (6.10), the system of equations above admits as

---

[1] For the metric perturbation, one can use the following dictionary between our notation and those of [34]: $H_{00} \to \Psi$, $H \to \Phi$ and $H_{0i} \to w_i$ to write the system of equations above.

consistent solution $H = H_{0i} = 0$, and also $H_{00} = 0$, using the remaining perturbed Einstein's equations. Indeed, these become sourceless Poisson's equation. Contrary, being Eq. (6.15) a wave equation, it admits non-trivial solutions even if sourceless. Furthermore, one can compute the conservation equations for the stress-energy tensor, $\delta_\alpha \left[\nabla_\mu T^\mu_\nu \right] = 0$. Using the line element in Eq. (6.12) it is easy to find

$$\partial_\tau \left[\delta_\alpha T^0_0 \right] - 3\dot{H}(\bar{\rho} + \bar{P}) + \partial_i \left[\delta_\alpha T^i_{\ 0} \right] = 0, \tag{6.16}$$

$$\partial_\tau \left[\delta_\alpha T^0_{\ i} \right] + 4\mathcal{H} \left[\delta_\alpha T^0_{\ i} \right] + \partial_j \left[\delta_\alpha T^j_{\ i} \right] + (\bar{\rho} + \bar{P})\,\partial_i H_{00} = 0, \tag{6.17}$$

where $\mathcal{H} \equiv a'/a$ is the comoving Hubble parameter. From the equations above, it is clear that the tensor modes γ_{ij} don't contribute to $\delta_\alpha \left[\nabla_\mu T^\mu_\nu \right] = 0$. Indeed, the linearized Einstein's equations, because of the Bianchi identities, develop non-trivial scalar and vector potentials designed exactly to achieve the conservation of the stress-energy tensor, covariantly and at first order in α. The tensor modes have a different role and are not uniquely fixed by Einstein's equation (one always has the freedom to add a freely propagating wave, satisfying the same equation of motion but sourceless). This is a usual result, considering that the latter do not fix the Riemann tensor, $R_{\mu\nu\rho\sigma}$, but only its trace and GWs are contained in the Weyl part of it [32]. We point out that the existence/absence of the scalar and vector potentials is not a gauge artifact. To illustrate this point we make the case of electromagnetism where Maxwell's equations are,

$$\boldsymbol{\nabla} \cdot \boldsymbol{E} = \boldsymbol{\nabla} \cdot \boldsymbol{E}_\parallel = 4\pi\rho, \qquad -\partial_\tau \boldsymbol{E}_\parallel = 4\pi \boldsymbol{J}_\parallel, \qquad \boldsymbol{\nabla} \times \boldsymbol{B} - \partial_\tau \boldsymbol{E}_\perp = 4\pi \boldsymbol{J}_\perp, \tag{6.18}$$

from which it is clear that $\boldsymbol{E}$, the electric field, develops a longitudinal component which guarantees charge conservation

$$\partial_\tau \rho + \boldsymbol{\nabla} \cdot \boldsymbol{J} = \partial_\tau \rho + \boldsymbol{\nabla} \cdot \boldsymbol{J}_\parallel = 4\pi \left(\partial_\tau \boldsymbol{\nabla} \cdot \boldsymbol{E}_\parallel - \partial_\tau \boldsymbol{\nabla} \cdot \boldsymbol{E}_\parallel \right) = 0. \tag{6.19}$$

Since the longitudinal component is present at the level of the observable electric field, it is not a gauge artifact [426], rather Maxwell's equations contain a redundant scalar equation so that charge conservation is directly built into them. Similar reasoning can be done about General Relativity, where it can be shown that the scalar and vector cosmological potentials contribute to the Riemann tensor, thus to the geodesic deviation equation, which is a physical observable [131]. Therefore, the classical matter approximation is designed to remove the conserved symmetry charges at first order in α, i.e. $\delta_\alpha T^\mu_\nu$, so that the equations of motion do not need to develop extra components of $h_{\mu\nu}$ in order to guarantee their conservation. Indeed, when assuming Eqs. (6.8) and (6.10), Eqs. (6.13)- (6.17) admit as consistent solution $H = H_{0i} = H_{00} = 0$ and the only non-null part of $h_{\mu\nu}$ are the tensor modes. All of the above can be simply restated as: every gauge symmetry comes with a Gauss' law, whose role is to conserve the charge.

The discussion above holds regardless of the choice of background, $\bar{g}_{\mu\nu}$. However, for less symmetric spacetimes scalar, vector and tensor modes couple at leading order,

making the derivation above less clear and reason why in the main text we opted for the covariant de-Donder gauge choice. Upon using Eq. (6.8) in Eq. (6.6), we find

$$\bar{\Box}\tilde{h}_{\mu\nu} + 2\bar{R}_{\lambda\mu\alpha\nu}h^{\lambda\alpha} - \bar{g}_{\mu\nu}h^{\alpha\beta}\bar{R}_{\alpha\beta} = 0, \tag{6.20}$$

which will be the starting point of the next Sections. Note that in this gauge choice, the constraint equations (time-time and time-space components of Eq. (6.20)) are not implemented through first order differential equations as usual, they are wave equations too. This is a consequence the gauge choice: the system of perturbed equations implements causality automatically because the gauge choice is covariant. Poisson's gauge, which relies on the slicing of the spacetime, leads indeed to a-causal Poisson's equations [34]. Therefore, looking for components of the metric perturbation satisfying first order differential equations is not a good strategy to isolate GWs from scalar and vector potentials because it is a gauge dependent statement. Nevertheless, observables do not depend on the gauge choice, and an explicit computation of the equivalence between a covariant versus a non-covariant gauge choice can be found in [427] for the electromagnetic field.

Given all of these considerations, we conclude that the role of the *classical matter approximation* is to isolate the freely propagating modes when the background spacetime is highly non-symmetric, and one cannot rely on the scalar-vector-tensor decomposition. It achieves so by setting to zero the sources of Gauss' laws (if we opted for a gauge which explicitly breaks covariance).

6.3. Linearization and perturbative scheme

The literature of wave-optics for gravitational waves is very extended. All the papers build up on the pioneering work [162] where the authors solve the gravitational wave equation propagating in a static background containing a single lens, and obtaining the solution in Eq. (1.101) for the perturbed gravitational wave. A number of simplifying assumptions have been made to arrive to this form of the GW, as discussed in Section 1.3.2 of the Introduction. The computation which we set up here, is very similar in spirit to the procedure that lead to Eq. (1.101), but without the assumption that the GW is a scalar wave and in an expanding Universe. So, the first step is to make explicit the form of the background metric, $\bar{g}_{\mu\nu}$, which follows from a choice of the matter content curving it.

6.3.1. Matter stress energy tensor and background metric

Since our goal is to describe wave-optics effects, we include in the matter content: an almost perfect fluid, accounting for the cosmological background and large-scale structures of the Universe, plus a pressureless perfect fluid of lenses tracing the dark

matter distribution,

$$\bar{T}_{\mu\nu} = \bar{\rho}\, \bar{u}_\mu \bar{u}_\nu + (P^I + P^B)\bar{\Lambda}_{\mu\nu} + \bar{\Sigma}_{\mu\nu}\,, \qquad \bar{\rho} = \rho^{FLRW} + \epsilon\, \rho^{LSS} + \rho^L \tag{6.21}$$

where $\bar{\Lambda}_{\mu\nu} \equiv \bar{g}_{\mu\nu} + \bar{u}_\mu \bar{u}_\nu$ is the orthogonal projector to $\bar{u}^\mu$, P^I and P^B are respectively the isotropic and bulk pressure contributions and $\bar{\Sigma}_{\mu\nu}$ represents the shear stresses which we take traceless and flow-orthogonal, i.e. $\bar{u}^\mu \bar{\Sigma}_{\mu\nu} = 0$ [34]. Note that we are introducing again the expansion parameter ϵ, keeping track of the cosmic structures, and that we are neglecting any velocity bias between the lenses and the large-sale structure. Compatibly with this definition of $\bar{T}_{\mu\nu}$, we choose as background metric

$$\mathrm{d}\bar{s}^2 = \bar{g}_{\mu\nu}\mathrm{d}x^\mu \mathrm{d}x^\nu = a^2(\tau)\left[-(1+2\epsilon\,\Phi(x))\mathrm{d}\eta^2 + (1-2\epsilon\,\Psi(x))\mathrm{d}\mathbf{x}^2\right], \tag{6.22}$$

following the notation of Section 1.1.2. Note that we are choosing the so-called *restricted Poisson's gauge*, where we are neglecting the vector and tensor perturbations in Eq. (1.14). This is a good approximation in the late time Universe, where vectors have had time to dilute out, and the relativistic species possibly carrying anisotropic shear stress are subdominant. In this case, Eq. (1.31) of Section 1.1.2 holds, and we can set $\Psi = \Phi$. Assuming to be in the late time Universe, is a good representation for astrophysical GWs, whose sources were not present during the radiation dominated epoch, and for the cosmological ones, because tensor modes that enter the horizon at early time are greatly damped. Moreover, the last primordial modes to reenter the horizon are those characterized by longer wavelength and hence could be the more suited to study wave-optics effects. We stress that $\Psi = \Phi$ holds only for the first orders gravitational potentials, as the second orders ones would be different from each other regardless of the shear viscosity being zero. We also point out that our formalism is able to accommodate various perturbative approaches for the background metric, such as the standard weak field limit, or the post-Newtonian [37, 39], the parameterized Post-Friedmann [118, 119] or hybrids ones [134]. Neglecting the radiation contribution make the classical matter approximation even more solid, since tensor modes interact with matter via quadrupole anisotropies.

6.3.2. Linearization of GW equations of motion

The equations obtained by plugging Eq. (6.22) into Eq. (6.20), are linear in α, but not in ϵ. Given how complicated these are, and in the same spirit of the wave-optics literature (see e.g. [149, 162, 165, 169]), we expand Eq. (6.20) up to linear order in ϵ. Before doing so, it is convenient to perform a conformal transformation, defining the metric $\hat{g}_{\mu\nu}$ as

$$\bar{g}_{\mu\nu} = a^2\,\hat{g}_{\mu\nu}\,, \qquad \bar{g}^{\mu\nu} = \hat{g}^{\mu\nu}/a^2\,, \tag{6.23}$$

this way the background spacetime at order ϵ^0 is flat. We also introduce $H_{\mu\nu}$

$$H^\mu_\nu \equiv h^\mu_\nu\,, \qquad H^{\mu\nu} \equiv \hat{g}^{\rho\nu} H^\mu_\rho = a^2\, h^{\mu\nu}\,, \qquad H_{\mu\nu} \equiv \hat{g}_{\mu\rho} H^\rho_\nu = \frac{1}{a^2}\, h_{\mu\nu}\,, \tag{6.24}$$

so that its indices are raised and lowered with the conformal metric, and

$$\hat{u}^\mu \equiv a\,\bar{u}^\mu, \qquad \hat{u}_\mu \equiv \hat{g}_{\mu\nu}\,\hat{u}^\nu = \frac{\bar{u}_\mu}{a}, \tag{6.25}$$

such that $\hat{u}^\mu$ is normalized to -1 with $\hat{g}_{\mu\nu}$. The system of equations describing the GWs is composed of: the gauge condition in Eq. (6.4), the compatibility condition in Eq. (6.11) and the equation of motion in Eq. (6.20), and we rewrite all of them in the conformal frame. After some manipulations, the de-Donder gauge condition in conformal frame reads

$$\hat{\nabla}_\mu \tilde{H}^\mu_\nu - 4\mathcal{H}\,\hat{n}^\mu H_{\mu\nu} + \mathcal{H} H\,\hat{n}_\nu \quad = \quad 0, \tag{6.26}$$

where $\hat{\nabla}_\mu$ is the covariant derivative associated to $\hat{g}_{\mu\nu}$, $\hat{n}^\mu = (1,0,0,0)$ and $\tilde{H}_{\mu\nu} = H_{\mu\nu} - \frac{1}{2}\hat{g}_{\mu\nu}H$ with $H \equiv \hat{g}^{\mu\nu}H_{\mu\nu}$. Condition (6.11) is mapped into

$$\hat{u}^\mu \hat{u}^\nu H_{\mu\nu} = 0. \tag{6.27}$$

Similarly, the GW equation of motion (6.20) becomes

$$\hat{\Box}\tilde{H}_{\mu\nu} - 2\mathcal{H}\hat{n}^\lambda \hat{\nabla}_\lambda \tilde{H}_{\mu\nu} + 2\hat{R}_{\mu\alpha\nu\beta}H^{\alpha\beta} - \hat{g}_{\mu\nu}H^{\alpha\beta}\hat{R}_{\alpha\beta} + 2\hat{g}_{\mu\nu}\mathcal{H}^2(\hat{n}^\alpha\hat{n}^\beta\tilde{H}_{\alpha\beta}) + 4\mathcal{H}^2 H\hat{n}_\mu\hat{n}_\nu +$$

$$+ \frac{2}{a}\left[\tilde{H}^\alpha_\mu\hat{\nabla}_\alpha\hat{\nabla}_\nu a + \tilde{H}^\alpha_\nu\hat{\nabla}_\alpha\hat{\nabla}_\mu a\right] - 2\mathcal{H}\hat{n}^\alpha\left[\hat{\nabla}_\mu\tilde{H}_{\nu\alpha} + \hat{\nabla}_\nu\tilde{H}_{\mu\alpha}\right] + \hat{g}_{\mu\nu}H\frac{\hat{\Box}a}{a} = 0, \tag{6.28}$$

with $\hat{\Lambda}_{\mu\nu} \equiv \eta_{\mu\nu} + \hat{n}_\mu\hat{n}_\nu$, and $\eta_{\mu\nu}$ the Minkwoski metric.

The next step is to linearize to first order in ϵ Eqs. (6.26), (6.27) and (6.28), similarly to what is done in, e.g., [165]. To do so, we introduce also the perturbation of the fluid 4-velocity

$$\hat{u}^\mu = \hat{n}^\mu + \epsilon\delta\hat{u}^\mu = (1 - \epsilon\Phi, \epsilon v^i) = (1 - \epsilon\Phi, \epsilon\partial^i v), \tag{6.29}$$

where, compatibly with the background metric in Eq. (6.22), we kept only the irrotational part of the peculiar velocity. This quantity can be obtained via Eq. (1.19) and $\hat{u}^\mu \equiv a\,\bar{u}^\mu$. The expansion of Eq. (6.26) up to order $\mathcal{O}(\epsilon)$ leads to

$$\left[\partial^\mu\left(H_{\mu\nu} - \frac{1}{2}\eta_{\mu\nu}(\eta^{\alpha\beta}H_{\alpha\beta})\right) - 4\mathcal{H}\,\hat{n}^\mu H_{\mu\nu} + H\mathcal{H}\,\hat{n}_\nu\right] + \epsilon\left[2\Phi\partial^\mu\tilde{H}_{\mu\nu} + 8\mathcal{H}\,\Phi\,\hat{n}^\mu H_{\mu\nu} +\right.$$

$$\left. + 2\mathcal{H}\,\Phi H\hat{n}_\nu + 4\mathcal{H}\,\Phi\,\hat{n}_\nu(\hat{n}^\alpha\hat{n}^\beta H_{\alpha\beta}) + 4\Phi'\,\hat{n}^\mu H_{\mu\nu} + 4\Phi\,\hat{n}^\mu H'_{\mu\nu} - 2\Phi\,\hat{n}^\alpha\hat{n}^\beta\partial_\nu H_{\alpha\beta}\right] = 0, \tag{6.30}$$

while the one of Eq. (6.27) gives

$$H_{\mu\nu}\hat{n}^\mu\hat{n}^\mu + 2\epsilon H_{\mu\nu}\hat{n}^\mu\delta\hat{u}^\nu = 0. \tag{6.31}$$

The first order expansion of Eq. (6.28) is, on the other hand, very complicated, and we report explicitly in the Appendix in Eqs. (6.147) and (6.148). Here, we write it schematically as:

$$[\mathcal{O}_0 H]_{\mu\nu} + \epsilon\,[\mathcal{O}_1 H]_{\mu\nu} = 0. \tag{6.32}$$

6.3.3. Perturbative scheme

Given the complexity of Eq. (6.32), we have no other choice than to solve it introducing an approximation scheme. As in [165] and in the Section 1.3.2, we expand also the gravitational wave in powers of ϵ

$$H_{\mu\nu} = H_{\mu\nu}^{(0)} + \epsilon H_{\mu\nu}^{(1)} + \epsilon^2 H_{\mu\nu}^{(2)} + \dots \tag{6.33}$$

and solve the system of equations iteratively. The meaning of such decomposition is that the $i - th$ order GW is a solution of a particular equation at $i - th$ order in ϵ. The expansion in Eq. (6.33) allows accounting for the effects of the matter inhomogeneities on the propagating GWs perturbatively. More in details, we will show that $H_{\mu\nu}^{(0)}$ constitutes GW propagating on a FRLW Universe, $H_{\mu\nu}^{(1)}$ accounts for the first order corrections induced by cosmic structures, and so on. Looking at the equations of motion in Eq. (6.32) we find that each $i - th$ modes satisfy

$$\left[\mathcal{O}_0 H^{(i)} \right]_{\mu\nu} + \left[\mathcal{O}_1 H^{(i-1)} \right]_{\mu\nu} = 0, \tag{6.34}$$

where $i = 0, 1, 2, \dots$ and with the convention $H_{\mu\nu}^{(-1)} = 0$ and we apply the same procedure to Eqs. (6.30) and (6.31). Since we neglected terms of order $\geq \epsilon^2$ to find Eqs. (6.31), (6.30) and (6.32), we consider only $H_{\mu\nu} = H_{\mu\nu}^{(0)} + \epsilon H_{\mu\nu}^{(1)}$. Considering only terms at first order in ϵ is equivalent to performing a Born approximation [165, 169].

6.4. The zero-th order gravitational wave

In this Section, we derive the equation of motion for the zeroth order GW, namely $H_{\mu\nu}^{(0)}$, and solve it introducing its transfer function and the polarization basis.

6.4.1. Equation of motion

The equations that $H_{\mu\nu}^{(0)}$ satisfies can be found by setting $H_{\mu\nu} = H_{\mu\nu}^{(0)}$ and taking the ϵ^0 order of Eqs. (6.32), (6.30) and (6.31). From the last two we find

$$\hat{n}^\mu \hat{n}^\nu H_{\mu\nu}^{(0)} = 0, \qquad \partial^\mu \tilde{H}_{\mu\nu}^{(0)} - 4\mathcal{H} \, n^\mu H_{\mu\nu}^{(0)} + H^{(0)} \mathcal{H} \, \hat{n}_\nu = 0, \tag{6.35}$$

where $\tilde{H}_{\mu\nu}^{(0)}$ is the zeroth order trace reversed metric perturbation, $\tilde{H}_{\mu\nu}^{(0)} = H_{\mu\nu}^{(0)} - \frac{1}{2}\eta_{\mu\nu}H^{(0)}$ with $H^{(0)} = \eta^{\alpha\beta}H_{\alpha\beta}^{(0)}$. We use these conditions in the equations of motion of $H_{\mu\nu}^{(0)}$, and find

$$\left[\mathcal{O}_0 H^{(0)} \right]_{\mu\nu} = \Box_\eta \tilde{H}_{\mu\nu}^{(0)} - 2\mathcal{H}(\tilde{H}_{\mu\nu}^{(0)})' + \mathcal{H}\left(\hat{n}_\nu \partial_\mu H^{(0)} + \hat{n}_\mu \partial_\nu H^{(0)} \right) - (\hat{n}_\mu \hat{n}_\nu + \hat{\Lambda}_{\mu\nu})\mathcal{H}' H^{(0)} -$$
$$- 2\mathcal{H}\left(\hat{n}^\alpha \partial_\mu H_{\alpha\nu}^{(0)} + \hat{n}^\alpha \partial_\nu H_{\alpha\mu}^{(0)} \right) + 2(\mathcal{H}' + \mathcal{H}^2)\hat{n}^\alpha \left(\hat{n}_\mu H_{\alpha\nu}^{(0)} + \hat{n}_\nu H_{\alpha\mu}^{(0)} \right). \tag{6.36}$$

The details of the computations can be found in Appendix A and B, especially Eqs. (6.147), (6.148) and (6.154). From Eq. (6.36) we extract the time-time and time-space components

$$\frac{1}{2}\Box_\eta H^{(0)} - 3\mathcal{H}(H^{(0)})' - \mathcal{H}'H^{(0)} = 0 \qquad \text{Time-Time} \qquad (6.37)$$

$$\Box_\eta H^{(0)}_{0i} - 4\mathcal{H}(H^{(0)}_{0i})' + H^{(0)}_{0i}(6\mathcal{H}^2 - 2\mathcal{H}') - \mathcal{H}\partial_i H^{(0)} = 0 \qquad \text{Space-Time} \qquad (6.38)$$

where $\Box_\eta = \eta^{\mu\nu}\partial_\mu\partial_\nu = -\partial_\tau^2 + \partial^i\partial_i$ is the wave-operator on flat spacetimes and $H^{(0)}_{0i} \equiv \hat{n}^\mu H^{(0)}_{\mu i}$. The two equations above admit as consistent solution

$$H^{(0)} = H^{(0)}_{0i} = 0, \qquad (6.39)$$

which we choose also invoking the fact that in General Relativity there are no scalar sources, not even far away. In this case, Eq. (6.35) tells us that the zeroth order GW is transverse and traceless, namely

$$\partial^\mu H^{(0)}_{\mu\nu} = 0, \qquad \text{and} \qquad \eta^{\mu\nu} H^{(0)}_{\mu\nu} = 0. \qquad (6.40)$$

Using all of these results, the zeroth order GW equation is

$$\Box_\eta H^{(0)}_{ij} - 2\mathcal{H}(H^{(0)}_{ij})' = 0, \qquad (6.41)$$

as it is shown in Appendix B. As expected, we have found that on FLRW $H^{(0)}_{\mu\nu}$ is purely spatial, traceless, transverse, and it satisfies the standard damped wave equation. This result is not surprising, but it is instructive to see an explicit example of how the classical matter approximation works in a gauge different than Poisson's, as we did in Section 6.2.3. Indeed, at order ϵ^0, we are simply studying the propagation of a metric perturbation on the FLRW Universe, and we shouldn't exect to find anything different than the standard propagation equation for tensor modes.

6.4.2. Solution

We look for an explicit solution of Eq. (6.41). In Fourier space, each **k** mode of $H^{(0)}_{\mu\nu}$ satisfies

$$\eta^{\mu\nu} H^{(0)}_{\mu\nu,\mathbf{k}} = 0, \quad H^{(0)}_{0\nu,\mathbf{k}} = 0, \quad k^i H^{(0)}_{i\nu,\mathbf{k}} = 0, \quad (H^{(0)}_{ij,\mathbf{k}})'' + 2\mathcal{H}(H^{(0)}_{ij,\mathbf{k}})' + k^2 H^{(0)}_{ij,\mathbf{k}} = 0. \quad (6.42)$$

where $k^2 \equiv \delta_{ij} k^i k^j$ and $H^{(0)}_{0\nu,\mathbf{k}} \equiv \hat{n}^\mu H^{(0)}_{\mu\nu,\mathbf{k}}$. At this order, the GW depends only on the modulus of **k**, hence we shall write $H^{(0)}_{\mu\nu,k}$. We define the 4-vector $k^\mu \equiv \{k^0, k^i\}$ such that $k^0 \equiv -\hat{n}^\mu k_\mu$. We point out that this vector is not necessarily null because the zero component is not fixed by a dispersion relation. However, since the 0ν components of the GW vanish, the GW is orthogonal to the entire 4-vector k^μ.

We introduce an almost null tetrad basis [413, 428–430] $\{\hat{e}^{\mu}_{\hat{a}}\} = \{e^{\mu}_{\hat{0}}, m^{\mu}, \bar{m}^{\mu}, e^{\mu}_{\hat{3}}\}$ such that

$$\hat{e}^{\mu}_{\hat{0}} = \hat{n}^{\mu}, \qquad \hat{e}^{\mu}_{\hat{3}} = \frac{[k^{\mu} - k^{0}\hat{n}^{\mu}]}{k} = \begin{bmatrix} 0 \\ \hat{k}^{i} \end{bmatrix}, \tag{6.43}$$

with $k^{i} = k\hat{k}^{i}$. The scalar products between the elements of $\{\hat{e}^{\mu}_{\hat{a}}\}$ are summarized in

$$\eta_{\hat{a}\hat{b}} = \begin{bmatrix} -1 & 0 & 0 & 0 \\ 0 & 0 & 1 & 0 \\ 0 & 1 & 0 & 0 \\ 0 & 0 & 0 & 1 \end{bmatrix}. \tag{6.44}$$

It is important to keep in mind that, since $m^{\mu}, \bar{m}^{\mu}$ are orthogonal to $\hat{e}^{\mu}_{\hat{3}}$, they implicitly depend on the direction of the propagating wave, $\hat{k}^{i}$. Additionally, these two vectors are related to the two legs of an orthonormal tetrad $\{e^{\mu}_{\hat{0}}, e^{\mu}_{\hat{1}}, e^{\mu}_{\hat{2}}, e^{\mu}_{\hat{3}}\}$ as

$$m^{\mu} \equiv \frac{\hat{e}^{\mu}_{\hat{1}} + i\hat{e}^{\mu}_{\hat{2}}}{\sqrt{2}}, \qquad \bar{m}^{\mu} \equiv \frac{\hat{e}^{\mu}_{\hat{1}} - i\hat{e}^{\mu}_{\hat{2}}}{\sqrt{2}}. \tag{6.45}$$

Using all of these geometrical objects, we build a basis for rank-2 symmetric tensors as

$$\Theta^{\mu\nu}_{\hat{a}\hat{b}}(\hat{k}) \equiv \frac{1}{4}\left(\hat{e}^{\mu}_{\hat{a}}\hat{e}^{\nu}_{\hat{b}} + \hat{e}^{\nu}_{\hat{a}}\hat{e}^{\mu}_{\hat{b}}\right) \qquad \text{with} \qquad \{e^{\mu}_{\hat{a}}, e^{\mu}_{\hat{b}}\} \in \{e^{\mu}_{\hat{0}}, m^{\mu}, \bar{m}^{\mu}, e^{\mu}_{\hat{3}}\}, \tag{6.46}$$

and decompose each k of the GW mode as

$$H^{(0)}_{\mu\nu,k}(\tau) = \sum_{\hat{a},\hat{b}} H^{(0)}_{\hat{a}\hat{b},\mathbf{k}}(\tau) \Theta^{\hat{a}\hat{b}}_{\mu\nu}(\hat{k}), \qquad \text{with} \qquad H^{(0)}_{\hat{a}\hat{b},\mathbf{k}} = H^{(0)}_{\hat{b}\hat{a},\mathbf{k}}. \tag{6.47}$$

Because the basis elements in Eq. (6.46) depends on the direction of propagation, then also the coefficients $H^{(0)}_{\hat{a}\hat{b},\mathbf{k}}$ must depend on $\hat{k}$ as well, in a way that precisely balances every contribution so that the left-hand side of Eq. (6.47) is direction-independent. This subtlety is a key point in our discussion, and it will be at the core of the study of the polarization content of $H^{(1)}_{ij}$.

We plug the decomposition in Eq. (6.47) into Eqs. (6.42) and, using the scalar product rules in Eq. (6.44), we find

$$\hat{n}^{\mu}H^{(0)}_{\mu\nu,k} = 0 \quad \rightarrow \quad H^{(0)}_{\hat{0}\hat{a},\mathbf{k}} = 0, \qquad k^{\mu}H^{(0)}_{\mu\nu,k} = 0 \rightarrow H^{(0)}_{\hat{3}\hat{a},\mathbf{k}} = 0, \tag{6.48}$$

amounting to seven conditions. The eighth one is fixed by the tracelessness of the GW,

$$\eta^{\mu\nu}H^{(0)}_{\mu\nu,k} = \eta^{\mu\nu}\left[H^{(0)}_{mm,\mathbf{k}}\Theta^{mm}_{\mu\nu} + H^{(0)}_{\bar{m}\bar{m},\mathbf{k}}\Theta^{\bar{m}\bar{m}}_{\mu\nu} + H^{(0)}_{m\bar{m},\mathbf{k}}\Theta^{m\bar{m}}_{\mu\nu}\right] = H^{(0)}_{m\bar{m},\mathbf{k}} = 0. \tag{6.49}$$

To sum up, the decomposition of the GW on the polarization basis is made of exlucsively two contributions

$$H^{(0)}_{\mu\nu,k} = H^{(0)}_{mm,\mathbf{k}}\Theta^{mm}_{\mu\nu}(\hat{k}) + H^{(0)}_{\bar{m}\bar{m},\mathbf{k}}\Theta^{\bar{m}\bar{m}}_{\mu\nu}(\hat{k}), \tag{6.50}$$

which is the standard expression in terms of left ($H^{(0)}_{mm,\mathbf{k}}$) and right ($H^{(0)}_{\bar{m}\bar{m},\mathbf{k}}$) helicity modes. In fact, under a rotation of angle φ about the $\hat{k}^i$ axis, we have that

$$
\begin{bmatrix} \hat{e}'_{\hat{1}} \\ \hat{e}'_{\hat{2}} \end{bmatrix} = \begin{bmatrix} \cos\varphi & -\sin\varphi \\ \sin\varphi & \cos\varphi \end{bmatrix} \begin{bmatrix} \hat{e}_{\hat{1}} \\ \hat{e}_{\hat{2}} \end{bmatrix} \quad \rightarrow \quad \begin{bmatrix} \Theta'_{mm} \\ \Theta'_{\bar{m}\bar{m}} \end{bmatrix} = \begin{bmatrix} e^{2i\varphi} & 0 \\ 0 & e^{-2i\varphi} \end{bmatrix} \begin{bmatrix} \Theta_{mm} \\ \Theta_{\bar{m}\bar{m}} \end{bmatrix}, \tag{6.51}
$$

using Eq. (6.45) and the definition of $\Theta^{\mu\nu}_{mm}$ and $\Theta^{\mu\nu}_{\bar{m}\bar{m}}$. Since $H^{(0)}_{\mu\nu,k}$ must be a scalar under the same transformation, we have that

$$
\begin{bmatrix} H^{(0)\prime}{}_{mm,\mathbf{k}} \\ H^{(0)\prime}{}_{\bar{m}\bar{m},\mathbf{k}} \end{bmatrix} = \begin{bmatrix} e^{-2i\varphi} & 0 \\ 0 & e^{2i\varphi} \end{bmatrix} \begin{bmatrix} H^{(0)}_{mm,\mathbf{k}} \\ H^{(0)}_{\bar{m}\bar{m},\mathbf{k}} \end{bmatrix}, \tag{6.52}
$$

under the same transformation, as expected for the left and right helicity modes. By contracting the equation of motion of $H^{(0)}_{ij}$ in Fourier space with the polarization basis elements, and using the decomposition in Eq. (6.50), we find that each polarization mode satisfies

$$
(H^{(0)}_{\mathring{a},\mathbf{k}})'' + 2\mathcal{H}(H^{(0)}_{\mathring{a},\mathbf{k}})' + k^2 H^{(0)}_{\mathring{a},\mathbf{k}} = 0, \tag{6.53}
$$

where we introduce the index notation $\mathring{a} = \{mm, \bar{m}\bar{m}\}$. This standard result allows us to introduce gravitational waves transfer function $\mathcal{T}^H$ as

$$
H^{(0)}_{\mathring{a}}(\tau, \mathbf{k}) \equiv H_{\mathring{a}}(\tau_s, \mathbf{k}) \, \mathcal{T}^H(\tau, k) \tag{6.54}
$$

where $H^{(0)}_{\mathring{a}}(\tau_s, \mathbf{k})$ is the amplitude of the wave's $\mathbf{k}$ mode at the source conformal time. The transfer function is normalized to

$$
\mathcal{T}^H(\tau_s, k) = 1, \tag{6.55}
$$

and satisfies the same differential equation of $H^{(0)}_{\mathring{a},\mathbf{k}}$, namely Eq. (6.53), but with the different boundary conditions. We absorbed the dependence on the direction $\hat{k}$, entirely due to the choice of elements in the tetrad, in the initial condition $H^{(0)}_{\mathring{a},\mathbf{k}}(\tau_s)$. In fact, once the choice is made, the way in which GWs propagate is independent of the spatial direction. Since the two polarization modes evolve identically, the transfer function $\mathcal{T}^H(\tau, k)$ doesn't depend on the polarization state.

Gravitational wave transfer functions

We solve Eq. (6.53) in two epochs: matter and Λ domination eras. To do so, we need the explicit solutions of the Hubble function, $\mathcal{H}$, which can be found in Eq. (1.9) of Section 1.1.1, in terms of the comoving distance. The generic solution of Eq. (6.53), then, is given by

$$
\mathcal{T}^H_{\mathrm{MD}}(\chi, k) = \sqrt{\frac{2k}{\pi}} \frac{1}{\chi_i - \chi} \left[A\, j_1[k(\chi_i - \chi)] + B\, y_1[k(\chi_i - \chi)] \right], \tag{6.56}
$$

during matter domination, while when dark energy is the main driver for the Universe's expansion we have

$$\mathcal{T}_{\Lambda D}^{H}(\chi, k) = \sqrt{\frac{2k}{\pi}} (\chi + \chi_{\Lambda})^2 \left[C\, j_1[k(\chi + \chi_{\Lambda})] + D\, y_1[k(\chi + \chi_{\Lambda})] \right]. \tag{6.57}$$

In the two previous equations, $j_1(x)$ and $y_1(x)$ are the spherical Bessel functions of order one and of type one and two respectively, given by

$$j_1(x) \quad = \quad \frac{\sin x}{x^2} - \frac{\cos x}{x}, \qquad y_1(x) = -\frac{\cos x}{x^2} - \frac{\sin x}{x}. \tag{6.58}$$

The two solutions presented here for $\mathcal{T}^H$, are well known in literature (see e.g. [160, 431] for matter dominated Universe and for solutions in de Sitter Universe [22, 23]) and the values of χ_i and χ_{Λ} can be found in Table 1.1.

The integration constants A, B, C, D are fixed imposing suitable boundary conditions. To this end, we distinguish two cases according to the epoch in which the GW source is located. In the case of the GW source located after the moment of matter-Λ equality, i.e. $\chi_s < \chi_{M\Lambda}$, where χ_s is the comoving distance of the wave's source, we impose

$$\mathcal{T}_{\Lambda D}^{H}(\chi_s) = 1, \qquad \frac{\partial \mathcal{T}_{\Lambda D}^{H}}{\partial \chi}(\chi_s) = 0, \tag{6.59}$$

assuming that the amplitude of the emitted GWs is maximum at the source position. With these prescription we find

$$C_{\Lambda D} = -\sqrt{\frac{\pi k}{2}} \frac{\cos[k(\chi_s + \chi_{\Lambda})]}{(\chi_s + \chi_{\Lambda})}, \qquad D_{\Lambda D} = -\sqrt{\frac{\pi k}{2}} \frac{\sin[k(\chi_s + \chi_{\Lambda})]}{(\chi_s + \chi_{\Lambda})}. \tag{6.60}$$

If the GW source is located prior to the equivalence, i.e. $\chi_s > \chi_{M\Lambda}$, we also perform a matching of the solutions and require

$$\mathcal{T}_{\Lambda D}^{H} = \mathcal{T}_{MD}^{H}\Big|_{\chi_{M\Lambda}}, \qquad \frac{\partial \mathcal{T}_{\Lambda D}^{H}}{\partial \chi} = \frac{\partial \mathcal{T}_{MD}^{H}}{\partial \chi}\Big|_{\chi_{M\Lambda}}, \qquad \mathcal{T}_{MD}^{H}(\chi_s) = 1, \qquad \frac{\partial \mathcal{T}_{MD}^{H}}{\partial \chi}(\chi_s) = 0, \tag{6.61}$$

with the resulting boundary conditions

$$A_{MD} = -\sqrt{\frac{\pi k}{2}} (\chi_s - \chi_i)^2 \left[3y_1[k(\chi_s - \chi_i)] + \cos[k(\chi_s - \chi_i)] \right], \tag{6.62}$$

$$B_{MD} = -\sqrt{\frac{\pi k}{2}} (\chi_s - \chi_i)^2 \left[\sin(k(\chi_s - \chi_i)) - 3j_1[k(\chi_s - \chi_i)] \right], \tag{6.63}$$

$$C_{MD} = \frac{\left[\Xi_1 \cos(k\chi_*) + \Xi_2 \sin(k\chi_*) + \Xi_3 \cos(3k\chi_*) + \Xi_4 \sin(3k\chi_*) \right]}{32 k^3 \chi_*^6}, \tag{6.64}$$

$$D_{MD} = \frac{\left[\Xi_2 \cos(k\chi_*) - \Xi_1 \sin(k\chi_*) - \Xi_4 \cos(3k\chi_*) + \Xi_3 \sin(3k\chi_*) \right]}{32 k^3 \chi_*^6}, \tag{6.65}$$

and where χ_* can be found in Table 1.1 and the coefficients Ξ_i are

$$\Xi_1 = 3(B_{\rm MD} - A_{\rm MD}\, k\chi_*), \qquad \Xi_3 = 3B_{\rm MD} - 9A_{\rm MD}\,(k\chi_*) - 12B_{\rm MD}(k\chi_*)^2 + 8A_{\rm MD}(k\chi_*)^3 \tag{6.66}$$

$$\Xi_2 = 3(A_{\rm MD} + B_{\rm MD}\, k\chi_*), \qquad \Xi_4 = 3A_{\rm MD} + 9B_{\rm MD}\,(k\chi_*) - 12A_{\rm MD}(k\chi_*)^2 - 8B_{\rm MD}(k\chi_*)^3. \tag{6.67}$$

A plot of these transfer functions for different values of k can be found in Fig. 6.1.
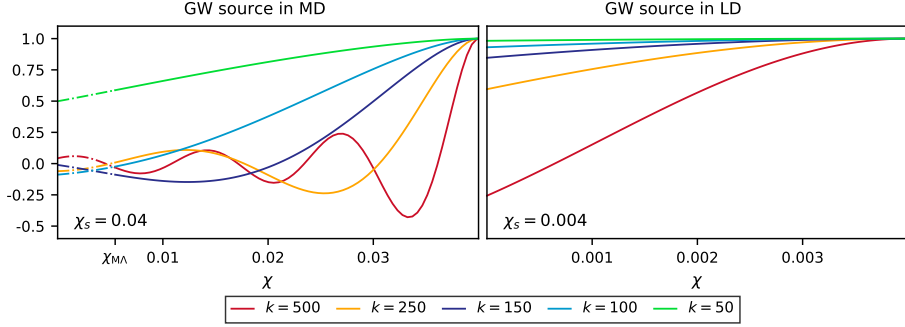

Figure 6.1: GW transfer functions for different values of k. In the left panel the source is located in matter domination, at a comoving distance of $\chi_s = 0.04$, while in the right panel it is in Λ domination, at $\chi_s = 0.004$. Solid versus dashed-dot lines, in the left panel, stands for the transfer function in the two epochs of the Universe, showing their matching at the moment of equivalence.

6.5. The first order gravitational wave

In this Section, we derive the equation of motion for $H^{(1)}_{\mu\nu}$, following the procedure outlined in Section 6.3.3. We will see that the GW at this order develops additional polarization components on top of the standard transverse and traceless modes. Then, we find a decoupled equation for the first order tensor modes, which we solve using a Green's function.

6.5.1. First order equation

We start by working out the gauge and compatibility conditions. Inserting Eq. (6.33) into Eqs. (6.30) and (6.31), and extracting the ϵ^1 order, we find that $H^{(1)}_{\mu\nu}$ satisfies

$$\hat{n}^\mu \hat{n}^\nu H^{(1)}_{\mu\nu} = 0, \qquad \partial^\mu \tilde{H}^{(1)}_{\mu\nu} - 4\mathcal{H}\,\hat{n}^\mu H^{(1)}_{\mu\nu} + H^{(1)}\,\mathcal{H}\,\hat{n}_\nu = 0, \tag{6.68}$$

where we have used also Eq. (6.39). Notice that the trace is defined as $H^{(1)} \equiv \eta^{\mu\nu} H^{(1)}_{\mu\nu}$ and also $\tilde{H}^{(1)}_{\mu\nu} = H^{(1)}_{\mu\nu} - \frac{1}{2}\eta_{\mu\nu}H^{(1)}$. From the first condition, we conclude that the time-time component of the first order GW is null, even at this order of perturbation.

The structure of the equation of motion of $H^{(1)}_{\mu\nu}$ has the form

$$\left[\mathcal{O}_0 H^{(1)}\right]_{\mu\nu} = -\left[\mathcal{O}_1 H^{(0)}\right]_{\mu\nu}, \tag{6.69}$$

from which we see that the adopted perturbation scheme generated, effectively a source, as the right-hand-side of doesn't depend on $H^{(1)}_{\mu\nu}$. This suorce describres the interaction between the freely propagating waves and the gravitational potentials describing the matter inhomogeneities. In light of what discussed in Section 6.2.3, we expect that $H^{(1)}_{\mu\nu}$, then, develops additional components whose role is to enforce the conservation of such source. Indeed, the left-hand-side of Eq. (6.69) is nothing but the first order Einstein tensor, evaluated in $H^{(1)}_{\mu\nu}$, which satisfies the linearized Bianchi identities. Therefore, $H^{(1)}_{\mu\nu}$ will contain scalar - vector and tensors modes, exactly as it was for $\delta g_{\mu\nu}$ in Section 1.1.2, generated through the interaction of the waves and the matter overdensities.

By plugging the solution of $H^{(0)}_{\mu\nu}$ in the first order Eq. (6.69), after a short manipulation, we find

$$
\begin{aligned}
\left[\mathcal{O}_0 H^{(1)}\right]_{\mu\nu} =\ & \Box_\eta \tilde{H}^{(1)}_{\mu\nu} - 2\mathcal{H}(\tilde{H}^{(1)}_{\mu\nu})' + \mathcal{H}\left(\hat{n}_\nu \partial_\mu H^{(1)} + \hat{n}_\mu \partial_\nu H^{(1)}\right) - \\
& - 2\mathcal{H}\left(\hat{n}^\alpha \partial_\mu H^{(1)}_{\alpha\nu} + \hat{n}^\alpha \partial_\nu H^{(1)}_{\alpha\mu}\right) + 2(\mathcal{H}' + \mathcal{H}^2)\hat{n}^\alpha\left(\hat{n}_\mu H^{(1)}_{\alpha\nu} + \hat{n}_\nu H^{(1)}_{\alpha\mu}\right) - \\
& - (\hat{n}_\mu \hat{n}_\nu + \hat{\Lambda}_{\mu\nu})\mathcal{H}' H^{(1)}
\end{aligned}
\tag{6.70}
$$

$$
\begin{aligned}
\left[\mathcal{O}_1 H^{(0)}\right]_{\mu\nu} =\ & 4\Phi \Delta H^{(0)}_{\mu\nu} + 2 H^{(0)}_{\mu\nu}\left[\Box_\eta \Phi - 2\mathcal{H}\Phi'\right] + 4\partial^k \Phi \partial_k H^{(0)}_{\mu\nu} + \\
& - 2\hat{n}_\mu D^\alpha \Phi\left(H^{(0)'}_{\ \ \nu\alpha} + \mathcal{H} H^{(0)}_{\nu\alpha}\right) - 2\hat{n}_\nu D^\alpha \Phi\left(H^{(0)'}_{\ \ \mu\alpha} + \mathcal{H} H^{(0)}_{\mu\alpha}\right) \\
& - 2 D_\mu\left(H^{(0)}_{\alpha\nu} D^\alpha \Phi\right) - 2 D_\nu\left(H^{(0)}_{\alpha\mu} D^\alpha \Phi\right) + \\
& + 2(\eta_{\mu\nu} + 2\hat{n}_\mu \hat{n}_\nu) H^{(0)}_{\alpha\beta} D^\alpha D^\beta \Phi
\end{aligned}
\tag{6.71}
$$

where $D_\mu \equiv \hat{\Lambda}^\nu_\mu \partial_\nu$. The details of this computations are in Appendix A and B.

6.5.2. Scalar and vector modes

As previously done, we look at the constraint equations, namely the time-time and the time-space components of Eq. (6.69). Using its explicit expression in Eqs. (6.70) and (6.71), we find

$$\frac{1}{2}\Box_\eta H^{(1)} - 3\mathcal{H}(H^{(1)})' - \mathcal{H}' H^{(1)} = -2 H^{(0)}_{ij}\partial^i \partial^j \Phi, \qquad \text{Time-Time} \tag{6.72}$$

$$\Box_\eta H^{(1)}_{0i} - 4\mathcal{H}(H^{(1)}_{0i})' - \mathcal{H}\partial_i H^{(1)} - 2(\mathcal{H}^2 + \mathcal{H}')H^{(1)}_{0i} = -\frac{2}{a}\partial^k \Phi\,(a H^{(0)}_{ki})'. \quad \text{Space-Time} \tag{6.73}$$

Extracting also the space component of gauge condition in Eq. (6.68), we find

$$\partial^j H^{(1)}_{ij} = (H^{(1)}_{0i})' + 4\mathcal{H} H^{(1)}_{0i} + \frac{\partial_i H^{(1)}}{2}\,. \tag{6.74}$$

The constraint equations and the gauge conditions relate the trace, the time-space component and the spatial divergence of $H^{(1)}_{\mu\nu}$, to (functions of) the projection of the zero-order gravitational wave along the gradient of the scalar gravitational potential. As already explained, such equations are second order in time derivatives, rather than first, because we are imposing a covariant gauge choice. The only components of $H^{(1)}_{\mu\nu}$ that do not take part to the constraint equations, are the transverse-traceless and spatial ones.

We explicitly decompose $H^{(1)}_{\mu\nu}$ as

$$H^{(1)}_{\mu\nu} = \left[\begin{array}{c|c} 0 & H^{(1)}_{0i} \\ \hline H^{(1)}_{i0} & \gamma^{(1)}_{ij} + E^{(1)}_{ij} + \frac{1}{3}\delta_{ij} H^{(1)} \end{array} \right] \tag{6.75}$$

so that $\gamma^{(1)}_{ij}$ is the tensor mode: it is spatial, traceless $\delta^{ij}\gamma^{(1)}_{ij} = 0$ and transverse $\partial^i \gamma^{(1)}_{ij} = 0$. We introduce a projector operator $\hat{\mathscr{P}}^{ab}_{ij}$, whose expression will be given later, with the aim of extracting these components of $H^{(1)}_{\mu\nu}$. With all these new ingredients, Eq. (6.74) reads

$$\partial^j E^{(1)}_{ij} = (H^{(1)}_{0i})' + 4\mathcal{H} H^{(1)}_{0i} + \frac{\partial_i H^{(1)}}{6}\,. \tag{6.76}$$

The main equations of this part are Eqs. (6.72), (6.73) and (6.76) which relate the first order trace $H^{(1)}$ and the components $H^{(1)}_{0i}, E^{(1)}_{ij}$ to products of the form $\sim H^{(0)}_{ij}\partial^i \Phi$. Since Eqs. (6.72), (6.73) are sourced wave equations, we cannot set $H^{(1)}$ and $H^{(1)}_{0i}$ to zero, contrary to what done for the zero-th order GW in the previous Section, and neither $E^{(1)}_{ij}$ because this has to satisfy Eq. (6.76). Since the presence or absence of $H^{(1)}, H^{(1)}_{0i}, E^{(1)}_{ij}$ depends entirely on the zeroth order GW, we claim that they do not represent any new degree of freedom as no new initial condition is needed to solve the system of equations. Nevertheless, if one was to look at the geoedisc deviation equation to understand the polarization content of the GW, as we did in Chapter 5, it would be easy to realize that these modes participate to it, and therefore they are physical and not gauge artifacts (a similar computation can be done also for $\delta g_{\mu\nu}$ see [131]).

6.5.3. Tensor modes

To finish characterizing the first order GW, $H_{\mu\nu}^{(1)}$, we need to find the evolution equation of $\gamma_{ij}^{(1)}$. This can be obtained by projecting Eq. (6.69) as

$$\hat{\mathscr{P}}_{ij}^{ab}\left[\mathcal{O}_0\, H^{(1)}\right]_{ab} = -\hat{\mathscr{P}}_{ij}^{ab}\left[\mathcal{O}_1\, H^{(0)}\right]_{ab}. \tag{6.77}$$

In the expression above, a, b are spacetime spatial indices, not to be confused with the polarization ones $\hat{a}, \hat{b}$ or $\mathring{a}, \mathring{b}$. As in [140, 141], the projector operator is most easily defined in Fourier space and using the polarization basis. Its action on a generic spacetime tensor, $A_{ij}(x)$, is given by

$$\hat{\mathscr{P}}_{ij}^{ab}\, A_{ab}(x) \equiv \int \frac{d^3k}{(2\pi)^3}\, e^{i\mathbf{k}\cdot\mathbf{x}}\left[\Theta_{ij}^{mm}(\hat{k})\Theta_{\bar{m}\bar{m}}^{ab}(\hat{k}) + \Theta_{ij}^{\bar{m}\bar{m}}(\hat{k})\Theta_{mm}^{ab}(\hat{k})\right] A_{ab}(\mathbf{k}, \tau) \tag{6.78}$$

where $A_{ij}(\mathbf{k}, \tau)$ is the Fourier transform of $A_{ij}(x)$.

We start by working out the left-hand side of Eq. (6.77). By taking the space-space components of Eq. (6.70) and applying the projector operator, we find

$$\begin{aligned}
\hat{\mathscr{P}}_{ij}^{ab}\left[\mathcal{O}_0\, H^{(1)}\right]_{ab} &= \hat{\mathscr{P}}_{ij}^{ab}\left[\Box_\eta \tilde{H}_{ab}^{(1)} - 2\mathcal{H}(\tilde{H}_{ab}^{(1)})' - \delta_{ab}\mathcal{H}'H^{(1)} - 2\mathcal{H}\left(\partial_a H_{0b}^{(1)} + \partial_b H_{0a}^{(1)}\right)\right] \\
&= \Box_\eta \gamma_{ij}^{(1)} - 2\mathcal{H}(\gamma_{ij}^{(1)})', \tag{6.79}
\end{aligned}$$

where we have used that $\gamma_{ij}^{(1)} = \hat{\mathscr{P}}_{ij}^{ab} H_{ab}^{(1)}$ by definition, and the orthogonality properties of the polarization basis elements (see Eqs. (6.46) and (6.44)).

Working out the right-hand side of Eq. (6.77) is more tricky as the source is non-linear in the fields (it is quadratic in Φ and $H_{ij}^{(0)}$). We will proceed with the following steps:

1. select the space-space components of Eq. (6.71) and perform a 3D Fourier transform,

2. apply the projector operator,

3. use the decomposition of $H_{\mu\nu}^{(0)}$ on the polarization basis, i.e. Eq. (6.50) and rotate such basis to compute the scalar products.

Step i.

We start by taking the space-space components of Eq. (6.71) and go in Fourier space. Since $\left[\mathcal{O}_1\, H^{(0)}\right]_{ij}$ is quadratic in the fields, its 3D Fourier transform will be given by the convolution

$$\left[\mathcal{O}_1\, H^{(0)}\right]_{ij}(\mathbf{k}, \tau) = \int \frac{d^3p}{(2\pi)^3}\, f_{ij}(\mathbf{p}, \mathbf{k}-\mathbf{p}, \tau) \tag{6.80}$$

with f_{ij} defined as

$$f_{ij}(\mathbf{p},\mathbf{k}-\mathbf{p},\tau) = -2H^{(0)}_{ij,\mathbf{p}}\left[\Phi''_{|\mathbf{k}-\mathbf{p}|}+2\mathcal{H}\Phi'_{|\mathbf{k}-\mathbf{p}|}+\Phi_{|\mathbf{k}-\mathbf{p}|}(p^2+k^2)\right]+$$
$$+2\Phi_{|\mathbf{k}-\mathbf{p}|}\left[H^{(0)}_{mi,\mathbf{p}}k^m k_j + H^{(0)}_{mj,\mathbf{p}}k^m k_i - \delta_{ij}H^{(0)}_{lm,\mathbf{p}}k^l k^m\right] \qquad (6.81)$$

where all the fields are evaluated at same confomal time τ. The integral over all possible momenta implies that multiple $\boldsymbol{p}$ modes contribute to a single $\mathbf{k}$ mode in $\gamma^{(1)}_{ij}$. This mixing is going to modulate the properties of the final wave, such as intensity and polarization, and accounts for the wave-optics effects.

Step ii.

We can understand already that the second line of Eq. (6.81) won't contribute to the final tensor modes equation. This is easy to see by considering that it is composed by vectors ($\propto k_i$) or scalar ($\propto \delta_{ij}$) type of terms which will vanish when using the projector operator $\hat{\mathscr{P}}^{ab}_{ij}$. We can show this explicitly by considering the right-hand-side of Eq. (6.77)

$$\hat{\mathscr{P}}^{ab}_{ab}[\mathcal{O}_1 H^{(0)}]_{ab} = \int \frac{d^3 k}{(2\pi)^3}\, e^{i\mathbf{k}\cdot\mathbf{x}}\left[\Theta^{mm}_{ij}(\hat{k})\Theta^{ab}_{\bar{m}\bar{m}}(\hat{k})+\Theta^{\bar{m}\bar{m}}_{ij}(\hat{k})\Theta^{ab}_{mm}(\hat{k})\right][\mathcal{O}_1 H^{(0)}]_{ab}(\mathbf{k},\tau)$$

$$= \int \frac{d^3 k\, d^3 p}{(2\pi)^6}\, e^{i\mathbf{k}\cdot\mathbf{x}}\left[\Theta^{mm}_{ij}(\hat{k})\Theta^{ab}_{\bar{m}\bar{m}}(\hat{k})+\Theta^{\bar{m}\bar{m}}_{ij}(\hat{k})\Theta^{ab}_{mm}(\hat{k})\right]f_{ab}(\mathbf{p},\mathbf{k}-\mathbf{p},\tau)$$

$$= \int \frac{d^3 k\, d^3 p}{(2\pi)^6}\, e^{i\mathbf{k}\cdot\mathbf{x}}\left[\Theta^{mm}_{ij}(\hat{k})\Theta^{ab}_{\bar{m}\bar{m}}(\hat{k})+\Theta^{\bar{m}\bar{m}}_{ij}(\hat{k})\Theta^{ab}_{mm}(\hat{k})\right]\times$$
$$\times\left\{-2H^{(0)}_{ab,\mathbf{p}}\left[\Phi''_{|\mathbf{k}-\mathbf{p}|}+2\mathcal{H}\Phi'_{|\mathbf{k}-\mathbf{p}|}+\Phi_{|\mathbf{k}-\mathbf{p}|}(p^2+k^2)\right]+\right.$$
$$\left.+2\Phi_{|\mathbf{k}-\mathbf{p}|}\left[H^{(0)}_{ma,\mathbf{p}}k^m k_b + H^{(0)}_{mb,\mathbf{p}}k^m k_a - \delta_{ab}H^{(0)}_{lm,\mathbf{p}}k^l k^m\right]\right\}$$

$$= \int \frac{d^3 k\, d^3 p}{(2\pi)^6}\, e^{i\mathbf{k}\cdot\mathbf{x}}\left[\Theta^{mm}_{ij}(\hat{k})\Theta^{ab}_{\bar{m}\bar{m}}(\hat{k})+\Theta^{\bar{m}\bar{m}}_{ij}(\hat{k})\Theta^{ab}_{mm}(\hat{k})\right]\times$$
$$\times\left\{-2H^{(0)}_{ab,\mathbf{p}}\left[\Phi''_{|\mathbf{k}-\mathbf{p}|}+2\mathcal{H}\Phi'_{|\mathbf{k}-\mathbf{p}|}+\Phi_{|\mathbf{k}-\mathbf{p}|}(p^2+k^2)\right]\right\} \qquad (6.82)$$

where in the last line we used that $\Theta^{ab}_{mm}(\hat{k})\,k_b = \Theta^{ab}_{\bar{m}\bar{m}}(\hat{k})\,k_b = 0$ and $\Theta^{ab}_{mm}(\hat{k})\,\delta_{ab} = \Theta^{ab}_{\bar{m}\bar{m}}(\hat{k})\,\delta_{ab} = 0$, since m^k and $\bar{m}^{k2}$ are orthogonal to $\hat{k}$ and traceless, to eliminate the third raw of the intermediate step in the computation above.

---

[2] $m^k = m(\hat{k})$ and $\bar{m}^k = \bar{m}(\hat{k})$, to clarify that these vectors are built orthogonal to $\hat{k}$.
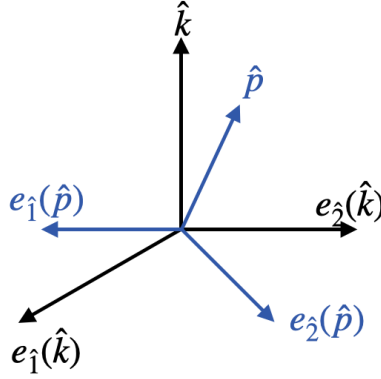
Figure 6.2: Representation of $\{\hat{e}^i_{\hat{1}}(\hat{p}), \hat{e}^i_{\hat{2}}(\hat{p}), \hat{p}^i\}$ in the basis relative to $\hat{k}$.

Step iii.

To complete the computation, we must perform the scalar products between the polarization basis elements and $H^{(0)}_{ab,\mathbf{p}}$. In order to do so, we use the decomposition of $H^{(0)}_{\mu\nu}$ on the polarization basis, i.e. Eq. (6.50), which we can rewrite in compact form as

$$H^{(0)}_{ab,\mathbf{p}} = H^{(0)}_{\mathring{a}}(\mathbf{p}, \tau) \Theta^{\mathring{a}}_{ab}(\hat{p}) \tag{6.83}$$

since $\mathring{a} = \{mm, \bar{m}\bar{m}\}$, while a, b are spatial indices, and where the polarization basis is built with respect to $\mathbf{p}$. Looking at Eq. (6.82), it is easy to realize that we have to compute scalar products of the form $\sim \Theta^{ij}_{\mathring{a}}(\hat{k}) \Theta^{\mathring{b}}_{ij}(\hat{p})$, namely products of basis elements bult with respect to two different directions: $\hat{k}$ and $\hat{p}$. These products do not follow the rules in Eq. (6.44), so first we have to express $\Theta^{\mathring{a}\mathring{b}}_{ij}(\hat{p})$ in terms of $\Theta^{\mathring{a}\mathring{b}}_{ij}(\hat{k})$. This can be achieved by a rotation of the tetrad basis elemets $\{\hat{e}^{\mu}_{\mathring{a}}(\hat{p})\}$. Once this rotation is performed, we can make use of the scalar products in Eq. (6.44).

Choosing $\hat{k}^i$ along the z-axis and $\hat{e}^i_{\hat{1}}(\hat{k}) = (1, 0, 0)$ and $\hat{e}^i_{\hat{2}}(\hat{k}) = (0, 1, 0)$, we can express $\{\hat{e}^i_{\hat{1}}(\hat{p}), \hat{e}^i_{\hat{2}}(\hat{p}), \hat{p}^i\}$ as [5, 407]

$$\hat{p}^i = \begin{bmatrix} \sin\theta\cos\varphi \\ \sin\theta\sin\varphi \\ \cos\theta \end{bmatrix}, \qquad \hat{e}^i_{\hat{1}}(\hat{p}) = \begin{bmatrix} \cos\theta\cos\varphi \\ \cos\theta\sin\varphi \\ -\sin\theta \end{bmatrix}, \qquad \hat{e}^i_{\hat{2}}(\hat{p}) = \begin{bmatrix} -\sin\varphi \\ \cos\varphi \\ 0 \end{bmatrix}, \tag{6.84}$$

where θ is the angle between $\hat{k}$ and $\hat{p}$, namely $\cos\theta = \hat{k} \cdot \hat{p}$, and it can be checked that these vectors satisfy the proper orthogonality relations (see Figure 6.2). Conse-

quently, we have that

$$
\begin{bmatrix} m^p \\ \bar{m}^p \\ \hat{p} \end{bmatrix} = \begin{bmatrix} \frac{1}{\sqrt{2}} & \frac{i}{\sqrt{2}} & 0 \\ \frac{1}{\sqrt{2}} & \frac{-i}{\sqrt{2}} & 0 \\ 0 & 0 & 1 \end{bmatrix} \begin{bmatrix} \cos\theta\cos\varphi & \cos\theta\sin\varphi & -\sin\theta \\ -\sin\varphi & \cos\varphi & 0 \\ \sin\theta\cos\varphi & \sin\theta\sin\varphi & \cos\theta \end{bmatrix} \begin{bmatrix} \frac{1}{\sqrt{2}} & \frac{1}{\sqrt{2}} & 0 \\ \frac{-i}{\sqrt{2}} & \frac{i}{\sqrt{2}} & 0 \\ 0 & 0 & 1 \end{bmatrix} \begin{bmatrix} m^k \\ \bar{m}^k \\ \hat{k} \end{bmatrix} =
$$

$$
= \begin{bmatrix} \cos^2\left(\frac{\theta}{2}\right)e^{-i\varphi} & -\sin^2\left(\frac{\theta}{2}\right)e^{i\varphi} & -\frac{\sin\theta}{\sqrt{2}} \\ -\sin^2\left(\frac{\theta}{2}\right)e^{-i\varphi} & \cos^2\left(\frac{\theta}{2}\right)e^{i\varphi} & -\frac{\sin\theta}{\sqrt{2}} \\ \frac{1}{\sqrt{2}}e^{-i\varphi}\sin\theta & \frac{1}{\sqrt{2}}e^{i\varphi}\sin\theta & \cos\theta \end{bmatrix} \begin{bmatrix} m^k \\ \bar{m}^k \\ \hat{k} \end{bmatrix} . \tag{6.85}
$$

From the matrix above, one can read m^p and $\bar{m}^p$ in terms of $\{m^k, \bar{m}^k, \hat{k}\}$ and write $\{\Theta_{ij}^{mm}(\hat{p}), \Theta_{ij}^{\bar{m}\bar{m}}(\hat{p})\}$ in terms of the basis $\Theta_{ij}^{\hat{a}\hat{b}}(\hat{k})$ following its definition in Eq. (6.46). We find

$$
\Theta_{ij}^{\bar{m}\bar{m}}(\hat{p}) = \frac{\sin^2\theta}{2}\Theta_{ij}^s(\hat{k}) + 2\sqrt{2}\sin\theta\left[\sin^2\left(\frac{\theta}{2}\right)e^{-i\varphi}\Theta_{ij}^{km}(\hat{k}) - \cos^2\left(\frac{\theta}{2}\right)e^{i\varphi}\Theta_{ij}^{k\bar{m}}(\hat{k})\right]
$$
$$
+ \left[\sin^4\left(\frac{\theta}{2}\right)e^{-2i\varphi}\Theta_{ij}^{mm}(\hat{k}) + \cos^4\left(\frac{\theta}{2}\right)e^{2i\varphi}\Theta_{ij}^{\bar{m}\bar{m}}(\hat{k})\right] , \tag{6.86}
$$

$$
\Theta_{ij}^{mm}(\hat{p}) = \frac{\sin^2\theta}{2}\Theta_{ij}^s(\hat{k}) + 2\sqrt{2}\sin\theta\left[\sin^2\left(\frac{\theta}{2}\right)e^{i\varphi}\Theta_{ij}^{k\bar{m}}(\hat{k}) - \cos^2\left(\frac{\theta}{2}\right)e^{-i\varphi}\Theta_{ij}^{km}(\hat{k})\right]
$$
$$
+ \left[\cos^4\left(\frac{\theta}{2}\right)e^{-2i\varphi}\Theta_{ij}^{mm}(\hat{k}) + \sin^4\left(\frac{\theta}{2}\right)e^{2i\varphi}\Theta_{ij}^{\bar{m}\bar{m}}(\hat{k})\right] , \tag{6.87}
$$

where we have called $\Theta_{ij}^s(\hat{k}) \equiv \Theta_{ij}^{kk}(\hat{k}) - \Theta_{ij}^{m\bar{m}}(\hat{k})$. The trigonometric functions in the last equation are actually spin 2 spherical harmonics, namely

$$
{}_{\pm 2}Y_0^2(\theta, \varphi) = \frac{1}{4}\sqrt{\frac{15}{2\pi}}\sin^2\theta , \tag{6.88}
$$

$$
{}_{\pm 2}Y_{\pm 1}^2(\theta, \varphi) = \mp\frac{1}{2}\sqrt{\frac{5}{\pi}}\sin\theta\sin^2\left(\frac{\theta}{2}\right)e^{\pm i\varphi} \tag{6.89}
$$

$$
{}_{\mp 2}Y_{\pm 1}^2(\theta, \varphi) = \pm\frac{1}{2}\sqrt{\frac{5}{\pi}}\sin\theta\cos^2\left(\frac{\theta}{2}\right)e^{\pm i\varphi} \tag{6.90}
$$

$$
{}_{\pm 2}Y_{\pm 2}^2(\theta, \varphi) = \frac{1}{2}\sqrt{\frac{5}{\pi}}\sin^4\left(\frac{\theta}{2}\right)e^{\pm 2i\varphi} \tag{6.91}
$$

$$
{}_{\mp 2}Y_{\pm 2}^2(\theta, \varphi) = \frac{1}{2}\sqrt{\frac{5}{\pi}}\cos^4\left(\frac{\theta}{2}\right)e^{\pm 2i\varphi} , \tag{6.92}
$$

whose definition can be found in Appendix C along with more details. We introduce the compact notation and rewrite

$$
\Theta_{ij}^{\hat{a}}(\hat{p}) = [\mathscr{R}(\hat{p}, \hat{k})]^{\hat{a}}{}_{\hat{b}}\Theta_{ij}^{\hat{b}}(\hat{k}) \tag{6.93}
$$

with the rotation matrix defined by

$$[\mathcal{R}(\hat{p},\hat{k})]^{\mathring{a}}_{\ \mathring{b}} = \sqrt{\frac{4\pi}{5}} \begin{bmatrix} \sqrt{\frac{2}{3}}[_{-2}Y_0^2(\theta,\varphi)] & -2\sqrt{2}[_{-2}Y_1^2(\theta,\varphi)] & 2\sqrt{2}[_{-2}Y_{-1}^2(\theta,\varphi)] & [_{-2}Y_2^2(\theta,\varphi)] & [_{-2}Y_{-2}^2(\theta,\varphi)] \\ \sqrt{\frac{2}{3}}[_2Y_0^2(\theta,\varphi)] & -2\sqrt{2}[_2Y_1^2(\theta,\varphi)] & 2\sqrt{2}[_2Y_{-1}^2(\theta,\varphi)] & [_2Y_2^2(\theta,\varphi)] & [_2Y_{-2}^2(\theta,\varphi)] \end{bmatrix}$$
(6.94)

where $\mathring{a} \in \{mm, \bar{m}\bar{m}\}$ and, with an abuse of notation, we indicate from here onward $\hat{a} \in \{s, k\bar{m}, km, \bar{m}\bar{m}, mm\}$. The rotation matrix in Eq. (6.94), is such that when $\cos\theta = 1$, so parallel $\mathbf{k}$ and $\mathbf{p}$, it reduces to

$$[\mathcal{R}(\hat{p},\hat{k})]^{\mathring{a}}_{\ \hat{b}} = \begin{bmatrix} 0 & 0 & 0 & e^{2i\varphi} & 0 \\ 0 & 0 & 0 & 0 & e^{-2i\varphi} \end{bmatrix},$$
(6.95)

as expected, as the two polarization basis, $\Theta_{ij}^{\hat{a}\hat{b}}(\hat{p})$ and $\Theta_{ij}^{\hat{a}\hat{b}}(\hat{k})$, can, in principle, be the same. We note that there is still the possibility of rotating the basis vectors in the orthogonal plane to the direction of propagation, justifying the factors $e^{\pm 2i\varphi}$ in the equation above and reflecting the spin-2 nature of the tensor modes. We point out that similar rotation matrices appear also in the treatment of CMB polarization [407, 432, 433]. Given all of these tools, we finish up the computation of the first order gravitational wave equation by performing the contractions

$$\Theta_{\bar{m}\bar{m}}^{ab}(\hat{k}) H_{ab,\mathbf{p}}^{(0)} = \sum_{\mathring{c}} H_{\mathring{c},\mathbf{p}}^{(0)} \Theta_{\bar{m}\bar{m}}^{ab}(\hat{k}) \Theta_{ab}^{\mathring{c}}(\hat{p}) = \sum_{\mathring{c}\hat{b}} H_{\mathring{c},\mathbf{p}}^{(0)} [\mathcal{R}(\hat{p},\hat{k})]^{\mathring{c}}_{\ \hat{b}} \Theta_{\bar{m}\bar{m}}^{ab}(\hat{k}) \Theta_{ab}^{\hat{b}}(\hat{k}) =$$

$$= \frac{1}{4} \sum_{\mathring{c}} H_{\mathring{c},\mathbf{p}}^{(0)} [\mathcal{R}(\hat{p},\hat{k})]^{\mathring{c}}_{\ mm},$$
(6.96)

$$\Theta_{mm}^{ab}(\hat{k}) H_{ab,\mathbf{p}}^{(0)} = \sum_{\mathring{c}} H_{\mathring{c},\mathbf{p}}^{(0)} \Theta_{mm}^{ab}(\hat{k}) \Theta_{ab}^{\mathring{c}}(\hat{p}) = \sum_{\mathring{c}\hat{b}} H_{\mathring{c},\mathbf{p}}^{(0)} [\mathcal{R}(\hat{p},\hat{k})]^{\mathring{c}}_{\ \hat{b}} \Theta_{mm}^{ab}(\hat{k}) \Theta_{ab}^{\hat{b}}(\hat{k}) =$$

$$= \frac{1}{4} \sum_{\mathring{c}} H_{\mathring{c},\mathbf{p}}^{(0)} [\mathcal{R}(\hat{p},\hat{k})]^{\mathring{c}}_{\ \bar{m}\bar{m}},$$
(6.97)

where we used Eq. (6.50), the definition of the polarization basis elements Eq. (6.46), and the orthogonality relations of the tetrad legs Eq. (6.44). Plugging these results into Eq. (6.82) we find

$$\hat{\mathcal{P}}_{ij}^{ab}[\mathcal{O}_1 H^{(0)}]_{ab} = -\frac{1}{2} \int \frac{d^3k\, d^3p}{(2\pi)^6} e^{i\mathbf{k}\cdot\mathbf{x}} \left[\Phi_{\mathbf{k}-\mathbf{p}}'' + 2\mathcal{H}\Phi_{\mathbf{k}-\mathbf{p}}' + \Phi_{\mathbf{k}-\mathbf{p}}(p^2+k^2) \right] \times$$

$$\times \sum_{\mathring{c}} H_{\mathring{c},\mathbf{p}}^{(0)} \left[\Theta_{ij}^{mm}(\hat{k}) [\mathcal{R}(\hat{p},\hat{k})]^{\mathring{c}}_{\ mm} + \Theta_{ij}^{\bar{m}\bar{m}}(\hat{k}) [\mathcal{R}(\hat{p},\hat{k})]^{\mathring{c}}_{\ \bar{m}\bar{m}} \right],$$
(6.98)

from which, together with Eq. (6.79), we can read off the equation of motion of the two spin-2 modes of the first order gravitational wave, namely

$$(\gamma_{\mathring{a},\mathbf{k}}^{(1)})'' + 2\mathcal{H}(\gamma_{\mathring{a},\mathbf{k}}^{(1)})' + k^2 \gamma_{\mathring{a},\mathbf{k}}^{(1)} = \mathcal{S}_{\mathring{a},\mathbf{k}}$$
(6.99)

with

$$\mathcal{S}_{\mathring{a},\mathbf{k}} = -\frac{1}{2} \sum_{\mathring{c}} \int \frac{d^3p}{(2\pi)^3} \left[\Phi_{|\mathbf{k}-\mathbf{p}|}'' + 2\mathcal{H}\Phi_{|\mathbf{k}-\mathbf{p}|}' + \Phi_{|\mathbf{k}-\mathbf{p}|}(p^2+k^2) \right] H_{\mathring{c},\mathbf{p}}^{(0)} [\mathcal{R}(\hat{p},\hat{k})]^{\mathring{c}}_{\ \mathring{a}}, \quad (6.100)$$

where $[\mathcal{R}(\hat{p}, \hat{k})]^{\mathring{c}}{}_{\mathring{a}}$ is the 2×2 sub-matrix of the rotation matrix in Eq. (6.94) corresponding to the $\mathring{a} = \{mm, \bar{m}\bar{m}\}$ indices. Eq. (6.100) is the first main result of this Chapter, and it displays many interesting features:

- Using Eqs. (6.91) and (6.92) we rewrite

$$[\mathcal{R}(\hat{p}, \hat{k})]^{\mathring{c}}{}_{\mathring{a}} = \begin{bmatrix} \cos^4\left(\frac{\theta}{2}\right) e^{2i\varphi} & \sin^4\left(\frac{\theta}{2}\right) e^{-2i\varphi} \\ \sin^4\left(\frac{\theta}{2}\right) e^{2i\varphi} & \cos^4\left(\frac{\theta}{2}\right) e^{-2i\varphi} \end{bmatrix} \tag{6.101}$$

where we can see the standard $e^{\pm 2i\varphi}$ exponential factors stemming for the spin-2 nature of these polarization modes and reflecting their dependence on the choice of $\{\hat{e}_{\hat{1}}, \hat{e}_{\hat{2}}\}$. This matrix is diagonal exclusively when $\cos\theta = 1$. Therefore, unless in the very specific case of $\hat{k} \| \hat{p}$, each polarization mode of $\gamma_{\mathring{a}}^{(1)}$, is sourced by a linear combination of the two helicity eigenstates of the zero-order GW. Only in the symmetric scenario of the two wave-vectors aligned, a left- mode of $H_{\mathring{a},\mathbf{p}}^{(0)}$, sources a left- mode of $\gamma_{\mathring{a}}^{(1)}$, and similarly for the right-ones. Among the classical relativistic effects, the one that is responsible for orthogonal changes in direction of the GW's trajectory is gravitational lensing [156, 157, 228, 230]. Even though in the context of wave-optics the concept of geodesics is not well-defined, our result suggests that a similar effect to the lensing on CMB polarization [231, 405, 406] is taking place here.

- The integral over all possible 3-momenta accounts for the interference between GW and gravitational potential modes. For a monochromatic source, $H_{\mathring{c},\mathbf{p}}^{(0)}$ is peaked on a certain wave vector, making the integral over $d^3 p$ trivial. This problem doesn't occur in a stochastic background, being a superposition of many different waves by definition.

It is convenient to introduce the transfer function of the gravitational potential and of the gravitational wave (see Section 1.1.2) and rewrite the source $\mathcal{S}_{\mathring{a},\mathbf{k}}$ as

$$\mathcal{S}_{\mathring{a},\mathbf{k}}(\tau) = \sum_{\mathring{c}} \int \frac{d^3 p}{(2\pi)^3} \mathcal{F}(\mathbf{p}, \mathbf{k} - \mathbf{p}, \tau) \mathcal{T}_p^H(\tau) [\mathcal{R}(\hat{p}, \hat{k})]^{\mathring{c}}{}_{\mathring{a}} H_{\mathring{c},\mathbf{p}}^{(0)}(\tau^s) \Phi_{|\mathbf{k}-\mathbf{p}|}^{\tau_{in}} \tag{6.102}$$

where $\Phi_{|\mathbf{k}-\mathbf{p}|}^{\tau_{in}}$ is the initial value of the gravitational potential and

$$\mathcal{F}(\mathbf{p}, \mathbf{k} - \mathbf{p}, \tau) \equiv -\frac{9 T_m(|\mathbf{k} - \mathbf{p}|)}{20} \left[\left(\frac{D_m(a)}{a}\right)'' + 2\mathcal{H}\left(\frac{D_m(a)}{a}\right)' + \left(\frac{D_m(a)}{a}\right)(p^2 + k^2) \right], \tag{6.103}$$

where we used

$$\Phi(a, k) = \frac{9}{10} T_m(k) \frac{D_m(a)}{a} \Phi_k^{in}. \tag{6.104}$$

In the expressions above, $D_m(a)$ is the matter growth factor and $T_m(k)$ its transfer function, usually evaluated numerically by Einstein-Boltzmann solvers codes such

as `CAMB` [41], `CLASS` [42]. Since the gravitational potential is constant in matter domination (see Section 1.1.2), in Eq. (6.103) the first two terms are negligible for $a < a_{M\Lambda}$, while in the late universe the term proportional to the second derivative of the growth factor dominates. Of course this also depends on the scale considered: our background includes also the lenses, however one can consider their gravitational potentials constant in time as in Eq. (1.97), for instance. Figure 6.3 shows the behavior of $\mathcal{F}(\mathbf{p}, \mathbf{k} - \mathbf{p}, \tau)/T_m(|\mathbf{k} - \mathbf{p}|)$ as a function of the scale factor, which we plotted using the fitting formula in Eq. (1.43) [35, 46]. In the late time Universe, after the end of the radiation dominated epoch, the transfer function is constant [5], meaning that $\mathcal{F}(\mathbf{p}, \mathbf{k} - \mathbf{p}, \tau)/T_m(|\mathbf{k} - \mathbf{p}|) \sim \mathcal{F}(\mathbf{p}, \mathbf{k} - \mathbf{p}, \tau)$ and it becomes a function of only k, p and τ.
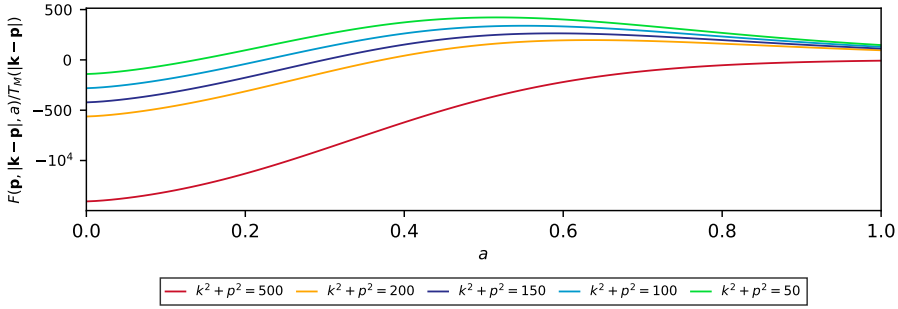

Figure 6.3: Plot of $\mathcal{F}(\mathbf{p}, \mathbf{k} - \mathbf{p}, \tau)/T_m(|\mathbf{k} - \mathbf{p}|)$ for different values of $k^2 + p^2$ as a function of the scale factor. During the matter dominated epoch, the last term of Eq. (6.103) dominates, making the difference between various values of $k^2 + p^2$ more marked, while in the late universe such term is overpowered by the second derivative of the growth factor.

Finally, we recall that the first order gravitational wave components $H^{(1)}, H^{(1)}_{0i}$ and $E^{(1)}_{ij}$ are different from zero, satisfying their respective equation given previously. We expect all of these modes to contribute to observables, for instance to the geodesic deviation equation through the first order Riemann tensor [131]. They contain valuable information as well, and solving their equations of motion and assessing their order of magnitude will be the object of future works. However, we can already make the following remark. In Eqs. (6.99) and (6.100) there are three direction dependencies: the wave-vector of the perturbed GW $\mathbf{k}$, the one of the unperturbed wave $\mathbf{p}$ and the gravitational potential mode $\mathbf{k} - \mathbf{p}$. We already claimed that when $\mathbf{p}$ and $\mathbf{k}$ are aligned, the rotation matrix in Eq. (6.101) becomes diagonal, leading to a more trivial sourcing of the polarization modes of $\gamma_{\mathring{a}}$. Not only, when these two vectods are parallel, we also have that

$$H^{(0)}_{ij} \partial^i \Phi \sim H^{(0)}_{ij,p} \Phi_{\mathbf{k}-\mathbf{p}} (\mathbf{k} - \mathbf{p})^i = 0, \qquad (6.105)$$

using the transversality of $H^{(0)}_{ij}$, implying that the sources of trace and time-space

components of the first order GW in Eqs. (6.72) and (6.73) vanish. In this case, the system of equations admits as solution $H^{(1)} = H_{0i}^{(1)} = 0$, and similarly for $E_{ij}^{(1)}$ via Eq. (6.76). This would mean that, in the case where all the 3D Fourier vectors are aligned, not only there is no mixing between the tensor modes, but also no scalar or vector polarization is generated. In practice, this results states that $H_{\mu\nu}^{(1)}$ doesn't develop extra components only when the free GW, $H_{\mu\nu}^{(0)}$, falls straight inside the gravitational potential well, toward its center. In less symmetric situation, non-trivial mixing of the polarization modes of $H_{\mu\nu}^{(0)}$ arise, and $H_{\mu\nu}^{(1)}$ gains extra components in order for the gauge conditions to be satisfied and its source (i.e. $\left[\mathcal{O}_1 H^{(0)}\right]_{\mu\nu}$) to be conserved.

6.5.4. Contact with literature

To make contact with the literature of wave-optics effects, we write Eq. (6.99) in coordinate basis. By considering $\mathcal{S}_{ij}(\mathbf{k}) = \sum_{\mathring{a}} \mathcal{S}_{\mathring{a}} \Theta_{ij}^{\mathring{a}}(\hat{k})$, starting from Eq. (6.100) we have that

$$\mathcal{S}_{ij}(\mathbf{k}) = -\frac{1}{2} \int \frac{d^3p}{(2\pi)^3} \left[\Phi''_{|\mathbf{k}-\mathbf{p}|} + 2\mathcal{H}\Phi'_{|\mathbf{k}-\mathbf{p}|} + \Phi_{|\mathbf{k}-\mathbf{p}|}(p^2+k^2)\right] \sum_{\mathring{a}\mathring{c}} H_{\mathring{c},\mathbf{p}}^{(0)} [\mathscr{R}(\hat{p},\hat{k})]^{\mathring{c}}{}_{\mathring{a}}(\hat{k}) \Theta_{ij}^{\mathring{a}}(\hat{k})$$

$$= -\frac{1}{2} \int \frac{d^3p}{(2\pi)^3} \left[\Phi''_{|\mathbf{k}-\mathbf{p}|} + 2\mathcal{H}\Phi'_{|\mathbf{k}-\mathbf{p}|} + \Phi_{|\mathbf{k}-\mathbf{p}|}(p^2+k^2)\right] H_{ij,p}^{(0)}. \tag{6.106}$$

Similarly $\gamma_{ij}^{(1)}(\mathbf{k}) = \sum_{\mathring{a}} \gamma_{\mathring{a}}^{(1)} \Theta_{ij}^{\mathring{a}}(\hat{k})$, so that Eq. (6.99) in coordinate basis and real space is

$$\Box_\eta \gamma_{ij}^{(1)} - 2\mathcal{H}(\gamma_{ij}^{(1)})' = -4\Phi\Delta H_{ij}^{(0)} - 2H_{ij}^{(0)}\left[\Box_\eta\Phi - 2\mathcal{H}\Phi'\right] - 4\partial^k\Phi\partial_k H_{ij}^{(0)}. \tag{6.107}$$

The equation above can be rewritten as

$$\Box_\eta \breve{\gamma}_{ij}^{(1)} - 2\mathcal{H}(\breve{\gamma}_{ij}^{(1)})' = -4\Phi\Delta H_{ij}^{(0)}. \tag{6.108}$$

where $\breve{\gamma}_{ij}^{(1)} = \gamma_{ij}^{(1)} + 2H_{ij}^{(0)}\Phi$, in the same way as done in [434], which is the standard starting point of all the works treating wave-optics effects. We point out that in [434] a different gauge choice is made and, thus, while the equations for $\breve{\gamma}_{ij}^{(1)}$ coincide, those for $H^{(1)}, H_{0i}^{(1)}$ and $E_{ij}^{(1)}$ are different. This is not a problem, since observables are gauge independent and will not be affected by the different choice.

Note that in [435] the authors study the evolution equation for second order tensor modes on a perturbed Universe which includes both scalar and tensor perturbations. Even though the settings of the two works are different, effectively the methodologies employed in this Chapter and in [435] shares some similarities. In our case, $H_{\mu\nu}^{(1)}$ is only sourced by second order combinations built from one scalar and one tensor mode, while [435] also considers the possibility of having scalar-scalar and tensor-tensor sources. Our formalism doesn't include these cases by construction, however tensor-tensor sources could be included by adding a background tensor mode

to Eq. (6.22). Additionally, the authors of [435] consider only second order tensor modes, hence they cannot account for the scalar and vector polarization which we find at the perturbed level, namely $H^{(1)}, H^{(1)}_{0i}, E^{(1)}_{ij}$. Regardless of these differences and similarities, the scalar-tensor source $\mathcal{S}_{ij}(\mathbf{k})$, show some different numerical factors.

6.5.5. Solution via the Green's function

In Section 6.4.2 we found the solutions to the propagation equations of a GW travelling freely in an isotropic and homogeneous background. In this Section, we solve Eq. (6.99) introducing the Green's function

$$(\partial_\tau^2 + 2\mathcal{H}\partial_\tau + k^2)\, g_k(\tau,\tau') = \delta(\tau - \tau'),\tag{6.109}$$

in such a way that the first order tensor mode is given by

$$\gamma^{(1)}_{\mathring{a},\mathbf{k}}(\tau) = \int_{\tau_s}^{\tau} d\tau'\, g_k(\tau,\tau')\,\mathcal{S}_{\mathring{a},\mathbf{k}}(\tau'),\tag{6.110}$$

where the integral runs from the conformal time of the GW source, up to τ, so that $\gamma^{(1)}_{\mathring{a}}(\tau_s, \mathbf{k}) = 0$. Indeed, we are choosing the first order GW to satisfy the boundary condition, $H^{(1)}_{\mu\nu}(\tau_s, \mathbf{x}) = 0$ since iin Eq. (6.54) we have normalized the zero-th order GW to the total emitted amplitude. This is also in line with our previous statement about the degrees of freedom: the number of initial conditions needed to solve the problem doesn't increase when considering the first order GW as its source is the unperturbed wave.

We can build the Green's function $g_k(\tau,\tau')$ out of two solutions, $u(\tau)$ and $v(\tau)$, of the homogeneous associated problem as [140], as

$$g_k(\tau,\tilde{\tau}) = \frac{v_k(\tau)u_k(\tilde{\tau}) - u_k(\tau)v_k(\tilde{\tau})}{v'_k(\tilde{\tau})u_k(\tilde{\tau}) - u'_k(\tilde{\tau})v_k(\tilde{\tau})}.\tag{6.111}$$

In the case analyzed here, the homogeneous solutions are

$$u^{\mathrm{MD}}_{\mathbf{k}} = \frac{j_1[k(\tau+\tau_i)]}{(\tau+\tau_i)}, \qquad u^{\Lambda\mathrm{D}}_{\mathbf{k}} = (\tau_\Lambda - \tau)^2 j_1[k(\tau_\Lambda - \tau)]\tag{6.112}$$

$$v^{\mathrm{MD}}_{\mathbf{k}} = \frac{y_1[k(\tau+\tau_i)]}{(\tau+\tau_i)}, \qquad v^{\Lambda\mathrm{D}}_{\mathbf{k}} = (\tau_\Lambda - \tau)^2 y_1[k(\tau_\Lambda - \tau)],\tag{6.113}$$

where $\tau_i = \chi_i - \tau_0$ and $\tau_\Lambda = \tau_0 + \chi_\Lambda$ with τ_0 today's conformal time and the values of the comoving distance can be found in Table 1.1. Combining all of this information, we find

$$g_k(\tau,\tilde{\tau}) = \begin{cases} \dfrac{k(\tilde{\tau}+\tau_i)^3}{(\tau+\tau_i)}\Big[j_1[k(\tau+\tau_i)]y_1[k(\tilde{\tau}+\tau_i)] - y_1[k(\tau+\tau_i)]j_1[k(\tilde{\tau}+\tau_i)]\Big] & \mathrm{MD} \\[2ex] k(\tau_\Lambda - \tau)^2\Big[j_1[k(\tau_\Lambda - \tau)]y_1[k(\tau_\Lambda - \tilde{\tau})] - y_1[k(\tau_\Lambda - \tau)]j_1[k(\tau_\Lambda - \tilde{\tau})]\Big] & \Lambda\mathrm{D} \end{cases}.\tag{6.114}$$

6.6. Polarization tensor and density matrix

The formalism developed so far describes the propagation of GWs through the large scale structures of the Universe without relying on assumptions typical of geometric optics. In this Section, we consider the stochastic gravitational wave background (SGWB), namely the incoherent superposition of many GW signals, by promoting the amplitude of the GW to a random variable characterized by its n-point functions. In order to have more handy results, we slowly introduce different assumptions, e.g. gaussianity, statistical homogeneity and isotropy or an unpolarized zeroth order background. Such hypotheses are more or less accurate according to the type of SGWB taken into consideration. For instance, primordial gravitational waves generated in standard inflationary scenarios are expected to be well described by them. For gravitational waves of astrophysical origin, on the other hand, this hypothesis might break down depending on the type of sources. Nonetheless, the central limit theorem ensures that the statistics will approach that of a Gaussian random field if the SGWB is sourced by a sufficiently large number of independent events and any high-signal-to-noise outliers have been subtracted from the detector time streams [371, 436]. A detail characterization of each background type is beyond the scope of this Chapter and will be the subject of further investigations, here we are mainly interested in laying out the general formalism and we do so in the simplest possible scenario. The goal of this Chapter is to produce a description of the polarization of the SGWB analogous to the one of the CMB.

Even though the full solution of the first order gravitational wave includes also the scalar and vector modes, encoded in $H^{(1)}, H^{(1)}_{0i}$ and $E^{(1)}_{ij}$, in this Section we focus in building the polarization tensor for the transverse and traceless modes, which in the polarization basis corresponds to the $\mathring{a} = \{mm, \bar{m}\bar{m}\}$ indices. Therefore, we consider

$$H_{\mathring{a}}(\mathbf{k}, \tau) = H^{(0)}_{\mathring{a}}(\mathbf{k}, \tau) + \epsilon \gamma^{(1)}_{\mathring{a}}(\mathbf{k}, \tau). \tag{6.115}$$

We build the polarization matrix as in [407] [3]

$$\rho_{\mathring{a}\mathring{b}}(\mathbf{k}_1, \tau_1; \mathbf{k}_2, \tau_2) = H^*_{\mathring{a}}(\mathbf{k}_1, \tau_1) H_{\mathring{b}}(\mathbf{k}_2, \tau_2), \tag{6.116}$$

and the polarization tensor will be given by

$$\mathcal{P}_{\mathring{a}\mathring{b}}(\mathbf{k}_1, \tau_1; \mathbf{k}_2, \tau_2) = \left\langle \rho_{\mathring{a}\mathring{b}}(\mathbf{k}_1, \tau_1; \mathbf{k}_2, \tau_2) \right\rangle, \tag{6.117}$$

where the average is an ensemble average or a volume one upon invoking statistical homogeneity and isotropy [22, 380, 436]. If one wants to compute the properties of the SGWB generated by astrophysical sources, then a summation over all possible unresolved sources is also understood [400]. We can look at the different orders in ϵ

---

[3]Note that $\rho_{(ij)(ab)}(\mathbf{k}_1, \tau_1; \mathbf{k}_2, \tau_2) = \sum_{\mathring{a}\mathring{b}} \rho_{\mathring{a}\mathring{b}}(\mathbf{k}_1, \tau_1; \mathbf{k}_2, \tau_2) \Theta^{\mathring{a}}_{ij}(\hat{k}_1) \Theta^{\mathring{b}}_{ab}(\hat{k}_2).$

of the polarization tensor and divide them into

$$\mathcal{P}^{(0)}_{\mathring{a}\mathring{b}}(\mathbf{k}_1,\tau_1;\mathbf{k}_2,\tau_2) = \left\langle H^{(0)\,*}_{\mathring{a}}(\mathbf{k}_1,\tau_1)\,H^{(0)}_{\mathring{b}}(\mathbf{k}_2,\tau_2) \right\rangle, \tag{6.118}$$

$$\mathcal{P}^{(1)}_{\mathring{a}\mathring{b}}(\mathbf{k}_1,\tau_1;\mathbf{k}_2,\tau_2) = \left\langle H^{(0)\,*}_{\mathring{a}}(\mathbf{k}_1,\tau_1)\,\gamma^{(1)}_{\mathring{b}}(\mathbf{k}_2,\tau_2) \right\rangle + \left\langle \gamma^{(1)\,*}_{\mathring{a}}(\mathbf{k}_1,\tau_1)\,H^{(0)}_{\mathring{b}}(\mathbf{k}_2,\tau_2) \right\rangle, \tag{6.119}$$

$$\mathcal{P}^{(2)}_{\mathring{a}\mathring{b}}(\mathbf{k}_1,\tau_1;\mathbf{k}_2,\tau_2) = \left\langle \gamma^{(1)\,*}_{\mathring{a}}(\mathbf{k}_1,\tau_1)\,\gamma^{(1)}_{\mathring{b}}(\mathbf{k}_2,\tau_2) \right\rangle, \tag{6.120}$$

which we analyze one at the time in the next Sections. Before doing so, we introduce the Stokes parameters, which are defined through particular linear combinations of the matrix elements of the polarization tensor. In particular, since this is a 2×2 tensor, we can decompose it over the Pauli matrices, plus the Identity, basis as

$$\mathcal{P}_{\mathring{a}\mathring{b}} = \frac{1}{2}\left(I\,\sigma^0_{\mathring{a}\mathring{b}} + Q\,\sigma^1_{\mathring{a}\mathring{b}} + U\,\sigma^2_{\mathring{a}\mathring{b}} + V\,\sigma^3_{\mathring{a}\mathring{b}} \right) = \frac{1}{2}\begin{bmatrix} I+V & Q-iU \\ Q+iU & I-V \end{bmatrix}, \tag{6.121}$$

where σ_i are the Pauli matrices

$$\sigma_0 = \begin{bmatrix} 1 & 0 \\ 0 & 1 \end{bmatrix}, \quad \sigma_1 = \begin{bmatrix} 0 & 1 \\ 1 & 0 \end{bmatrix}, \quad \sigma_2 = \begin{bmatrix} 0 & -i \\ i & 0 \end{bmatrix}, \quad \sigma_3 = \begin{bmatrix} 1 & 0 \\ 0 & -1 \end{bmatrix}, \tag{6.122}$$

and I, U, V, Q the Stokes parameters. Using the Pauli matrices property $\mathrm{Tr}(\sigma_i\sigma_j) = 2\delta_{ij}$, we can extract the various Stokes parameters as

$$I = \sigma_0\cdot\mathcal{P}, \qquad Q = \sigma_1\cdot\mathcal{P}, \qquad U = \sigma_2\cdot\mathcal{P}, \qquad V = \sigma_3\cdot\mathcal{P}. \tag{6.123}$$

As discussed in [153, 437], the different parameters can be related to the amplitudes of the left and right polarization modes as

$$I = |H_R|^2 + |H_L|^2, \tag{6.124}$$

$$V = |H_R|^2 - |H_L|^2, \tag{6.125}$$

$$Q = 2\,\mathrm{Re}\left(H_R^*\,H_L\right), \tag{6.126}$$

$$U = 2\,\mathrm{Im}\left(H_R^*\,H_L\right), \tag{6.127}$$

from which we can easily make the following interpretations: I represents the intensity of the SGWB, namely the average power per unit area, V the net difference between the right- and left- helicity modes, and hence it is related to parity breaking processes, and it represents the amount of circular polarization, while Q and U represents the linear polarization of the SGWB due to a difference of the phases of the two polarizations, and they are related by a $45°$ angle rotation of the orthonormal basis used to decompose the wave. Together, the four Stokes parameters provide a complete description of the polarization state of the SGWB, since any polarization state can be represented as a linear combination of them.

6.6.1. Zeroth order polarization tensor

Now we evaluate the lowest order polarization tensor, namely the one at $\mathcal{O}(\epsilon^0)$. This is given by

$$\mathcal{P}^{(0)}_{\mathring{a}\mathring{b}}(\mathbf{k}_1, \tau_1; \mathbf{k}_2, \tau_2) = \sum_{\tau_1^s, \tau_2^s} \left\langle H^{(0)\,*}_{\mathring{a}}(\mathbf{k}_1, \tau_1)\, H^{(0)}_{\mathring{b}}(\mathbf{k}_2, \tau_2) \right\rangle =$$

$$= \sum_{\tau_1^s, \tau_2^s} \left[\begin{matrix} \left\langle H^{(0)\,*}_{\bar{m}\bar{m}}(\mathbf{k}_1, \tau_1) H^{(0)}_{\bar{m}\bar{m}}(\mathbf{k}_2, \tau_2) \right\rangle & \left\langle H^{(0)\,*}_{\bar{m}\bar{m}}(\mathbf{k}_1, \tau_1) H^{(0)}_{mm}(\mathbf{k}_2, \tau_2) \right\rangle \\ \left\langle H^{(0)\,*}_{mm}(\mathbf{k}_1, \tau_1) H^{(0)}_{\bar{m}\bar{m}}(\mathbf{k}_2, \tau_2) \right\rangle & \left\langle H^{(0)\,*}_{mm}(\mathbf{k}_1, \tau_1) H^{(0)}_{mm}(\mathbf{k}_2, \tau_2) \right\rangle \end{matrix} \right], \tag{6.128}$$

where we introduced the sum over the sources, to be consistent with other works in literature about the astrophysical SGWB. Unless the GWs production mechanism prefers one polarization mode over the other, as it could be the case in parity violating theories [438], one should expect to observe an unpolarized SGWB [371] at $\mathcal{O}(\epsilon^0)$. Indeed, in the standard gravitational theory, the propagation of the two helicity modes is independent of their polarization state (the transfer function in Eq. (6.54) is shared between the two modes), and an unpolarized background at the source, remains unpolarized after the propagation process. We take this case and write the zeroth order polarization tensor as

$$\mathcal{P}^{(0)}_{\mathring{a}\mathring{\beta}}(\mathbf{k}_1, \tau_1; \mathbf{k}_2, \tau_2) = \mathrm{I}^{(0)}(\mathbf{k}_1, \tau_1; \mathbf{k}_2, \tau_2) \frac{\delta_{\mathring{a}\mathring{\beta}}}{2}. \tag{6.129}$$

The intensity $\mathrm{I}^{(0)}(\mathbf{k}_1, \tau_1; \mathbf{k}_2, \tau_2)$ is the usual tensor mode's power spectrum [22].

6.6.2. First order polarization tensor

We now turn to Eq. (6.119) and work it out one part at the time. Using Eq. (6.102), we can write

$$\left\langle H^{(0)\,*}_{\mathring{a}}(\mathbf{k}_1, \tau_1)\, \gamma^{(1)}_{\mathring{b}}(\mathbf{k}_2, \tau_2) \right\rangle =$$

$$= \sum_{\tau_1^s, \tau_2^s} \int_{\tau_2^s}^{\tau_2} d\tau_2'\, \mathcal{T}^H_{\mathbf{k}_1}(\tau_1)\, g_{k_2}(\tau_2, \tau_2') \left\langle H^{(0)\,*}_{\mathring{a}}(\mathbf{k}_1, \tau_1^s)\, S_{\mathring{b}}(\mathbf{k}_2, \tau_2) \right\rangle =$$

$$= \sum_{\tau_1^s, \tau_2^s} \sum_{\mathring{c}} \int_{\tau_2^s}^{\tau_2} d\tau_2'\, \mathcal{T}^H_{\mathbf{k}_1}(\tau_1)\, g_{k_2}(\tau_2, \tau_2') \int \frac{d^3 p}{(2\pi)^3}\, \mathcal{T}^H_{\mathbf{p}}(\tau_2')\, \mathcal{F}(\mathbf{p}, \mathbf{k}_2 - \mathbf{p}, \tau_2') \times$$

$$\times \left[\mathcal{R}(\hat{p}, \hat{k}_2) \right]^{\mathring{c}}_{\mathring{b}} \left\langle \Phi^{\tau_{in}}_{\mathbf{k}_2 - \mathbf{p}}\, H^{(0)\,*}_{\mathring{a}}(\mathbf{k}_1, \tau_1^s)\, H^{(0)}_{\mathring{c}}(\mathbf{p}, \tau_2^s) \right\rangle. \tag{6.130}$$

According to the type of situation taken in consideration the three point function may or may not vanish. In the case in which the fields involved are uncorrelated Gaussian random fields, as it is usually the case for a SGWB of primordial origin, then the three point function above would be equal to zero, but more complicated

situations could give different results. For the astrophysical background, gaussianity follows from the emission from many uncorrelated regions, a condition which might not represent the case of sources tracing the underlying dark matter distribution [22]. Modeling properly the statistics of astrophysical GW sources can be a highly non-trivial task, and it requires introducing the concept of GW bias [439], a topic which is beyond the scope of this Chapter. Additionally, if the GW's sources follow the distribution of the dark matter potential wells, it is not necessarily longer true that the fields are uncorrelated. However, we take this opportunity to clarify that possible dark matter tracers, both playing the role of source or of lens, can be accommodated in our formalism at the level of transfer functions relating the specific tracer and the gravitational potential. Similar considerations are also valid for the second term in Eq. (6.119).

6.6.3. Second order polarization tensor

Now we work out the second order polarization tensor of Eq. (6.120). This tensor represents the power spectrum of the anisotropies of the SGWB. Using again Eq. (6.110) we have that

$$
\mathcal{P}^{(2)}_{\mathring{a}\mathring{b}}(\mathbf{k}_1,\tau_1;\mathbf{k}_2,\tau_2) = \left\langle \gamma^{(1)\,*}_{\mathring{a}}(\mathbf{k}_1,\tau_1)\,\gamma^{(1)}_{\mathring{b}}(\mathbf{k}_2,\tau_2) \right\rangle =
$$
$$
= \sum_{\tau^s_1,\tau^s_2} \int_{\tau^s_1}^{\tau_1} d\tau'_1 \int_{\tau^s_2}^{\tau_2} d\tau'_2 \, g^*_{k_1}(\tau_1,\tau'_1)\, g_{k_2}(\tau_2,\tau'_2)\, \left\langle \mathcal{S}^*_{\mathring{a}}(\mathbf{k}_1,\tau'_1)\, S_{\mathring{b}}(\mathbf{k}_2,\tau'_2) \right\rangle
$$
$$(6.131)$$

with the source correlation function given by

$$
\left\langle \mathcal{S}^*_{\mathring{a}}(\mathbf{k}_1,\tau'_1)\, S_{\mathring{b}}(\mathbf{k}_2,\tau'_2) \right\rangle =
$$
$$
= \sum_{\mathring{c}\mathring{d}} \int \frac{d^3 p_1 d^3 p_2}{(2\pi)^6} \mathcal{T}^H_{p_1}(\tau'_1)\, \mathcal{T}^H_{p_2}(\tau'_2)\, \mathcal{F}^*(\mathbf{p}_1,\mathbf{k}_1-\mathbf{p}_1,\tau'_1)\, \mathcal{F}(\mathbf{p}_2,\mathbf{k}_2-\mathbf{p}_2,\tau'_2) \times
$$
$$
\times \left[\mathscr{R}^*(\hat{p}_1,\hat{k}_1)\right]^{\mathring{c}}_{\mathring{a}} \left[\mathscr{R}(\hat{p}_2,\hat{k}_2)\right]^{\mathring{d}}_{\mathring{b}} \left\langle \Phi^{\tau_{in}\,*}_{\mathbf{k}_1-\mathbf{p}_1}\, \Phi^{\tau_{in}}_{\mathbf{k}_2-\mathbf{p}_2}\, H^{(0)\,*}_{\mathring{c}}(\mathbf{p}_1,\tau^s_1)\, H^{(0)}_{\mathring{d}}(\mathbf{p}_2,\tau^s_2) \right\rangle,
$$
$$(6.132)$$

where we used Eq. (6.102). To proceed further, we slowly add assumptions. First, we choose the case where $\Phi^{\tau_{in}}_{\mathbf{k}}$ and $H^{(0)}_{\mathring{c}}(\mathbf{p},\tau^s)$ are both Gaussian random fields so that we can evaluate the expectation value in the last line value using Wick's theorem

$$
\left\langle \Phi^{\tau_{in}\,*}_{\mathbf{k}_1-\mathbf{p}_1}\, \Phi^{\tau_{in}}_{\mathbf{k}_2-\mathbf{p}_2}\, H^{(0)\,*}_{\mathring{c},\mathbf{p}_1}(\tau^s_1)\, H^{(0)}_{\mathring{d},\mathbf{p}_2}(\tau^s_2) \right\rangle =
$$
$$
= \left\langle \Phi^{\tau_{in}\,*}_{\mathbf{k}_1-\mathbf{p}_1}\, \Phi^{\tau_{in}}_{\mathbf{k}_2-\mathbf{p}_2} \right\rangle \left\langle H^{(0)\,*}_{\mathring{c},\mathbf{p}_1}(\tau^s_1)\, H^{(0)}_{\mathring{d},\mathbf{p}_2}(\tau^s_2) \right\rangle +
$$
$$
+ \left\langle \Phi^{\tau_{in}\,*}_{\mathbf{k}_1-\mathbf{p}_1}\, H^{(0)\,*}_{\mathring{c},\mathbf{p}_1}(\tau^s_1) \right\rangle \left\langle \Phi^{\tau_{in}}_{\mathbf{k}_2-\mathbf{p}_2}\, H^{(0)}_{\mathring{d},\mathbf{p}_2}(\tau^s_2) \right\rangle +
$$
$$
+ \left\langle \Phi^{\tau_{in}}_{\mathbf{k}_2-\mathbf{p}_2}\, H^{(0)\,*}_{\mathring{c},\mathbf{p}_1}(\tau^s_1) \right\rangle \left\langle \Phi^{\tau_{in}\,*}_{\mathbf{k}_1-\mathbf{p}_1}\, H^{(0)}_{\mathring{d},\mathbf{p}_2}(\tau^s_2) \right\rangle.
$$
$$(6.133)$$

Secondly, we assume that the initial gravitational scalar potential and the GW's amplitude at the source position are uncorrelated, that the 0th order SGWB is unpolarized and that both of the random fields are statistically homogeneous and isotropic. This situation can represent a SGWB of cosmological origins, for instance. Introducing also the scalar potential power spectrum, we consider the following expectation values

$$\left\langle \Phi_{\mathbf{k}}^{\tau_{in}*} \Phi_{\mathbf{p}}^{\tau_{in}} \right\rangle = (2\pi)^3 \delta^3(\mathbf{k} - \mathbf{p}) \frac{P_{in}^{\Phi}(k)}{k^3}, \tag{6.134}$$

$$\left\langle H_{\mathring{c},\mathbf{p}_1}^{(0)*}(\tau_1^s) H_{\mathring{d},\mathbf{p}_2}^{(0)}(\tau_2^s) \right\rangle = (2\pi)^3 \delta_{\mathring{c}\mathring{d}} \delta^3(\mathbf{p}_1 - \mathbf{p}_2) \frac{I^{(0)}(p_1, \tau_1^s, \tau_2^s)}{2} \tag{6.135}$$

$$\left\langle \Phi_{\mathbf{k}_2 - \mathbf{p}_2}^{\tau_{in}} H_{\mathring{d},\mathbf{p}_2}^{(0)}(\tau_2^s) \right\rangle = 0. \tag{6.136}$$

Assuming for simplicity a standard inflationary model, write $P_{in}^{\Phi}(k) = A_s(k/k_*)^{n_s - 1}$. The constraints on n_s by the Planck [3] indicate that $P_{in}^{\Phi}(k)$ is almost scale invariant, hence $P_{in}^{\Phi}(k)/k^3 \sim 1/k^3$. With these results, the source two point function reads

$$\left\langle \mathcal{S}_{\mathring{a}}^*(\mathbf{k}_1, \tau_1') S_{\mathring{b}}(\mathbf{k}_2, \tau_2') \right\rangle =$$
$$= \delta^3(\mathbf{k}_1 - \mathbf{k}_2) \int d^3 p \, \mathcal{T}_p^H(\tau_1') \mathcal{T}_p^H(\tau_2') \mathcal{F}^*(\mathbf{p}, \mathbf{k}_1 - \mathbf{p}, \tau_1') \mathcal{F}(\mathbf{p}, \mathbf{k}_1 - \mathbf{p}, \tau_2') \times$$
$$\times \frac{P_{in}^{\Phi}(|\mathbf{k}_1 - \mathbf{p}|)}{|\mathbf{k}_1 - \mathbf{p}|^3} \frac{I^{(0)}(p, \tau_1^s, \tau_2^s)}{2} \sum_{\mathring{c}} \left[\mathscr{R}^*(\hat{p}, \hat{k}_1) \right]_{\mathring{a}}^{\mathring{c}} \left[\mathscr{R}(\hat{p}, \hat{k}_1) \right]_{\mathring{b}}^{\mathring{c}}, \tag{6.137}$$

where we notice the interesting divergence when $|\mathbf{k}_1 - \mathbf{p}_1| \to 0$. This effect, which is also found in the context of scalar induced gravitational waves [140, 143], encodes the constructive interference of modes which is able, possibly, to enhance the signal.

We can evaluate the product of the two rotation matrices with the aid of Eq. (6.94) and the properties of spin weighted spherical harmonics and their product rules in terms of the Clebsch - Gordan coefficients (see Appendix C). In particular, we have that

$$\sum_{\mathring{c}} [\mathscr{R}^*(\theta, \varphi)]_{\mathring{a}}^{\mathring{c}} [\mathscr{R}(\theta, \varphi)]_{\mathring{b}}^{\mathring{c}} = \frac{8\sqrt{\pi}}{21} \left[\begin{matrix} \left(\frac{21 Y_0^0}{2} + 3\sqrt{5} Y_0^2 + \frac{Y_0^4}{4} \right) & \sqrt{\frac{35}{8}} Y_{-4}^4 \\ \sqrt{\frac{35}{8}} Y_4^4 & \left(\frac{21 Y_0^0}{2} + 3\sqrt{5} Y_0^2 + \frac{Y_0^4}{4} \right) \end{matrix} \right], \tag{6.138}$$

where all the functions in the matrix above are spin-0 spherical harmonics evaluated in (θ, φ). Combining Eqs. (6.131), (6.137) and (6.138), and their definitions in Eq. (6.123), allow us to write the Stokes parameters at $\mathcal{O}(\epsilon^2)$. For the V one, related to a net circular polarization of the SGWB, we find

$$V^{(1)}(\mathbf{k}_1, \tau_1; \mathbf{k}_2, \tau_2) = 0, \tag{6.139}$$

while the expressions of the intensity and the linear polarizations are more compli-
cated, and they read

$$
I^{(1)}(\mathbf{k}_1, \tau_1; \mathbf{k}_2, \tau_2) = \sqrt{\pi} \delta^3(\mathbf{k}_1 - \mathbf{k}_2) \sum_{\tau_1^s, \tau_2^s} \int_{\tau_1^s}^{\tau_1} d\tau_1' \int_{\tau_2^s}^{\tau_2} d\tau_2' \, g_{k_1}^*(\tau_1, \tau_1') \, g_{k_1}(\tau_2, \tau_2') \times
$$

$$
\times \int d^3 p \, \mathcal{T}_p^H(\tau_1') \, \mathcal{T}_p^H(\tau_2') \, \mathcal{F}^*(\mathbf{p}, \mathbf{k}_1 - \mathbf{p}, \tau_1') \, \mathcal{F}(\mathbf{p}, \mathbf{k}_1 - \mathbf{p}, \tau_2') \times
$$

$$
\times \frac{P_{in}^\Phi(|\mathbf{k}_1 - \mathbf{p}|)}{|\mathbf{k}_1 - \mathbf{p}|^3} \times I^{(0)}(p, \tau_1^s, \tau_2^s) \times \left(4 Y_0^0(\theta, \varphi) + \frac{8\sqrt{5}}{7} Y_0^2(\theta, \varphi) + \frac{2}{21} Y_0^4(\theta, \varphi) \right),
$$

$$(6.140)$$

and

$$
(Q^{(1)} \pm i U^{(1)})(\mathbf{k}_1, \tau_1; \mathbf{k}_2, \tau_2) = \sqrt{\pi} \delta^3(\mathbf{k}_1 - \mathbf{k}_2) \sum_{\tau_1^s, \tau_2^s} \int_{\tau_1^s}^{\tau_1} d\tau_1' \int_{\tau_2^s}^{\tau_2} d\tau_2' \, g_{k_1}^*(\tau_1, \tau_1') \, g_{k_1}(\tau_2, \tau_2') \times
$$

$$
\times \int d^3 p \, \mathcal{T}_p^H(\tau_1') \, \mathcal{T}_p^H(\tau_2') \, \mathcal{F}^*(\mathbf{p}, \mathbf{k}_1 - \mathbf{p}, \tau_1') \, \mathcal{F}(\mathbf{p}, \mathbf{k}_1 - \mathbf{p}, \tau_2') \times
$$

$$
\times \frac{P_{in}^\Phi(|\mathbf{k}_1 - \mathbf{p}|)}{|\mathbf{k}_1 - \mathbf{p}|^3} \times I^{(0)}(p, \tau_1^s, \tau_2^s) \times \left(\sqrt{\frac{40}{63}} Y_{\mp 4}^4(\theta, \varphi) \right).
$$

$$(6.141)$$

Eqs. (6.140), (6.139) and (6.141) constitute another of the key results of this Chapter.
The information that they encode is

- Eq. (6.139) clearly states that the Stokes parameter V is null also at order $\mathcal{O}(\epsilon^2)$.
  Hence, our result implies that the interaction with structures doesn't violate
  parity creating a net difference in the amounts of left- and right- helicity states.
  This result was expected for two reasons: we assumed a GW generation mech-
  anism that doesn't prefer one state over the other, and in our analysis the two
  tensor modes propagate in the same fashion.

- Because of the orthogonality properties of the spherical harmonics, the angu-
  lar integrals in Eqs. (6.140) and (6.141) select specific multipoles of their in-
  tegrands. The dependence on the angle θ, namely the angle between $\mathbf{k}_1$ and
  $\mathbf{p}$ shows both in the spherical harmonics and in the functions of the variable
  $|\mathbf{k}_1 - \mathbf{p}|$, since this is equal to $\sqrt{k_1^2 + p^2 - 2 p k \cos\theta}$. Among these, we have
  $\mathcal{F}(\mathbf{p}, \mathbf{k}_1 - \mathbf{p}, \tau)$ and the scalar power spectrum. One can look at the expression
  of $\mathcal{F}$ in Eq. (6.103) and realize that only $T_m(|\mathbf{k}_1 - \mathbf{p}|)$ is angle dependent, as the
  rest of the expression contains only the modulus of $\mathbf{k}_1$ and $\mathbf{p}$, and the matter
  growth factor. However, the matter transfer function is essentially constant in
  the late time Universe, since its role is mainly to diversify the modes entering
  the horizon in radiation domination, versus those in matter domination (see
  discussion in Section 1.1.2). Overall, this means that the main dependence on
  the angle θ in Eqs. (6.140) and (6.141) is in the scalar potential power spectrum,
  $P_{in}^\Phi(|\mathbf{k}_1 - \mathbf{p}|)/|\mathbf{k}_1 - \mathbf{p}|^3$, and in the spherical harmonics.

- An interesting feature of Eq. (6.140) is that all values of ℓ from 0 to 4 contribute to the intensity $I^{(1)}$. This result is also found in [419], where they claim that this fact is due to the long range interaction nature of gravity, and also for the CMB, with the due differences, in [433].

- The spherical harmonics in Eq. (6.141) are such that

$$Y^4_{\pm 4}(\theta, \varphi) \propto e^{\pm 4 i \varphi}, \qquad (6.142)$$

reflecting the spin-4 nature of these Stokes parameters, and the spin-2 one of the GWs vicariously. The angle φ depends on the choice of the tetrad's elements $\{\hat{e}_{\hat{1}}(\hat{k}), \hat{e}_{\hat{2}}(\hat{k})\}$ made to construct the polarization basis for $H_{\hat{a}\hat{b},\mathbf{k}}(\tau)$. To get rid of this arbitrariness, in parallel with CMB computations [407, 432], one could define E and B modes for the SGWB as

$$E \pm i B \equiv e^{\mp 4 i \varphi} \left[Q \pm i U \right]. \qquad (6.143)$$

Note also that we are considering the combination $Q^{(1)} \pm i U^{(1)}$, instead of $Q^{(1)}$ and $U^{(1)}$ separately, to deal with an object with a well-defined character under parity transformations. However, their individual expressions can be readily found from Eq. (6.141).

- Note that the integral in Eq. (6.141) is actually zero, because the integral over the angle φ vanishes, since none of the other functions in the expression depend on it. Nevertheless, it is instructive to have the expression of $Q^{(1)} \pm i U^{(1)}$ written out this way, as it makes easier to understand which are the prerequisites of the scalar and tensor power spectra in order to have a non-trivial polarization profile. For instance, if one of them was not statistically isotropic, Eq. (6.141) would give a non trivial result.

- A very relevant quantity in describing the SGWB is the two-point correlation function

$$\left\langle H_{\hat{a}}(\mathbf{x}, \tau) \, H_{\hat{b}}(\mathbf{y}, \tau) \right\rangle \equiv \int d^3 k \, d^3 p \, e^{i(\mathbf{y} \cdot \mathbf{p} - \mathbf{x} \cdot \mathbf{k})} \, \mathcal{P}_{\hat{a}\hat{b}}(\mathbf{k}, \tau; \mathbf{p}, \tau), \qquad (6.144)$$

especially when evaluated in the same spacetime coordinate [22]. If the SGWB is statistically homogeneous and isotropic then the polarization tensor is $\propto \delta^3(\mathbf{k} - \mathbf{p})$ and in this case one can compute

$$\left\langle H_{\hat{a}}(\mathbf{x}, \tau) \, H_{\hat{b}}(\mathbf{x}, \tau) \right\rangle = \int_0^{+\infty} \frac{dk}{k} \left[\int_{\mathcal{S}^2} d^2 \hat{n} \, k^3 \, \mathcal{P}_{\hat{a}\hat{b}}(\mathbf{k}, \tau) \right], \qquad (6.145)$$

so that $k^3 \mathcal{P}_{\hat{a}\hat{b}}$ represents the amount of GW power in each logarithmic k bin, if one focuses on the diagonal elements of the polarization tensor. We have extracted the factor $1/k^3$ to have a dimensionless power spectrum. To make contact with observation, it is also customary to define the frequency of the

wave as $f \equiv k/(2\pi a_0)$, where a_0 is the value of the scale factor today [22]. One can also sum over the two polarization modes to obtain the total power spectrum.

- Starting from Eq. (6.144) one can compute the angular power spectrum by expanding the fields, evaluated on the 2− sphere, on the spherical harmonics basis. Despite the exciting prospects [245], the poor angular resolution typical of GW detectors still poses a serious challenge in accessing the high multipoles of the SGWB anisotropies (ET is expected to probe multipoles up to $\ell \lesssim 50$, while LISA $\ell \lesssim 15$ [400, 440, 441]).

6.7. Discussion and Conclusions

Detecting the stochastic gravitational wave background is one of the main science goals of many future gravitational wave observatories [370, 380–382]. Multi-band GW observation will also open a new observational window in cosmology, as the different behaviors in the various energy regimes can be used to break degeneracies between intrinsic and induced properties of the SGWB. In this Chapter, we developed a formalism able to describe the intensity and the polarization of the SGWB, across the entire frequency spectrum, accounting for its interaction with the matter structures present in the Universe. Working under the *classical matter approximation*, justified in Section 6.2.3, we found and solved the equations of motion of the metric perturbation. The direct consequence of such approach is to produce a source for the first order GW, $H^{(1)}_{\mu\nu}$, composed by the freely propagating GWs, $H^{(0)}_{\mu\nu}$, and the gravitational scalar potential, Φ. The matter density fluctuations, generating such potential wells do not have to be small, hence Φ can also describe the gravitational potential wells of compact lenses. Because of the presence of this second order source, as explained in Section 6.2.3, $H^{(1)}_{\mu\nu}$ develops scalar and vector components, on top of the tensor ones, whose evolution equations are Eqs. (6.72), (6.73) and (6.76) in the chosen gauge, which are physical since they source components of the Riemann tensor participating in the geodesics tidal motion [131]. We proceed in our analysis with the first order tensor mode, $\gamma^{(1)}_{ij}$, and found its propagation equation by applying the projector operator to Eq. (6.69). This operation led us to the first main result of the Chapter, namely Eqs. (6.99) and (6.100), where we can see the interference effects at play: the source in Eq. (6.100) is given by the integral over all possible momenta, **p**, of the free GW. At this stage, our results can are valid for both the SGWB or single waves in case of resolved sources. We commented that, the appearance of scalar and vector modes, $H^{(1)}, H^{(1)}_{ij}$ and $E^{(1)}_{ij}$ is related to a change in the direction of propagation between the perturbed and unperturbed GW. Indeed, when their wave vectors, k^i and p^i, are parallel, their sources vanishes (see Eq. (6.105)). Even though the concept of GW trajectory becomes unclear in the wave-optics regime, this effect must be re-

lated to gravitational lensing which, in geometric optics, displaces the GWs direction of propagation toward the center of the gravitational potential well. Similar simplifications also occur in the tensor sector. Looking at the source (6.100), we commented that each helicity component of the first order modes, i.e. $\gamma^{(1)}_{\mathring{a}}$, is sourced by a non-trivial linear combination of the two background ones, i.e. $H^{(0)}_{\mathring{a}}$, unless k^i and p^i are parallel. We claimed that this mixing, which in turns generates the polarization pattern in the SGWB, can be interpreted under the light of lensing as well: it is known that this is responsible for the production of secondary scalar-induced B-modes in the CMB [231, 405–407].

In Section 6.6 we built the GW's tensor modes' power spectrum, namely Eq. (6.117). To draw conclusions on the SGWB, we increasingly introduced assumptions; we required that the unperturbed SGWB is unpolarized, statistically homogeneous and isotropic and that all the fields are uncorrelated Gaussian random fields. In this case, we derived the expression of the Stokes parameters in Eqs. (6.140), (6.139) and (6.141). We claimed that it is an interplay of the free SGWB and the matter distribution which generates the first order effects, namely the anisotropies in the intensity and polarization. In particular, the intensity of the background receives contributions for the $\ell = 0, 2, 4$, $m = 0$ multipoles of the integrand in Eq. (6.137). On the other hand, the polarization parameters Q and U are sourced by the $\ell = 4$, $m = \pm 4$ multipoles, compatibly with the fact that we are considering only the tensor modes of $H^{(1)}_{ij}$. However, we have showed that the interaction between two statistically homogeneous and isotropic backgrounds does not produce these polarization modes, as the integral over the polar angle φ in Eq. (6.141) vanishes. As expected, we found that the Stokes parameter V, related to an asymmetry between left- and right- helicity eigenstates, remains zero: the interaction with matter does not act as a source or sink of one state over the other.

The amount of possible ramifications that can be addressed starting from the results presented in this Chapter is remarkable, and they all revolve around the two key ingredients of our analysis: the statistics of the GW's sources, encoded in $I(k)$, and the one of the gravitational potential wells, described by $P^{\Phi}_{in}(k)$. For instance, by changing the scalar potential power spectrum, one could use Eq. (6.140) to probe scale dependent features in the primordial power spectrum, usually linked to the formation of primordial black holes [145, 146, 388, 389]. To break the degeneracy among the effects of the two stochastic processes taking place, namely the generation of the GW and the propagation effects induced by matter overdensities, one could perform cross-correlations with other tracers, such as galaxy surveys or CMB experiments. Characterizing the order of magnitude of the effects predicted here, in different scenarios, will be the topic of future investigations.

Appendices

A. Expansion of equations of motion

Here we write explicitly the equations used in the main text. In particular, the linearized form of Eq. (6.28) once we choose Eq. (6.22) as background metric, setting $\Phi = \Psi$. To perform these computations, we use the Mathematica package *xPand* [442]: a suit to compute cosmological perturbations. We organize Eq. (6.28) as

$$[\mathcal{O}_0 H]_{\mu\nu} + \epsilon \, [\mathcal{O}_1 H]_{\mu\nu} = 0 \,, \tag{6.146}$$

with the explicit expressions of the two terms

$$
\begin{aligned}
[\mathcal{O}_0 H]_{\mu\nu} &= \Box_\eta \left(H_{\mu\nu} - \frac{1}{2}\eta_{\mu\nu}H \right) - 2\mathcal{H}\left(H_{\mu\nu} - \frac{1}{2}\eta_{\mu\nu}H \right)' + \hat{n}_\mu \hat{n}_\nu (4\mathcal{H}^2 - \mathcal{H}')H - \hat{\Lambda}_{\mu\nu}\mathcal{H}'H \\
&+ 2\mathcal{H}\left(\hat{n}_\nu \partial^\alpha H_{\alpha\mu} + \hat{n}_\mu \partial^\alpha H_{\alpha\nu} - \hat{n}^\alpha \partial_\mu H_{\alpha\nu} - \hat{n}^\alpha \partial_\nu H_{\alpha\mu} \right) + 2\eta_{\mu\nu}\mathcal{H}^2 \left(\hat{n}^\alpha \hat{n}^\beta H_{\alpha\beta} \right) \\
&+ (2\mathcal{H}' - 6\mathcal{H}^2)\hat{n}^\alpha \left(\hat{n}_\mu H_{\alpha\nu} + \hat{n}_\nu H_{\alpha\mu} \right)
\end{aligned} \tag{6.147}
$$

$$
\begin{aligned}
\left[\mathcal{O}_1 H\right]_{\mu\nu} &= 2H_{\mu\nu}\left[\Box_\eta \Phi - 2\mathcal{H}\Phi'\right] + 2\Phi\Box_\eta \tilde{H}_{\mu\nu} + 4\Phi\,\tilde{H}''_{\mu\nu} + 2\hat{n}_\mu \hat{n}_\nu \Phi\Box_\eta H + \\
&+ 4\eta_{\mu\nu}\left[\mathcal{H}\,\hat{n}^\gamma \Phi - D^\gamma \Phi\right]\partial_\gamma(\hat{n}^\alpha \hat{n}^\beta H_{\alpha\beta}) + (\partial_\mu H_{\nu\alpha} + \partial_\nu H_{\mu\alpha})\left[4\mathcal{H}\,\Phi'\hat{n}^\alpha - 2\partial^\alpha \Phi\right] + \\
&+ 4\partial_\alpha H_{\mu\beta}\left[\hat{n}^\alpha \hat{n}^\beta(\partial_\nu \Phi - 2\mathcal{H}\hat{n}_\nu \Phi) + \hat{n}_\nu(\hat{n}^\beta D^\alpha \Phi - \hat{n}^\alpha D^\beta \Phi)\right] + \\
&+ 4\partial_\alpha H_{\nu\beta}\left[\hat{n}^\alpha \hat{n}^\beta(\partial_\mu \Phi - 2\mathcal{H}\hat{n}_\mu \Phi) + \hat{n}_\mu(\hat{n}^\beta D^\alpha \Phi - \hat{n}^\alpha D^\beta \Phi)\right] + \\
&+ 4\partial_\alpha \tilde{H}_{\mu\nu}\left[\mathcal{H}\hat{n}^\alpha \Phi + D^\alpha \Phi\right] - 4\mathcal{H}\,\Phi\,\hat{n}_\mu \hat{n}_\nu \hat{n}^\alpha \partial_\alpha H - 2\eta_{\mu\nu}\Phi\Box_\eta(\hat{n}^\alpha \hat{n}^\beta H_{\alpha\beta}) + \\
&+ 2\partial^\alpha H_{\alpha\mu}\left[\partial_\nu \Phi + 2\mathcal{H}\,\hat{n}_\nu \Phi\right] + 2\partial^\alpha H_{\alpha\nu}\left[\partial_\mu \Phi + 2\mathcal{H}\,\hat{n}_\mu \Phi\right] + \\
&+ H\left[2\hat{\Lambda}_{\mu\nu}\Phi'' - 2\eta_{\mu\nu}\Delta\Phi + \Phi(2\mathcal{H}'\eta_{\mu\nu} + 8\mathcal{H}^2\hat{n}_\mu \hat{n}_\nu) + \mathcal{H}\Phi'(4\eta_{\mu\nu} - 4\hat{n}_\mu \hat{n}_\nu) - \\
&- 2\hat{n}_\mu D_\nu \Phi' - 2\hat{n}_\nu D_\mu \Phi'\right] + \\
&+ (H^{\alpha\beta}\hat{n}_\alpha \hat{n}_\beta)\left[\Phi\mathcal{H}^2(12\eta_{\mu\nu} - 8\hat{n}_\mu \hat{n}_\nu) + \Phi\mathcal{H}'(4\eta_{\mu\nu} + 8\hat{n}_\mu \hat{n}_\nu) + \eta_{\mu\nu}\Phi''\right] + \\
&+ H^{\alpha\beta}\left[(2\eta_{\mu\nu} + 4\hat{n}_\mu \hat{n}_\nu)\left(D_\alpha D_\beta \Phi + 2\mathcal{H}\,\hat{n}_\alpha D_\beta \Phi\right) - \\
&- 4\hat{n}^\alpha \left[\hat{n}_\mu D_\beta D_\nu \Phi + \hat{n}_\nu D_\beta D_\mu \Phi\right] + 4\hat{n}_\alpha \hat{n}_\beta\left[D_\nu D_\mu \Phi - H\hat{n}_\mu D_\nu \Phi - H\hat{n}_\nu D_\mu \Phi\right]\right] + \\
&+ H^\alpha_\mu\left[\hat{n}_\alpha \hat{n}_\nu(12\mathcal{H}^2\Phi - 4\mathcal{H}'\Phi + 4\mathcal{H}\Phi' - 4\Phi'' + 2\Delta\Phi) - 2D_\alpha D_\nu \Phi\right] + \\
&+ H^\alpha_\mu\left[2\mathcal{H}\hat{n}^\alpha D_\nu \Phi + 4\hat{n}_\alpha D_\nu \Phi' - 2\mathcal{H}\hat{n}_\nu D_\alpha \Phi\right] + \\
&+ H^\alpha_\nu\left[\hat{n}_\alpha \hat{n}_\mu(12\mathcal{H}^2\Phi - 4\mathcal{H}'\Phi + 4\mathcal{H}\Phi' - 4\Phi'' + 2\Delta\Phi) - 2D_\alpha D_\mu \Phi\right] + \\
&+ H^\alpha_\nu\left[2\mathcal{H}\hat{n}^\alpha D_\mu \Phi + 4\hat{n}_\alpha D_\nu \Phi' - 2\mathcal{H}\hat{n}_\mu D_\alpha \Phi\right]
\end{aligned} \tag{6.148}
$$

where $H = \eta^{\mu\nu} H_{\mu\nu}$, $\tilde{H}_{\mu\nu} \equiv H_{\mu\nu} - \eta_{\mu\nu} H/2$ and where we introduced the notation $D_\mu \equiv \hat{\Lambda}_\mu^\nu \partial_\nu$ with $\hat{\Lambda}_{\mu\nu} = \eta_{\mu\nu} + \hat{n}_\mu \hat{n}_\nu$ the orthogonal projector to $\hat{n}^\mu$. The derivatives D_μ are simply a covariant way of writing spatial partial derivatives, i.e. $D_\mu = \delta_\mu^i \partial_i$. Along with the equations of motion, the GW satisfies the de-Donder gauge condition, i.e. Eq. (6.26), whose linearization takes the form

$$\left[\partial^\mu \left(H_{\mu\nu} - \frac{1}{2} \eta_{\mu\nu} (\eta^{\alpha\beta} H_{\alpha\beta}) \right) - 4\mathcal{H} \, \hat{n}^\mu H_{\mu\nu} + H \mathcal{H} \, \hat{n}_\nu \right] + \epsilon \left[2\Phi \partial^\mu \tilde{H}_{\mu\nu} + 8\mathcal{H} \, \Phi \, \hat{n}^\mu H_{\mu\nu} + \right.$$
$$\left. + 2\mathcal{H} \, \Phi H \, \hat{n}_\nu + 4\mathcal{H} \, \Phi \, \hat{n}_\nu (\hat{n}^\alpha \hat{n}^\beta H_{\alpha\beta}) + 4\Phi' \, \hat{n}^\mu \, H_{\mu\nu} + 4\Phi \, \hat{n}^\mu \, H'_{\mu\nu} - 2\Phi \, \hat{n}^\alpha \hat{n}^\beta \partial_\nu H_{\alpha\beta} \right] = 0 \,,$$
$$(6.149)$$

while the compatibility Eq. (6.27) gives

$$H_{\mu\nu} \hat{n}^\mu \hat{n}^\mu + 2\epsilon H_{\mu\nu} \hat{n}^\mu \delta \hat{u}^\nu = 0 \,. \tag{6.150}$$

B. zeroth and first order equations

Now we can plug in $H_{\mu\nu} = H_{\mu\nu}^{(0)} + \epsilon H_{\mu\nu}^{(1)}$ in all the equations above, and find properties of $H_{\mu\nu}^{(0)}$ and $H_{\mu\nu}^{(1)}$ by equating order by order in the ϵ expansion. In particular, from Eqs. (6.149) and (6.150) we find

$$\hat{n}^\mu \hat{n}^\nu H_{\mu\nu}^{(0)} = 0 \,, \qquad \partial^\mu \tilde{H}_{\mu\nu}^{(0)} - 4\mathcal{H} \, \hat{n}^\mu H_{\mu\nu}^{(0)} + H^{(0)} \mathcal{H} \, \hat{n}_\nu = 0 \,, \qquad (6.151)$$
$$\hat{n}^\mu \hat{n}^\nu H_{\mu\nu}^{(1)} + 2\hat{n}^\nu \delta \hat{u}^\mu H_{\mu\nu}^{(0)} = 0 \,, \qquad \partial^\mu \tilde{H}_{\mu\nu}^{(1)} - 4\mathcal{H} \, \hat{n}^\mu H_{\mu\nu}^{(1)} + H^{(1)} \mathcal{H} \, \hat{n}_\nu = 0 \,, \qquad (6.152)$$

where the trace is $H^{(i)} = \eta^{\mu\nu} H_{\mu\nu}^{(i)}$ and introducing $\tilde{H}_{\mu\nu}^{(i)} = H_{\mu\nu}^{(i)} - \frac{1}{2} \eta_{\mu\nu} H^{(i)}$. On the other hand, the two equations of motion are

$$\left[\mathcal{O}_0 H^{(0)} \right]_{\mu\nu} = 0 \,, \qquad \text{and} \qquad \left[\mathcal{O}_0 H^{(1)} \right]_{\mu\nu} + \left[\mathcal{O}_1 H^{(0)} \right]_{\mu\nu} = 0 \,, \tag{6.153}$$

and their explicit expressions can be found from Eqs. (6.147) and (6.148), upon using Eqs. (6.151) and (6.152). These are

$$\left[\mathcal{O}_0 H^{(0)} \right]_{\mu\nu} = \Box_\eta \tilde{H}_{\mu\nu}^{(0)} - 2\mathcal{H} (\tilde{H}_{\mu\nu}^{(0)})' + \mathcal{H} \left(\hat{n}_\nu \partial_\mu H^{(0)} + \hat{n}_\mu \partial_\nu H^{(0)} \right) - (\hat{n}_\mu \hat{n}_\nu + \hat{\Lambda}_{\mu\nu}) \mathcal{H}' H^{(0)} -$$
$$- 2\mathcal{H} \left(\hat{n}^\alpha \partial_\mu H_{\alpha\nu}^{(0)} + \hat{n}^\alpha \partial_\nu H_{\alpha\mu}^{(0)} \right) + 2(\mathcal{H}' + \mathcal{H}^2) \hat{n}^\alpha \left(\hat{n}_\mu H_{\alpha\nu}^{(0)} + \hat{n}_\nu H_{\alpha\mu}^{(0)} \right)$$
$$(6.154)$$

$$\left[\mathcal{O}_0 H^{(1)} \right]_{\mu\nu} = \Box_\eta \tilde{H}_{\mu\nu}^{(1)} - 2\mathcal{H} (\tilde{H}_{\mu\nu}^{(1)})' + \mathcal{H} \left(\hat{n}_\nu \partial_\mu H^{(1)} + \hat{n}_\mu \partial_\nu H^{(1)} \right) - (\hat{n}_\mu \hat{n}_\nu + \hat{\Lambda}_{\mu\nu}) \mathcal{H}' H^{(1)} -$$
$$- 2\mathcal{H} \left(\hat{n}^\alpha \partial_\mu H_{\alpha\nu}^{(1)} + \hat{n}^\alpha \partial_\nu H_{\alpha\mu}^{(1)} \right) + 2(\mathcal{H}' + \mathcal{H}^2) \hat{n}^\alpha \left(\hat{n}_\mu H_{\alpha\nu}^{(1)} + \hat{n}_\nu H_{\alpha\mu}^{(1)} \right) +$$
$$+ 2\eta_{\mu\nu} \mathcal{H}^2 (\hat{n}^\alpha \hat{n}^\beta H_{\alpha\beta}^{(1)}) \,. \tag{6.155}$$

The expression of $[\mathcal{O}_1 H^{(0)}]_{\mu\nu}$ depends on the solution of $H^{(0)}_{\mu\nu}$, hence we first solve its equations. Taking the time-time and space-time component of Eq (6.154) we obtain

$$\frac{1}{2}\Box_\eta H^{(0)} - 3\mathcal{H}(H^{(0)})' - \mathcal{H}'H^{(0)} = 0 \qquad \text{Time-Time} \qquad (6.156)$$

$$\Box_\eta H^{(0)}_{0i} - 4\mathcal{H}(H^{(0)}_{0i})' + H^{(0)}_{0i}(6\mathcal{H}^2 - 2\mathcal{H}') - \mathcal{H}\partial_i H^{(0)} = 0 \qquad \text{Space-Time} \quad (6.157)$$

of which we take the solution $H^{(0)} = H^{(0)}_{0i} = 0$ as explained in the main text. This way Eqs. (6.154) and (6.151) give

$$\Box_\eta H^{(0)}_{ij} - 2\mathcal{H}(H^{(0)}_{ij})' = 0, \qquad \partial^i H^{(0)}_{ij} = 0, \qquad (6.158)$$

which we use to compute the source of the first order GW, namely

$$\begin{aligned}
[\mathcal{O}_1 H^{(0)}]_{\mu\nu} &= 4\Phi\,\Delta H^{(0)}_{\mu\nu} + 2H^{(0)}_{\mu\nu}\left[\Box_\eta\Phi - 2\mathcal{H}\Phi'\right] + 4\partial^k\Phi\,\partial_k H^{(0)}_{\mu\nu} - \\
&\quad - 2\hat{n}_\mu D^\alpha\Phi\left(H^{(0)'}_{\nu\alpha} + \mathcal{H}H^{(0)}_{\nu\alpha}\right) - 2\hat{n}_\nu D^\alpha\Phi\left(H^{(0)'}_{\mu\alpha} + \mathcal{H}H^{(0)}_{\mu\alpha}\right) - \\
&\quad - 2D_\mu\left(H^{(0)}_{\alpha\nu}D^\alpha\Phi\right) - 2D_\nu\left(H^{(0)}_{\alpha\mu}D^\alpha\Phi\right) \\
&\quad + 2(\eta_{\mu\nu} + 2\hat{n}_\mu\hat{n}_\nu)H^{(0)}_{\alpha\beta}D^\alpha D^\beta\Phi.
\end{aligned} \qquad (6.159)$$

We look again at the constraint equations, namely the time-time and space-time of $[\mathcal{O}_0 H^{(1)}]_{\mu\nu} + [\mathcal{O}_1 H^{(0)}]_{\mu\nu} = 0$. These are

$$\frac{1}{2}\Box_\eta H^{(1)} - 3\mathcal{H}(H^{(1)})' - \mathcal{H}'H^{(1)} = -2H^{(0)}_{ij}\partial^i\partial^j\Phi, \qquad \text{Time-Time}$$
$$(6.160)$$

$$\Box_\eta H^{(1)}_{0i} - 4\mathcal{H}(H^{(1)}_{0i})' - \mathcal{H}\partial_i H^{(1)} - 2(\mathcal{H}^2 + \mathcal{H}')H^{(1)}_{0i} = -\frac{2}{a}\partial^k\Phi\,(aH^{(0)}_{ki})', \qquad \text{Space-Time}$$
$$(6.161)$$

as it can be checked by using Eqs. (6.155) and (6.159).

C. Spin-weighted spherical harmonics and Clebsch-Gordan coefficients

The content of this Section follows [407, 432]. The spin-0 spherical harmonics are given by

$$Y^\ell_m(\theta, \varphi) = (-1)^m\sqrt{\frac{(2\ell+1)}{4\pi}\frac{(\ell-m)!}{(\ell+m)!}}\,e^{im\varphi}P_{\ell m}(\cos\theta) \qquad (6.162)$$

where $P_{\ell m}(x)$ is the associated Legendre polynomial. The spin weighted spherical harmonics are defined as

$$
{}_sY^\ell_m(\theta,\varphi) = (-1)^m \sqrt{\frac{(2\ell+1)}{4\pi} \frac{(\ell+m)!(\ell-m)!}{(\ell+s)!(\ell-s)!}} \left[\sin\left(\frac{\theta}{2}\right)\right]^{2\ell} e^{im\varphi} \times
$$
$$
\times \sum_r \binom{\ell-s}{r}\binom{\ell+s}{r+s-m}(-1)^{\ell-r-s}\left[\cot\left(\frac{\theta}{2}\right)\right]^{2r+s-m}. \tag{6.163}
$$

The sum over r runs over those values for which the binomial coefficients are non-vanishing, namely $\max\{0, m-s\} \le r \le \min\{\ell-s,\ell+m\}$. The spin weighted spherical harmonics are defined for $|s| \le \ell$ and $|m| \le \ell$ and, under the complex conjugation and a parity transformation, respect the following relations

$$
\left({}_sY^\ell_m(\theta,\varphi)\right)^* = (-1)^{s+m}\,{}_{-s}Y^\ell_{-m}(\theta,\varphi) \tag{6.164}
$$
$$
{}_sY^\ell_m(\pi-\theta,\pi+\varphi) = (-1)^\ell\,{}_{-s}Y^\ell_m(\theta,\varphi). \tag{6.165}
$$

The products of two spin weighted spherical harmonics is given by

$$
{}_{s_1}Y^{\ell_1}_{m_1}(\theta,\varphi)\,{}_{s_2}Y^{\ell_2}_{m_2}(\theta,\varphi) = \frac{\sqrt{(2\ell_1+1)(2\ell_2+2)}}{4\pi} \sum_{j=|\ell_1-\ell_2|}^{j=\ell_1+\ell_2} \sqrt{\frac{4\pi}{(2j+1)}}\,{}_sY^j_m(\theta,\varphi)
$$
$$
\times \langle \ell_1,\ell_2; m_1,m_2 | j,m \rangle \langle \ell_1,\ell_2; -s_1,-s_2 | j,-s \rangle \tag{6.166}
$$

where $s = s_1 + s_2$, $m = m_1 + m_2$ and the Clebsh-Gordan coefficients can be computed as

$$
\langle \ell_1,\ell_2; m_1,m_2 | j,m_1+m_2 \rangle =
$$
$$
= \sqrt{\frac{(\ell_1+\ell_2-j)!(j+\ell_1-\ell_2)!(j+\ell_2-\ell_1)!(2j+1)}{(j+\ell_1+\ell_2+1)!}} \times
$$
$$
\times \sum_k \left[\frac{(-1)^k \sqrt{(\ell_1+m_1)!(\ell_1-m_1)!(\ell_2+m_2)!(\ell_2-m_2)!}}{k!(\ell_1+\ell_2-j-k)!(\ell_1-m_1-k)!} \right.
$$
$$
\left. \times \frac{\sqrt{(j+m_1+m_2)!(j-m_1-m_2)!}}{(\ell_2+m_2-k)!(j-\ell_2+m_1+k)!(j-\ell_1-m_2+k)!} \right] \tag{6.167}
$$

where the sum over k goes from $\max\{0, \ell_2-j-m_1, \ell_1-j+m_2\} \le k \le \min\{\ell_1+\ell_2-j, \ell_1-m_1, \ell_2+m_2\}$.

Bibliography

[1] **LIGO Scientific, Virgo** Collaboration, B. P. Abbott et al., *Observation of Gravitational Waves from a Binary Black Hole Merger, Phys. Rev. Lett.* **116** (2016), no. 6 061102, [`arXiv:1602.03837`].

[2] **WMAP** Collaboration, C. L. Bennett et al., *First year Wilkinson Microwave Anisotropy Probe (WMAP) observations: Preliminary maps and basic results, Astrophys. J. Suppl.* **148** (2003) 1–27, [`astro-ph/0302207`].

[3] **Planck** Collaboration, Y. Akrami et al., *Planck 2018 results. X. Constraints on inflation, Astron. Astrophys.* **641** (2020) A10, [`arXiv:1807.06211`].

[4] **Planck** Collaboration, N. Aghanim et al., *Planck 2018 results. VI. Cosmological parameters, Astron. Astrophys.* **641** (2020) A6, [`arXiv:1807.06209`]. [Erratum: Astron.Astrophys. 652, C4 (2021)].

[5] S. Dodelson and F. Schmidt, *Modern cosmology.* Academic Press, 2020.

[6] **Supernova Search Team** Collaboration, A. G. Riess et al., *Observational evidence from supernovae for an accelerating universe and a cosmological constant, Astron. J.* **116** (1998) 1009–1038, [`astro-ph/9805201`].

[7] **Supernova Cosmology Project** Collaboration, S. Perlmutter et al., *Measurements of Ω and Λ from 42 high redshift supernovae, Astrophys. J.* **517** (1999) 565–586, [`astro-ph/9812133`].

[8] **SDSS** Collaboration, K. Abazajian et al., *The First data release of the Sloan Digital Sky Survey, Astron. J.* **126** (2003) 2081, [`astro-ph/0305492`].

[9] L. Amendola et al., *Cosmology and fundamental physics with the Euclid satellite, Living Rev. Rel.* **21** (2018), no. 1 2, [`arXiv:1606.00180`].

[10] **SKA** Collaboration, D. J. Bacon et al., *Cosmology with Phase 1 of the Square Kilometre Array: Red Book 2018: Technical specifications and performance forecasts, Publ. Astron. Soc. Austral.* **37** (2020) e007, [`arXiv:1811.02743`].

[11] O. Doré et al., *Cosmology with the SPHEREX All-Sky Spectral Survey,* [`arXiv:1412.4872`].

[12] **LSST** Collaboration, Z. Ivezic et al., *LSST: from Science Drivers to Reference Design and Anticipated Data Products, Astrophys. J.* **873** (2019), no. 2 111, [`arXiv:0805.2366`].

[13] E. Abdalla et al., *Cosmology intertwined: A review of the particle physics, astrophysics, and cosmology associated with the cosmological tensions and anomalies, JHEAp* **34** (2022) 49–211, [`arXiv:2203.06142`].

[14] L. Perivolaropoulos and F. Skara, *Challenges for ΛCDM: An update, New Astron. Rev.* **95** (2022) 101659, [`arXiv:2105.05208`].

[15] E. Di Valentino, O. Mena, S. Pan, L. Visinelli, W. Yang, A. Melchiorri, D. F. Mota, A. G. Riess, and J. Silk, *In the realm of the Hubble tension—a review of solutions, Class. Quant. Grav.* **38** (2021), no. 15 153001, [`arXiv:2103.01183`].

[16] **LIGO Scientific, VIRGO, KAGRA** Collaboration, R. Abbott et al., *GWTC-3: Compact Binary Coalescences Observed by LIGO and Virgo During the Second Part of the Third Observing Run*, [`arXiv:2111.03606`].

[17] **KAGRA, LIGO Scientific, Virgo, VIRGO** Collaboration, B. P. Abbott et al., *Prospects for observing and localizing gravitational-wave transients with Advanced LIGO, Advanced Virgo and KAGRA, Living Rev. Rel.* **21** (2018), no. 1 3, [`arXiv:1304.0670`].

[18] M. Maggiore et al., *Science Case for the Einstein Telescope, JCAP* **03** (2020) 050, [`arXiv:1912.02622`].

[19] D. Reitze et al., *Cosmic Explorer: The U.S. Contribution to Gravitational-Wave Astronomy beyond LIGO, Bull. Am. Astron. Soc.* **51** (2019), no. 7 035, [`arXiv:1907.04833`].

[20] G. Scelfo, N. Bellomo, A. Raccanelli, S. Matarrese, and L. Verde, *GW×LSS: chasing the progenitors of merging binary black holes, JCAP* **09** (2018) 039, [`arXiv:1809.03528`].

[21] B. J. Carr and S. W. Hawking, *Black holes in the early Universe, Mon. Not. Roy. Astron. Soc.* **168** (1974) 399–415.

[22] C. Caprini and D. G. Figueroa, *Cosmological Backgrounds of Gravitational Waves, Class. Quant. Grav.* **35** (2018), no. 16 163001, [`arXiv:1801.04268`].

[23] M. C. Guzzetti, N. Bartolo, M. Liguori, and S. Matarrese, *Gravitational waves from inflation, Riv. Nuovo Cim.* **39** (2016), no. 9 399–495, [`arXiv:1605.01615`].

[24] N. Bartolo et al., *Science with the space-based interferometer LISA. IV: Probing inflation with gravitational waves, JCAP* **12** (2016) 026, [`arXiv:1610.06481`].

[25] P. Amaro-Seoane et al., *Laser Interferometer Space Antenna*, [`arXiv:1702.00786`].

[26] J. Crowder and N. J. Cornish, *Beyond LISA: Exploring future gravitational wave missions, Phys. Rev. D* **72** (2005) 083005, [`gr-qc/0506015`].

[27] W.-H. Ruan, Z.-K. Guo, R.-G. Cai, and Y.-Z. Zhang, *Taiji program: Gravitational-wave sources, Int. J. Mod. Phys. A* **35** (2020), no. 17 2050075, [arXiv:1807.09495].

[28] **TianQin** Collaboration, J. Luo et al., *TianQin: a space-borne gravitational wave detector, Class. Quant. Grav.* **33** (2016), no. 3 035010, [arXiv:1512.02076].

[29] R. Manchester, *The international pulsar timing array, Classical and Quantum Gravity* **30** (2013), no. 22 224010.

[30] **NANOGrav** Collaboration, Z. Arzoumanian et al., *The NANOGrav Nine-year Data Set: Limits on the Isotropic Stochastic Gravitational Wave Background, Astrophys. J.* **821** (2016), no. 1 13, [arXiv:1508.03024].

[31] A. Weltman et al., *Fundamental physics with the Square Kilometre Array, Publ. Astron. Soc. Austral.* **37** (2020) e002, [arXiv:1810.02680].

[32] R. M. Wald, *General Relativity.* Chicago Univ. Pr., Chicago, USA, 1984.

[33] M. V. Sazhin, O. S. Sazhina, and U. Chadayammuri, *The Scale Factor in the Universe with Dark Energy*, [arXiv:1109.2258].

[34] E. Bertschinger, *Cosmological dynamics: Course 1*, in *Les Houches Summer School on Cosmology and Large Scale Structure (Session 60)*, pp. 273–348, 8, 1993. astro-ph/9503125.

[35] S. M. Carroll, W. H. Press, and E. L. Turner, *The Cosmological constant, Ann. Rev. Astron. Astrophys.* **30** (1992) 499–542.

[36] H. Kodama and M. Sasaki, *Cosmological Perturbation Theory, Prog. Theor. Phys. Suppl.* **78** (1984) 1–166.

[37] K. A. Malik and D. Wands, *Cosmological perturbations, Phys. Rept.* **475** (2009) 1–51, [arXiv:0809.4944].

[38] M. Maggiore, *Gravitational Waves. Vol. 2: Astrophysics and Cosmology.* Oxford University Press, 3, 2018.

[39] C.-P. Ma and E. Bertschinger, *Cosmological perturbation theory in the synchronous and conformal Newtonian gauges, Astrophys. J.* **455** (1995) 7–25, [astro-ph/9506072].

[40] J. M. Bardeen, *Gauge Invariant Cosmological Perturbations, Phys. Rev. D* **22** (1980) 1882–1905.

[41] A. Lewis, A. Challinor, and A. Lasenby, *Efficient computation of CMB anisotropies in closed FRW models, Astrophys. J.* **538** (2000) 473–476, [astro-ph/9911177].

[42] J. Lesgourgues and T. Tram, *The cosmic linear anisotropy solving system (class) iv: efficient implementation of non-cold relics, Journal of Cosmology and Astroparticle Physics* **2011** (2011), no. 09 032.

[43] D. J. Eisenstein and W. Hu, *Baryonic features in the matter transfer function, Astrophys. J.* **496** (1998) 605, [`astro-ph/9709112`].

[44] D. J. Eisenstein and W. Hu, *Power spectra for cold dark matter and its variants, Astrophys. J.* **511** (1997) 5, [`astro-ph/9710252`].

[45] A. J. S. Hamilton, *Formulae for growth factors in expanding universes containing matter and a cosmological constant, Mon. Not. Roy. Astron. Soc.* **322** (2001) 419, [`astro-ph/0006089`].

[46] E. V. Linder and A. Jenkins, *Cosmic structure and dark energy, Mon. Not. Roy. Astron. Soc.* **346** (2003) 573, [`astro-ph/0305286`].

[47] J. A. Peacock, *Cosmological physics.* Cambridge Univ. Pr., 1999.

[48] S. Weinberg, *Cosmology.* Oxford Univ. Pr., 2008.

[49] N. Kaiser, *Clustering in real space and in redshift space, Mon. Not. Roy. Astron. Soc.* **227** (1987) 1–27.

[50] **SDSS** Collaboration, M. Tegmark et al., *The 3-D power spectrum of galaxies from the SDSS, Astrophys. J.* **606** (2004) 702–740, [`astro-ph/0310725`].

[51] A. Joyce, B. Jain, J. Khoury, and M. Trodden, *Beyond the Cosmological Standard Model, Phys. Rept.* **568** (2015) 1–98, [`arXiv:1407.0059`].

[52] T. Clifton, P. G. Ferreira, A. Padilla, and C. Skordis, *Modified Gravity and Cosmology, Phys. Rept.* **513** (2012) 1–189, [`arXiv:1106.2476`].

[53] H. Ruegg and M. Ruiz-Altaba, *The Stueckelberg field, Int. J. Mod. Phys. A* **19** (2004) 3265–3348, [`hep-th/0304245`].

[54] A. Silvestri and M. Trodden, *Approaches to Understanding Cosmic Acceleration, Rept. Prog. Phys.* **72** (2009) 096901, [`arXiv:0904.0024`].

[55] P. J. E. Peebles and B. Ratra, *Cosmology with a Time Variable Cosmological Constant, Astrophys. J. Lett.* **325** (1988) L17.

[56] C. Brans and R. H. Dicke, *Mach's principle and a relativistic theory of gravitation, Phys. Rev.* **124** (1961) 925–935.

[57] A. Nicolis, R. Rattazzi, and E. Trincherini, *The Galileon as a local modification of gravity, Phys. Rev. D* **79** (2009) 064036, [`arXiv:0811.2197`].

[58] C. Armendariz-Picon, V. F. Mukhanov, and P. J. Steinhardt, *Essentials of k essence*, Phys. Rev. D **63** (2001) 103510, [`astro-ph/0006373`].

[59] A. De Felice and S. Tsujikawa, *Cosmology of a covariant Galileon field*, Phys. Rev. Lett. **105** (2010) 111301, [`arXiv:1007.2700`].

[60] G. W. Horndeski, *Second-order scalar-tensor field equations in a four-dimensional space*, Int. J. Theor. Phys. **10** (1974) 363–384.

[61] C. Deffayet, X. Gao, D. A. Steer, and G. Zahariade, *From k-essence to generalised Galileons*, Phys. Rev. D **84** (2011) 064039, [`arXiv:1103.3260`].

[62] T. Kobayashi, M. Yamaguchi, and J. Yokoyama, *Generalized G-inflation: Inflation with the most general second-order field equations*, Prog. Theor. Phys. **126** (2011) 511–529, [`arXiv:1105.5723`].

[63] M. Zumalacárregui and J. García-Bellido, *Transforming gravity: from derivative couplings to matter to second-order scalar-tensor theories beyond the Horndeski Lagrangian*, Phys. Rev. D **89** (2014) 064046, [`arXiv:1308.4685`].

[64] J. Gleyzes, D. Langlois, F. Piazza, and F. Vernizzi, *Healthy theories beyond Horndeski*, Phys. Rev. Lett. **114** (2015), no. 21 211101, [`arXiv:1404.6495`].

[65] D. Langlois and K. Noui, *Degenerate higher derivative theories beyond Horndeski: evading the Ostrogradski instability*, JCAP **1602** (2016) 034, [`arXiv:1510.06930`].

[66] D. Langlois, *Dark energy and modified gravity in degenerate higher-order scalar–tensor (DHOST) theories: A review*, Int. J. Mod. Phys. **D28** (2019), no. 05 1942006, [`arXiv:1811.06271`].

[67] M. Crisostomi, K. Koyama, and G. Tasinato, *Extended Scalar-Tensor Theories of Gravity*, JCAP **1604** (2016) 044, [`arXiv:1602.03119`].

[68] J. Ben Achour, M. Crisostomi, K. Koyama, D. Langlois, K. Noui, and G. Tasinato, *Degenerate higher order scalar-tensor theories beyond Horndeski up to cubic order*, JHEP **12** (2016) 100, [`arXiv:1608.08135`].

[69] C. de Rham and A. Matas, *Ostrogradsky in Theories with Multiple Fields*, JCAP **06** (2016) 041, [`arXiv:1604.08638`].

[70] D. Langlois, M. Mancarella, K. Noui, and F. Vernizzi, *Effective Description of Higher-Order Scalar-Tensor Theories*, JCAP **1705** (2017) 033, [`arXiv:1703.03797`].

[71] T. Baker and P. Bull, *Observational signatures of modified gravity on ultra-large scales*, Astrophys. J. **811** (2015) 116, [`arXiv:1506.00641`].

[72] T. Baker, P. G. Ferreira, C. D. Leonard, and M. Motta, *New Gravitational Scales in Cosmological Surveys, Phys. Rev. D* **90** (2014), no. 12 124030, [arXiv:1409.8284].

[73] E. Bertschinger and P. Zukin, *Distinguishing Modified Gravity from Dark Energy, Phys. Rev. D* **78** (2008) 024015, [arXiv:0801.2431].

[74] K. Koyama, *Cosmological Tests of Modified Gravity, Rept. Prog. Phys.* **79** (2016), no. 4 046902, [arXiv:1504.04623].

[75] J. M. Ezquiaga and M. Zumalacárregui, *Dark Energy After GW170817: Dead Ends and the Road Ahead, Phys. Rev. Lett.* **119** (2017), no. 25 251304, [arXiv:1710.05901].

[76] P. Creminelli and F. Vernizzi, *Dark Energy after GW170817 and GRB170817A, Phys. Rev. Lett.* **119** (2017), no. 25 251302, [arXiv:1710.05877].

[77] T. Baker, E. Bellini, P. G. Ferreira, M. Lagos, J. Noller, and I. Sawicki, *Strong constraints on cosmological gravity from GW170817 and GRB 170817A, Phys. Rev. Lett.* **119** (2017), no. 25 251301, [arXiv:1710.06394].

[78] T. Baker et al., *Novel Probes Project: Tests of gravity on astrophysical scales, Rev. Mod. Phys.* **93** (2021), no. 1 015003, [arXiv:1908.03430].

[79] **LIGO Scientific, Virgo, Fermi-GBM, INTEGRAL** Collaboration, B. P. Abbott et al., *Gravitational Waves and Gamma-rays from a Binary Neutron Star Merger: GW170817 and GRB 170817A, Astrophys. J. Lett.* **848** (2017), no. 2 L13, [arXiv:1710.05834].

[80] J. M. Ezquiaga, W. Hu, M. Lagos, M.-X. Lin, and F. Xu, *Modified gravitational wave propagation with higher modes and its degeneracies with lensing, JCAP* **08** (2022), no. 08 016, [arXiv:2203.13252].

[81] M. Lagos, T. Baker, P. G. Ferreira, and J. Noller, *A general theory of linear cosmological perturbations: scalar-tensor and vector-tensor theories, JCAP* **08** (2016) 007, [arXiv:1604.01396].

[82] C. Cheung, P. Creminelli, A. L. Fitzpatrick, J. Kaplan, and L. Senatore, *The Effective Field Theory of Inflation, JHEP* **03** (2008) 014, [arXiv:0709.0293].

[83] P. Creminelli, G. D'Amico, J. Norena, and F. Vernizzi, *The Effective Theory of Quintessence: the w<-1 Side Unveiled, JCAP* **02** (2009) 018, [arXiv:0811.0827].

[84] M. Park, K. M. Zurek, and S. Watson, *A Unified Approach to Cosmic Acceleration, Phys. Rev. D* **81** (2010) 124008, [arXiv:1003.1722].

[85] J. K. Bloomfield and E. E. Flanagan, *A Class of Effective Field Theory Models of Cosmic Acceleration*, JCAP **10** (2012) 039, [arXiv:1112.0303].

[86] G. Gubitosi, F. Piazza, and F. Vernizzi, *The Effective Field Theory of Dark Energy*, JCAP **02** (2013) 032, [arXiv:1210.0201].

[87] F. Piazza and F. Vernizzi, *Effective Field Theory of Cosmological Perturbations*, Class. Quant. Grav. **30** (2013) 214007, [arXiv:1307.4350].

[88] J. Gleyzes, D. Langlois, F. Piazza, and F. Vernizzi, *Essential Building Blocks of Dark Energy*, JCAP **08** (2013) 025, [arXiv:1304.4840].

[89] B. Hu, M. Raveri, N. Frusciante, and A. Silvestri, *Effective Field Theory of Cosmic Acceleration: an implementation in CAMB*, Phys. Rev. D **89** (2014), no. 10 103530, [arXiv:1312.5742].

[90] B. Hu, M. Raveri, N. Frusciante, and A. Silvestri, *EFTCAMB/EFTCosmoMC: Numerical Notes v3.0*, [arXiv:1405.3590].

[91] E. Bellini and I. Sawicki, *Maximal freedom at minimum cost: linear large-scale structure in general modifications of gravity*, JCAP **07** (2014) 050, [arXiv:1404.3713].

[92] M. Lagos, E. Bellini, J. Noller, P. G. Ferreira, and T. Baker, *A general theory of linear cosmological perturbations: stability conditions, the quasistatic limit and dynamics*, JCAP **03** (2018) 021, [arXiv:1711.09893].

[93] N. Frusciante and L. Perenon, *Effective field theory of dark energy: A review*, Phys. Rept. **857** (2020) 1–63, [arXiv:1907.03150].

[94] N. Frusciante, G. Papadomanolakis, and A. Silvestri, *An Extended action for the effective field theory of dark energy: a stability analysis and a complete guide to the mapping at the basis of EFTCAMB*, JCAP **07** (2016) 018, [arXiv:1601.04064].

[95] N. Frusciante, G. Papadomanolakis, S. Peirone, and A. Silvestri, *The role of the tachyonic instability in Horndeski gravity*, JCAP **02** (2019) 029, [arXiv:1810.03461].

[96] M. Raveri, B. Hu, N. Frusciante, and A. Silvestri, *Effective Field Theory of Cosmic Acceleration: constraining dark energy with CMB data*, Phys. Rev. D **90** (2014), no. 4 043513, [arXiv:1405.1022].

[97] S. Peirone, M. Martinelli, M. Raveri, and A. Silvestri, *Impact of theoretical priors in cosmological analyses: the case of single field quintessence*, Phys. Rev. D **96** (2017), no. 6 063524, [arXiv:1702.06526].

[98] M. Chevallier and D. Polarski, *Accelerating universes with scaling dark matter,* *Int. J. Mod. Phys. D* **10** (2001) 213–224, [gr-qc/0009008].

[99] E. V. Linder, *Exploring the expansion history of the universe,* *Phys. Rev. Lett.* **90** (2003) 091301, [astro-ph/0208512].

[100] **DES** Collaboration, T. Abbott et al., *Dark Energy Survey year 1 results: Cosmological constraints from galaxy clustering and weak lensing,* *Phys. Rev. D* **98** (2018), no. 4 043526, [arXiv:1708.01530].

[101] **DES** Collaboration, T. Abbott et al., *The Dark Energy Survey: more than dark energy – an overview,* *Mon. Not. Roy. Astron. Soc.* **460** (2016), no. 2 1270–1299, [arXiv:1601.00329].

[102] **DES** Collaboration, T. M. C. Abbott et al., *Dark Energy Survey Year 3 results: Cosmological constraints from galaxy clustering and weak lensing,* *Phys. Rev. D* **105** (2022), no. 2 023520, [arXiv:2105.13549].

[103] J. T. A. de Jong, G. A. Verdoes Kleijn, K. H. Kuijken, and E. A. Valentijn, *The Kilo-Degree Survey,* *Experimental Astronomy* **35** (Jan., 2013) 25–44, [arXiv:1206.1254].

[104] E. van Uitert et al., *KiDS+GAMA: cosmology constraints from a joint analysis of cosmic shear, galaxy–galaxy lensing, and angular clustering,* *Mon. Not. Roy. Astron. Soc.* **476** (2018), no. 4 4662–4689, [arXiv:1706.05004].

[105] **EUCLID** Collaboration, R. Laureijs et al., *Euclid Definition Study Report,* [arXiv:1110.3193].

[106] LSST Science Collaboration, *LSST Science Book, Version 2.0,* *arXiv e-prints* (Dec., 2009) arXiv:0912.0201, [arXiv:0912.0201].

[107] **LSST Dark Energy Science** Collaboration, R. Mandelbaum et al., *The LSST Dark Energy Science Collaboration (DESC) Science Requirements Document,* [arXiv:1809.01669].

[108] D. Spergel et al., *Wide-Field InfrarRed Survey Telescope-Astrophysics Focused Telescope Assets WFIRST-AFTA 2015 Report,* [arXiv:1503.03757].

[109] L. Pogosian, A. Silvestri, K. Koyama, and G.-B. Zhao, *How to optimally parametrize deviations from General Relativity in the evolution of cosmological perturbations?,* *Phys. Rev. D* **81** (2010) 104023, [arXiv:1002.2382].

[110] L. Pogosian and A. Silvestri, *What can cosmology tell us about gravity? Constraining Horndeski gravity with Σ and μ,* *Phys. Rev. D* **94** (2016), no. 10 104014, [arXiv:1606.05339].

[111] T. Baker, P. G. Ferreira, and C. Skordis, *A Fast Route to Modified Gravitational Growth*, Phys. Rev. D **89** (2014), no. 2 024026, [arXiv:1310.1086].

[112] B. Jain and P. Zhang, *Observational Tests of Modified Gravity*, Phys. Rev. D **78** (2008) 063503, [arXiv:0709.2375].

[113] L. Amendola, M. Kunz, and D. Sapone, *Measuring the dark side (with weak lensing)*, JCAP **04** (2008) 013, [arXiv:0704.2421].

[114] S. F. Daniel, R. R. Caldwell, A. Cooray, and A. Melchiorri, *Large Scale Structure as a Probe of Gravitational Slip*, Phys. Rev. **D77** (2008) 103513, [arXiv:0802.1068].

[115] Y.-S. Song, G.-B. Zhao, D. Bacon, K. Koyama, R. C. Nichol, and L. Pogosian, *Complementarity of Weak Lensing and Peculiar Velocity Measurements in Testing General Relativity*, Phys. Rev. D **84** (2011) 083523, [arXiv:1011.2106].

[116] F. Simpson et al., *CFHTLenS: Testing the Laws of Gravity with Tomographic Weak Lensing and Redshift Space Distortions*, Mon. Not. Roy. Astron. Soc. **429** (2013) 2249, [arXiv:1212.3339].

[117] S. Peirone, K. Koyama, L. Pogosian, M. Raveri, and A. Silvestri, *Large-scale structure phenomenology of viable Horndeski theories*, Phys. Rev. D **97** (2018), no. 4 043519, [arXiv:1712.00444].

[118] W. Hu and I. Sawicki, *A Parameterized Post-Friedmann Framework for Modified Gravity*, Phys. Rev. D **76** (2007) 104043, [arXiv:0708.1190].

[119] W. Hu, *Parametrized Post-Friedmann Signatures of Acceleration in the CMB*, Phys. Rev. D **77** (2008) 103524, [arXiv:0801.2433].

[120] P. G. Ferreira, T. Baker, and C. Skordis, *Testing general relativity with cosmology: a synopsis of the parametrized post-Friedmann approach*, Gen. Rel. Grav. **46** (2014) 1788.

[121] T. Baker, P. G. Ferreira, and C. Skordis, *The Parameterized Post-Friedmann framework for theories of modified gravity: concepts, formalism and examples*, Phys. Rev. D **87** (2013), no. 2 024015, [arXiv:1209.2117].

[122] **LISA Cosmology Working Group** Collaboration, E. Belgacem et al., *Testing modified gravity at cosmological distances with LISA standard sirens*, JCAP **07** (2019) 024, [arXiv:1906.01593].

[123] A. Nishizawa, *Generalized framework for testing gravity with gravitational-wave propagation. I. Formulation*, Phys. Rev. **D97** (2018), no. 10 104037, [arXiv:1710.04825].

[124] I. D. Saltas, I. Sawicki, L. Amendola, and M. Kunz, *Anisotropic Stress as a Signature of Nonstandard Propagation of Gravitational Waves*, Phys. Rev. Lett. **113** (2014), no. 19 191101, [`arXiv:1406.7139`].

[125] **LIGO Scientific, Virgo** Collaboration, B. P. Abbott et al., *GW170817: Observation of Gravitational Waves from a Binary Neutron Star Inspiral*, Phys. Rev. Lett. **119** (2017), no. 16 161101, [`arXiv:1710.05832`].

[126] A. Dima and F. Vernizzi, *Vainshtein Screening in Scalar-Tensor Theories before and after GW170817: Constraints on Theories beyond Horndeski*, Phys. Rev. D **97** (2018), no. 10 101302, [`arXiv:1712.04731`].

[127] D. Bettoni, J. M. Ezquiaga, K. Hinterbichler, and M. Zumalacárregui, *Speed of Gravitational Waves and the Fate of Scalar-Tensor Gravity*, Phys. Rev. **D95** (2017), no. 8 084029, [`arXiv:1608.01982`].

[128] R. Kase and S. Tsujikawa, *Dark energy in Horndeski theories after GW170817: A review*, Int. J. Mod. Phys. D **28** (2019), no. 05 1942005, [`arXiv:1809.08735`].

[129] C. de Rham and S. Melville, *Gravitational Rainbows: LIGO and Dark Energy at its Cutoff*, Phys. Rev. Lett. **121** (2018), no. 22 221101, [`arXiv:1806.09417`].

[130] L. Bordin, E. J. Copeland, and A. Padilla, *Dark energy loopholes some time after GW170817*, JCAP **11** (2020) 063, [`arXiv:2006.06652`].

[131] E. E. Flanagan and S. A. Hughes, *The Basics of gravitational wave theory*, New J. Phys. **7** (2005) 204, [`gr-qc/0501041`].

[132] K. S. Thorne, *Gravitational waves*, in *Particle and nuclear astrophysics and cosmology in the next millennium. Proceedings, Summer Study, Snowmass, USA, June 29-July 14, 1994*, pp. 0160–184, 1995. `gr-qc/9506086`.

[133] A. Buonanno, *TASI lectures on gravitational waves from the early universe*, in *Theoretical Advanced Study Institute in Elementary Particle Physics (TASI 2002): Particle Physics and Cosmology: The Quest for Physics Beyond the Standard Model(s)*, pp. 855–892, 3, 2003. `gr-qc/0303085`.

[134] C. Carbone and S. Matarrese, *A Unified treatment of cosmological perturbations from super-horizon to small scales*, Phys. Rev. D **71** (2005) 043508, [`astro-ph/0407611`].

[135] P. Auclair et al., *Probing the gravitational wave background from cosmic strings with LISA*, JCAP **04** (2020) 034, [`arXiv:1909.00819`].

[136] A. C. Jenkins and M. Sakellariadou, *Anisotropies in the stochastic gravitational-wave background: Formalism and the cosmic string case*, Phys. Rev. D **98** (2018), no. 6 063509, [`arXiv:1802.06046`].

[137] S. Kuroyanagi, K. Takahashi, N. Yonemaru, and H. Kumamoto, *Anisotropies in the gravitational wave background as a probe of the cosmic string network*, *Phys. Rev. D* **95** (2017), no. 4 043531, [`arXiv:1604.00332`].

[138] M. Geller, A. Hook, R. Sundrum, and Y. Tsai, *Primordial Anisotropies in the Gravitational Wave Background from Cosmological Phase Transitions*, *Phys. Rev. Lett.* **121** (2018), no. 20 201303, [`arXiv:1803.10780`].

[139] C. Caprini et al., *Science with the space-based interferometer eLISA. II: Gravitational waves from cosmological phase transitions*, *JCAP* **04** (2016) 001, [`arXiv:1512.06239`].

[140] D. Baumann, P. J. Steinhardt, K. Takahashi, and K. Ichiki, *Gravitational Wave Spectrum Induced by Primordial Scalar Perturbations*, *Phys. Rev. D* **76** (2007) 084019, [`hep-th/0703290`].

[141] K. N. Ananda, C. Clarkson, and D. Wands, *The Cosmological gravitational wave background from primordial density perturbations*, *Phys. Rev. D* **75** (2007) 123518, [`gr-qc/0612013`].

[142] K. Kohri and T. Terada, *Semianalytic calculation of gravitational wave spectrum nonlinearly induced from primordial curvature perturbations*, *Phys. Rev. D* **97** (2018), no. 12 123532, [`arXiv:1804.08577`].

[143] G. Domènech, *Scalar Induced Gravitational Waves Review*, *Universe* **7** (2021), no. 11 398, [`arXiv:2109.01398`].

[144] J. Fumagalli, S. Renaux-Petel, and L. T. Witkowski, *Oscillations in the stochastic gravitational wave background from sharp features and particle production during inflation*, *JCAP* **08** (2021) 030, [`arXiv:2012.02761`].

[145] R. Saito and J. Yokoyama, *Gravitational-Wave Constraints on the Abundance of Primordial Black Holes*, *Prog. Theor. Phys.* **123** (2010) 867–886, [`arXiv:0912.5317`]. [Erratum: Prog.Theor.Phys. 126, 351–352 (2011)].

[146] N. Bartolo, V. De Luca, G. Franciolini, A. Lewis, M. Peloso, and A. Riotto, *Primordial Black Hole Dark Matter: LISA Serendipity*, *Phys. Rev. Lett.* **122** (2019), no. 21 211301, [`arXiv:1810.12218`].

[147] S. Pi and M. Sasaki, *Gravitational Waves Induced by Scalar Perturbations with a Lognormal Peak*, *JCAP* **09** (2020) 037, [`arXiv:2005.12306`].

[148] E. Dimastrogiovanni, M. Fasiello, A. Malhotra, and G. Tasinato, *Enhancing gravitational wave anisotropies with peaked scalar sources*, *JCAP* **01** (2023) 018, [`arXiv:2205.05644`].

[149] P. Schneider, J. Ehlers, and E. E. Falco, *Gravitational Lenses.* Springer, 1992.

[150] M. Maggiore, *Gravitational Waves. Vol. 1: Theory and Experiments*. Oxford Master Series in Physics. Oxford University Press, 2007.

[151] R. A. Isaacson, *Gravitational Radiation in the Limit of High Frequency. I. The Linear Approximation and Geometrical Optics, Phys. Rev.* **166** (1968) 1263–1271.

[152] R. A. Isaacson, *Gravitational Radiation in the Limit of High Frequency. II. Nonlinear Terms and the Effective Stress Tensor, Phys. Rev.* **166** (1968) 1272–1279.

[153] A. M. Anile and R. A. Breuer, *Gravitational stokes parameters, The Astrophysical Journal* **189** (1974) 39–50.

[154] S. R. Dolan, *Higher-order geometrical optics for electromagnetic waves on a curved spacetime*, [`arXiv:1801.02273`].

[155] A. I. Harte, *Gravitational lensing beyond geometric optics: I. Formalism and observables, Gen. Rel. Grav.* **51** (2019), no. 1 14, [`arXiv:1808.06203`].

[156] F. Schmidt and D. Jeong, *Cosmic Rulers, Phys. Rev. D* **86** (2012) 083527, [`arXiv:1204.3625`].

[157] D. Bertacca, A. Raccanelli, N. Bartolo, and S. Matarrese, *Cosmological perturbation effects on gravitational-wave luminosity distance estimates, Phys. Dark Univ.* **20** (2018) 32–40, [`arXiv:1702.01750`].

[158] A. Garoffolo, G. Tasinato, C. Carbone, D. Bertacca, and S. Matarrese, *Gravitational waves and geometrical optics in scalar-tensor theories, JCAP* **11** (2020) 040, [`arXiv:1912.08093`].

[159] C. R. Contaldi, *Anisotropies of Gravitational Wave Backgrounds: A Line Of Sight Approach, Phys. Lett. B* **771** (2017) 9–12, [`arXiv:1609.08168`].

[160] C. W. Misner, K. S. Thorne, and J. A. Wheeler, *Gravitation*. W. H. Freeman, San Francisco, 1973.

[161] M. Lagos, M. Fishbach, P. Landry, and D. E. Holz, *Standard sirens with a running Planck mass, Phys. Rev.* **D99** (2019), no. 8 083504, [`arXiv:1901.03321`].

[162] T. T. Nakamura and S. Deguchi, *Wave optics in gravitational lensing, Progress of Theoretical Physics Supplement* **133** (1999) 137–153.

[163] Y. Nambu, *Wave Optics and Image Formation in Gravitational Lensing, J. Phys. Conf. Ser.* **410** (2013) 012036, [`arXiv:1207.6846`].

[164] R. Takahashi and T. Nakamura, *Wave effects in gravitational lensing of gravitational waves from chirping binaries, Astrophys. J.* **595** (2003) 1039–1051, [`astro-ph/0305055`].

[165] R. Takahashi, T. Suyama, and S. Michikoshi, *Scattering of gravitational waves by the weak gravitational fields of lens objects, Astron. Astrophys.* **438** (2005) L5, [`astro-ph/0503343`].

[166] M. Oguri and R. Takahashi, *Amplitude and phase fluctuations of gravitational waves magnified by strong gravitational lensing, Phys. Rev. D* **106** (2022), no. 4 043532, [`arXiv:2204.00814`].

[167] K. Yamamoto, *Path integral formulation for wave effect in multi-lens system*, [`astro-ph/0309696`].

[168] J. Feldbrugge and N. Turok, *Gravitational lensing of binary systems in wave optics*, [`arXiv:2008.01154`].

[169] R. Takahashi, *Amplitude and phase fluctuations for gravitational waves propagating through inhomogeneous mass distribution in the universe, Astrophys. J.* **644** (2006) 80–85, [`astro-ph/0511517`].

[170] J. M. Diego, O. A. Hannuksela, P. L. Kelly, T. Broadhurst, K. Kim, T. G. F. Li, G. F. Smoot, and G. Pagano, *Observational signatures of microlensing in gravitational waves at LIGO/Virgo frequencies, Astron. Astrophys.* **627** (2019) A130, [`arXiv:1903.04513`].

[171] A. K. Meena and J. S. Bagla, *Gravitational lensing of gravitational waves: wave nature and prospects for detection, Mon. Not. Roy. Astron. Soc.* **492** (2020), no. 1 1127–1134, [`arXiv:1903.11809`].

[172] K.-H. Lai, O. A. Hannuksela, A. Herrera-Martín, J. M. Diego, T. Broadhurst, and T. G. F. Li, *Discovering intermediate-mass black hole lenses through gravitational wave lensing, Phys. Rev. D* **98** (2018), no. 8 083005, [`arXiv:1801.07840`].

[173] S. Jung and C. S. Shin, *Gravitational-Wave Fringes at LIGO: Detecting Compact Dark Matter by Gravitational Lensing, Phys. Rev. Lett.* **122** (2019), no. 4 041103, [`arXiv:1712.01396`].

[174] X. Guo and Y. Lu, *Probing the nature of dark matter via gravitational waves lensed by small dark matter halos, Phys. Rev. D* **106** (2022), no. 2 023018, [`arXiv:2207.00325`].

[175] M. Oguri and R. Takahashi, *Probing Dark Low-mass Halos and Primordial Black Holes with Frequency-dependent Gravitational Lensing Dispersions of Gravitational Waves, Astrophys. J.* **901** (2020), no. 1 58, [`arXiv:2007.01936`].

[176] Z. Gao, X. Chen, Y.-M. Hu, J.-D. Zhang, and S.-J. Huang, *A higher probability of detecting lensed supermassive black hole binaries by LISA, Mon. Not. Roy. Astron. Soc.* **512** (2022), no. 1 1–10, [arXiv:2102.10295].

[177] **LISA Cosmology Working Group** Collaboration, P. Auclair et al., *Cosmology with the Laser Interferometer Space Antenna*, [arXiv:2204.05434].

[178] L. Dai, S.-S. Li, B. Zackay, S. Mao, and Y. Lu, *Detecting Lensing-Induced Diffraction in Astrophysical Gravitational Waves, Phys. Rev. D* **98** (2018), no. 10 104029, [arXiv:1810.00003].

[179] T. T. Nakamura, *Gravitational lensing of gravitational waves from inspiraling binaries by a point mass lens, Phys. Rev. Lett.* **80** (1998) 1138–1141.

[180] M. Çalışkan, L. Ji, R. Cotesta, E. Berti, M. Kamionkowski, and S. Marsat, *Observability of lensing of gravitational waves from massive black hole binaries with LISA*, [arXiv:2206.02803].

[181] G. Tambalo, M. Zumalacárregui, L. Dai, and M. H.-Y. Cheung, *Gravitational wave lensing as a probe of halo properties and dark matter*, [arXiv:2212.11960].

[182] C. Dalang, P. Fleury, and L. Lombriser, *Scalar and tensor gravitational waves, Phys. Rev. D* **103** (2021), no. 6 064075, [arXiv:2009.11827].

[183] E. Belgacem, Y. Dirian, S. Foffa, and M. Maggiore, *Gravitational-wave luminosity distance in modified gravity theories, Phys. Rev.* **D97** (2018), no. 10 104066, [arXiv:1712.08108].

[184] E. Belgacem, Y. Dirian, S. Foffa, and M. Maggiore, *Modified gravitational-wave propagation and standard sirens, Phys. Rev. D* **98** (2018), no. 2 023510, [arXiv:1805.08731].

[185] S. Mukherjee, B. D. Wandelt, and J. Silk, *Testing the general theory of relativity using gravitational wave propagation from dark standard sirens, Mon. Not. Roy. Astron. Soc.* **502** (2021), no. 1 1136–1144, [arXiv:2012.15316].

[186] T. Baker and I. Harrison, *Constraining Scalar-Tensor Modified Gravity with Gravitational Waves and Large Scale Structure Surveys, JCAP* **01** (2021) 068, [arXiv:2007.13791].

[187] K. Leyde, S. Mastrogiovanni, D. A. Steer, E. Chassande-Mottin, and C. Karathanasis, *Current and future constraints on cosmology and modified gravitational wave friction from binary black holes, JCAP* **09** (2022) 012, [arXiv:2202.00025].

[188] A. Finke, S. Foffa, F. Iacovelli, M. Maggiore, and M. Mancarella, *Cosmology with LIGO/Virgo dark sirens: Hubble parameter and modified gravitational wave propagation*, JCAP **08** (2021) 026, [`arXiv:2101.12660`].

[189] A. Finke, S. Foffa, F. Iacovelli, M. Maggiore, and M. Mancarella, *Modified gravitational wave propagation and the binary neutron star mass function*, Phys. Dark Univ. **36** (2022) 100994, [`arXiv:2108.04065`].

[190] A. Finke, S. Foffa, F. Iacovelli, M. Maggiore, and M. Mancarella, *Probing modified gravitational wave propagation with strongly lensed coalescing binaries*, Phys. Rev. D **104** (2021), no. 8 084057, [`arXiv:2107.05046`].

[191] L. Amendola, I. Sawicki, M. Kunz, and I. D. Saltas, *Direct detection of gravitational waves can measure the time variation of the Planck mass*, JCAP **08** (2018) 030, [`arXiv:1712.08623`].

[192] R. D'Agostino and R. C. Nunes, *Probing observational bounds on scalar-tensor theories from standard sirens*, Phys. Rev. **D100** (2019), no. 4 044041, [`arXiv:1907.05516`].

[193] M. Mancarella, A. Finke, S. Foffa, E. Genoud-Prachex, F. Iacovelli, and M. Maggiore, *Cosmology and modified gravity with dark sirens from GWTC-3*, in *56th Rencontres de Moriond on Gravitation*, 3, 2022. `arXiv:2203.09238`.

[194] M. Mancarella, E. Genoud-Prachex, and M. Maggiore, *Cosmology and modified gravitational wave propagation from binary black hole population models*, Phys. Rev. D **105** (2022), no. 6 064030, [`arXiv:2112.05728`].

[195] E. Belgacem, Y. Dirian, S. Foffa, E. J. Howell, M. Maggiore, and T. Regimbau, *Cosmology and dark energy from joint gravitational wave-GRB observations*, JCAP **08** (2019) 015, [`arXiv:1907.01487`].

[196] F. Iacovelli, A. Finke, S. Foffa, M. Maggiore, and M. Mancarella, *Modified gravitational wave propagation: information from strongly lensed binaries and the BNS mass function*, in *56th Rencontres de Moriond on Gravitation*, 3, 2022. `arXiv:2203.09237`.

[197] B. F. Schutz, *Determining the Hubble Constant from Gravitational Wave Observations*, Nature **323** (1986) 310–311.

[198] N. Dalal, D. E. Holz, S. A. Hughes, and B. Jain, *Short GRB and binary black hole standard sirens as a probe of dark energy*, Phys. Rev. D **74** (2006) 063006, [`astro-ph/0601275`].

[199] N. Tamanini, C. Caprini, E. Barausse, A. Sesana, A. Klein, and A. Petiteau, *Science with the space-based interferometer eLISA. III: Probing the expansion*

of the Universe using gravitational wave standard sirens, JCAP **04** (2016) 002, [arXiv:1601.07112].

[200] H.-Y. Chen, M. Fishbach, and D. E. Holz, *A two per cent Hubble constant measurement from standard sirens within five years, Nature* **562** (2018), no. 7728 545–547, [arXiv:1712.06531].

[201] S. Mukherjee, A. Krolewski, B. D. Wandelt, and J. Silk, *Cross-correlating dark sirens and galaxies: measurement of H_0 from GWTC-3 of LIGO-Virgo-KAGRA,* [arXiv:2203.03643].

[202] **DES, LIGO Scientific, Virgo** Collaboration, M. Soares-Santos et al., *First Measurement of the Hubble Constant from a Dark Standard Siren using the Dark Energy Survey Galaxies and the LIGO/Virgo Binary–Black-hole Merger GW170814, Astrophys. J.* **876** (2019), no. 1 L7, [arXiv:1901.01540].

[203] S. M. Feeney, H. V. Peiris, A. R. Williamson, S. M. Nissanke, D. J. Mortlock, J. Alsing, and D. Scolnic, *Prospects for resolving the Hubble constant tension with standard sirens, Phys. Rev. Lett.* **122** (2019), no. 6 061105, [arXiv:1802.03404].

[204] S. Nissanke, D. E. Holz, S. A. Hughes, N. Dalal, and J. L. Sievers, *Exploring short gamma-ray bursts as gravitational-wave standard sirens, Astrophys. J.* **725** (2010) 496–514, [arXiv:0904.1017].

[205] **LIGO Scientific, Virgo, 1M2H, Dark Energy Camera GW-E, DES, DLT40, Las Cumbres Observatory, VINROUGE, MASTER** Collaboration, B. P. Abbott et al., *A gravitational-wave standard siren measurement of the Hubble constant, Nature* **551** (2017), no. 7678 85–88, [arXiv:1710.05835].

[206] S. R. Taylor and J. R. Gair, *Cosmology with the lights off: standard sirens in the Einstein Telescope era, Phys. Rev. D* **86** (2012) 023502, [arXiv:1204.6739].

[207] S. Mukherjee, B. D. Wandelt, S. M. Nissanke, and A. Silvestri, *Accurate precision Cosmology with redshift unknown gravitational wave sources, Phys. Rev. D* **103** (2021), no. 4 043520, [arXiv:2007.02943].

[208] M. Oguri, *Measuring the distance-redshift relation with the cross-correlation of gravitational wave standard sirens and galaxies, Phys. Rev. D* **93** (2016), no. 8 083511, [arXiv:1603.02356].

[209] J. R. Gair et al., *The Hitchhiker's guide to the galaxy catalog approach for gravitational wave cosmology,* [arXiv:2212.08694].

[210] M. Mancarella, N. Borghi, S. Foffa, E. Genoud-Prachex, F. Iacovelli, M. Maggiore, M. Moresco, and M. Schulz, *Gravitational-wave cosmology with*

dark sirens: state of the art and perspectives for 3G detectors, PoS **ICHEP2022** (11, 2022) 127, [`arXiv:2211.15512`].

[211] J. M. Ezquiaga and M. Zumalacárregui, *Dark Energy in light of Multi-Messenger Gravitational-Wave astronomy, Front. Astron. Space Sci.* **5** (2018) 44, [`arXiv:1807.09241`].

[212] M. Sasaki, *The Magnitude - Redshift relation in a perturbed Friedmann universe, Mon. Not. Roy. Astron. Soc.* **228** (1987) 653–669.

[213] T. Pyne and M. Birkinshaw, *The luminosity distance in perturbed flrw spacetimes, Mon. Not. Roy. Astron. Soc.* **348** (2004) 581, [`astro-ph/0310841`].

[214] D. E. Holz and E. V. Linder, *Safety in numbers: Gravitational lensing degradation of the luminosity distance-redshift relation, Astrophys. J.* **631** (2005) 678–688, [`astro-ph/0412173`].

[215] L. Hui and P. B. Greene, *Correlated Fluctuations in Luminosity Distance and the (Surprising) Importance of Peculiar Motion in Supernova Surveys, Phys. Rev.* **D73** (2006) 123526, [`astro-ph/0512159`].

[216] C. Bonvin, R. Durrer, and M. A. Gasparini, *Fluctuations of the luminosity distance, Phys. Rev.* **D73** (2006) 023523, [`astro-ph/0511183`]. [Erratum: Phys. Rev.D85,029901(2012)].

[217] P. Laguna, S. L. Larson, D. Spergel, and N. Yunes, *Integrated Sachs-Wolfe Effect for Gravitational Radiation, Astrophys. J. Lett.* **715** (2010) L12, [`arXiv:0905.1908`].

[218] B. Kocsis, Z. Frei, Z. Haiman, and K. Menou, *Finding the electromagnetic counterparts of cosmological standard sirens, Astrophys. J.* **637** (2006) 27–37, [`astro-ph/0505394`].

[219] C. Bonvin, C. Caprini, R. Sturani, and N. Tamanini, *Effect of matter structure on the gravitational waveform, Phys. Rev.* **D95** (2017), no. 4 044029, [`arXiv:1609.08093`].

[220] C. M. Hirata, D. E. Holz, and C. Cutler, *Reducing the weak lensing noise for the gravitational wave Hubble diagram using the non-Gaussianity of the magnification distribution, Phys. Rev.* **D81** (2010) 124046, [`arXiv:1004.3988`].

[221] L. Dai, T. Venumadhav, and K. Sigurdson, *Effect of lensing magnification on the apparent distribution of black hole mergers, Phys. Rev.* **D95** (2017), no. 4 044011, [`arXiv:1605.09398`].

[222] S. Mukherjee, B. D. Wandelt, and J. Silk, *Multimessenger tests of gravity with weakly lensed gravitational waves*, Phys. Rev. **D101** (2020), no. 10 103509, [arXiv:1908.08950].

[223] S. Mukherjee, B. D. Wandelt, and J. Silk, *Probing the theory of gravity with gravitational lensing of gravitational waves and galaxy surveys*, Mon. Not. Roy. Astron. Soc. **494** (2020), no. 2 1956–1970, [arXiv:1908.08951].

[224] S. Mukherjee, G. Lavaux, F. R. Bouchet, J. Jasche, B. D. Wandelt, S. M. Nissanke, F. Leclercq, and K. Hotokezaka, *Velocity correction for Hubble constant measurements from standard sirens*, Astron. Astrophys. **646** (2021) A65, [arXiv:1909.08627].

[225] D. E. Holz and S. A. Hughes, *Using gravitational-wave standard sirens*, Astrophys. J. **629** (2005) 15–22, [astro-ph/0504616].

[226] C. Shapiro, D. Bacon, M. Hendry, and B. Hoyle, *Delensing Gravitational Wave Standard Sirens with Shear and Flexion Maps*, Mon. Not. Roy. Astron. Soc. **404** (2010) 858–866, [arXiv:0907.3635].

[227] D. Jeong, F. Schmidt, and C. M. Hirata, *Large-scale clustering of galaxies in general relativity*, "Phys. Rev. D" **85** (Jan., 2012) 023504, [arXiv:1107.5427].

[228] D. Jeong and F. Schmidt, *Large-Scale Structure Observables in General Relativity*, Class. Quant. Grav. **32** (2015), no. 4 044001, [arXiv:1407.7979].

[229] J. Yoo, A. L. Fitzpatrick, and M. Zaldarriaga, *New perspective on galaxy clustering as a cosmological probe: General relativistic effects*, "Phys. Rev. D" **80** (Oct., 2009) 083514, [arXiv:0907.0707].

[230] C. Bonvin and R. Durrer, *What galaxy surveys really measure*, Phys. Rev. D **84** (2011) 063505, [arXiv:1105.5280].

[231] A. Lewis and A. Challinor, *Weak gravitational lensing of the CMB*, Phys. Rept. **429** (2006) 1–65, [astro-ph/0601594].

[232] C. D. Leonard, T. Baker, and P. G. Ferreira, *Exploring degeneracies in modified gravity with weak lensing*, Phys. Rev. D **91** (2015), no. 8 083504, [arXiv:1501.03509].

[233] J. Espejo, S. Peirone, M. Raveri, K. Koyama, L. Pogosian, and A. Silvestri, *Phenomenology of Large Scale Structure in scalar-tensor theories: joint prior covariance of w_{DE}, Σ and μ in Horndeski*, Phys. Rev. D **99** (2019), no. 2 023512, [arXiv:1809.01121].

[234] C. Cutler and D. E. Holz, *Ultra-high precision cosmology from gravitational waves*, Phys. Rev. **D80** (2009) 104009, [arXiv:0906.3752].

[235] C. Dalang, P. Fleury, and L. Lombriser, *Horndeski gravity and standard sirens*, *Phys. Rev. D* **102** (2020), no. 4 044036, [`arXiv:1912.06117`].

[236] E. Babichev and C. Deffayet, *An introduction to the Vainshtein mechanism*, *Class. Quant. Grav.* **30** (2013) 184001, [`arXiv:1304.7240`].

[237] C. Burrage and J. Sakstein, *Tests of Chameleon Gravity*, *Living Rev. Rel.* **21** (2018), no. 1 1, [`arXiv:1709.09071`].

[238] Y.-S. Song, W. Hu, and I. Sawicki, *The Large Scale Structure of f(R) Gravity*, *Phys. Rev. D* **75** (2007) 044004, [`astro-ph/0610532`].

[239] S. Peirone, M. Raveri, M. Viel, S. Borgani, and S. Ansoldi, *Constraining f(R) Gravity with Planck Sunyaev-Zel'dovich Clusters*, *Phys. Rev. D* **95** (2017), no. 2 023521, [`arXiv:1607.07863`].

[240] A. De Felice and S. Tsujikawa, *Generalized Brans-Dicke theories*, *JCAP* **07** (2010) 024, [`arXiv:1005.0868`].

[241] F. Perrotta, C. Baccigalupi, and S. Matarrese, *Extended quintessence*, *Phys. Rev. D* **61** (1999) 023507, [`astro-ph/9906066`].

[242] C. Baccigalupi, S. Matarrese, and F. Perrotta, *Tracking extended quintessence*, *Phys. Rev. D* **62** (2000) 123510, [`astro-ph/0005543`].

[243] A. R. Cooray, D. E. Holz, and R. Caldwell, *Measuring dark energy spatial inhomogeneity with supernova data*, *JCAP* **11** (2010) 015, [`arXiv:0812.0376`].

[244] F. Calore, A. Cuoco, T. Regimbau, S. Sachdev, and P. D. Serpico, *Cross-correlating galaxy catalogs and gravitational waves: a tomographic approach*, *Phys. Rev. Res.* **2** (2020), no. 2 2, [`arXiv:2002.02466`].

[245] J. Baker et al., *High angular resolution gravitational wave astronomy*, *Exper. Astron.* **51** (2021), no. 3 1441–1470, [`arXiv:1908.11410`].

[246] R. Hounsell et al., *Simulations of the WFIRST Supernova Survey and Forecasts of Cosmological Constraints*, *Astrophys. J.* **867** (2018), no. 1 23, [`arXiv:1702.01747`].

[247] C. L. MacLeod and C. J. Hogan, *Precision of Hubble constant derived using black hole binary absolute distances and statistical redshift information*, *Phys. Rev. D* **77** (2008) 043512, [`arXiv:0712.0618`].

[248] W. Del Pozzo, *Inference of the cosmological parameters from gravitational waves: application to second generation interferometers*, *Phys. Rev. D* **86** (2012) 043011, [`arXiv:1108.1317`].

[249] **LISA Cosmology Working Group** Collaboration, E. Belgacem et al., *Testing modified gravity at cosmological distances with LISA standard sirens*, JCAP **07** (2019) 024, [arXiv:1906.01593].

[250] **LSST Science, LSST Project** Collaboration, P. A. Abell et al., *LSST Science Book, Version 2.0*, [arXiv:0912.0201].

[251] G. M. Harry, P. Fritschel, D. A. Shaddock, W. Folkner, and E. S. Phinney, *Laser interferometry for the big bang observer*, *Class. Quant. Grav.* **23** (2006) 4887–4894. [Erratum: Class.Quant.Grav. 23, 7361 (2006)].

[252] S. Kawamura et al., *The Japanese space gravitational wave antenna: DECIGO*, *Class. Quant. Grav.* **28** (2011) 094011.

[253] L. McNeill, R. A. Mardling, and B. Müller, *Gravitational waves from dynamical tides in white dwarf binaries*, *Mon. Not. Roy. Astron. Soc.* **491** (2020), no. 2 3000–3012, [arXiv:1901.09045].

[254] A. Maselli, S. Marassi, and M. Branchesi, *Binary white dwarfs and decihertz gravitational wave observations: From the Hubble constant to supernova astrophysics*, *Astron. Astrophys.* **635** (2020) A120, [arXiv:1910.00016].

[255] T. Kinugawa, H. Takeda, A. Tanikawa, and H. Yamaguchi, *Probe for Type Ia Supernova Progenitor in Decihertz Gravitational Wave Astronomy*, *Astrophys. J.* **938** (2022), no. 1 52, [arXiv:1910.01063].

[256] D. Maoz and F. Mannucci, *Type-Ia supernova rates and the progenitor problem, a review*, *Publ. Astron. Soc. Austral.* **29** (2012) 447, [arXiv:1111.4492].

[257] A. Gupta, D. Fox, B. S. Sathyaprakash, and B. F. Schutz, *Calibrating the cosmic distance ladder using gravitational-wave observations*, [arXiv:1907.09897].

[258] **LIGO Scientific, Virgo** Collaboration, B. P. Abbott et al., *GWTC-1: A Gravitational-Wave Transient Catalog of Compact Binary Mergers Observed by LIGO and Virgo during the First and Second Observing Runs*, *Phys. Rev. X* **9** (2019), no. 3 031040, [arXiv:1811.12907].

[259] **LIGO Scientific, Virgo** Collaboration, R. Abbott et al., *GWTC-2: Compact Binary Coalescences Observed by LIGO and Virgo During the First Half of the Third Observing Run*, *Phys. Rev. X* **11** (2021) 021053, [arXiv:2010.14527].

[260] **KAGRA** Collaboration, T. Akutsu et al., *Overview of KAGRA : KAGRA science*, [arXiv:2008.02921].

[261] C. M. Hirata, D. E. Holz, and C. Cutler, *Reducing the weak lensing noise for the gravitational wave Hubble diagram using the non-Gaussianity of the magnification distribution*, *Phys. Rev. D* **81** (6, 2010) 124046, [arXiv:1004.3988].

[262] S. Camera and A. Nishizawa, *Beyond Concordance Cosmology with Magnification of Gravitational-Wave Standard Sirens, Phys. Rev. Lett.* **110** (2013), no. 15 151103, [`arXiv:1303.5446`].

[263] S. Libanore, M. C. Artale, D. Karagiannis, M. Liguori, N. Bartolo, Y. Bouffanais, M. Mapelli, and S. Matarrese, *Clustering of Gravitational Wave and Supernovae events: a multitracer analysis in Luminosity Distance Space, JCAP* **02** (2022), no. 02 003, [`arXiv:2109.10857`].

[264] G. Scelfo, M. Spinelli, A. Raccanelli, L. Boco, A. Lapi, and M. Viel, *Gravitational waves × HI intensity mapping: cosmological and astrophysical applications, JCAP* **01** (2022), no. 01 004, [`arXiv:2106.09786`].

[265] G. Scelfo, M. Berti, A. Silvestri, and M. Viel, *Testing gravity with gravitational waves × electromagnetic probes cross-correlations*, [`arXiv:2210.02460`].

[266] G. Congedo and A. Taylor, *Joint cosmological inference of standard sirens and gravitational wave weak lensing, Phys. Rev. D* **99** (2019), no. 8 083526, [`arXiv:1812.02730`].

[267] C. T. Mpetha, G. Congedo, and A. Taylor, *Future prospects on testing extensions to ΛCDM through the weak lensing of gravitational waves*, [`arXiv:2208.05959`].

[268] W. M. Farr, M. Fishbach, J. Ye, and D. Holz, *A Future Percent-Level Measurement of the Hubble Expansion at Redshift 0.8 With Advanced LIGO, Astrophys. J. Lett.* **883** (2019), no. 2 L42, [`arXiv:1908.09084`].

[269] S. Mastrogiovanni, K. Leyde, C. Karathanasis, E. Chassande-Mottin, D. A. Steer, J. Gair, A. Ghosh, R. Gray, S. Mukherjee, and S. Rinaldi, *On the importance of source population models for gravitational-wave cosmology, "Phys.Rev.D"* **104** (Sept., 2021) 062009, [`arXiv:2103.14663`].

[270] S. Mukherjee, *The redshift dependence of black hole mass distribution: is it reliable for standard sirens cosmology?, Mon. Not. Roy. Astron. Soc.* **515** (2022), no. 4 5495–5505, [`arXiv:2112.10256`].

[271] J. M. Ezquiaga and D. E. Holz, *Spectral Sirens: Cosmology from the Full Mass Distribution of Compact Binaries, Phys. Rev. Lett.* **129** (2022), no. 6 061102, [`arXiv:2202.08240`].

[272] S. Nissanke, D. E. Holz, N. Dalal, S. A. Hughes, J. L. Sievers, and C. M. Hirata, *Determining the Hubble constant from gravitational wave observations of merging compact binaries*, [`arXiv:1307.2638`].

[273] S. Ronchini, M. Branchesi, G. Oganesyan, B. Banerjee, U. Dupletsa, G. Ghirlanda, J. Harms, M. Mapelli, and F. Santoliquido, *Perspectives for multi-messenger astronomy with the next generation of gravitational-wave detectors and high-energy satellites*, Astron. Astrophys. **665** (2022) A97, [arXiv:2204.01746].

[274] S. Vitale and H.-Y. Chen, *Measuring the Hubble constant with neutron star black hole mergers*, Phys. Rev. Lett. **121** (2018), no. 2 021303, [arXiv:1804.07337].

[275] S. M. Feeney, H. V. Peiris, S. M. Nissanke, and D. J. Mortlock, *Prospects for Measuring the Hubble Constant with Neutron-Star–Black-Hole Mergers*, Phys. Rev. Lett. **126** (2021), no. 17 171102, [arXiv:2012.06593].

[276] A. Caputo, L. Sberna, A. Toubiana, S. Babak, E. Barausse, S. Marsat, and P. Pani, *Gravitational-wave detection and parameter estimation for accreting black-hole binaries and their electromagnetic counterpart*, Astrophys. J. **892** (2020), no. 2 90, [arXiv:2001.03620].

[277] N. Tamanini, *Late time cosmology with LISA: probing the cosmic expansion with massive black hole binary mergers as standard sirens*, J. Phys. Conf. Ser. **840** (2017), no. 1 012029, [arXiv:1612.02634].

[278] F. Cattorini, B. Giacomazzo, F. Haardt, and M. Colpi, *Fully General Relativistic Magnetohydrodynamic Simulations of Accretion Flows onto Spinning Massive Black Hole Binary Mergers*, Phys. Rev. D **103** (2021), no. 10 103022, [arXiv:2102.13166].

[279] S. D'Ascoli, S. C. Noble, D. B. Bowen, M. Campanelli, J. H. Krolik, and V. Mewes, *Electromagnetic Emission from Supermassive Binary Black Holes Approaching Merger*, Astrophys. J. **865** (2018), no. 2 140, [arXiv:1806.05697].

[280] D. Bertacca, A. Raccanelli, N. Bartolo, and S. Matarrese, *Cosmological perturbation effects on gravitational-wave luminosity distance estimates*, Phys. Dark Univ. **20** (2018) 32–40.

[281] A. Garoffolo, M. Raveri, A. Silvestri, G. Tasinato, C. Carbone, D. Bertacca, and S. Matarrese, *Detecting Dark Energy Fluctuations with Gravitational Waves*, Phys. Rev. D **103** (2021), no. 8 083506, [arXiv:2007.13722].

[282] N. Kaiser, *Weak gravitational lensing of distant galaxies*, Astrophys. J. **388** (1992) 272.

[283] M. LoVerde and N. Afshordi, *Extended Limber Approximation*, Phys. Rev. D **78** (2008) 123506, [arXiv:0809.5112].

[284] T. D. Kitching, J. Alsing, A. F. Heavens, R. Jimenez, J. D. McEwen, and L. Verde, *The Limits of Cosmic Shear, Mon. Not. Roy. Astron. Soc.* **469** (2017), no. 3 2737–2749, [`arXiv:1611.04954`].

[285] M. Kilbinger et al., *Precision calculations of the cosmic shear power spectrum projection, Mon. Not. Roy. Astron. Soc.* **472** (2017), no. 2 2126–2141, [`arXiv:1702.05301`].

[286] P. Lemos, A. Challinor, and G. Efstathiou, *The effect of Limber and flat-sky approximations on galaxy weak lensing, JCAP* **05** (2017) 014, [`arXiv:1704.01054`].

[287] W. L. Matthewson and R. Durrer, *The Flat Sky Approximation to Galaxy Number Counts, JCAP* **02** (2021) 027, [`arXiv:2006.13525`].

[288] **Euclid** Collaboration, A. Blanchard et al., *Euclid preparation: VII. Forecast validation for Euclid cosmological probes, Astron. Astrophys.* **642** (2020) A191, [`arXiv:1910.09273`].

[289] N. Frusciante, S. Peirone, S. Casas, and N. A. Lima, *Cosmology of surviving Horndeski theory: The road ahead, Phys. Rev. D* **99** (2019), no. 6 063538, [`arXiv:1810.10521`].

[290] C. Deffayet, O. Pujolas, I. Sawicki, and A. Vikman, *Imperfect Dark Energy from Kinetic Gravity Braiding, JCAP* **10** (2010) 026, [`arXiv:1008.0048`].

[291] M. Tegmark, A. Taylor, and A. Heavens, *Karhunen-Loeve eigenvalue problems in cosmology: How should we tackle large data sets?, Astrophys. J.* **480** (1997) 22, [`astro-ph/9603021`].

[292] M. Raveri, M. Martinelli, G. Zhao, and Y. Wang, *Information Gain in Cosmology: From the Discovery of Expansion to Future Surveys*, [`arXiv:1606.06273`].

[293] M. Raveri, M. Martinelli, G. Zhao, and Y. Wang, *CosmicFish Implementation Notes V1.0*, [`arXiv:1606.06268`].

[294] A. Amara and T. Kitching, *Figures of merit for testing standard models: application to dark energy experiments in cosmology, Mon. Not. Roy. Astron. Soc.* **413** (2011), no. 3 1505–1514, [`arXiv:1009.3274`].

[295] M. Pieroni, A. Ricciardone, and E. Barausse, *Detectability and parameter estimation of stellar origin black hole binaries with next generation gravitational wave detectors*, [`arXiv:2203.12586`].

[296] D. W. Hogg, *Distance measures in cosmology*, [`astro-ph/9905116`].

[297] H.-Y. Chen, D. E. Holz, J. Miller, M. Evans, S. Vitale, and J. Creighton, *Distance measures in gravitational-wave astrophysics and cosmology, Class. Quant. Grav.* **38** (2021), no. 5 055010, [arXiv:1709.08079].

[298] M. Oguri, *Strong gravitational lensing of explosive transients, Rept. Prog. Phys.* **82** (2019), no. 12 126901, [arXiv:1907.06830].

[299] D. M. Eardley, D. L. Lee, A. P. Lightman, R. V. Wagoner, and C. M. Will, *Gravitational-wave observations as a tool for testing relativistic gravity, Phys. Rev. Lett.* **30** (1973) 884–886.

[300] D. M. Eardley, D. L. Lee, and A. P. Lightman, *Gravitational-wave observations as a tool for testing relativistic gravity, Phys. Rev. D* **8** (1973) 3308–3321.

[301] J. M. Ezquiaga and M. Zumalacárregui, *Gravitational wave lensing beyond general relativity: birefringence, echoes and shadows, Phys. Rev. D* **102** (2020), no. 12 124048, [arXiv:2009.12187].

[302] **LIGO Scientific, Virgo** Collaboration, B. P. Abbott et al., *Properties of the binary neutron star merger GW170817, Phys. Rev. X* **9** (2019), no. 1 011001, [arXiv:1805.11579].

[303] I. Sawicki, I. D. Saltas, M. Motta, L. Amendola, and M. Kunz, *Nonstandard gravitational waves imply gravitational slip: On the difficulty of partially hiding new gravitational degrees of freedom, Phys. Rev.* **D95** (2017), no. 8 083520, [arXiv:1612.02002].

[304] S. Arai and A. Nishizawa, *Generalized framework for testing gravity with gravitational-wave propagation. II. Constraints on Horndeski theory, Phys. Rev.* **D97** (2018), no. 10 104038, [arXiv:1711.03776].

[305] A. Vijaykumar, S. J. Kapadia, and P. Ajith, *Constraints on the time variation of the gravitational constant using gravitational wave observations of binary neutron stars*, [arXiv:2003.12832].

[306] S. Mastrogiovanni, L. Haegel, C. Karathanasis, I. M. n. Hernandez, and D. A. Steer, *Gravitational wave friction in light of GW170817 and GW190521, JCAP* **02** (2021) 043, [arXiv:2010.04047].

[307] S. Mastrogiovanni, D. Steer, and M. Barsuglia, *Probing modified gravity theories and cosmology using gravitational-waves and associated electromagnetic counterparts, Phys. Rev.* **D102** (2020), no. 4 044009, [arXiv:2004.01632].

[308] A. Nishizawa and S. Arai, *Generalized framework for testing gravity with gravitational-wave propagation. III. Future prospect, Phys. Rev.* **D99** (2019), no. 10 104038, [arXiv:1901.08249].

[309] J. Fier, X. Fang, B. Li, S. Mukohyama, A. Wang, and T. Zhu, *Gravitational wave cosmology: High frequency approximation, Phys. Rev. D* **103** (2021), no. 12 123021, [arXiv:2102.08968].

[310] I. Etherington, *Republication of: LX. On the definition of distance in general relativity, Gen. Relativ. Gravit.* **39** (2007) 1055.

[311] G. Ellis, *On the definition of distance in general relativity: I. m. h. etherington (philosophical magazine ser. 7, vol. 15, 761 (1933)), General Relativity and Gravitation* **39** (07, 2007) 1047–1052.

[312] M. Martinelli, C. J. A. P. Martins, S. Nesseris, D. Sapone, I. Tutusaus, A. Avgoustidis, S. Camera, C. Carbone, S. Casas, S. Ilić, Z. Sakr, V. Yankelevich, N. Auricchio, A. Balestra, C. Bodendorf, D. Bonino, E. Branchini, M. Brescia, J. Brinchmann, V. Capobianco, J. Carretero, M. Castellano, S. Cavuoti, R. Cledassou, G. Congedo, L. Conversi, L. Corcione, F. Dubath, A. Ealet, M. Frailis, E. Franceschi, M. Fumana, B. Garilli, B. Gillis, C. Giocoli, F. Grupp, S. V. H. Haugan, W. Holmes, F. Hormuth, K. Jahnke, S. Kermiche, M. Kilbinger, T. D. Kitching, B. Kubik, M. Kunz, H. Kurki-Suonio, S. Ligori, P. B. Lilje, I. Lloro, O. Marggraf, K. Markovic, R. Massey, S. Mei, M. Meneghetti, G. Meylan, L. Moscardini, S. Niemi, C. Padilla, S. Paltani, F. Pasian, V. Pettorino, S. Pires, G. Polenta, M. Poncet, L. Popa, L. Pozzetti, F. Raison, J. Rhodes, M. Roncarelli, R. Saglia, P. Schneider, A. Secroun, S. Serrano, C. Sirignano, G. Sirri, F. Sureau, A. N. Taylor, I. Tereno, R. Toledo-Moreo, L. Valenziano, T. Vassallo, Y. Wang, N. Welikala, J. Weller, and A. Zacchei, *Euclid: Forecast constraints on the cosmic distance duality relation with complementary external probes, Astron. Astrophys.* **644** (Dec., 2020) A80, [arXiv:2007.16153].

[313] N. B. Hogg, M. Martinelli, and S. Nesseris, *Constraints on the distance duality relation with standard sirens, JCAP* **12** (2020) 019, [arXiv:2007.14335].

[314] R. F. L. Holanda, J. A. S. Lima, and M. B. Ribeiro, *Testing the Distance-Duality Relation with Galaxy Clusters and Type Ia Supernovae, Astrophys. J. Lett.* **722** (2010) L233–L237, [arXiv:1005.4458].

[315] R. F. L. Holanda, R. S. Gonçalves, and J. S. Alcaniz, *A test for cosmic distance duality, JCAP* **06** (2012) 022, [arXiv:1201.2378].

[316] X. Zheng, K. Liao, M. Biesiada, S. Cao, T.-H. Liu, and Z.-H. Zhu, *Multiple measurements of quasars acing as standard probes: exploring the cosmic distance duality relation at higher redshift,* [arXiv:2002.09909].

[317] F. Renzi and A. Silvestri, *Hubble speed from first principles, Phys. Rev. D* **107** (2023), no. 2 023520, [arXiv:2011.10559].

[318] G. Tasinato, *Symmetries for scalarless scalar theories, Phys. Rev.* **D102** (2020), no. 8 084009, [arXiv:2009.02157].

[319] T. Treu and P. J. Marshall, *Time Delay Cosmography, Astron. Astrophys. Rev.* **24** (2016), no. 1 11, [arXiv:1605.05333].

[320] B. Shiralilou, M. Martinelli, G. Papadomanolakis, S. Peirone, F. Renzi, and A. Silvestri, *Strong Lensing Time Delay Constraints on Dark Energy: a Forecast, JCAP* **04** (2020) 057, [arXiv:1910.03566].

[321] S. H. Suyu, T.-C. Chang, F. Courbin, and T. Okumura, *Cosmological distance indicators, Space Sci. Rev.* **214** (2018), no. 5 91, [arXiv:1801.07262].

[322] M. Oguri, *Effect of gravitational lensing on the distribution of gravitational waves from distant binary black hole mergers, Mon. Not. Roy. Astron. Soc.* **480** (2018), no. 3 3842–3855, [arXiv:1807.02584].

[323] E. L. Turner, *Gravitational lensing limits on the cosmological constant in a flat universe, Astrophys. J. Lett.* **365** (1990) L43.

[324] Y. Wang, A. Stebbins, and E. L. Turner, *Gravitational lensing of gravitational waves from merging neutron star binaries, Phys. Rev. Lett.* **77** (1996) 2875–2878, [astro-ph/9605140].

[325] Y. Wang, *Analytical modeling of the weak lensing of standard candles, Astrophys. J.* **525** (1999) 651, [astro-ph/9901212].

[326] J.-P. Macquart, *Scattering of gravitational radiation: Second order moments of the wave amplitude, Astron. Astrophys.* **422** (2004) 761–775, [astro-ph/0402661].

[327] N. Seto, *Strong gravitational lensing and localization of merging massive black hole binaries with LISA, Phys. Rev.* **D69** (2004) 022002, [astro-ph/0305605].

[328] C.-M. Yoo, K.-i. Nakao, H. Kozaki, and R. Takahashi, *Lensing effects on gravitational waves in a clumpy universe: effects of inhomogeneity on the distance-redshift relation, Astrophys. J.* **655** (2007) 691–703, [astro-ph/0604123].

[329] N. Seto, *Demagnified GWs from Cosmological Double Neutron Stars and GW Foreground Cleaning Around 1Hz, Phys. Rev.* **D80** (2009) 103001, [arXiv:0910.4812].

[330] M. Sereno, A. Sesana, A. Bleuler, P. Jetzer, M. Volonteri, and M. C. Begelman, *Strong lensing of gravitational waves as seen by LISA, Phys. Rev. Lett.* **105** (2010) 251101, [arXiv:1011.5238].

[331] C. Van Den Broeck, M. Trias, B. S. Sathyaprakash, and A. M. Sintes, *Weak lensing effects in the measurement of the dark energy equation of state with LISA, Phys. Rev.* **D81** (2010) 124031, [`arXiv:1001.3099`].

[332] M. Sereno, P. Jetzer, A. Sesana, and M. Volonteri, *Cosmography with strong lensing of LISA gravitational wave sources, Mon. Not. Roy. Astron. Soc.* **415** (2011) 2773, [`arXiv:1104.1977`].

[333] T. Baker and M. Trodden, *Multimessenger time delays from lensed gravitational waves, Phys. Rev.* **D95** (2017), no. 6 063512, [`arXiv:1612.02004`].

[334] K. Kyutoku and N. Seto, *Gravitational-wave cosmography with LISA and the Hubble tension, Phys. Rev. D* **95** (2017), no. 8 083525, [`arXiv:1609.07142`].

[335] T. E. Collett and D. Bacon, *Testing the speed of gravitational waves over cosmological distances with strong gravitational lensing, Phys. Rev. Lett.* **118** (2017), no. 9 091101, [`arXiv:1602.05882`].

[336] L. Dai and T. Venumadhav, *On the waveforms of gravitationally lensed gravitational waves*, [`arXiv:1702.04724`].

[337] K. Haris, A. K. Mehta, S. Kumar, T. Venumadhav, and P. Ajith, *Identifying strongly lensed gravitational wave signals from binary black hole mergers*, [`arXiv:1807.07062`].

[338] S. Hou, X.-L. Fan, K. Liao, and Z.-H. Zhu, *Gravitational Wave Interference via Gravitational Lensing: Measurements of Luminosity Distance, Lens Mass, and Cosmological Parameters, Phys. Rev.* **D101** (2020), no. 6 064011, [`arXiv:1911.02798`].

[339] B. Liu, Z. Li, and Z.-H. Zhu, *Complementary constraints on dark energy equation of state from strongly lensed gravitational wave, Mon. Not. Roy. Astron. Soc.* **487** (2019), no. 2 1980–1985, [`arXiv:1904.11751`].

[340] O. A. Hannuksela, K. Haris, K. K. Y. Ng, S. Kumar, A. K. Mehta, D. Keitel, T. G. F. Li, and P. Ajith, *Search for gravitational lensing signatures in LIGO-Virgo binary black hole events, Astrophys. J. Lett.* **874** (2019), no. 1 L2, [`arXiv:1901.02674`].

[341] T. Morita and J. Soda, *Arrival Time Differences of Lensed Massive Gravitational Waves*, [`arXiv:1911.07435`].

[342] G. Cusin and N. Tamanini, *Characterization of lensing selection effects for LISA massive black hole binary mergers, Mon. Not. Roy. Astron. Soc.* **504** (2021), no. 3 3610–3618, [`arXiv:2011.15109`].

[343] P. T. H. Pang, O. A. Hannuksela, T. Dietrich, G. Pagano, and I. W. Harry, *Lensed or not lensed: Determining lensing magnifications for binary neutron star mergers from a single detection*, [`arXiv:2002.04893`].

[344] D. Rubin, I. Szapudi, B. J. Shappee, and G. S. Anand, *Does Gravity Fall Down? Evidence for Gravitational-wave Deflection along the Line of Sight to GW170817*, Astrophys. J. Lett. **890** (2020), no. 1 L6, [`arXiv:2001.01710`].

[345] J. M. Ezquiaga, D. E. Holz, W. Hu, M. Lagos, and R. M. Wald, *Phase effects from strong gravitational lensing of gravitational waves*, Phys. Rev. D **103** (2021), no. 6 064047, [`arXiv:2008.12814`].

[346] J. M. Ezquiaga, W. Hu, and M. Lagos, *Apparent Superluminality of Lensed Gravitational Waves*, Phys. Rev. D **102** (2020), no. 2 023531, [`arXiv:2005.10702`].

[347] R. Takahashi, *Arrival time differences between gravitational waves and electromagnetic signals due to gravitational lensing*, Astrophys. J. **835** (2017), no. 1 103, [`arXiv:1606.00458`].

[348] T. Suyama, *On arrival time difference between lensed gravitational waves and light*, Astrophys. J. **896** (2020), no. 1 46, [`arXiv:2003.11748`].

[349] O. Contigiani, *Lensing efficiency for gravitational wave mergers*, Mon. Not. Roy. Astron. Soc. **492** (2020), no. 3 3359–3363, [`arXiv:2001.01135`].

[350] F. Renzi, N. B. Hogg, M. Martinelli, and S. Nesseris, *Strongly lensed supernovae as a self-sufficient probe of the distance duality relation*, Phys. Dark Univ. **32** (2021) 100824, [`arXiv:2010.04155`].

[351] R. Arjona, H.-N. Lin, S. Nesseris, and L. Tang, *Machine learning forecasts of the cosmic distance duality relation with strongly lensed gravitational wave events*, Phys. Rev. D **103** (2021), no. 10 103513, [`arXiv:2011.02718`].

[352] **LSST** Collaboration, v. Ivezić et al., *LSST: from Science Drivers to Reference Design and Anticipated Data Products*, Astrophys. J. **873** (2019), no. 2 111, [`arXiv:0805.2366`].

[353] **SKA** Collaboration, D. J. Bacon et al., *Cosmology with Phase 1 of the Square Kilometre Array: Red Book 2018: Technical specifications and performance forecasts*, Publ. Astron. Soc. Austral. **37** (2020) e007, [`arXiv:1811.02743`].

[354] J. K. Bloomfield, E. E. Flanagan, M. Park, and S. Watson, *Dark energy or modified gravity? An effective field theory approach*, JCAP **08** (2013) 010, [`arXiv:1211.7054`].

[355] M. Zumalacárregui, E. Bellini, I. Sawicki, J. Lesgourgues, and P. G. Ferreira, *hi_class: Horndeski in the Cosmic Linear Anisotropy Solving System*, JCAP **08** (2017) 019, [`arXiv:1605.06102`].

[356] R. Bluhm, *Gravity with background fields and diffeomorphism breaking*, in *14th Marcel Grossmann Meeting on Recent Developments in Theoretical and Experimental General Relativity, Astrophysics, and Relativistic Field Theories*, 1, 2016. `arXiv:1601.00331`.

[357] S. Hou, Y. Gong, and Y. Liu, *Polarizations of Gravitational Waves in Horndeski Theory*, Eur. Phys. J. C **78** (2018), no. 5 378, [`arXiv:1704.01899`].

[358] S. Mirshekari, N. Yunes, and C. M. Will, *Constraining Generic Lorentz Violation and the Speed of the Graviton with Gravitational Waves*, Phys. Rev. D **85** (2012) 024041, [`arXiv:1110.2720`].

[359] T. Baker, D. Psaltis, and C. Skordis, *Linking Tests of Gravity On All Scales: from the Strong-Field Regime to Cosmology*, Astrophys. J. **802** (2015) 63, [`arXiv:1412.3455`].

[360] A. Garoffolo and O. Contigiani, *Unifying gravitational waves and dark energy*, [`arXiv:2110.14689`].

[361] P. Brax, A.-C. Davis, B. Li, and H. A. Winther, *A Unified Description of Screened Modified Gravity*, Phys. Rev. D **86** (2012) 044015, [`arXiv:1203.4812`].

[362] P. Brax and P. Valageas, *Impact on the power spectrum of screening in modified gravity scenarios*, "Phys. Rev. D" **88** (July, 2013) 023527, [`arXiv:1305.5647`].

[363] L. Lombriser, F. Simpson, and A. Mead, *Unscreening Modified Gravity in the Matter Power Spectrum*, "Phys. Rev. Lett." **114** (June, 2015) 251101, [`arXiv:1501.04961`].

[364] H. Desmond, P. G. Ferreira, G. Lavaux, and J. Jasche, *Fifth force constraints from the separation of galaxy mass components*, Phys. Rev. D **98** (2018), no. 6 064015, [`arXiv:1807.01482`].

[365] G. Tasinato, A. Garoffolo, D. Bertacca, and S. Matarrese, *Gravitational-wave cosmological distances in scalar-tensor theories of gravity*, JCAP **06** (2021) 050, [`arXiv:2103.00155`].

[366] J. Khoury and A. Weltman, *Chameleon fields: Awaiting surprises for tests of gravity in space*, Phys. Rev. Lett. **93** (2004) 171104, [`astro-ph/0309300`].

[367] T. Katsuragawa, T. Nakamura, T. Ikeda, and S. Capozziello, *Gravitational Waves in $F(R)$ Gravity: Scalar Waves and the Chameleon Mechanism*, Phys. Rev. D **99** (2019), no. 12 124050, [`arXiv:1902.02494`].

[368] J. Khoury and A. Weltman, *Chameleon cosmology*, *Phys. Rev. D* **69** (2004) 044026, [`astro-ph/0309411`].

[369] K. Hinterbichler, J. Khoury, A. Levy, and A. Matas, *Symmetron Cosmology*, *Phys. Rev. D* **84** (2011) 103521, [`arXiv:1107.2112`].

[370] T. Regimbau, *The astrophysical gravitational wave stochastic background*, *Res. Astron. Astrophys.* **11** (2011) 369–390, [`arXiv:1101.2762`].

[371] A. I. Renzini, B. Goncharov, A. C. Jenkins, and P. M. Meyers, *Stochastic Gravitational-Wave Backgrounds: Current Detection Efforts and Future Prospects*, *Galaxies* **10** (2022), no. 1 34, [`arXiv:2202.00178`].

[372] A. J. Farmer and E. S. Phinney, *The gravitational wave background from cosmological compact binaries*, *Mon. Not. Roy. Astron. Soc.* **346** (2003) 1197, [`astro-ph/0304393`].

[373] P. Amaro-Seoane et al., *Astrophysics with the Laser Interferometer Space Antenna*, [`arXiv:2203.06016`].

[374] K. Crocker, V. Mandic, T. Regimbau, K. Belczynski, W. Gladysz, K. Olive, T. Prestegard, and E. Vangioni, *Model of the stochastic gravitational-wave background due to core collapse to black holes*, *Phys. Rev. D* **92** (2015), no. 6 063005, [`arXiv:1506.02631`].

[375] B. Allen and A. C. Ottewill, *Detection of anisotropies in the gravitational wave stochastic background*, *Phys. Rev. D* **56** (1997) 545–563, [`gr-qc/9607068`].

[376] S. R. Taylor and J. R. Gair, *Searching For Anisotropic Gravitational-wave Backgrounds Using Pulsar Timing Arrays*, *Phys. Rev. D* **88** (2013) 084001, [`arXiv:1306.5395`].

[377] **LIGO Scientific, Virgo** Collaboration, B. P. Abbott et al., *GW150914: Implications for the stochastic gravitational wave background from binary black holes*, *Phys. Rev. Lett.* **116** (2016), no. 13 131102, [`arXiv:1602.03847`].

[378] **KAGRA, Virgo, LIGO Scientific** Collaboration, R. Abbott et al., *Search for anisotropic gravitational-wave backgrounds using data from Advanced LIGO and Advanced Virgo's first three observing runs*, *Phys. Rev. D* **104** (2021), no. 2 022005, [`arXiv:2103.08520`].

[379] **NANOGrav** Collaboration, Z. Arzoumanian et al., *The NANOGrav 12.5 yr Data Set: Search for an Isotropic Stochastic Gravitational-wave Background*, *Astrophys. J. Lett.* **905** (2020), no. 2 L34, [`arXiv:2009.04496`].

[380] J. D. Romano and N. J. Cornish, *Detection methods for stochastic gravitational-wave backgrounds: a unified treatment*, *Living Rev. Rel.* **20** (2017), no. 1 2, [`arXiv:1608.06889`].

[381] A. I. Renzini, J. D. Romano, C. R. Contaldi, and N. J. Cornish, *Comparison of maximum-likelihood mapping methods for gravitational-wave backgrounds*, *Phys. Rev. D* **105** (2022), no. 2 023519, [arXiv:2107.02292].

[382] S. C. Hotinli, M. Kamionkowski, and A. H. Jaffe, *The search for anisotropy in the gravitational-wave background with pulsar-timing arrays*, *Open J. Astrophys.* **2** (2019), no. 1 8, [arXiv:1904.05348].

[383] L. V. Dall'Armi, A. Ricciardone, and D. Bertacca, *The Dipole of the Astrophysical Gravitational-Wave Background*, [arXiv:2206.02747].

[384] A. Raccanelli, E. D. Kovetz, S. Bird, I. Cholis, and J. B. Munoz, *Determining the progenitors of merging black-hole binaries*, *Phys. Rev. D* **94** (2016), no. 2 023516, [arXiv:1605.01405].

[385] A. C. Jenkins, R. O'Shaughnessy, M. Sakellariadou, and D. Wysocki, *Anisotropies in the astrophysical gravitational-wave background: The impact of black hole distributions*, *Phys. Rev. Lett.* **122** (2019), no. 11 111101, [arXiv:1810.13435].

[386] G. Cusin, I. Dvorkin, C. Pitrou, and J.-P. Uzan, *Properties of the stochastic astrophysical gravitational wave background: astrophysical sources dependencies*, *Phys. Rev. D* **100** (2019), no. 6 063004, [arXiv:1904.07797].

[387] G. Cusin, I. Dvorkin, C. Pitrou, and J.-P. Uzan, *Stochastic gravitational wave background anisotropies in the mHz band: astrophysical dependencies*, *Mon. Not. Roy. Astron. Soc.* **493** (2020), no. 1 L1–L5, [arXiv:1904.07757].

[388] S. S. Bavera, G. Franciolini, G. Cusin, A. Riotto, M. Zevin, and T. Fragos, *Stochastic gravitational-wave background as a tool for investigating multi-channel astrophysical and primordial black-hole mergers*, *Astron. Astrophys.* **660** (2022) A26, [arXiv:2109.05836].

[389] S. Wang, K. Kohri, and V. Vardanyan, *Probing Primordial Black Holes with Anisotropies in Stochastic Gravitational-Wave Background*, [arXiv:2107.01935].

[390] A. Klein et al., *The last three years: multiband gravitational-wave observations of stellar-mass binary black holes*, [arXiv:2204.03423].

[391] D. Gerosa, S. Ma, K. W. K. Wong, E. Berti, R. O'Shaughnessy, Y. Chen, and K. Belczynski, *Multiband gravitational-wave event rates and stellar physics*, *Phys. Rev. D* **99** (2019), no. 10 103004, [arXiv:1902.00021].

[392] T. Baker, E. Barausse, A. Chen, C. de Rham, M. Pieroni, and G. Tasinato, *Testing gravitational wave propagation with multiband detections*, [arXiv:2209.14398].

[393] E. Dimastrogiovanni, M. Fasiello, A. Malhotra, P. D. Meerburg, and G. Orlando, *Testing the early universe with anisotropies of the gravitational wave background*, JCAP **02** (2022), no. 02 040, [arXiv:2109.03077].

[394] V. Alba and J. Maldacena, *Primordial gravity wave background anisotropies*, JHEP **03** (2016) 115, [arXiv:1512.01531].

[395] E. Dimastrogiovanni, M. Fasiello, and G. Tasinato, *Searching for Fossil Fields in the Gravity Sector*, Phys. Rev. Lett. **124** (2020), no. 6 061302, [arXiv:1906.07204].

[396] C. Pitrou, G. Cusin, and J.-P. Uzan, *Unified view of anisotropies in the astrophysical gravitational-wave background*, Phys. Rev. D **101** (2020), no. 8 081301, [arXiv:1910.04645].

[397] G. Cusin, C. Pitrou, and J.-P. Uzan, *Anisotropy of the astrophysical gravitational wave background: Analytic expression of the angular power spectrum and correlation with cosmological observations*, Phys. Rev. D **96** (2017), no. 10 103019, [arXiv:1704.06184].

[398] G. Cusin, C. Pitrou, and J.-P. Uzan, *The signal of the gravitational wave background and the angular correlation of its energy density*, Phys. Rev. D **97** (2018), no. 12 123527, [arXiv:1711.11345].

[399] N. Bartolo, D. Bertacca, S. Matarrese, M. Peloso, A. Ricciardone, A. Riotto, and G. Tasinato, *Characterizing the cosmological gravitational wave background: Anisotropies and non-Gaussianity*, Phys. Rev. D **102** (2020), no. 2 023527, [arXiv:1912.09433].

[400] **LISA Cosmology Working Group** Collaboration, N. Bartolo et al., *Probing Anisotropies of the Stochastic Gravitational Wave Background with LISA*, [arXiv:2201.08782].

[401] L. Valbusa Dall'Armi, A. Ricciardone, N. Bartolo, D. Bertacca, and S. Matarrese, *Imprint of relativistic particles on the anisotropies of the stochastic gravitational-wave background*, Phys. Rev. D **103** (2021), no. 2 023522, [arXiv:2007.01215].

[402] G. Cusin, I. Dvorkin, C. Pitrou, and J.-P. Uzan, *First predictions of the angular power spectrum of the astrophysical gravitational wave background*, Phys. Rev. Lett. **120** (2018) 231101, [arXiv:1803.03236].

[403] D. Bertacca, A. Ricciardone, N. Bellomo, A. C. Jenkins, S. Matarrese, A. Raccanelli, T. Regimbau, and M. Sakellariadou, *Projection effects on the observed angular spectrum of the astrophysical stochastic gravitational wave background*, Phys. Rev. D **101** (2020), no. 10 103513, [arXiv:1909.11627].

[404] N. Bellomo, D. Bertacca, A. C. Jenkins, S. Matarrese, A. Raccanelli, T. Regimbau, A. Ricciardone, and M. Sakellariadou, *CLASS_GWB: robust modeling of the astrophysical gravitational wave background anisotropies*, *JCAP* **06** (2022), no. 06 030, [arXiv:2110.15059].

[405] L. Dai, *Rotation of the cosmic microwave background polarization from weak gravitational lensing*, *Phys. Rev. Lett.* **112** (2014), no. 4 041303, [arXiv:1311.3662].

[406] W. Hu, *Weak lensing of the CMB: A harmonic approach*, *Phys. Rev. D* **62** (2000) 043007, [astro-ph/0001303].

[407] R. Durrer, *The Cosmic Microwave Background.* Cambridge University Press, Cambridge, 2008.

[408] C. Dalang, G. Cusin, and M. Lagos, *Polarization distortions of lensed gravitational waves*, *Physical Review D* (2022).

[409] T. Callister, A. S. Biscoveanu, N. Christensen, M. Isi, A. Matas, O. Minazzoli, T. Regimbau, M. Sakellariadou, J. Tasson, and E. Thrane, *Polarization-based Tests of Gravity with the Stochastic Gravitational-Wave Background*, *Phys. Rev. X* **7** (2017), no. 4 041058, [arXiv:1704.08373].

[410] H. Omiya and N. Seto, *Searching for anomalous polarization modes of the stochastic gravitational wave background with LISA and Taiji*, *Phys. Rev. D* **102** (2020), no. 8 084053, [arXiv:2010.00771].

[411] E. Belgacem and M. Kamionkowski, *Chirality of the gravitational-wave background and pulsar-timing arrays*, *Phys. Rev. D* **102** (2020), no. 2 023004, [arXiv:2004.05480].

[412] L. Sorbo, *Parity violation in the Cosmic Microwave Background from a pseudoscalar inflaton*, *JCAP* **06** (2011) 003, [arXiv:1101.1525].

[413] D. M. Eardley, D. L. Lee, and A. P. Lightman, *Gravitational-wave observations as a tool for testing relativistic gravity*, *Physical Review D* **8** (1973) 3308–3321.

[414] R. C. Nunes, *Searching for modified gravity in the astrophysical gravitational wave background: Application to ground-based interferometers*, *Phys. Rev. D* **102** (2020), no. 2 024071, [arXiv:2007.07750].

[415] G. W. Horndeski, *Second-Order Scalar-Tensor Field Equations in a Four-Dimensional Space*, *International Journal of Theoretical Physics* **10** (Sept., 1974) 363–384.

[416] G. Orlando, *Probing parity-odd bispectra with anisotropies of GW V modes*, *JCAP* **12** (2022) 019, [arXiv:2206.14173].

[417] N. Seto and A. Taruya, *Polarization analysis of gravitational-wave backgrounds from the correlation signals of ground-based interferometers: Measuring a circular-polarization mode, Phys. Rev. D* **77** (2008) 103001, [arXiv:0801.4185].

[418] Y. Hu, P.-P. Wang, Y.-J. Tan, and C.-G. Shao, *Testing the polarization of gravitational wave background with LISA-TianQin network*, [arXiv:2209.07049].

[419] L. Pizzuti, A. Tomella, C. Carbone, M. Calabrese, and C. Baccigalupi, *Boltzmann equations for astrophysical Stochastic Gravitational Wave Backgrounds scattering off of massive objects*, [arXiv:2208.02800].

[420] G. Cusin, R. Durrer, and P. G. Ferreira, *Polarization of a stochastic gravitational wave background through diffusion by massive structures, Phys. Rev. D* **99** (2019), no. 2 023534, [arXiv:1807.10620].

[421] R. A. Matzner and M. P. Ryan, *Low-frequency limit of gravitational scattering, Phys. Rev. D* **16** (Sep, 1977) 1636–1642.

[422] P. J. Westervelt, *Scattering of electromagnetic and gravitational waves by a static gravitational field: comparison between the classical and quantum field-theoretic results.*, .

[423] P. C. Peters, *Differential cross-sections for weak-field gravitational scattering, Phys. Rev. D* **13** (Feb, 1976) 775–777.

[424] N. Sanchez, *Scattering of scalar waves from a schwarzschild black hole., Journal of Mathematical Physics* **17** (1976) 688–692.

[425] S. R. Dolan, *Scattering of long-wavelength gravitational waves, Phys. Rev. D* **77** (Feb, 2008) 044004.

[426] O. L. Brill and B. Goodman, *Causality in the coulomb gauge, American Journal of Physics* **35** (1967), no. 9 832–837.

[427] C. W. Gardiner and P. D. Drummond, *Causality in the coulomb gauge: A direct proof, Phys. Rev. A* **38** (Nov, 1988) 4897–4898.

[428] E. Newman and R. Penrose, *An Approach to Gravitational Radiation by a Method of Spin Coefficients, Journal of Mathematical Physics* **3** (May, 1962) 566–578.

[429] C. M. Will, *Theory and Experiment in Gravitational Physics.* Cambridge University Press, 9, 2018.

[430] S. Chandrasekhar and S. Chandrasekhar, *The mathematical theory of black holes*, vol. 69. Oxford university press, 1998.

[431] T. Kite, J. Chluba, A. Ravenni, and S. P. Patil, *Clarifying transfer function approximations for the large-scale gravitational wave background in ΛCDM*, *Mon. Not. Roy. Astron. Soc.* **509** (2021), no. 1 1366–1376, [arXiv:2107.13351].

[432] W. Hu and M. J. White, *CMB anisotropies: Total angular momentum method*, *Phys. Rev. D* **56** (1997) 596–615, [astro-ph/9702170].

[433] Y.-T. Lin and B. D. Wandelt, *A Beginner's guide to the theory of CMB temperature and polarization power spectra in the line-of-sight formalism*, *Astropart. Phys.* **25** (2006) 151–166, [astro-ph/0409734].

[434] P. C. Peters, *Index of refraction for scalar, electromagnetic, and gravitational waves in weak gravitational fields*, *Phys. Rev. D* **9** (Apr, 1974) 2207–2218.

[435] Z. Chang, X. Zhang, and J.-Z. Zhou, *Gravitational waves from primordial scalar and tensor perturbations*, [arXiv:2209.07693].

[436] A. I. Renzini and C. R. Contaldi, *Mapping Incoherent Gravitational Wave Backgrounds*, *Mon. Not. Roy. Astron. Soc.* **481** (2018), no. 4 4650–4661, [arXiv:1806.11360].

[437] A. Kosowsky, *Cosmic microwave background polarization*, *Annals Phys.* **246** (1996) 49–85, [astro-ph/9501045].

[438] S. Alexander and N. Yunes, *Chern-Simons Modified General Relativity*, *Phys. Rept.* **480** (2009) 1–55, [arXiv:0907.2562].

[439] S. Libanore, M. C. Artale, D. Karagiannis, M. Liguori, N. Bartolo, Y. Bouffanais, N. Giacobbo, M. Mapelli, and S. Matarrese, *Gravitational Wave mergers as tracers of Large Scale Structures*, *JCAP* **02** (2021) 035, [arXiv:2007.06905].

[440] C. Ungarelli and A. Vecchio, *Studying the anisotropy of the gravitational wave stochastic background with LISA*, *Phys. Rev. D* **64** (2001) 121501, [astro-ph/0106538].

[441] N. Seto and A. Cooray, *LISA measurement of gravitational wave background anisotropy: Hexadecapole moment via a correlation analysis*, *Phys. Rev. D* **70** (2004) 123005, [astro-ph/0403259].

[442] C. Pitrou, X. Roy, and O. Umeh, *xPand: An algorithm for perturbing homogeneous cosmologies*, *Class. Quant. Grav.* **30** (2013) 165002, [arXiv:1302.6174].

Samenvatting

De directe detectie van zwaartekrachtgolven (ZG) is een baanbrekende wetenschappelijke prestatie van het afgelopen decennium. Het betekende onder andere het begin van de ZG-kosmologie: de mogelijkheid om het heelal, vanaf de oerfase tot vandaag, te bestuderen met behulp van deze nieuwe fascinerende detectiemethode. Gravitatiegolven bevatten waardevolle informatie over hun bronnen en de ruimtetijd waarin ze zich voortplanten. Daarom kunnen ze inzichten onthullen in het homogene en isotrope heelal en de kosmische structuren die hierdoor verstoord worden. Hoewel de huidige technologie voor de detectie van deze golven geen kosmologische gegevens van vergelijkbare kwaliteit kan leveren als die vanuit elektromagnetische signalen worden verzameld, blijft het inherente potentieel van gravitatiegolven bestaan. Vooruitkijkend naar toekomstige missies beoogt dit proefschrift te begrijpen wat gravitatiegolven ons kunnen vertellen over de dynamiek van het heelal op kosmologische schalen, met een bijzondere nadruk op donkere energie en grootschalige structuren. Na **Hoofdstuk 1**, waarin we alle noodzakelijke concepten betreffende kosmologie en gravitatiegolven introduceren, is de rest van het proefschrift verdeeld in drie onderdelen:

1. In het eerste deel wordt een poging ondernomen de kracht van de fluctuaties in de helderheidsafstand van gravitatiegolven te benutten als een robuust instrument om scalar-tensor theorieën van de zwaartekracht te onderzoeken. Dit zijn uitgebreide zwaartekrachttheorieën waarin een scalair veld een extra zwaartekrachtinteractie bemiddelt. De aanwezigheid van het scalaire veld laat sporen na in de zogenaamde *relativistische effecten*: vervormingen van de ZGen door de aanwezigheid van kosmische structuren langs het voortplantingstraject. Aangezien het groeipatroon van de zwaartekrachtpotentialen van de materie afhangt van de zwaartekrachttheorie, dragen relativistische effecten informatie over het scalaire veld. De analyse wordt uitgevoerd in het geometrische optica regime, waar de frequentie van de gravitatiegolven veel groter is dan de karakteristieke energieschaal van de ondervonden obstakels. **Hoofdstuk 2** stelt een nieuwe schattingsfactor voor, die gebruik maakt van ZG en Type-Ia Supernovae observaties, om de onderscheidende signaturen geassocieerd met de lopende Planck massa en de clustering van donkere energie te detecteren. Volgens onze analyse is in het meest optimistische scenario nabij 10^{14} effectief aantal gebeurtenissen nodig om dergelijke signaturen op

te sporen. **Hoofdstuk 3** verlegt de aandacht naar de zwakke lensing convergentieterm, het meest prominente relativistische effect. We onderzoeken de mogelijkheden ervan om de parameters van het uitgebreide kosmologische model in te perken, waarbij we ZG-missies alleen of in combinatie met sterrenstelselonderzoeken beschouwen. Wij concluderen dat ZGen het inperkend vermogen kunnen vergroten als hun statistiek vergelijkbaar wordt met die van sterrenstelsels.

2. Het tweede deel van het proefschrift formuleert aanvullende testen voor scalair-tensor theorieën van de zwaartekracht. Opnieuw werkend in de hoge frequentie benadering, introduceerden we in **Hoofdstuk 4** de energie-impulstensor voor zwaartekrachtsgolven in de subklasse van dergelijke theorieën waar de tensormodi zich voortplanten met de lichtsnelheid. Uit dit resultaat hebben we de zwaartekrachtgolfafstanden afgeleid, d_L^{GW} en d_A^{GW}, en aangetoond dat beide expliciet gewijzigd kunnen worden door de aanwezigheid van het scalaire veld. We hebben ook de geldigheid van de reciprociteitswet van Etherington bewezen en de implicaties van ons resultaat in de context van sterke lensing tijdsvertraging onderzocht. **Hoofdstuk 5** onderzoekt de mogelijkheden van directe detectie van scalaire veldgolven met de focus op twee screeningsmechanismen: *chameleon* en *symmetron*. Wil een scalair-tensor theorie namelijk aanvaardbaar zijn, dan moet deze voorzien zijn van een mechanisme dat het scalaire veld onderdrukt in gebieden met een hoge dichtheid, zoals bijvoorbeeld het Zonnestelsel. Wij tonen aan dat in beide scenario's de interactie tussen de scalaire golven en de testdeeltjes wordt onderdrukt. Daarom concluderen wij dat scalaire golven in deze theorieën niet waarneembaar zouden moeten zijn.

3. In het derde deel onderzoeken we de voortplanting van ZGen in het golfoptische regime binnen de algemene relativiteitstheorie. De reden achter deze keuze is om aan te tonen dat bepaalde effecten, die gewoonlijk worden toegeschreven aan bijkomende dynamische veldinhoud, degeneratie kunnen vertonen met golfoptische effecten. In **Hoofdstuk 6** hebben we laten zien dat de voortplantingseffecten zelfs in de algemene relativiteitstheorie waarneembare scalaire en vectoriële polarisatiemodi kunnen voortbrengen. Hoewel de verkregen resultaten van toepassing blijven op opgeloste ZG-gebeurtenissen, hebben we ons in dit deel gericht op de *stochastische ZG-achtergrond* en de polarisatie-inhoud hiervan. Voor het eenvoudige geval van een ongepolariseerde, Gaussische, statistisch homogene beginachtergrond hebben we laten zien dat de interactie met materiestructuren geen netto verschil veroorzaakt in de hoeveelheid links- en rechtsdraaiende tensormodi. Wij hebben ook geconstateerd dat, om Q- en U-polarisatiemodes te produceren, een hexadecapool anisotropie vereist is.

Summary

The direct detection of gravitational waves (GW) is a groundbreaking scientific achievement of the past decade. Among others, it marked the beginning of GW-cosmology: the possibility of studying the Universe, from its primordial phase until today, using this new fascinating probe. Gravitational waves carry valuable information about their sources and the spacetime through which they propagate. For this reason, they have the power of revealing insights into the homogeneous and isotropic Universe, and the cosmic structures that perturb it. While the current technology for their detection is not able to deliver cosmological data of comparable quality as the one gathered through electromagnetic signals, the inherent potential of gravitational waves still remains. Looking ahead to future missions, this Thesis aims at understanding what gravitational waves can tell us about the dynamics of the Universe on cosmological scales, with particular emphasis on dark energy and large-scale structures. After **Chapter 1**, where we introduce all the necessary concepts regarding cosmology and gravitational waves, the rest of the Thesis is divided in three main parts:

1. The first Part seeks to harness the power of *gravitational waves luminosity distance fluctuations* as a robust tool to investigate scalar-tensor theories of gravity. The latter are extended gravitational theories where a scalar field mediates an additional gravitational interaction. The presence of the scalar field leaves traces in the so-called *relativistic effects*: distortions of the GWs due to the presence of cosmic structures along the propagation path. Since the growth pattern of the matter gravitational potentials depends on the gravitational theory, relativistic effects carry information about the scalar field. The analysis is conducted in the geometric optics regime, where the frequency of the gravitational waves greatly exceeds the characteristic energy scale of the encountered obstacles. **Chapter 2** proposes a novel estimator, which exploits GW and Type-Ia Supernovae observation, to detect the distinctive signatures associated with the running Planck's Mass and the clustering of dark energy. According to our analysis, in the most optimistic scenario, a total of 10^{14} effective number of events is needed to pick up such signatures. **Chapter 3** shifts the focus to the weak lensing convergence term, the most prominent relativistic effect. We investigate its potentiality in constraining the parameters of the extended cosmological model, considering GW-missions alone or in combi-

nation with galaxy surveys. We concluded that GWs can help the constraining power if their statistic becomes comparable with the one of galaxies.

2. The second Part of the Thesis formulates additional tests for scalar-tensor theories of gravity. Working again in the high frequency approximation, in **Chapter 4** we introduced the *gravitational wave stress-energy tensor* in the subclass of such theories where tensor modes propagate at the speed of light. From this result, we derived the gravitational wave distances, d_L^{GW} and d_A^{GW}, and showed that both of them can be explicitly modified by the presence of the scalar field. We also proved the validity of the *Etherington's reciprocity law* and investigated the implications of our result in the context of strong lensing time delay. **Chapter 5** explores the direct detection prospect of the scalar field waves in light of two screening mechanisms: *chameleon* and *symmetron*. Indeed, in order for a scalar-tensor theory to be viable, it must be equipped of a mechanism which suppresses the scalar field in high-density regions, such as the Solar System. We show that, in both scenarios, the interaction between the scalar waves and test particles is suppressed. Because of this, we concluded that scalar waves in these theories should not be observable.

3. In the third Part, we investigate the propagation of gravitational waves in the wave-optics regime within General. The reason behind this choice is to demonstrate that certain effects, commonly attributed to additional dynamical field content, may exhibit degeneracy with wave-optics effects. In **Chapter 6** we showed that the propagation effects can produce observable scalar and vector polarization modes even in General Relativity. While the results obtained remain applicable to resolved gravitational wave events, in this part we focused on the *stochastic gravitational wave background* and its polarization content. For the simple case of an unpolarized, Gaussian, statistically homogeneous initial background, we showed that the interaction with matter structures does not generate a net difference in the amount of left- and right-helicity tensor modes. We also observed that, in order to produce Q- and U-polarization modes, a hexadecapole anisotropy is required.

List of Publications

1. " Gravitational waves and geometrical optics in scalar tensor theories",

   A. Garoffolo, G. Tasinato, C. Carbone, D. Bertacca, S. Matarrese.
   JCAP, 11 (2020) 040

2. "Detecting dark energy fluctuations with gravitational waves",

   A. Garoffolo, M. Raveri, A. Silvestri, G. Tasinato, C. Carbone, D. Bertacca,
   S. Matarrese.
   Phys.Rev.D, 103 (2021) 8, 083506.

3. "Gravitational wave cosmological distances in scalar-tensor theories of gravity",

   G. Tasinato, **A. Garoffolo**, D. Bertacca, S. Matarrese.
   JCAP, 06 (2021) 050.

4. "Unifying gravitational waves and dark energy",

   A. Garoffolo, O. Contigiani,
   e-Print: 2110.14689, submitted to *Phys.Rev.D*.

5. "Prospects of testing late-time cosmology with weak lensing of gravitational
   waves and galaxy surveys",

   A. Balaudo, **A. Garoffolo**, M. Martinelli, S. Mukherjee, A. Silvestri,
   e-Print: 2210.06398, submitted to *JCAP*.

6. "Wave-optics limit of the stochastic gravitational wave background", **A. Garoffolo**,
   e-Print: 2210.05718, submitted to *JCAP*.

Curriculum Vitae

I was born in Milan on November 24th, 1993, where I attended high school and university. Despite what one might assume from reading this Thesis, my interest in physics sparked, quite late, at the Gran Sasso laboratories while observing a liquid scintillator for low-energy solar neutrinos. Before that physics was not my top priority, perhaps partly because I skipped the first year of its teaching due to attending my third year of high school at Poudre High in Fort Collins, Colorado. Nevertheless, when I found myself face-to-face with such an enormous detector, with its interior walls all covered in "light bulbs", something clicked. Drifting towards more theoretical pursuits, I obtained my bachelor's degree from the University of Milan in 2016. The title of my thesis was *Study of stochastic properties of forces in long-range interaction systems*. If any, the role of this thesis was to make me appreciate the physics of plasmas. During my master's studies, I discovered that cosmology essentially involves studying an unimaginably vast one in a spacetime that is also expanding. This realization led me to the University of Padova, where I worked on my master thesis, *Propagation of Gravitational Waves through Cosmic Inhomogeneities in Modified Gravity*, in the group of Prof. S. Matarrese. I started my PhD in September 2019, in the theoretical cosmology group at the Lorentz Institute of Leiden University, under the supervision of Prof. dr. Ana Achúcarro and Dr. Alessandra Silvestri. During my time in Leiden, I had the pleasure to supervise multiple master students in their thesis work, and I was the teaching assistant of the courses "Quantum Field Theory" and "Theory of General Relativity". I participated in a number of schools and conferences and had the opportunity of presenting my work in various seminars in the Netherlands, Italy, Germany, Belgium, United Kingdom, France, Canada and the United States.

In the fall of 2023, I will start a postdoc at the University of Pennsylvania, Philadelphia, where I plan to continue my research on gravitational wave cosmology.

Acknowledgements

I would like to express my deepest gratitude to all those who have contributed to the completion of this PhD. Your support, guidance, and encouragement have been instrumental in this journey of academic and personal growth. Sometimes quietly and sometimes loudly, my perspective on many things has changed since I arrived in the Netherlands. I truly believe that these changes have been for the better, and I am filled with curiosity and excitement to witness the ongoing evolution that lies ahead.